Targeted Nanocarriers for HIV Therapy

Shijie Cao

A dissertation

submitted in partial fulfillment of the

requirements for the degree of

Doctor of Philosophy

University of Washington

2018

Reading Committee:

Kim A. Woodrow, Chair

Rodney J.Y. Ho

Ying Zheng

Program Authorized to Offer Degree:

Bioengineering

University of Washington

Abstract

Targeted Nanocarriers for HIV Therapy

Shijie Cao

Chair of the Supervisory Committee:
Professor Kim A. Woodrow
Bioengineering

Highly active antiretroviral therapy (HAART) can successfully suppress HIV-1 replication in plasma to undetectable levels, but is not capable of eradicating the virus from long-live cellular reservoirs. The latent reservoir for HIV-1 is sustained by the longevity and proliferative capacity of resting CD4 T cells containing HIV in a highly suppressed state, rendering the infection invisible to the immune system. Numerous approaches are aimed at diminishing these latent HIV reservoirs, such as early initiation of HAART, or reactivation of latent virus by use of latency reversing agents (LRAs). However, none has yet been proven effective in actually reducing the reservoir in vivo. A synergistic approach will likely be needed to deplete the reservoir and establish a cure. In addition, HIV persistence in some anatomical sites has been attributed to lower concentrations of

anti-HIV drugs. In this work, we focused on developing targeted nanocarriers (NCs) to deliver synergistic anti-HIV drugs to cellular or anatomical viral reservoirs.

One aim of our work is to deliver antiretroviral drugs (ARVs) to the gut-associated lymphoid tissue (GALT), a major sanctuary site for HIV infection. The α4β7 integrin gut homing receptor leads to migration of infected cells to the GALT and facilitates HIV infection. We developed a core-shell nanoparticle incorporating the α4β7 monoclonal antibody (mAb) as a dual-functional ligand for selectively targeting a protease inhibitor to gut-homing T cells in the GALT while simultaneously blocking HIV infection. This targeted NC showed specific binding to α4β7+ CD4 T lymphocytes from rhesus macaque ileum and higher levels of accumulation in α4β7+ cells from the small intestine when administered in mice. A second aim of our work is to deliver mechanistically distinct LRAs to reactivate CD4 T cells in the lymph nodes. We screened a variety of LRAs that were incorporated into NCs through different loading strategies, and determined LRA combinations that displayed synergistic latency reversal and low cytotoxicity in both human T cell line model and CD4+ T cells from HIV-infected patients under suppressive HAART. Our targeted NCs demonstrated long-acting and selective activation of CD4+ T cells in the mice lymph nodes and significantly reduced local toxicity compared to free drug. Our NCs for T cell and lymphatic tissue targeting also show promise in delivering other types of anti-HIV agents, vaccines, and immune-modulating drugs for many biomedical applications.

TABLE OF CONTENTS

LIST OF FIGURES

LIST OF TABLES

ACKNOWLEDGEMENTS

I would like to express my deepest thanks to my advisor, Prof. Kim Woodrow for her continuous support throughout of my PhD study. Kim's curiosity and creativity on research, and her passion and enthusiasm on science always impressed and affected me. I am grateful for many great opportunities she provided to me, such as publishing research, writing review papers, presenting at conferences, reviewing others' work, and mentoring undergraduate students. I also very appreciate her detailed and insightful edits, comments, and critics on all my manuscripts and abstracts, as well as her great advises on every talk I practiced for public presentations. always inspires me with new ideas and makes me think more critically.

I thank all members of my Supervisory Committee: Prof. Rodney Ho, Prof. Ying Zheng, Prof. Buddy Ratner, and Prof. Ann Collier. I very appreciate their time, constructive feedback and valuable input from various expertise and aspects on my research projects. They always came up with great ideas on every committee meeting and my general exam.

I thank those people I have worked with in the last five years. I particularly thank Dr. Yonghou Jiang, who has worked closely with me and taught me skills especially in antiretroviral studies. I thank Dr. Hangyu Zhang for his help on taking TEM images and making peptides for my studies. Thank you to Dr. Jaehyung Park, Dr. Emily Krogstad, Dr. Renuka Ramanathan, and Dr. Sharon Golan-Paz, Hannah Frizzell, Rachel Creighton, and Jamie Hernandaz for their valuable discussions, advices, and help. Thank you to the undergraduate students who have worked with me, Sarah Slack and Nina Kondza. I very appreciate their hard work and creativity, I couldn't have done all the work without them. I thank Rick Edmark, who was such a great lab manager and provided a great lab environment for us. I also want to thank our collaborators, especially Sean

Hughes and Claire Levy from Hladik Lab who did a lot of hard work for us, provided us great suggestions and feedback, and also helped me with manuscripts. I am so fortunate to work with all these wonderful people.

I would like to thank my loved ones who have been my support through all these years. To my parents Hui Cao and Minhua Le, no words can truly express how grateful I am for your unconditional love and support. Thank you for always being there and having my back. I especially appreciate your support on whatever decision I made for all these years. You always believe me and encourage me to pursue what I dreamed of and want me to be happy.

To Bowen Ruan, thank you for being with me all along this journey. I always love to share my joy, sadness, complaints, and many trivial matters with you. You're truly my best friend and have provided such an affinity amount of support and care. We have grown up together throughout our PhD, and I'm excited to step into next adventures with you.

To my friends in BIOE, Gary Liu, Zhongdi Chu, Yoon Jung Choi, Ida Su, Jason Miklas, Pakapreud Khumwan, and Efren Lee, I enjoyed our dim sum and bubble tea time, and will miss that. I also thank Gary, Ida, and Pak for helping me with my practice talks. Thank you to my previous roommates Yuan Wen, Puze Li, and Tianye Lv, you made me feel like having a home here in Seattle. Thank you to my dear friend Fangda Xu, who has provided long-distance support along the journey. Thank you to my college roommates and friends for welcoming me back home every time I passed by Shanghai. Thank you to my mentor in college, Dr. Huile Gao, who brought me into this exciting drug delivery field.

DEDICATION

This work is dedicated to all of those who are fighting against HIV.

Chapter 1. Executive summary and specific aims

Combination antiretroviral therapy has revolutionized the treatment of HIV-1 infection, but a reservoir of latent HIV-1 in resting memory CD4+ T cells remains a barrier to achieving complete virus eradication and cure. The major anatomical sites, including gut-associated lymphoid tissue (GALT), lymph nodes (LNs), and spleen, that harbor a vast amount of infected cells, exhibit limited access to anti-HIV drugs which may contribute to viral persistence[1-4]. Numerous approaches are proposed to eradicate these HIV reservoirs, but none of them has achieved success in clinical settings, and some of them are still in the early pre-clinical stage. Due to the complexity of HIV pathogenesis, combination of more efficient therapeutic and novel reservoir-targeted drug delivery approaches may be needed for a better therapy. In addition, studies suggest that an HIV cure may not require complete elimination of latent reservoir[5], and targeting cell subsets and tissues that harbor the majority of latently infected cells might be sufficient to control infection. Here, we hypothesize that targeted nanocarrier (NC) delivery systems will increase local concentrations of drug combinations to effectively reduce the HIV reservoir size. Our hypothesis is based on several key observations. First, we have shown that NCs can be designed to target tissues and cells associated with the latent reservoir, which may potentially increase efficacy of these therapeutic agents while decreasing toxicity. Second, sufficient reduction of the latent pool to curative levels may require mechanistically distinct latency reversing agents (LRAs) used in combination[6-7]. Lastly, we have shown that NCs can combine therapeutic agents to synergistically enhance potency while also reducing toxicity[8], which may be useful for delivering the LRA combinations needed for robust latency reversal. In this research, we established a targeted nanocarrier system which can carry antiretroviral drugs and specifically target gut-homing T cells

(Aim 1). We then optimized the NCs and functionalized it to target CD4 T cells (Aim 2). In order to eradicate latently HIV infected T cells, we incorporated latency reversing agents (LRAs) into our CD4-targeting NCs to selective activate CD4+ T cells in the lymph nodes (Aim 3).

1.1 Aim 1. Develop targeted lipid-polymer hybrid nanoparticles that can co-deliver ARV and antibody to gut-homing T cells.

The gut-associated lymphoid tissue (GALT) is a major site for latently infected cells and is also a sanctuary site for residual virus replication and emergence of ARV drug resistance[9-10]. The α4β7 integrin (gut homing receptor) is a promising therapeutic target for the virus reservoir due to its dual-function. First, α4β7 demarcates a subset of CD4+ T cells that are highly susceptible to HIV-1 infection, and also causes their migration and accumulation to the GALT[11-12]. Second, HIV envelop has been shown to bind to and signal through α4β7 thereby facilitating productive infection[13]. Animal studies have shown that targeting α4β7 using a monoclonal antibody reduces SIV transmission in macaques[14-16]. Here, we conjugated anti-α4β7 antibodies (α4β7 mAb) to lipid-coated PLGA nanoparticles (A4B7-LCNPs) loaded with a protease inhibitor (PI). We hypothesized that A4B7-LCNPs would target gut-homing T cells in the GALT, where the delivered PIs could block infected cells from producing new HIV virions and the delaminated antibodies could protect uninfected T cells by blocking virus binding to α4β7.

1.2 Aim 2. Optimize and compare CD4-targeting hybrid nanoparticles using different binding ligands.

Recently, CD4+ T lymphocytes have attracted more attention as a target for nanocarrier (NC)-based therapies in conditions such as HIV, cancer, and autoimmune diseases. Especially, CD4+ T cells are major targets for HIV and the resting CD4+ T cells are considered the major HIV reservoir

cells. Monoclonal antibodies (mAbs) against CD4 and CD4 binding peptides2 have been developed and conjugated to the surface of NCs for targeting[17-18]. However, targeting efficacy may vary with their specificity, affinity or avidity when linked to NCs. In addition, the physicochemical properties of NCs could also affect the ligand function. Here, we used a hybrid nanoparticle system to investigate the targeting of several CD4 binding ligands conjugate to NCs. We demonstrate that unlike positively charged or neutral LCNPs, a negative surface charge showed dramatically lower nonspecific binding and had preferential bindings to CD4+ T cells when conjugated with CD4 mAbs or its fragments. CD4-targeed LCNPs have great promise for delivery of anti-HIV cure agents, vaccines and gene-modifying oligonucleotide drugs that can be applied in a variety of biomedical areas.

1.3 Aim 3. Incorporate diverse LRAs into targeted NCs for selective CD4+ T cell reactivation and HIV-1 latency reversal.

A proposed strategy to cure HIV, known as "shock and kill", uses latency-reversing agents (LRAs) to reactivate latent proviruses for the purge of HIV reservoirs[19-20]. A variety of small molecule LRAs have been identified, but none has yet been proven effective in actually reducing the reservoir size in vivo partially due to their low potency, poor solubility, and toxicity issues[21]. Additionally, the diverse physicochemical properties of LRAs also limit their combination to achieve maximal latency reversal. Nanocarriers (NC) address these challenges by improving drug solubility, safety, and providing sustained drug release and simultaneous delivery of multiple drugs to target tissues and cells. Here, we formulated targeted NCs that incorporate physicochemically diverse LRAs. We screened all formulations and determined an LRA combination that displayed synergistic latency reversal and low cytotoxicity in a human HIV-1 latency T cell line model, and verified it on CD4+ T cells from HIV-infected patients under suppressive antiretroviral therapy.

Furthermore, our targeted NCs provided long-acting and selective activation of CD4+ T cells in the mice lymph nodes, and significantly reduced local toxicity compared to free drug. This platform might enable new solutions for delivering anti-HIV agents towards an HIV cure.

1.4 References

1. Murray, A. J.; Kwon, K. J.; Farber, D. L.; Siliciano, R. F., The Latent Reservoir for HIV-1: How Immunologic Memory and Clonal Expansion Contribute to HIV-1 Persistence. *The Journal of Immunology* **2016,** *197* (2), 407-417.
2. Ostrowski, M.; Benko, E.; Yue, F. Y.; Kim, C. J.; Huibner, S.; Lee, T.; Singer, J.; Pankovich, J.; Laeyendecker, O.; Kaul, R.; Kandel, G.; Kovacs, C., Intensifying Antiretroviral Therapy With Raltegravir and Maraviroc During Early Human Immunodeficiency Virus (HIV) Infection Does Not Accelerate HIV Reservoir Reduction. *Open Forum Infectious Diseases* **2015,** *2* (4), ofv138.
3. Fletcher, C. V.; Staskus, K.; Wietgrefe, S. W.; Rothenberger, M.; Reilly, C.; Chipman, J. G.; Beilman, G. J.; Khoruts, A.; Thorkelson, A.; Schmidt, T. E.; Anderson, J.; Perkey, K.; Stevenson, M.; Perelson, A. S.; Douek, D. C.; Haase, A. T.; Schacker, T. W., Persistent HIV-1 replication is associated with lower antiretroviral drug concentrations in lymphatic tissues. *Proceedings of the National Academy of Sciences* **2014,** *111* (6), 2307-2312.
4. Estes, J. D.; Kityo, C.; Ssali, F.; Swainson, L.; Makamdop, K. N.; Del Prete, G. Q.; Deeks, S. G.; Luciw, P. A.; Chipman, J. G.; Beilman, G. J.; Hoskuldsson, T.; Khoruts, A.; Anderson, J.; Deleage, C.; Jasurda, J.; Schmidt, T. E.; Hafertepe, M.; Callisto, S. P.; Pearson, H.; Reimann, T.; Schuster, J.; Schoephoerster, J.; Southern, P.; Perkey, K.; Shang, L.; Wietgrefe, S. W.; Fletcher, C. V.; Lifson, J. D.; Douek, D. C.; McCune, J. M.; Haase, A. T.; Schacker, T. W., Defining total-body AIDS-virus burden with implications for curative strategies. *Nature Medicine* **2017,** *23*, 1271.
5. Hill, A. L.; Rosenbloom, D. I. S.; Fu, F.; Nowak, M. A.; Siliciano, R. F., Predicting the outcomes of treatment to eradicate the latent reservoir for HIV-1. *Proceedings of the National Academy of Sciences* **2014,** *111* (37), 13475-13480.
6. Blazkova, J.; Chun, T.-W.; Belay, B. W.; Murray, D.; Justement, J. S.; Funk, E. K.; Nelson, A.; Hallahan, C. W.; Moir, S.; Wender, P. A.; Fauci, A. S., Effect of Histone Deacetylase Inhibitors on HIV Production in Latently Infected, Resting CD4(+) T Cells From Infected Individuals Receiving Effective Antiretroviral Therapy. *The Journal of Infectious Diseases* **2012,** *206* (5), 765-769.
7. Laird, G. M.; Bullen, C. K.; Rosenbloom, D. I.; Martin, A. R.; Hill, A. L.; Durand, C. M.; Siliciano, J. D.; Siliciano, R. F., Ex vivo analysis identifies effective HIV-1 latency-reversing drug combinations. *J Clin Invest* **2015,** *125* (5), 1901-12.
8. Jiang, Y.; Cao, S.; Bright, D. K.; Bever, A. M.; Blakney, A. K.; Suydam, I. T.; Woodrow, K. A., Nanoparticle-Based ARV Drug Combinations for Synergistic Inhibition of Cell-Free and Cell–Cell HIV Transmission. *Molecular pharmaceutics* **2015,** *12* (12), 4363-4374.
9. Chun, T.-W.; Nickle, D. C.; Justement, J. S.; Meyers, J. H.; Roby, G.; Hallahan, C. W.; Kottilil, S.; Moir, S.; Mican, J. M.; Mullins, J. I.; Ward, D. J.; Joseph A., K.; Mannon, P. J.; Fauci, A. S., Persistence of HIV in Gut-Associated Lymphoid Tissue despite Long-Term Antiretroviral Therapy. *Journal of Infectious Diseases* **2008,** *197* (5), 714-720.

10. Brenchley, J. M.; Douek, D. C., HIV infection and the gastrointestinal immune system. *Mucosal immunology* **2008,** *1* (1), 23-30.
11. Cicala, C.; Martinelli, E.; McNally, J. P.; Goode, D. J.; Gopaul, R.; Hiatt, J.; Jelicic, K.; Kottilil, S.; Macleod, K.; O'Shea, A.; Patel, N.; Van Ryk, D.; Wei, D.; Pascuccio, M.; Yi, L.; McKinnon, L.; Izulla, P.; Kimani, J.; Kaul, R.; Fauci, A. S.; Arthos, J., The integrin α4β7 forms a complex with cell-surface CD4 and defines a T-cell subset that is highly susceptible to infection by HIV-1. *Proceedings of the National Academy of Sciences* **2009,** *106* (49), 20877-20882.
12. Poles, M. A.; Elliott, J.; Taing, P.; Anton, P. A.; Chen, I. S., A preponderance of CCR5+ CXCR4+ mononuclear cells enhances gastrointestinal mucosal susceptibility to human immunodeficiency virus type 1 infection. *Journal of virology* **2001,** *75* (18), 8390-8399.
13. Arthos, J.; Cicala, C.; Martinelli, E.; Macleod, K.; Van Ryk, D.; Wei, D.; Xiao, Z.; Veenstra, T. D.; Conrad, T. P.; Lempicki, R. A.; McLaughlin, S.; Pascuccio, M.; Gopaul, R.; McNally, J.; Cruz, C. C.; Censoplano, N.; Chung, E.; Reitano, K. N.; Kottilil, S.; Goode, D. J.; Fauci, A. S., HIV-1 envelope protein binds to and signals through integrin α4β7, the gut mucosal homing receptor for peripheral T cells. *Nat Immunol* **2008,** *9* (3), 301-309.
14. Byrareddy, S. N.; Kallam, B.; Arthos, J.; Cicala, C.; Nawaz, F.; Hiatt, J.; Kersh, E. N.; McNicholl, J. M.; Hanson, D.; Reimann, K. A.; Brameier, M.; Walter, L.; Rogers, K.; Mayne, A. E.; Dunbar, P.; Villinger, T.; Little, D.; Parslow, T. G.; Santangelo, P. J.; Villinger, F.; Fauci, A. S.; Ansari, A. A., Targeting α4β7 integrin reduces mucosal transmission of simian immunodeficiency virus and protects gut-associated lymphoid tissue from infection. *Nat Med* **2014,** *advance online publication*.
15. Ansari, A. A.; Reimann, K. A.; Mayne, A. E.; Takahashi, Y.; Stephenson, S. T.; Wang, R.; Wang, X.; Li, J.; Price, A. A.; Little, D. M., Blocking of α4β7 gut-homing integrin during acute infection leads to decreased plasma and gastrointestinal tissue viral loads in simian immunodeficiency virus-infected rhesus macaques. *The Journal of Immunology* **2011,** *186* (2), 1044-1059.
16. Byrareddy, S. N.; Arthos, J.; Cicala, C.; Villinger, F.; Ortiz, K. T.; Little, D.; Sidell, N.; Kane, M. A.; Yu, J.; Jones, J. W.; Santangelo, P. J.; Zurla, C.; McKinnon, L. R.; Arnold, K. B.; Woody, C. E.; Walter, L.; Roos, C.; Noll, A.; Van Ryk, D.; Jelicic, K.; Cimbro, R.; Gumber, S.; Reid, M. D.; Adsay, V.; Amancha, P. K.; Mayne, A. E.; Parslow, T. G.; Fauci, A. S.; Ansari, A. A., Virologic control in SIV+ macaques after antiretroviral and α4β7 antibody therapy. *Science* **2016,** *354* (6309), 197-202.
17. Eck, W.; Nicholson, A. I.; Zentgraf, H.; Semmler, W.; Bartling, S., Anti-CD4-targeted Gold Nanoparticles Induce Specific Contrast Enhancement of Peripheral Lymph Nodes in X-ray Computed Tomography of Live Mice. *Nano Letters* **2010,** *10* (7), 2318-2322.
18. Endsley, A. N.; Ho, R. J. Y., Design and Characterization of Novel Peptide-Coated Lipid Nanoparticles for Targeting Anti-HIV Drug to CD4 Expressing Cells. *The AAPS Journal* **2012,** *14* (2), 225-235.
19. Xing, S.; Siliciano, R. F., Targeting HIV latency: pharmacologic strategies toward eradication. *Drug Discovery Today* **2013,** *18* (11–12), 541-551.
20. Margolis, D. M.; Garcia, J. V.; Hazuda, D. J.; Haynes, B. F., Latency reversal and viral clearance to cure HIV-1. *Science* **2016,** *353* (6297).
21. Rasmussen, T. A.; Lewin, S. R., Shocking HIV out of hiding: where are we with clinical trials of latency reversing agents? *Current Opinion in HIV and AIDS* **2016,** *11* (4), 394-401.

Chapter 2. Introduction

Adapted from: Cao S, Woodrow KA. Nanotechnology approaches to eradicating HIV reservoirs. *European Journal of Pharmaceutics and Biopharmaceutics.* 2018. In press. DOI: 10.1016/j.ejpb.2018.06.002

2.1 Abstract

The advent of combination antiretroviral therapy (cART) has transformed HIV-1 infection into a controllable chronic disease, but these therapies are incapable of eradicating the virus to bring about an HIV cure. Multiple strategies have been proposed and investigated to eradicate latent viral reservoirs from various biological sanctuaries. However, due to the complexity of HIV infection and latency maintenance, a single drug is unlikely to eliminate all HIV reservoirs and novel strategies may be needed to achieve better efficacy while limiting systemic toxicity. In this review, we describe HIV latency in cellular and anatomical reservoirs, and present an overview of current strategies for HIV cure with a focus on their challenges for clinical translation. We then provide a summary of nanotechnology solutions that have been used to address challenges in HIV cure by delivering physicochemically diverse agents for combination therapy or targeting HIV reservoir sites. We also review nanocarrier-based gene delivery and immunotherapy used in cancer treatment but may have potential applications in HIV cure.

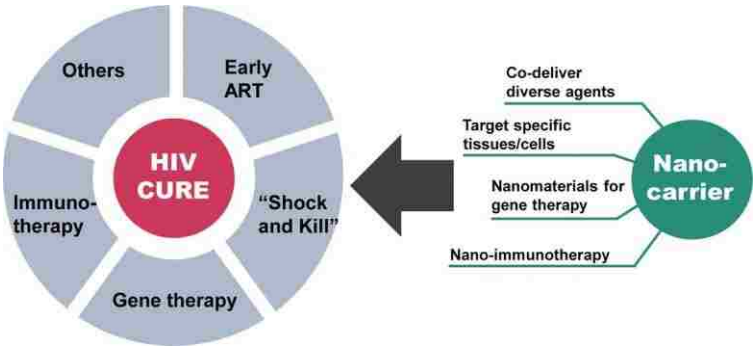

2.2 Introduction

At the end of 2016, the toll of the HIV/AIDS pandemic included 36.7 million infections and 1 million deaths [1]. The combination of antiretroviral drugs (ARVs) for HIV treatment, also referred to as highly active or combination antiretroviral therapy (HAART, cART), can successfully suppress viral replication in plasma to undetectable levels. These treatments have greatly extended the life span and improved the quality of life for people living with HIV-1 infection. However, none of these therapies are capable of eradicating the virus from long-lived cellular reservoirs, which leads to virus rebound once treatment is stopped. Moreover, a lifetime of cART is expensive and causes both short- and long-term side effects such as cardiovascular diseases, neurocognitive disorders, and liver injury [2-5].

Currently, there is no cure for HIV/AIDS, but a singular success has proven that a cure is possible and has galvanized the field [6]. The "Berlin Patient" describes the clinical case study of Timothy Ray Brown who underwent treatment for acute myeloid leukemia (AML), and was cured of both AML and HIV after transplantation with CCR5-deficient hematopoietic stem cells that are inherently resistant to HIV infection [7]. Chemotherapy and radiotherapy was used to eradicate all leukocytes including AML cells. Stem cell transplantation was used to reconstitute the immune system, which also effectively eliminated the need for cART to control plamsa viremia to undetectable levels. This remarkable case bolstered support for HIV cure research, but considerable and sustained efforts are needed to develop clinical approaches that can be applied safely and effectively with the lowest barriers to accessing healthcare.

Viral reservoirs are the primary obstacle that must be overcome to realize an HIV cure. These reservoirs can be defined as cellular sites (e.g. long-lived infected memory CD4+ T cells,

macrophages) where viral replication in infected cells is arrested, and anatomical sites (e.g., gut-associated lymphoid tissue, lymph node, genital tract, central nervous system) that harbor these latently infected cells [8]. These tissues exhibit limited access to ARVs which may contribute to viral persistence [9-10]. Numerous approaches are aimed at finding and diminishing these HIV reservoirs. For example, a number of studies have suggested that early initiation of cART during acute infection could be a realistic approach to cure HIV at the population level as it may block the initial establishment of latent reservoirs [11-12]. Another approach focuses on reactivation of HIV from latently infected cells by use of latency reversing agents (LRAs). Once these latent cells express viral antigen, they may become vulnerable to the immune system or other therapeutics that result in their elimination [13]. However, clinical studies of LRAs have failed to reduce the reservoir size, which might be due to insufficient potency of LRAs, off-target effects in uninfected cells leading to dose-limiting toxicities, or lack of effective "kill" strategies [14]. Cell and gene therapies have also been investigated for HIV cure, where immune cells have been engineered to be resistant to HIV, or HIV proviral DNA has been targeted for excision from latently-infected cells [15]. Other strategies such as broadly neutralizing HIV antibody (bnAb) [16-18], permanently silencing the HIV provirus [19], and anti-proliferative therapy have also been investigated [20].

Due to the complexity of HIV pathogenesis, more efficient therapeutic combinations and novel reservoir-targeted drug delivery approaches may be needed to optimize current approaches for eradicating latently infected cells. Nanocarrier drug delivery systems have unique attributes that are ideally suited to address challenges with targeting the HIV reservoir and eradicating the latent virus to realize an HIV cure. This technology has already shown enormous potential for use in the diagnosis and treatment of several diseases, with a major emphasis in cancer.

Nanocarrier attributes that may be ideally suited for HIV cure strategies include: (1) improvement of bioavailability and pharmacokinetic (PK) profiles of cure agents [21]; (2) reduction of drug toxicity [22], and avoidance of surface efflux pump mediated drug resistance [23]; (3) enhanced or synergistic efficacy through combination of multiple drugs in a single particle [24]; (4) ability to penetrate into HIV reservoir sites such as lymphatic tissues or to target specific vulnerable cells such as CD4+ T cells [25-29]; (5) ability to release therapeutics in controlled rates for sustained drug delivery [30-31].

In this review, we will describe HIV sanctuaries and the current strategies toward diminishing HIV reservoirs and provide an overview of current and future nanotechnology approaches to address HIV cure.

2.3 HIV reservoirs are the obstacle to a cure

The main obstacle to HIV eradication is the existence of reservoirs of latently infected cells. Two models have been proposed to explain the establishment of latency in long-lived memory cells. The pre-activation latency model hypothesizes that HIV can directly infect resting CD4+ T cells [32-33], and the post-activation latency model relies on an idea that the activated CD4+ memory T cells revert to a resting state instead of cell death after being infected by HIV [34]. HIV viral DNA integrates at various locations into the genome of these long-lived host cells [35], and the integration at specific sites (e.g. MKL2 and BACH2) has been attributed to cell clonal expansion and therefore persistent infection [36-37]. HIV latency is maintained under several molecular mechanisms including: (1) the recruitment of histone deacetylases (HDACs) and histone methyltransferases (HMTs) to HIV-1 long term repeat (LTR), leading to histone deacetylation and methylation on Nuc-0 and Nuc-1, which can restrict the initiation of transcription [38-39]; (2)

sequestration or inactivation of transcription and elongation factors such as nuclear factor κB (NF-κB) and NFAT, or positive transcription elongation factor b (P-TEFb) that are important for initiating or elongating transcription [40-41]; and (3) other mechanisms such as HIV-1 DNA methylation [42], post-transcriptional blocks [43], and cellular microRNAs that inhibit HIV-1 production [44]. Compared to virus-producing CD4+ T cells that have a half-life of only 0.7-1.1 days [45], latently-infected CD4+ T cells have a half-life ranging from 4.6 to 44.2 months based on different studies in patients receiving ART [46-48]. These long-lived infected CD4+ T cells with the ability of clonal expansion keep proliferate without releasing virus, leads to their high stability and persistence in sanctuary sites [49]. The variability of integration sites, complexity of latency maintenance, and clonal expansion of long-lived reservoirs are all challenges for the HIV cure field.

HIV latency can be found in different cell types and tissue compartments, which presents additional barriers to curative strategies (Figure 1) [8]. Cellular reservoirs include a wide-range of cell types that are susceptible to HIV infections, such as memory CD4+ T lymphocytes and macrophages. These cells are found in the peripheral blood, but also in anatomical reservoirs that include lymph nodes (LNs), spleen, gut-associated lymphoid tissue (GALT) and brain or central nervous system (CNS).

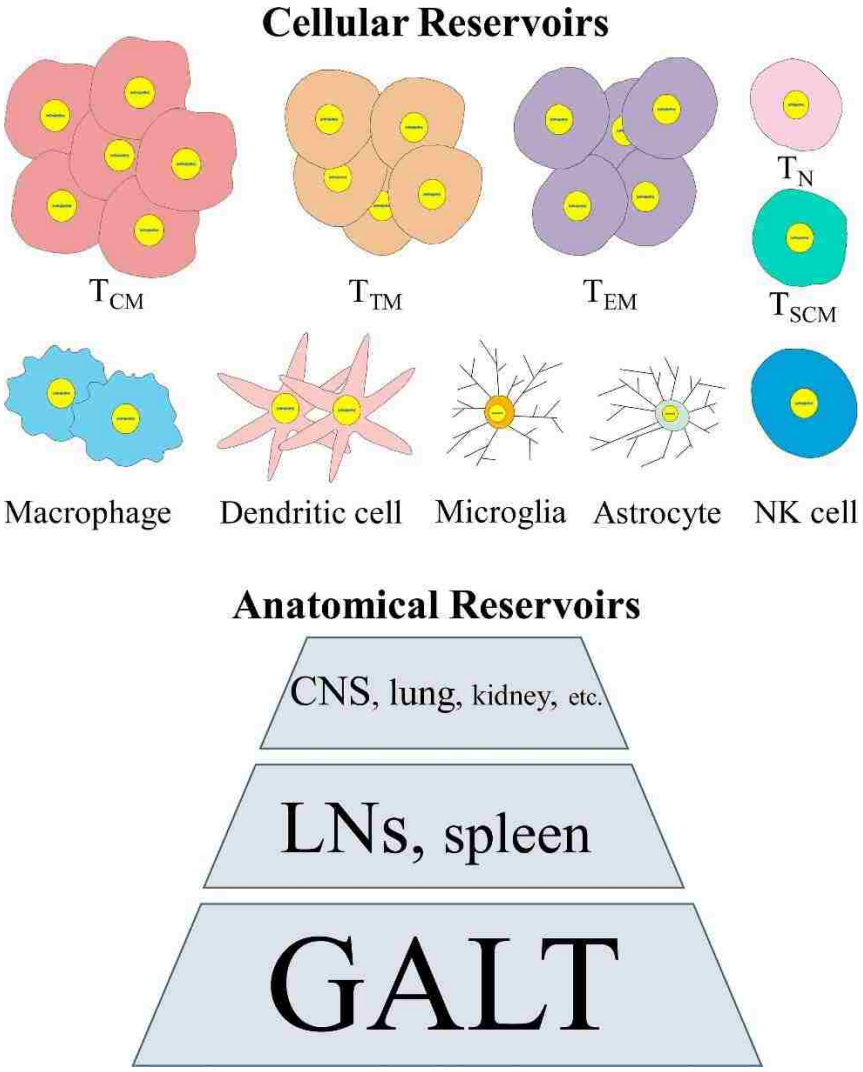

Figure 2.1. Schematic illustration on major HIV cellular and anatomical reservoirs. The relative size of the reservoir is represented by the size of the compartment as shown. TCM, central memory CD4+ T cells; TTM, transitional memory CD4+ T cells; TEM, effector memory CD4+ T cells; TN, naïve CD4+ T cells; TSCM, CD4+ T memory stem cells; NK cell, natural killer cell; CNS, central neural system; LNs, lymph nodes; GALT, gut-associated lymphoid tissue.

HIV proviral DNA is detected primarily in central memory (T_{CM}), transitional memory T cells (T_{TM}), and effector memory T cells (T_{EM}) which maintain latency and persistence through clonal expansion [49-51]. In particular, a subset of T_{CM} called peripheral T follicular helper cells (pTfh cells) are highly susceptible to HIV infection and contribute to HIV persistence [52]. CD4+ T memory stem cells (T_{SCM}) also significantly contribute to reservoir expansion and viral

persistence because these cells are long-lived and differentiate into mature memory T cells, although their proportion in circulating lymphocytes is only 2-4% [53-54]. Macrophages are also a chronic and latent HIV reservoir in infected patients that contributes to disease progression [55]. Macrophages are antigen presenting cells (APCs) that have been shown to spread virus particle to bystander CD4+ T cells [56], as well as recruit and activate latently-infected CD4+ T cells through chemokine and virus antigen production [57]. Macrophages are present in almost all organ systems, and can transmit virus to different anatomical sites including the brain (e.g., microglia as the resident macrophage in the brain and spinal cord) [58]. Infected macrophages have a much longer half-life (>30 days) and are less prone to cytopathic effects of the virus compared to CD4+ T cells [59-60]. In particular, HIV-infected microglia show a strong correlation with HIV-associated neurological symptoms due to neurotoxin secretion and attraction of adaptive immune responses to the brain that cause neural damage [58, 61]., Dendritic cells (DCs) are another type of APC that can be infected directly by HIV-1, although less efficiently than CD4+ T cells, but can transmit virus to T cells [62-63]. It has also been suggested that DC subtypes in the LNs, but not the peripheral blood, act as long-lived HIV reservoirs [64-65].

The major anatomical sites that harbor infected cells include lymphatic tissues (LNs, spleen, and GALT), CNS, and lung (Figure 1) [66]. HIV-1 or cells producing viral RNA (vRNA+ cells) can still be detected in many of these tissues of patients whose viral loads in the peripheral blood are undetectable [10]. Estes et al. have reported that in an NHP model, ~98.6% vRNA+ cells reside in lymphatic tissues (LNs, spleen, and GALT) [66]. Ineffective viral suppression in these tissues may be due to poor immune surveillance, less efficient drug penetration, high CD4+ T cell density that favors cell-to-cell HIV transmission, and interactions with autologous B cells or dendritic cells [67-69]. A clear majority of cells that contain HIV proviral DNA (vDNA+ cells) are found in

lymphoid tissues harboring significant numbers of memory T cells. A frequency on the order of ~10^5 vDNA+ cells/g was detected in both LN and GALT from patients under ART [66]. The GALT is one of the largest lymphoid organs infected by HIV-1 [70-71] estimated to contain ~62.3% of vRNA+ cells before ART and ~98.0% after the therapy in an NHP model [66]. Distinct from other lymphatic tissues, the frequency of vDNA+ cells in GALT does not decline after ART, leaving it as the largest sanctuary for HIV latency. The gut mucosal CD4+ lymphocytes are uniquely susceptible to HIV infections due to higher expression of chemokine receptor CCR5 and high levels of activation [72]. In addition, HIV-1 infected CD4+ T cells from other parts of the body regardless of the primary infection route can traffic to the GALT mediated by α4β7 and CCR9 [73-74]. It has also been reported that resting central memory α4β7+CD4+ cells are preferential targets of simian immunodeficiency virus (SIV) and contribute to reservoir establishment and expansion in mucosal sites [75]. Aside from these lymphatic tissues, the CNS is another key anatomical reservoir for HIV-1. The virus enters the brain at the early stage of infection and is difficult to eradicate, making the brain a lifelong virus pool [76]. Clinically, most ARVs have limited penetration into the CNS due to tight junctions of the blood-brain barrier (BBB) and transmembrane proteins that exist on the BBB to pump the drug out of the brain [77]. Other tissues such as lung and kidney have also been regarded as HIV reservoirs although they harbor much less proportions of latently infected cells [78-79].

2.4 Current strategies towards diminishing HIV reservoirs

With the recognition that viral reservoirs are major barriers to an HIV cure, several therapeutic strategies toward finding and diminishing latently infected cells have become the focus of recent research efforts. These cure strategies include early cART, reactivation of latently infected HIV reservoirs, gene therapy, and immunotherapy

2.4.1 *Minimizing the size of HIV reservoirs by early cART*

Many studies suggest that initiation of ART during the acute phase of infection could be an effective first step toward achieving sustained virologic remission. HIV latency is likely established early within days of acquiring infection although the specific timing in human is still uncertain [80-81]. Studies in non-human primates (NHPs) have observed high levels of integrated SIV DNA in resting CD4+ T cells within 10 days post-infection, but the seeding of the reservoir is thought to occur as early as 3 days. [82-84]. Patient initiated early ART has resulted in observed faster decay of HIV reservoirs and better preserved immunity against HIV compared to those who delayed ART [11, 46, 48, 85-87]. For example, the VISCONTI study investigating 14 patients who received ART during the acute-early phase of infection found that plasma viremia remained controlled for prolonged periods of time after cessation of therapy [12]. In a clinical case study known as the "Mississippi baby", an infant born to an HIV-positive mother had ART initiated at 30 hours from birth but discontinued therapy at 18 months of age and remained aviremic for more than 2 years [88]. Unfortunately, the child's plasma viremia ultimately rebounded and ART had to be reinitiated [89]. Aside from impeding the initial seeding and development of reservoirs, it has been suggested that early ART could also reverse chronic mucosal and systemic immune activation, which is the hallmark of HIV infection, contributes to reservoir size, and viral distribution through preservation of mucosal Th17 cells [90]. While multiple studies have shown that early ART can successfully suppress HIV in peripheral blood to undetectable levels, it has shown limited effect in inhibiting viral replication in lymphatic tissues such as intestinal tissues and lymph nodes which may contribute to viral rebound [91-92]. Collectively, the data suggests that early ART alone may not be sufficient to achieve virologic remission. The practicality of initiating ART at the population level during the early phase of HIV infection also remains a

challenge. As such, future direction may need to focus on combination therapy with other cure strategies, such as latency-reversing agents, therapeutic vaccines, or immune-modulating agents, as well as increase drug concentration in anatomical reservoir sites [81].

2.4.2 *Reactivating HIV reservoirs by LRAs*

Viral rebound normally occurs within 2-3 weeks after the interruption of ART, mainly due to viral reactivation in latently infected resting CD4+ T cells as well as other cellular reservoirs [93]. Several strategies for reducing the reservoir size have focused on targeting these cells. A widely investigated approach that has reached the clinic known as "shock and kill" reactivates HIV-1 proviruses while maintaining ART in order to prevent the spread of new infections and the establishment of new cellular reservoirs. These reactivated cells are then eliminated by viral cytopathic effects, the host immune response, or by a combination of therapies involving therapeutic vaccines, neutralizing antibodies or immune checkpoint blockade agents [94]. Several classes of LRAs have been identified and developed to overcome obstacles to transcription of the HIV-1 provirus that leads to maintenance of latency (Table 2.1). HDAC inhibitors (HDACi) unleashes the repression of viral LTR that is maintained by histone deacetylase to allow transcription of provirus [95]. While these drugs are effective and do not lead to global T cell activation, they may affect expression of a large numbers of genes [96]. HMT inhibitors (HMTi) similarly activate viral LTR through inhibition of histone H3 methylation [39]. HMTi can enhance the potency of HDACi but most agents are still under preliminary studies [97]. Protein kinase C (PKC) agonist activates NF-κB which binds to LTR to increase proviral transcription [98-99]. Many agents from this class are highly potent, but have major concerns such as nonspecific induction of many genes, toxicity, and tumor-promoting potential. P-TEFb activators, such as bromodomain extra-terminal (BET) inhibitor JQ1, enhance interaction of P-TEFb with LTR to

activate transcription [100]. JQ1 is also advantageous as it suppresses T cell proliferation and activation, which may be beneficial for cure therapy. DNA methyltransferase inhibitors function based on the role of DNA methylation on HIV latency [101]. This role is still controversial, and latency reversal from such inhibitors is relatively weak but could be strengthened when combined with other agents. Some agents may act based on multiple mechanisms. For instance, SAHA as an HDACi also activate latency through the activation of PI3K/Akt pathways [102]. Also, some short chain fatty acids induce latency by activating P-TEFb as well as inducing multiple histone modifications [103].

Table 2.1. Major latency reversing agent (LRA) categories and their representatives

Categories	Representative agents	Clinical trial number*	Reference
HDAC inhibitor	vorinostat (SAHA)	NCT01365065; NCT03198559; NCT02707900; NCT01319383; NCT03212989; NCT02475915; NCT02336074	102, 104-107
	panobinostat	NCT01680094; NCT02471430	108
	valproic acid (VPA)	NCT00312546; NCT00614458; NCT00000629; NCT00289952	109-110
	romidepsin	NCT02616874; NCT02092116; NCT01933594; NCT03041012; NCT02850016	111-113
	chidamide	NCT02513901; NCT02902185	114
	sodium butyrate	Not tested	115
HMT inhibitor	BIX01294	Not tested	116
	Chaetocin	Not tested	39
PKC agonist	prostratin	Not tested	117-118
	bryostatin-1	NCT02269605	119-120
	ingenol derivatives	Not tested	99, 121-122
P-TEFb activator	hexamethylene bisacetamide	Not tested	123
	JQ1	Not tested	100
DNA methyltransferase inhibitors	decitabine and its analog azacytidine	Not tested	124
unclassified	disulfiram	NCT00878306; NCT01944371; NCT03198559; NCT01286259; NCT00002065	125-127

*source: clinicaltrials.gov
HDAC, histone deacetylase; HMT, histone methyltransferase; PKC, protein kinase C; P-TEFb, positive transcription elongation factor b.

Several HDACi, (e.g., vorinostat [104-107], panobinostat [108], romidepsin [111], valproic acid [109] and chidamide [114]), disulfiram [126-127], and bryostatin-1 [119] have already been tested in clinical trials (Table 2.1), and other agents are under ongoing clinical trials (reviewed in [14, 128]). Many clinical studies of LRAs have shown an increase in cell-associated or plasma HIV RNA in CD4+ T cells. This is with the exception of bryostatin-1, where no effect on PKC activity or HIV latency

reversal was observed, which may due to low plasma concentrations after a single dose [119]. However, while all these LRAs have shown ability to reactivate HIV in patients, none have shown a reduction on the HIV reservoir size [14, 129]. This might be due to a lack of effective "kill" approaches used in these clinical trials, as only ART has been incorporated so far to suppress viral spreading. Only few "kill" strategies such as broadly neutralizing antibodies have been tested in combination with LRA in humanized mice [130]. It has been shown that some of these LRAs act synergistically to enhance potency when used in combination. The combination may also reduce the dose of single LRAs to minimize their toxicity. For example, HMTi can enhance proviral reactivation by HDAC inhibitors such as SAHA [97]. Recent studies from several groups have shown that protein kinase C activators such as prostratin, bryostatin 1, or ingenol-B synergistically and robustly induced HIV-1 transcription and virus production from *in vitro* or *ex vivo* models when combined with bromodomain inhibitor (also known as pTEFb-releasing agents as described above) or HDACi[121, 131-134].

"Shock and Kill" is still a controversial strategy especially based on recent safety issues and unenthusiastic outcomes from clinical studies. As such, whether or not a single LRAs is able to significantly reduce the size of HIV reservoirs is still questionable. A stronger focus is now on the use of LRAs combinations and combination with other therapeutics, as well as novel drug delivery systems to enhance therapeutic effects, avoid global immune cell activation, and reduce off-target side effects.

2.4.3 *Gene-editing approaches*

Gene-editing technologies are also being investigated for HIV cure strategies [15]. Gene-editing enzymes such as homing endonucleases, evolved recombinases, zinc finger nucleases (ZFNs),

transcription activator-like effector nucleases (TALENs), and CRISPR/Cas9 have been used to directly excise HIV provirus from the host genome and have proven effective in culture with cell lines and primary cells [135-138]. Recent studies in humanized mouse models have shown successful proviral excision in most major organs after single intravenous administration of *Staphylococcus aureus* Cas9 (saCas9) and multiplex single-guide RNAs (sgRNAs) using adeno-associated virus (AAV) [139-140]. However, due to various integration sites of latent virus and low percentage of latently infected cells, off-target effects and poor gene delivery efficiency remain big challenges towards clinical trials.

Gene-editing tools have also been used to knock out CCR5 in CD4+ T cells or hematopoietic stem/progenitor cells (HSPCs) in order to block virus entry [141], one of the mechanisms underlying the "Berlin Patient" case . ZFNs have been used to modify autologous CD4+ T cells and tested in HIV-infected patients [142]. However, patients that completed analytical treatment interruption (ATI) all had viral rebound after the therapy, even though the therapy resulted in a slower decay rate for the CCR5-modified CD4+ T cells compared to unmodified cells. A challenge for this approach is the low frequency of modified CD4+ T cells that are adoptively transferred, which likely limits its effect. CRISPP/Cas9 has been used successfully to disrupt CCR5 as well as CXCR4 on primary CD4+ T cells *in vitro* [143-145]. Gene-editing of primary CD4+ T cells *in vivo* is also likely to result in a low frequency of modified cells and would be associated with relatively high off-target effects. Disrupting CCR5 on HSPCs, which gives rise to all cell lineages that HIV-1 infects, has the advantages of producing longer-term effects than targeting CD4+ T cells. ZFNs or CRISPR/Cas9 have been used to modify HSPCs, showing successful CCR5 disruption and anti-HIV effect in reconstituted or transplanted mice [146-148]. Similarly, induced pluripotent stem cells (iPSCs) have been modified and can be differentiated

into HIV-resistant monocytes/macrophages *in vitro* [149-151]. Aside from generating HIV-resistant immune cells, human hematopoietic stem cells (HSCs) have also been induced to HIV-specific cytotoxic T lymphocytes to inhibit viral replication *in vivo* [152].

Permanently silencing the non-expressing provirus in latently infected cells has been investigated using different strategies. RNA interference (RNAi) with small interfering RNA (siRNA) silences the expression of viral RNA or cellular mRNAs that are necessary for viral production, and has been shown to control viral replication (reviewed in [19]). HIV-1 encoded genes such as *tat, rev, vif, gag, nef, pol, env, vpr* that are important for viral replication and are targets for siRNA silencing.

siRNAs have potential to overcome the high rate of HIV mutation through targeting highly conserved sequences [153]. These agents may offer an effective and safe approach towards an HIV cure, but still have challenges for reaching the clinic such as low delivery efficiency and instability. Challenges with gene editing strategies have included delivering genes or editing enzymes specifically to latently infected resting CD4+ T cells, off-target effects, and insufficient activity of enzymes that reach target cells *in vivo* [154]. These issues will collectively impact the efficacy and safety of gene editing therapies for HIV cure.

2.4.4 *Immunotherapy*

HIV therapeutic vaccines have focused on inducing HIV-1 specific CD8+ T cells responses to selectively kill virus-producing cells [155-156], and ultimately control the disease. Several therapeutic vaccines have been tested on HIV-1 infected individuals including vector-based vaccines that express HIV-1 antigens from harmless or attenuated viruses and plasmid DNA vaccines [157-160], but most have failed to show sufficient efficacy and some have raised safety

concerns. Nonetheless, several promising vaccines have been tested in preclinical studies and will go into clinical trials in the near future. For example, a vaccine based on cytomegalovirus (CMV) has been investigated and showed induction of broad cellular immune responses against novel epitopes resulting in efficient control of pathogenic SIV infection [161-162].

The use of broadly neutralizing antibodies (bnAbs) has also attracted attention as a therapeutic to prevent and treat HIV infection based on promising animal and human data. These bnAbs are also regarded as a potential cure strategy based on their antiviral activity as well as their ability to reduce reservoir size [163]. For the treatment of HIV, bnAbs have demonstrated remarkable efficacy in reducing viral load through clearance of free virus, elimination of infected T cells, as well as reduction of proviral DNA in the LN and GALT [16-18, 163-164]. bnAbs can also act as vaccines by enhancing autologous neutralizing antibody responses [165], or boosting and broadening humoral immunity [166]. Another strategy combines bnAbs and LRAs showed reduced viral rebound from the reservoir in established infections in humanized HIV- infected mice [130]. Currently, bnAbs still have challenges such as limited accessibility to certain anatomical reservoirs, as well as possible hurdles for clinical application related to their bioavailability, PK profile and high cost.

Many regulatory pathways designed to blunt cell activation are turned on during chronic infection, and one of the well-characterized immune regulators is the programmed cell death protein-1 (PD-1). For example, HIV-specific CD8 T cells that express high levels of PD-1 show functional exhaustion with low proliferation and cytotoxic effects [167]. The ligands for PD-1 (e.g., PD-L1 and PD-L2) are widely expressed in tissues, and inhibitors or blockades of the PD-1 pathway result in restoration of T cell function [168]. Thus, the blockades may enhance immune responses to clear chronic viral infections [169]. It has been demonstrated that the size of the

reservoirs is positively correlated with the frequency of PD-1 expressing cells [49, 170]. PD-1 inhibitors have been administered into SIV-infected macaques, and induce a significant viral load reduction and prolong survival [171]. It has been further shown that PD-1 blockade reduces hyperimmune activation in the blood and colorectal tissue and decreases microbial translocation [172].

Chimeric antigen receptor (CAR) T cell therapy has shown great promise in treating multiple cancers such as leukemia [173], and is also being investigated for HIV cure. The immunotherapy uses gene-editing tools to engineer T cells to express receptor on their surface in order to recognize and bind to specific target cells and then mediate cell lysis [174]. Previously, this technology has been applied to engineer CD8+ cytotoxic T cells to bind to and lyse HIV-infected CD4+ T cells [175], but has shown limited efficacy in clinical studies [176]. A recent study induced CAR onto HSPCs to consistently generate CAR T cells against SHIV infection in an NHP model of suppressive SHIV that are relevant to HIV cure research. They observed long-term (> 2 years) and stable production of CAR T cells in multiple lymphatic tissues, as well as a lower viral rebound after cessation of cART [177].

2.4.5 *Other strategies*

While early cART, reactivation of latently infected HIV reservoirs, gene therapy, and immunotherapy represent the most active areas of HIV cure research, several other approaches are also being actively pursued. One strategy known as “block and lock” is proposed to permanently inhibit transcription to prevent viral reactivation from latency, which may provide a functional cure for HIV infection. For example, ruxolitinib and tofacitinib are FDA-approved for myelofibrosis and rheumatoid arthritis (RA), respectively, and inhibit the JAK-STAT pathway

[178-179]. Another agent, didehydro-cortistatin A (dCA) binds to the HIV regulatory protein Tat and suppresses transcription [180-181]. While most of these agents are still under preclinical studies, the JAK inhibitor ruxolitinib (clinicaltrials.gov # NCT02475655) is currently being tested clinically in a phase 2 study. There is still concern about whether or not these agents alone are sufficient enough to permanently block viral reactivation, and they may need to be integrated with other strategies to realize an HIV cure in the future.

An innovative idea in cure research hypothesizes that reducing the proliferation of long-lived latently infected T cells could deplete the reservoir. Reeves et al. predicted that substantial reductions in the reservoir size may result from modest but continuous decreases in the proliferation rate of latently infected CD4 T cells with the use of mathematical modeling of the HIV reservoir under suppressive cART [20]. They identified that sustained anti-proliferation and ART treatment could potentially induce a functional cure within 2-10 years, which is much shorter than is predicted to occur with LRA and ART treatment. Mycophenolate mofetil (MMF) or its active metabolite, mycophenolic acid (MPA) have been tested in patients, and clinical trials for evaluating its effect on reducing reservoir size are currently enrolling patients [20] (clinicaltrials.gov # NCT03262441).

A recent study treated SIV+ macaques with a monoclonal antibody against the α4β7 integrin in combination with ART, and observed normal CD4+ T cell counts as well as undetectable viral loads in both plasma and GALT, even after cessation of ART [182-183]. α4β7 integrin is involved in trafficking of CD4+ T cells to GITs, where there are high levels of viral replication and viral reservoirs can be rapidly established [70]. CD4+ T cells that express high levels of α4β7 are also preferential targets of HIV during acute infection [74-75, 184]. While the mechanisms by which α4β7 mAb therapy promoted virologic control remains to be defined, it is hypothesized that the

antibody can block α4β7 binding to mucosal vascular addressin cell adhesion molecular 1 (MAdCAM-1) leading to interrupted cell migration to the GALT. It is noteworthy that α4β7 integrin is also a target for the HIV-1 envelop protein gp120, and binding leads to rapid activation of LFA that contributes to forming of virological synapses and facilitating cell-to-cell virus spreading [185]. More research efforts are needed to investigate this promising therapy for use in HIV treatment towards eradicating viral reservoirs.

2.5 Nanocarriers for eradicating HIV reservoirs

Many HIV cure strategies still face hurdles that limit their clinical translation. For example, clinical studies of LRAs have failed to meaningfully reduce reservoir size [42]. Sufficient reduction of the latent pool to curative levels may require mechanistically distinct LRAs used in combination. Many LRAs differ in solubility, bioavailability, and toxicity which make dosing and formulation challenging [131, 186]. Gene-based therapies must overcome challenges associated with off-target effects, low delivery efficiency, as well as safety issues especially when using viral-based vectors *in vivo* [187]. The complexity of HIV infection and latency may also require complimentary strategies for curing HIV, making it important but challenging to deliver physicochemically diverse cure agents simultaneously. HIV persistence in some anatomical sites has been attributed to lower concentrations of ARV drugs [10, 188], which could be addressed by novel drug delivery system to improve the bioavailability of cure therapeutics. New approaches are required to address these multiple complex molecular mechanisms associated with latent reservoir dynamics in cells and tissue compartments that present physiological barriers to therapeutic delivery *in vivo*. Nanotechnology has emerged as a promising approach for HIV cure due to several key attributes including ability to encapsulate diverse agents, increase circulation or tissue retention time, sustain drug release, enhance solubility and bioavailability, reduce

toxicity or side effects, and enhance drug potency [22, 189]. Some nanocarriers can also be modified to target specific cells or tissues, which have shown broad applications in cancer therapy [190]. Various types of nanocarriers including liposomes, polymeric nanoparticles, solid lipid nanoparticles, micelles, dendrimers, and inorganic nanoparticles have been reported for ARV drug delivery [191]. Some prodrugs or analogs of ARV drugs have also been developed and used to enhance drug loading or extend half-life when encapsulated in nanocarriers [192-193]. LRAs have been incorporated into nanocarriers for HIV cure applications and demonstrate CD4+ T cell specific reactivation both *in vitro* and *in vivo* [29, 194]. Here, we summarize current nanocarrier-based anti-HIV therapeutics and focus on strategies using drug combination or targeted nanocarriers to enhance drug potency and reduce toxicity. We also review nanocarrier-based gene delivery and immunotherapy approaches that have attracted more attention in cancer therapy and may have potential applications for curing HIV.

2.5.1 *Combination therapy using nanocarriers*

Based on multiple cellular mechanisms that suppress viral reactivation in latent cells and from results of preclinical studies, LRA combinations have been proposed to achieve a clinical cure by maximizing potency and minimizing toxicity [131]. However, there are several challenges that may limit such combinations using conventional drug formulations [195]. Co-dissolving of multiple hydrophobic drugs for injection may result in precipitation or aggregation, inaccuracy of dosing and risk of embolisms. Also, different drugs have their own bioavailability and PK profiles that make it more difficult to reach sufficient and safe concentrations in target tissues when delivered simultaneously.

Several nanotechnology-based systems have been developed to deliver incompatible drug combinations simultaneously, which is especially important and beneficial for both ARV and LRA therapies being considered for HIV cure. Table 2.2 summarizes recent studies that use nanocarriers to co-deliver multiple anti-HIV drugs to enhance their therapeutic effects. ARV drugs are physicochemically diverse and are used clinically in combination, but have been incorporated in nanocarriers for the dominant purpose of enhancing potency and prolonging drug residence time to reduce dosing frequency [24, 196-202]. For example, the Ho group has developed a long-acting triple-ARV drug combination using lipid nanoparticles that have shown enhanced drug exposure in primate blood and lymph nodes, as well as persistent drug levels in peripheral blood mononuclear cells (PBMCs) and lymph node mononuclear cells (LNMCs) [196-197, 203]. The synergistic enhancement of antiviral activity may be attributed to higher intracellular ARV drug concentrations, which has been observed by several studies (Table 2.2). Similar to ARV drugs, LRAs are mostly small molecule compounds and are physicochemically and mechanistically diverse. Several LRAs have been incorporated into nanocarriers individually. For example, Buehler et al. have reported a self-assembling vault nanoparticle incorporating a PKC agonist bryostatin-1. They demonstrated its ability to reactivate latent virus in a human cell line and induce CD69 expression in primary human PBMCs and mice after intravenous administration. However, whether or not the nanoparticle had any effect on the potency of free drug was not investigated. From studies investigating co-delivery of ARV drug combinations, nanocarriers also have the potential to deliver LRAs in combination. To date, single LRAs have been co-delivered with ARVs using nanocarriers [29-30, 204]. For example, Kovochich et al. loaded bryostatin-2 and a protease inhibitor nelfinavir into lipid nanoparticles. They observed that the nanoparticle formulation enhanced latency reactivation both in human T cell lines and PBMCs

from humanized mice with the ability to control viral spreading. In another study, Jayant et al. established ultrasmall magnetic nanoparticles (MNPs) used a layer-by-layer process to incorporate tenofovir (ARV) and vorinostat (LRA) for reactivating and suppressing HIV in a sustained manner for 5 days *in vitro* [30]. These promising preclinical studies will need to demonstrate PK, safety and efficacy *in vivo* before advancing into human clinical studies. Prioritizing drug combinations that are safe and effective for HIV cure is also challenging since there is a large pool of multiple combinations that are difficult to test in complex, expensive models such as patient blood or HIV- or SIV-infected animal models. These examples demonstrate that nanocarriers can overcome challenges with co-formulating physicochemically diverse drugs. Due to the higher potency of some combination drug therapies, dose-reduction could reduce toxicity that may be associated with single drugs. The toxicity associated with LRAs arises primarily from nonspecific induction and systemic release of cytokines [132]. Using biodegradable and non-toxic nanoparticles may further protect drug from degradation, increase circulation half-life and exhibit improved PK profiles, and lowering toxicity [22]. Thus, nanotechnology could provide alternative strategies to optimize latency reversal therapies. Future studies are being directed towards using a single nanocarrier to combine delivery of mechanistically distinct LRAs alone or co-formulated with other small molecule cure agents.

Table 2.2. Nanocarriers incorporating combinational therapeutics

Combination agents	Nanosystems	Test model	Observed effects	Ref.
ARVs (loponavir, ritonavir, and tenofovir)	Lipid nanoparticles	Nonhuman primates	Higher intracellular ARV concentrations in lymph nodes (50-fold higher than free drugs), long-acting plasma and lymphatic PK profiles	196-197, 203
ARVs (loponavir/ritonavir and efavirenz)	Biodegradable nanoparticles	*In vitro* cell lines	Higher intracellular ARV concentration	198
ARVs (binary or trinary combination of maraviroc, etravirine and raltegravir)	PLGA nanoparticles	*In vitro* cell lines, and *ex vivo* macaque cervicoviginal tissue	Higher intracellular ARV concentration, enhanced antiviral activities in relevant *in vitro* and *ex vivo* models	24
ARVs (tenofovir, alafenamide, and elvitegravir)	PLGA nanoparticles	Mice	Long residence time and exposure for both drugs	199
ARVs (atazanavir, ritonavir, and efavirenz)	NanoART	*In vitro* cell lines, *ex vivo* human primary cells, and *in vivo* in humanized mice	Attenuated viral replication and preserved CD4+ T cell numbers	200-201
ARVs (abacavir and lamivudine)	Glucose-coated gold nanoparticles	*In vitro* cell lines	Co-deliver and pH-mediated release of the drug and similar antiretroviral activity compared to free drug	202
ARVs (NNRTI: DAAN-14f, and HIV-1 fusion inhibitor: T1144)	PEG-PLA nanoparticles	*In vitro* cell lines and *in vivo* pharmacokinetic studies in rats	Enhanced *in vitro* antiviral activity against various HIV-1 strains and sustained controlled release both *in vitro* and *in vivo*	205
ARVs (zidovudine, efavirenz, and lamivudine)	Lactoferrin nanoparticles	*In vitro* cell lines and *in vivo* pharmacokinetic and safety studies in rats	Enhanced *in vitro* antiviral activity and improved pharmacokinetic and biodistribution profiles *in vivo*	206
LRA (bryostatin-2) + ARV (nelfinavir)	Lipid nanoparticles	*In vitro* cell lines, and *ex vivo* cells from an HIV-infected humanized mouse model	Reactivated latent virus and inhibited viral spreading simultaneously	29

LRA (vorinostat) + ARV (tenofovir)	Magnetic nanoparticles	*In vitro* HIV-infected human astrocytes	Reactivated latent virus and suppressed the viral replication	30
LRA (vorinostat) + ARV (nelfinavir)	PLGA-PEG nanoparticles	*In vitro* cell lines	Reactivated latent virus and suppressed the viral replication	204
ARV (nelfinavir) + sigma receptor antagonist (rimcazole)	Magnetic nanoparticles	*In vitro* cell lines	Mitigated co-effect of drug of abuse and inhibited HIV-1 infection	207
siRNAs (TNPO3, CD4, *tat,rev*)	PAMAM dendrimer	*In vitro* cell lines, *ex vivo* human primary cells, and *in vivo* in humanized mice	Suppressed HIV-1 infection and protected mice from CD4+ T cell loss	208
siRNAs (*p24*, *gag1*, *nef*)	Carbosilane dendrimers	*In vitro* cell lines, *ex vivo* human primary cells	Reduced HIV-1 replication	209
siRNAs (CCR5, *vif*, and *tat*)	Peptide carriers	*In vitro* cell lines and *in vivo* humanized mouse models	Suppressed HIV-1 replication and prevented mice from CD4+ T cell loss	153
siRNA (*tat/rev*) + RNA aptamer (gp120)	RNA nanoparticles	*In vitro* cell lines and *in vivo* humanized mouse models	Suppressed HIV-1 replication and prevented mice from CD4+ T cell loss	210-211
ARV, antiretroviral drugs; dsiRNA, dicer substrate small interfering RNA; NNRTI, Non-nucleoside reverse-transcriptase inhibitors; PAMAM, poly(amidoamine); PEG-PLA, polyethylene glycol–polylactic acid; PLGA, poly(lactic-co-glycolic acid).				

Many other HIV cure agents such as antiproliferative agents, bnAbs, and oligonucleotides drugs may also need combinations for achieving improved efficacy in eradicating HIV reservoirs. For example, antiproliferative agents are required to be dosed with ARVs in order to suppress both viral replication and reservoir proliferation, and show potential benefits when combined with LRAs [20]. Preclinical studies in humanized mice have demonstrated improved anti-HIV effects from treatment with a combination of multiple bnAbs [212-213] as well as single bnAbs combined with ARV drugs [214]. Combination gene therapies that target multiple HIV transcriptional genes as well as expression of CCR5 are being investigated to address rapid viral mutations and the complexity of HIV infection and latency maintenance [215].

Such combinations of antibodies, or nucleic acids with small molecules can be even more challenging due to their incompatibility, requirement of different vectors and administration routes, various PK or pharmacodynamic (PD) properties, and site of action. Nanocarriers have demonstrated their utility for co-delivering combinations of antibodies with chemotherapeutics [216], different RNAi targets [217], or siRNA with miRNA [218]. Due to the complexity of HIV integration sites and rapid mutation, combination might also bolster efficacy even for single gene therapies such as delivery of multiple siRNA. For example, Zhou et al. demonstrated the ability of poly(amidoamine) (PAMAM) dendrimer to deliver a combination of siRNAs to suppress HIV infection [208]. These siRNAs target viral as well as cellular transcripts for minimizing viral escape mutants and resulted in prolonged HIV suppression in humanized mice. However, dendrimer-siRNA nanoparticles primarily accumulated in PBMCs and liver, and biodistribution data was not provided for other major lymphatic tissues such as lymph nodes and GALT. Further investigation on biodistribution and PK profiles of these nanoparticles are needed to develop

nanocarriers that can deliver multiple agent more efficiently to different target sites relevant for HIV cure.

2.5.2 *Targeting tissue and cellular HIV sanctuaries by nanocarriers*

The compartments that harbor HIV are primarily the blood, lymphatic systems (e.g. lymph nodes, GALT, spleen, etc.), and CNS. Inconsistent ARV drug penetration and accumulation in some of these sites is a challenge for effective HIV treatment and can lead to HIV persistence [10]. Targeted nanocarriers have been investigated for delivering ARV drugs or HIV cure agents to specific cells or tissues that harbor latent virus (Table 2.3).

Table 2.3. Nanocarriers targeting HIV sanctuaries

	Target	Targeting ligands	Therapeutics	Nanosystems	Test model	Reference
Cellular Reservoirs	Leukocytes	LFA-1	anti-CCR5 siRNA	Liposome	*Ex vivo* human lymphocytes and *in vivo* humanized mouse model	219
	CD7-expressing T cells	Anti-CD7 single-chain antibody	siRNAs (CCR5, *vif* and *tat*)	Peptide carrier	*In vitro* cell lines and *in vivo* humanized mouse model	153
	CD4+ T cells	CD4-binding peptides	ARV (indinavir)	Lipid nanoparticles	*In vitro* cell lines	220-221
		anti-CD4 antibody	LRA (bryostatin-2) + ARV (nelfinavir)	Lipid nanoparticles	*In vitro* cell lines and *ex vivo* latently infected cells from humanized mouse model	29
	Resting memory T cells	CD45RO	LRA (vorinostat) + ARV (nelfinavir)	PEG-PLGA nanoparticles	*In vitro* cell lines	204
	Macrophage	Folate	ARV (atazanavir)	Polymer coated ARV nanoformulations (NanoART)	*In vitro* cell lines, *ex vivo* human primary cells, and *in vivo* mice	222-223
	Astrocytes	bradykinin B2 antibody	siRNA	Chitosan nanoparticles	*In vitro* cell lines	224
Anatomical Reservoirs	**Target**	**Administration route**	**Therapeutics**	**Nanosystems**	**Test model**	**Reference**
	Lymph nodes	SC	ARV (Indinavir)	Lipid-drug complexes	HIV-2287-infected macaques	225
		SC	ARV (lopinavir, ritonavir, and tenofovir)	Lipid nanoparticles	Pig-tailed macaques	196-197
	CNS	N/A	ARV (azidothymidine 5'-triphosphate, AZTTP)	Magnetic liposomal nanoformulation	*In vitro* BBB model	226

		IN	ARV (efavirenz)	PEO-PPO micelles	Rats	[227]
		IV	ARV (indinavir)	Transferrin coupled submicron lipid emulsions	Mice	[228]
		Oral or IV	ARV (saquinavir)	Nanoemulsion	Mice	[229]
		IP	ARV (azidothymidine)	Nanogel decorated with the peptide binding brain-specific apolipoprotein E receptor	Mice	[230]
		IV	ARV (nevirapine)	Surface modified nanosuspensions	Rats	[231]
		N/A	ARV (stavudine, delavirdine, or saquinavir)	PBCA, MMA-SPM, and SLN	*In vitro* BBB model, human brain-microvascular endothelial cells (HBMEC)	[232-233]
		IV	ARV (ritonavir)	TAT peptide conjugated PLA nanoparticles	Mice	[234]
		SC	ARV (atazanavir and ritonavir)	Macrophage-carriage system for nanoformulated crystalline ART (nanoART)	*In vitro* cell lines, *ex vivo* human primary cells, and *in vivo* mice	[235]
		Retro-orbital injection	siRNA (*nef*)	Carbosilane dendrimer	*In vitro* BBB model, human brain-microvascular endothelial cells (HBMEC), and *in vivo* mice	[236-237]

GALT: gut-associated lymphoid tissue; CNS: central neural system; SC: subcutaneous; IV: intravenous; IN: intranasal; IP: intraperitoneal; ARV: antiretroviral drugs; LRA: latency-reversing agents; PEG-PLGA: Poly(ethylene glycol) methyl ether-block-poly(lactide-co-glycolide); PEO-PPO: poly(ethylene oxide)-poly(propylene oxide); PBCA: Polybutylcyanoacrylate; MMA-SPM: methylmethacrylate-sulfopropylmethacrylate; SLN: solid lipid nanoparticle; TAT: trans-activating transcriptor; PLA: Poly(lactic acid); BBB: blood brain barrier.

Cell-specific accumulation of nanocarriers is achieved by the use of targeting moieties. Due to their high specificity, antibodies have also been widely used for targeting nanocarriers to T cells in various applications [26-28, 219, 238]. It has been suggested that anti-CD4 monoclonal antibodies, or its fragments, are good candidates to direct negatively-charged nanoparticles to CD4+ T cells [239]. Kovochich et al. reported lipid nanoparticles decorated with an anti-CD4 antibody for targeting both LRAs and ARVs to primary human CD4+ T cells in order to activate latent virus and inhibit viral spread [29]. The CD4 antibody led to specific targeting of nanoparticles to CD4+ T cells in PBMC culture, as well as preferential activation on CD4+ T cells over CD8+ T cells. This system shows great potential in systemic T cell targeting, however, PK profiles and biodistributions in some key HIV anatomical reservoirs were not investigated but would be important for future applications. Among CD4+ T cells, latent HIV viruses typically reside in resting memory (CD45RO+) T cells. Tang et al. conjugated anti-CD45RO antibody to PLGA-PEG nanoparticles that were loaded with a HDACi and protease inhibitors for targeting and eliminating latent HIV reservoirs *in vitro* [204]. They demonstrated that CD45RO antibody enhanced nanoparticle binding to human memory T cells, but the binding specificity was not measured and it is unclear how targeting improved drug potency. Aside from CD4+ T cells, macrophages are another target for ARV drug delivery and have been found to store and transport ARV drugs to lymph nodes and the CNS. Puligujja et al. developed folic acid (FA)-linked polymer-coated nanoformulated antiretroviral therapy (FA-nanoART), that induced five-fold enhanced plasma and tissue drug levels in mice and enabled 2.5-fold improvement in treating compared to untargeted nanoART [222-223]. These targeted nanocarriers demonstrate the potential for applications in HIV cure research, but most are still in early stages of development and need to be tested in relevant animal models. Also, there is a need of more options to select

binding ligands aside from whole antibodies to overcome high costs, nonspecific conjugation to nanocarriers, and effect on reducing nanocarrier circulation half-life for *in vivo* cellular targeting applications [240].

Several studies have focused on developing nanocarriers that preferentially distribute to lymph nodes after subcutaneous administration to address insufficient drug concentrations in these tissue [241-242]. Therapeutics administered subcutaneously are preferentially taken up by blood capillaries or lymphatic vessels depending on their physicochemical properties. Small molecular drugs, peptides, and proteins (<16 kDa) have been shown to be absorbed by blood capillaries while particulates between 10-100 nm diameter are transported through the interstitium and preferentially into the lymphatic system [243]. It has been reported that a lipid-drug or lipid nanoparticles (50-80 in diameter) enhanced delivery of ARV drugs to lymph nodes, increased intracellular drug concentration, acted as a long-acting dosage form, and led to significant virus load reduction after subcutaneous administration to NHP models [196-197, 225]. Such nanoparticle systems can be potentially used to enhance accumulation of other HIV cure agents in the lymph nodes, or direct multiple drugs with different PK profiles to lymph nodes for eradicating latent virus.

The GALT is an important site for early HIV replication and reservoir establishment, and has also shown significantly lower ARV concentrations compared with peripheral blood in patients under ART that are considered fully suppressive [10]. Nanoparticles have been used to target the GALT for various applications. For example, a variety of biodegradable antigen delivery systems have been developed for oral vaccines. Some of these were decorated with microfold cells (or M cells)-specific ligands to actively target delivery of nanoparticles to these cells in the GALT that transport nanoparticles across the intestinal epithelium [244]. Some limitations for this M cell

targeting strategy may be the low efficiencies for GALT delivery due to a small percentage of M cells in the follicle-associated epithelium [245]. Peers et al. used antibodies against the β7 integrin to target mutilamellar vesicles to specific leukocytes subsets involved in gut inflammation, showing more than 10-fold higher accumulation in the gut compared to an isotype antibody control group administered intravenously in mice [26]. These nanocarriers have been barely studied in the HIV field, but have potential to deliver HIV cure agents to the GALT.

Nanotechnology-based methods are also being developed to deliver ARVs into the brain, which shows limited accessibility of many drugs and is another key anatomical reservoir harboring the virus [76-77, 246]. Most investigations focus on crossing the BBB by developing nanocarriers with increased permeability, uptake, or transcytosis by brain microvascular endothelial cells (BMVECs) [247]. Many types of nanocarriers have been applied for the management of HIV infection in the CNS such as liposomes [226], micelles [227], nanoemulsions [228-229], nanogel [230], nanosuspensions [231], and polymeric nanoparticles [232-234]. Ligands such as transferrin and trans-acting transcriptional activator (TAT) peptide are widely used for targeting nanocarriers to the brain. For example, transferrin has been linked to indinavir lipid nanoemulsions and resulted in up to 5 times higher bioavailability in brain compared to free drug [228]. This has been attributed to the overexpression of transferrin receptors on brain cells that can mediate endocytosis and transcytosis of transferrin-coupled substances. The TAT-peptide has been shown to penetrate through cell membranes and enhance transport of nanocarriers across the BBB. Rao et al. demonstrated that TAT-conjugated poly (L-lactide) (PLA) nanoparticles efficiently enhance CNS bioavailability and maintain drug level of encapsulated ritonavir in the brain [234]. A peptide that binds to brain-specific apolipoprotein E receptor has also been decorated to cationic nanogels for delivering nucleoside reverse transcriptase inhibitors (NRTIs) against HIV infection

in the brain [230]. The macrophage-targeting nanoART described above showed the ability to be transferred from macrophages to human brain microvascular endothelial cells (HBMECs), and led to four-fold higher ARV levels in the mice brain compared to untargeted nanoART [235]. Alternative delivery routes such as intranasal delivery also offer a non-invasive way to transport drugs through olfactory neurons to the brain [227]. These solutions have demonstrated significant increases of ARV drug concentrations in the brain compared to free drug administration, therefore showing unique promise as efficient tools to deliver HIV cure agents into the brain.

2.5.3 *Future directions: nanocarrier-based gene- or immunotherapy*

Gene therapy offers promising solutions in treating multiple diseases including HIV, and has greatly advanced since the discovery of CRISPR as an easy and robust gene-editing tool. While current gene therapy for HIV cure has mostly relied on viral vectors, the advances in nanocarrier-based gene delivery technology may enhance its impact on the HIV cure field due to its lower risk, potential targeting abilities, and lower off-target effects. Some big hurdles for applying gene therapy to HIV cure research, particularly for strategies proposing to knock-out HIV provirus in the host genome, are low efficiency and targeting specificity *in vivo*. Currently, viral vectors such as adenoviruses and AAVs are still the most widely used for *in vivo* gene delivery due to their relatively high transfection efficiency but have associated concerns with off-target effects, immunogenicity, and toxicity. Non-viral vectors such as nanocarriers have been investigated as an alternative and safe way to deliver genes (reviewed in [248-250]). Studies have used lipid-based or polymer-based nanocarriers, or dendrimers as non-viral vectors to deliver exogeneous nucleic acids such as DNA, mRNA, siRNA and miRNA [249]. Many reports use nanoparticles for anti-HIV siRNA delivery [153, 208-211, 219, 236-237, 251-255]. For example, Weber et al. have used carbosilane dendrimers to deliver siRNAs targeting HIV *p24*, *gag1*, or *nef* genes [209]. The dendrimer-siRNA

complex showed highest transfection efficiency in both cell line and HIV-infected PBMCs without causing cytotoxicity, and protected siRNA from rapid degradation in the presence of RNase. A similar dendrimer system was also tested in mice and efficient siRNA transport across BBB was observed [237]. More investigations on siRNA transfection *in vivo*, particularly anti-HIV effects in relevant animal models are needed for future clinical applications. There are relatively few examples of using non-viral vectors to deliver whole genome editing systems such as ZFNs and CRISPR-Cas9 systems because they are large and complex [250]. Recently, Lee at al. developed a polymer-coated gold nanoparticle that can co-deliver CRISPR components, including the Cas9 and gRNA ribonucleoprotein (RNP) complex and donor DNA, resulting in efficient correction on the mutated dystrophin gene with low off-target effects [256].

HIV therapeutic vaccines, bnAbs, PD-1 blockades, and CAR T cell therapy have all shown promise in HIV cure but also have limitations such as low delivery efficiency to specific tissues or cells. Over the past decades, nanocarrier-based delivery platforms such as liposomes, polymeric nanoparticles, lipid-polymer hybrid nanoparticles, and virus-like nanoparticles have been used as carriers for vaccine delivery in the field of cancer immunotherapy (reviewed in [257]). The advantages of nanocarriers for delivering vaccines include simultaneous delivery of multiple antigens and adjuvants, rapid endocytosis by immune cells (especially DCs and macrophages), and accumulation to lymphatic tissues based on their size [257]. These attributes could be employed for nanocarriers to deliver HIV immunotherapeutics to specific cells or tissues that are inaccessible with current dosage forms.

PD-1 blockades, when delivered systematically, have concerns with systemic immune stimulation that is associated with some immune-related adverse effects [258]. The use of a drug delivery system to enhance accumulation of these blockades to specific cells or tissues may

reduce these side effects. For example, Kosmides et al. developed nanoparticles decorated with both anti-PD-L1 antibody and anti-4-1BB antibody (a costimulatory molecule), and observed increased targeting of CD8+ T cells, enhanced anti-tumor activities and low off-target toxicity *in vivo* [259]. Alternatively, Schmid et al. have used CD8 and PD-1 dual-targeting nanoparticles to deliver a TGFβR1 inhibitor, another immunostimulatory drug, to restore CD8+PD-1+ T cell functions for killing cancer cells [260]. These delivery systems may also be applied in delivering PD-1 blockade with other stimulators for targeting and activating HIV-specific CD8+ T cells that highly express PD-1. This targeted delivery system could achieve specific restoration of T cell function towards eradication of HIV infection.

Current CAR T cell-based immunotherapy that engineers T cells *ex vivo* may be too elaborate for widespread implementation for HIV and cancer treatment. This therapy involves complex procedures that requires expensive equipment and technical expertise for T cell isolation, modification, and expansion followed by infusion back into patients. Nanocarriers could offer an alternative and inexpensive solution by delivering modifying genes to program host T cells *in vivo*. Recently, Smith et al. have developed nanoparticles decorated with anti-CD3 antibody and loaded with leukemia-targeting CAR genes to target and engineer tumor-specific T cells directly *in situ* [261]. Such technology has potential to be applied to CAR T cell strategy to engineer CD8+ cytotoxic T cells *in vivo* to kill HIV-infected CD4+ T cells.

2.6 Conclusion

A variety of strategies have been developed to minimize HIV reservoirs, but several obstacles remain, such as insufficient potency and off-target effects in normal cells that may also result in dose-limiting toxicities [14]. Nanocarriers offer a promising treatment for HIV infection by

enhancing drug potency using synergistic combinations, or targeting specific and hard-to-reach sites that harbor virus. Nanocarriers also offer advantages compared to traditional delivery systems that include encapsulation of physicochemically diverse agents, sustained drug release, lower drug dosing, better bioavailability, and fewer or less severe side effects. These promising properties of nanocarriers help address problems in current novel strategies toward an HIV cure.

2.7 Acknowledgements

This work was supported in part by an NIH/NIAID grant (AI 094412) to KAW, and amfAR grant for Bringing Bioengineers to Cure HIV (109541-61-RGRL). The authors thank Jamie Hernandez for her critical reading and editing of the manuscript.

2.8 References

1. UNAIDS, Fact sheet - Latest global and regional statistics on the status of the AIDS epidemic. **2017**.
2. Group, T. D. C. o. A. E. o. A.-H. D. S., Combination Antiretroviral Therapy and the Risk of Myocardial Infarction. *New England Journal of Medicine* **2003,** *349* (21), 1993-2003.
3. Lai, S.; Bartlett, J.; Lai, H.; Moore, R.; Cofrancesco, J.; Pannu, H.; Tong, W.; Meng, W.; Sun, H.; Fishman, E. K., Long-Term Combination Antiretroviral Therapy Is Associated with the Risk of Coronary Plaques in African Americans with HIV Infection. *AIDS Patient Care and STDs* **2009,** *23* (10), 815-824.
4. Treisman, G. J.; Kaplin, A. I., Neurologic and psychiatric complications of antiretroviral agents. *AIDS* **2002,** *16* (9), 1201-1215.
5. Kovari, H.; Weber, R., Influence of antiretroviral therapy on liver disease. *Current Opinion in HIV and AIDS* **2011,** *6* (4), 272-277.
6. Hütter , G.; Nowak , D.; Mossner , M.; Ganepola , S.; Müßig , A.; Allers , K.; Schneider , T.; Hofmann , J.; Kücherer , C.; Blau , O.; Blau , I. W.; Hofmann , W. K.; Thiel , E., Long-Term Control of HIV by CCR5 Delta32/Delta32 Stem-Cell Transplantation. *New England Journal of Medicine* **2009,** *360* (7), 692-698.
7. Allers, K.; Hütter, G.; Hofmann, J.; Loddenkemper, C.; Rieger, K.; Thiel, E.; Schneider, T., Evidence for the cure of HIV infection by CCR5Δ32/Δ32 stem cell transplantation. *Blood* **2011,** *117* (10), 2791-2799.
8. Saksena, N. K.; Wang, B.; Zhou, L.; Soedjono, M.; Ho, Y. S.; Conceicao, V., HIV reservoirs in vivo and new strategies for possible eradication of HIV from the reservoir sites. *HIV AIDS (Auckl)* **2010,** *2*, 103-122.

9. Ostrowski, M.; Benko, E.; Yue, F. Y.; Kim, C. J.; Huibner, S.; Lee, T.; Singer, J.; Pankovich, J.; Laeyendecker, O.; Kaul, R.; Kandel, G.; Kovacs, C., Intensifying Antiretroviral Therapy With Raltegravir and Maraviroc During Early Human Immunodeficiency Virus (HIV) Infection Does Not Accelerate HIV Reservoir Reduction. *Open Forum Infectious Diseases* **2015,** *2* (4), ofv138.
10. Fletcher, C. V.; Staskus, K.; Wietgrefe, S. W.; Rothenberger, M.; Reilly, C.; Chipman, J. G.; Beilman, G. J.; Khoruts, A.; Thorkelson, A.; Schmidt, T. E.; Anderson, J.; Perkey, K.; Stevenson, M.; Perelson, A. S.; Douek, D. C.; Haase, A. T.; Schacker, T. W., Persistent HIV-1 replication is associated with lower antiretroviral drug concentrations in lymphatic tissues. *Proceedings of the National Academy of Sciences* **2014,** *111* (6), 2307-2312.
11. Hecht, F. M.; Wang, L.; Collier, A.; Little, S.; Markowitz, M.; Margolick, J.; Kilby, J. M.; Daar, E.; Conway, B.; Network, A., A multicenter observational study of the potential benefits of initiating combination antiretroviral therapy during acute HIV infection. *Journal of Infectious Diseases* **2006,** *194* (6), 725-733.
12. Sáez-Cirión, A.; Bacchus, C.; Hocqueloux, L.; Avettand-Fenoel, V.; Girault, I.; Lecuroux, C.; Potard, V.; Versmisse, P.; Melard, A.; Prazuck, T., Post-treatment HIV-1 controllers with a long-term virological remission after the interruption of early initiated antiretroviral therapy ANRS VISCONTI Study. *PLoS Pathog* **2013,** *9* (3), e1003211.
13. Margolis, D. M.; Garcia, J. V.; Hazuda, D. J.; Haynes, B. F., Latency reversal and viral clearance to cure HIV-1. *Science* **2016,** *353* (6297).
14. Rasmussen, T. A.; Lewin, S. R., Shocking HIV out of hiding: where are we with clinical trials of latency reversing agents? *Current Opinion in HIV and AIDS* **2016,** *11* (4), 394-401.
15. Wang, C. X.; Cannon, P. M., The clinical applications of genome editing in HIV. *Blood* **2016,** *127* (21), 2546-2552.
16. Caskey, M.; Klein, F.; Lorenzi, J. C. C.; Seaman, M. S.; West Jr, A. P.; Buckley, N.; Kremer, G.; Nogueira, L.; Braunschweig, M.; Scheid, J. F.; Horwitz, J. A.; Shimeliovich, I.; Ben-Avraham, S.; Witmer-Pack, M.; Platten, M.; Lehmann, C.; Burke, L. A.; Hawthorne, T.; Gorelick, R. J.; Walker, B. D.; Keler, T.; Gulick, R. M.; Fatkenheuer, G.; Schlesinger, S. J.; Nussenzweig, M. C., Viraemia suppressed in HIV-1-infected humans by broadly neutralizing antibody 3BNC117. *Nature* **2015,** *522* (7557), 487-491.
17. Lynch, R. M.; Boritz, E.; Coates, E. E.; DeZure, A.; Madden, P.; Costner, P.; Enama, M. E.; Plummer, S.; Holman, L.; Hendel, C. S.; Gordon, I.; Casazza, J.; Conan-Cibotti, M.; Migueles, S. A.; Tressler, R.; Bailer, R. T.; McDermott, A.; Narpala, S.; O'Dell, S.; Wolf, G.; Lifson, J. D.; Freemire, B. A.; Gorelick, R. J.; Pandey, J. P.; Mohan, S.; Chomont, N.; Fromentin, R.; Chun, T.-W.; Fauci, A. S.; Schwartz, R. M.; Koup, R. A.; Douek, D. C.; Hu, Z.; Capparelli, E.; Graham, B. S.; Mascola, J. R.; Ledgerwood, J. E., Virologic effects of broadly neutralizing antibody VRC01 administration during chronic HIV-1 infection. *Science Translational Medicine* **2015,** *7* (319), 319ra206.
18. Lu, C.-L.; Murakowski, D. K.; Bournazos, S.; Schoofs, T.; Sarkar, D.; Halper-Stromberg, A.; Horwitz, J. A.; Nogueira, L.; Golijanin, J.; Gazumyan, A.; Ravetch, J. V.; Caskey, M.; Chakraborty, A. K.; Nussenzweig, M. C., Enhanced clearance of HIV-1–infected cells by broadly neutralizing antibodies against HIV-1 in vivo. *Science* **2016,** *352* (6288), 1001-1004.
19. Bobbin, M. L.; Burnett, J. C.; Rossi, J. J., RNA interference approaches for treatment of HIV-1 infection. *Genome Medicine* **2015,** *7* (1), 50.
20. Reeves, D. B.; Duke, E. R.; Hughes, S. M.; Prlic, M.; Hladik, F.; Schiffer, J. T., Anti-proliferative therapy for HIV cure: a compound interest approach. *Scientific Reports* **2017,** *7* (1), 4011.

21. Sharma, P.; Garg, S., Pure drug and polymer based nanotechnologies for the improved solubility, stability, bioavailability and targeting of anti-HIV drugs. *Advanced Drug Delivery Reviews* **2010,** *62* (4), 491-502.
22. Yildirimer, L.; Thanh, N. T.; Loizidou, M.; Seifalian, A. M., Toxicology and clinical potential of nanoparticles. *Nano today* **2011,** *6* (6), 585-607.
23. Davis, M. E.; Chen, Z.; Shin, D. M., Nanoparticle therapeutics: an emerging treatment modality for cancer. *Nat Rev Drug Discov* **2008,** *7* (9), 771-782.
24. Jiang, Y.; Cao, S.; Bright, D. K.; Bever, A. M.; Blakney, A. K.; Suydam, I. T.; Woodrow, K. A., Nanoparticle-Based ARV Drug Combinations for Synergistic Inhibition of Cell-Free and Cell–Cell HIV Transmission. *Molecular pharmaceutics* **2015,** *12* (12), 4363-4374.
25. Freeling, J. P.; Ho, R. J. Y., Anti-HIV drug particles may overcome lymphatic drug insufficiency and associated HIV persistence. *Proceedings of the National Academy of Sciences of the United States of America* **2014,** *111* (25), E2512-E2513.
26. Peer, D.; Park, E. J.; Morishita, Y.; Carman, C. V.; Shimaoka, M., Systemic Leukocyte-Directed siRNA Delivery Revealing Cyclin D1 as an Anti-Inflammatory Target. *Science* **2008,** *319* (5863), 627-630.
27. Lee, J.; Yun, K.-S.; Choi, C. S.; Shin, S.-H.; Ban, H.-S.; Rhim, T.; Lee, S. K.; Lee, K. Y., T Cell-Specific siRNA Delivery Using Antibody-Conjugated Chitosan Nanoparticles. *Bioconjugate Chemistry* **2012,** *23* (6), 1174-1180.
28. Dinauer, N.; Balthasar, S.; Weber, C.; Kreuter, J.; Langer, K.; von Briesen, H., Selective targeting of antibody-conjugated nanoparticles to leukemic cells and primary T-lymphocytes. *Biomaterials* **2005,** *26* (29), 5898-5906.
29. Kovochich, M.; Marsden, M. D.; Zack, J. A., Activation of Latent HIV Using Drug-Loaded Nanoparticles. *PLoS ONE* **2011,** *6* (4), e18270.
30. Jayant, R. D.; Atluri, V. S. R.; Agudelo, M.; Sagar, V.; Kaushik, A.; Nair, M., Sustained-release nanoART formulation for the treatment of neuroAIDS. *International Journal of Nanomedicine* **2015,** *10*, 1077-1093.
31. Kamaly, N.; Yameen, B.; Wu, J.; Farokhzad, O. C., Degradable Controlled-Release Polymers and Polymeric Nanoparticles: Mechanisms of Controlling Drug Release. *Chemical Reviews* **2016,** *116* (4), 2602-2663.
32. Swiggard, W. J.; Baytop, C.; Yu, J. J.; Dai, J.; Li, C.; Schretzenmair, R.; Theodosopoulos, T.; O'Doherty, U., Human Immunodeficiency Virus Type 1 Can Establish Latent Infection in Resting CD4+ T Cells in the Absence of Activating Stimuli. *Journal of Virology* **2005,** *79* (22), 14179-14188.
33. Cameron, P. U.; Saleh, S.; Sallmann, G.; Solomon, A.; Wightman, F.; Evans, V. A.; Boucher, G.; Haddad, E. K.; Sekaly, R.-P.; Harman, A. N.; Anderson, J. L.; Jones, K. L.; Mak, J.; Cunningham, A. L.; Jaworowski, A.; Lewin, S. R., Establishment of HIV-1 latency in resting CD4+ T cells depends on chemokine-induced changes in the actin cytoskeleton. *Proceedings of the National Academy of Sciences* **2010,** *107* (39), 16934-16939.
34. Bosque, A.; Planelles, V., Induction of HIV-1 latency and reactivation in primary memory CD4+ T cells. *Blood* **2009,** *113* (1), 58-65.
35. Craigie, R.; Bushman, F. D., HIV DNA Integration. *Cold Spring Harbor Perspectives in Medicine* **2012,** *2* (7), a006890.
36. Wagner, T. A.; McLaughlin, S.; Garg, K.; Cheung, C. Y. K.; Larsen, B. B.; Styrchak, S.; Huang, H. C.; Edlefsen, P. T.; Mullins, J. I.; Frenkel, L. M., Proliferation of cells with HIV

integrated into cancer genes contributes to persistent infection. *Science (New York, N.Y.)* **2014,** *345* (6196), 570-573.
37. Maldarelli, F.; Wu, X.; Su, L.; Simonetti, F. R.; Shao, W.; Hill, S.; Spindler, J.; Ferris, A. L.; Mellors, J. W.; Kearney, M. F.; Coffin, J. M.; Hughes, S. H., Specific HIV integration sites are linked to clonal expansion and persistence of infected cells. *Science (New York, N.Y.)* **2014,** *345* (6193), 179-183.
38. Ylisastigui, L.; Coull, J. J.; Rucker, V. C.; Melander, C.; Bosch, R. J.; Brodie, S. J.; Corey, L.; Sodora, D. L.; Dervan, P. B.; Margolis, D. M., Polyamides Reveal a Role for Repression in Latency within Resting T Cells of HIV-Infected Donors. *Journal of Infectious Diseases* **2004,** *190* (8), 1429-1437.
39. Chéné, I. d.; Basyuk, E.; Lin, Y.-L.; Triboulet, R.; Knezevich, A.; Chable-Bessia, C.; Mettling, C.; Baillat, V.; Reynes, J.; Corbeau, P.; Bertrand, E.; Marcello, A.; Emiliani, S.; Kiernan, R.; Benkirane, M., Suv39H1 and HP1γ are responsible for chromatin-mediated HIV-1 transcriptional silencing and post-integration latency. *The EMBO Journal* **2007,** *26* (2), 424-435.
40. Barboric, M.; Kohoutek, J.; Price, J. P.; Blazek, D.; Price, D. H.; Peterlin, B. M., Interplay between 7SK snRNA and oppositely charged regions in HEXIM1 direct the inhibition of P-TEFb. *The EMBO Journal* **2005,** *24* (24), 4291-4303.
41. Yik, J. H. N.; Chen, R.; Nishimura, R.; Jennings, J. L.; Link, A. J.; Zhou, Q., Inhibition of P-TEFb (CDK9/Cyclin T) Kinase and RNA Polymerase II Transcription by the Coordinated Actions of HEXIM1 and 7SK snRNA. *Molecular Cell* **2003,** *12* (4), 971-982.
42. Xing, S.; Siliciano, R. F., Targeting HIV latency: pharmacologic strategies toward eradication. *Drug Discovery Today* **2013,** *18* (11–12), 541-551.
43. Lassen, K. G.; Ramyar, K. X.; Bailey, J. R.; Zhou, Y.; Siliciano, R. F., Nuclear Retention of Multiply Spliced HIV-1 RNA in Resting CD4(+) T Cells. *PLoS Pathogens* **2006,** *2* (7), e68.
44. Huang, J.; Wang, F.; Argyris, E.; Chen, K.; Liang, Z.; Tian, H.; Huang, W.; Squires, K.; Verlinghieri, G.; Zhang, H., Cellular microRNAs contribute to HIV-1 latency in resting primary CD4+ T lymphocytes. *Nature Medicine* **2007,** *13*, 1241.
45. Markowitz, M.; Louie, M.; Hurley, A.; Sun, E.; Di Mascio, M.; Perelson, A. S.; Ho, D. D., A novel antiviral intervention results in more accurate assessment of human immunodeficiency virus type 1 replication dynamics and T-cell decay in vivo. *Journal of virology* **2003,** *77* (8), 5037-5038.
46. Zhang , L.; Ramratnam , B.; Tenner-Racz , K.; He , Y.; Vesanen , M.; Lewin , S.; Talal , A.; Racz , P.; Perelson , A. S.; Korber , B. T.; Markowitz , M.; Guo , Y.; Duran , M.; Hurley , A.; Tsay , J.; Huang , Y.-C.; Wang , C.-C.; Ho , D. D., Quantifying Residual HIV-1 Replication in Patients Receiving Combination Antiretroviral Therapy. *New England Journal of Medicine* **1999,** *340* (21), 1605-1613.
47. Siliciano, J. D.; Kajdas, J.; Finzi, D.; Quinn, T. C.; Chadwick, K.; Margolick, J. B.; Kovacs, C.; Gange, S. J.; Siliciano, R. F., Long-term follow-up studies confirm the stability of the latent reservoir for HIV-1 in resting CD4+ T cells. *Nature Medicine* **2003,** *9*, 727.
48. Chun, T.-W.; Justement, J. S.; Moir, S.; Hallahan, C. W.; Maenza, J.; Mullins, J. I.; Collier, A. C.; Corey, L.; Fauci, A. S., Decay of the HIV reservoir in patients receiving antiretroviral therapy for extended periods: implications for eradication of virus. *Journal of Infectious Diseases* **2007,** *195* (12), 1762-1764.
49. Chomont, N.; El-Far, M.; Ancuta, P.; Trautmann, L.; Procopio, F. A.; Yassine-Diab, B.; Boucher, G.; Boulassel, M.-R.; Ghattas, G.; Brenchley, J. M.; Schacker, T. W.; Hill, B. J.;

Douek, D. C.; Routy, J.-P.; Haddad, E. K.; Sekaly, R.-P., HIV reservoir size and persistence are driven by T cell survival and homeostatic proliferation. *Nat Med* **2009,** *15* (8), 893-900.
50. Lorenzo-Redondo, R.; Fryer, H. R.; Bedford, T.; Kim, E.-Y.; Archer, J.; Kosakovsky Pond, S. L.; Chung, Y.-S.; Penugonda, S.; Chipman, J. G.; Fletcher, C. V.; Schacker, T. W.; Malim, M. H.; Rambaut, A.; Haase, A. T.; McLean, A. R.; Wolinsky, S. M., Persistent HIV-1 replication maintains the tissue reservoir during therapy. *Nature* **2016,** *530* (7588), 51-56.
51. Bui, J. K.; Sobolewski, M. D.; Keele, B. F.; Spindler, J.; Musick, A.; Wiegand, A.; Luke, B. T.; Shao, W.; Hughes, S. H.; Coffin, J. M.; Kearney, M. F.; Mellors, J. W., Proviruses with identical sequences comprise a large fraction of the replication-competent HIV reservoir. *PLOS Pathogens* **2017,** *13* (3), e1006283.
52. Pallikkuth, S.; Sharkey, M.; Babic, D. Z.; Gupta, S.; Stone, G. W.; Fischl, M. A.; Stevenson, M.; Pahwa, S., Peripheral T Follicular Helper Cells Are the Major HIV Reservoir within Central Memory CD4 T Cells in Peripheral Blood from Chronically HIV-Infected Individuals on Combination Antiretroviral Therapy. *Journal of Virology* **2016,** *90* (6), 2718-2728.
53. Buzon, M. J.; Sun, H.; Li, C.; Shaw, A.; Seiss, K.; Ouyang, Z.; Martin-Gayo, E.; Leng, J.; Henrich, T. J.; Li, J. Z.; Pereyra, F.; Zurakowski, R.; Walker, B. D.; Rosenberg, E. S.; Yu, X. G.; Lichterfeld, M., HIV-1 persistence in CD4(+) T cells with stem cell-like properties. *Nature medicine* **2014,** *20* (2), 139-142.
54. Gattinoni, L.; Lugli, E.; Ji, Y.; Pos, Z.; Paulos, C. M.; Quigley, M. F.; Almeida, J. R.; Gostick, E.; Yu, Z.; Carpenito, C.; Wang, E.; Douek, D. C.; Price, D. A.; June, C. H.; Marincola, F. M.; Roederer, M.; Restifo, N. P., A human memory T-cell subset with stem cell-like properties. *Nature medicine* **2011,** *17* (10), 1290-1297.
55. Kumar, A.; Herbein, G., The macrophage: a therapeutic target in HIV-1 infection. *Molecular and Cellular Therapies* **2014,** *2* (1), 10.
56. Groot, F.; Welsch, S.; Sattentau, Q. J., Efficient HIV-1 transmission from macrophages to T cells across transient virological synapses. *Blood* **2008,** *111* (9), 4660-4663.
57. Swingler, S.; Mann, A.; Jacque, J. M.; Brichacek, B.; Sasseville, V. G.; Williams, K.; Lackner, A. A.; Janoff, E. N.; Wang, R.; Fisher, D.; Stevenson, M., HIV-1 Nef mediates lymphocyte chemotaxis and activation by infected macrophages. *Nat Med* **1999,** *5* (9), 997-1003.
58. Rock, R. B.; Gekker, G.; Hu, S.; Sheng, W. S.; Cheeran, M.; Lokensgard, J. R.; Peterson, P. K., Role of Microglia in Central Nervous System Infections. *Clinical Microbiology Reviews* **2004,** *17* (4), 942-964.
59. Kelly, J.; Beddall, M. H.; Yu, D.; Iyer, S. R.; Marsh, J. W.; Wu, Y., Human macrophages support persistent transcription from unintegrated HIV-1 DNA. *Virology* **2008,** *372* (2), 300-312.
60. Carter, C. A.; Ehrlich, L. S., Cell Biology of HIV-1 Infection of Macrophages. *Annual Review of Microbiology* **2008,** *62* (1), 425-443.
61. Ghorpade, A.; Persidskaia, R.; Suryadevara, R.; Che, M.; Liu, X. J.; Persidsky, Y.; Gendelman, H. E., Mononuclear phagocyte differentiation, activation, and viral infection regulate matrix metalloproteinase expression: implications for human immunodeficiency virus type 1-associated dementia. *Journal of virology* **2001,** *75* (14), 6572-6583.
62. Loré, K.; Smed-Sörensen, A.; Vasudevan, J.; Mascola, J. R.; Koup, R. A., Myeloid and plasmacytoid dendritic cells transfer HIV-1 preferentially to antigen-specific CD4(+) T cells. *The Journal of Experimental Medicine* **2005,** *201* (12), 2023-2033.
63. Wu, L.; KewalRamani, V. N., Dendritic-cell interactions with HIV: infection and viral dissemination. *Nature reviews. Immunology* **2006,** *6* (11), 859-868.

64. Otero, M.; Nunnari, G.; Leto, D.; Sullivan, J.; Wang, F.-X.; Frank, I.; Xu, Y.; Patel, C.; Dornadula, G.; Kulkosky, J., Peripheral blood dendritic cells are not a major reservoir for HIV type 1 in infected individuals on virally suppressive HAART. *AIDS research and human retroviruses* **2003,** *19* (12), 1097-1103.
65. Spiegel, H.; Herbst, H.; Niedobitek, G.; Foss, H. D.; Stein, H., Follicular dendritic cells are a major reservoir for human immunodeficiency virus type 1 in lymphoid tissues facilitating infection of CD4+ T-helper cells. *The American Journal of Pathology* **1992,** *140* (1), 15-22.
66. Estes, J. D.; Kityo, C.; Ssali, F.; Swainson, L.; Makamdop, K. N.; Del Prete, G. Q.; Deeks, S. G.; Luciw, P. A.; Chipman, J. G.; Beilman, G. J.; Hoskuldsson, T.; Khoruts, A.; Anderson, J.; Deleage, C.; Jasurda, J.; Schmidt, T. E.; Hafertepe, M.; Callisto, S. P.; Pearson, H.; Reimann, T.; Schuster, J.; Schoephoerster, J.; Southern, P.; Perkey, K.; Shang, L.; Wietgrefe, S. W.; Fletcher, C. V.; Lifson, J. D.; Douek, D. C.; McCune, J. M.; Haase, A. T.; Schacker, T. W., Defining total-body AIDS-virus burden with implications for curative strategies. *Nature Medicine* **2017,** *23*, 1271.
67. Sigal, A.; Kim, J. T.; Balazs, A. B.; Dekel, E.; Mayo, A.; Milo, R.; Baltimore, D., Cell-to-cell spread of HIV permits ongoing replication despite antiretroviral therapy. *Nature* **2011,** *477* (7362), 95-98.
68. Döpper, S.; Wilflingseder, D.; Prodinger, W. M.; Stiegler, G.; Speth, C.; Dierich, M. P.; Stoiber, H., Mechanism(s) promoting HIV-1 infection of primary unstimulated T lymphocytes in autologous B cell/T cell co-cultures. *European Journal of Immunology* **2003,** *33* (8), 2098-2107.
69. Arrighi, J.-F.; Pion, M.; Garcia, E.; Escola, J.-M.; van Kooyk, Y.; Geijtenbeek, T. B.; Piguet, V., DC-SIGN–mediated Infectious Synapse Formation Enhances X4 HIV-1 Transmission from Dendritic Cells to T Cells. *The Journal of Experimental Medicine* **2004,** *200* (10), 1279-1288.
70. Veazey, R. S.; DeMaria, M.; Chalifoux, L. V.; Shvetz, D. E.; Pauley, D. R.; Knight, H. L.; Rosenzweig, M.; Johnson, R. P.; Desrosiers, R. C.; Lackner, A. A., Gastrointestinal Tract as a Major Site of CD4+ T Cell Depletion and Viral Replication in SIV Infection. *Science* **1998,** *280* (5362), 427-431.
71. Ling, B.; Mohan, M.; Lackner, A. A.; Green, L. C.; Marx, P. A.; Doyle, L. A.; Veazey, R. S., The Large Intestine as a Major Reservoir for Simian Immunodeficiency Virus in Macaques with Long-Term, Nonprogressing Infection. *Journal of Infectious Diseases* **2010,** *202* (12), 1846-1854.
72. Poles, M. A.; Elliott, J.; Taing, P.; Anton, P. A.; Chen, I. S., A preponderance of CCR5+ CXCR4+ mononuclear cells enhances gastrointestinal mucosal susceptibility to human immunodeficiency virus type 1 infection. *Journal of virology* **2001,** *75* (18), 8390-8399.
73. Shacklett, B. L.; Anton, P. A., HIV Infection and Gut Mucosal Immune Function: Updates on Pathogenesis with Implications for Management and Intervention. *Current Infectious Disease Reports* **2010,** *12* (1), 19-27.
74. Cicala, C.; Martinelli, E.; McNally, J. P.; Goode, D. J.; Gopaul, R.; Hiatt, J.; Jelicic, K.; Kottilil, S.; Macleod, K.; O'Shea, A.; Patel, N.; Van Ryk, D.; Wei, D.; Pascuccio, M.; Yi, L.; McKinnon, L.; Izulla, P.; Kimani, J.; Kaul, R.; Fauci, A. S.; Arthos, J., The integrin α4β7 forms a complex with cell-surface CD4 and defines a T-cell subset that is highly susceptible to infection by HIV-1. *Proceedings of the National Academy of Sciences* **2009,** *106* (49), 20877-20882.
75. Kader, M.; Wang, X.; Piatak, M.; Lifson, J.; Roederer, M.; Veazey, R.; Mattapallil, J. J., α4+β7hiCD4+ memory T cells harbor most Th-17 cells and are preferentially infected during acute SIV infection. *Mucosal Immunol* **2009,** *2* (5), 439-449.

76. Kanmogne, G. D.; Kennedy, R. C.; Grammas, P., HIV-1 gp120 Proteins and gp160 Peptides Are Toxic to Brain Endothelial Cells and Neurons: Possible Pathway for HIV Entry into the Brain and HIV-Associated Dementia. *Journal of Neuropathology & Experimental Neurology* **2002,** *61* (11), 992-1000.
77. McGee, B.; Smith, N.; Aweeka, F., HIV Pharmacology: Barriers to the Eradication of HIV from the CNS. *HIV Clinical Trials* **2006,** *7* (3), 142-153.
78. Costiniuk, C. T.; Jenabian, M.-A., The lungs as anatomical reservoirs of HIV infection. *Reviews in Medical Virology* **2014,** *24* (1), 35-54.
79. Fierer, D. S.; Klotman, M. E., Kidney and central nervous system as reservoirs of HIV infection. *Current opinion in HIV and AIDS* **2006,** *1* (2), 115-120.
80. Chun, T.-W.; Engel, D.; Berrey, M. M.; Shea, T.; Corey, L.; Fauci, A. S., Early establishment of a pool of latently infected, resting CD4+ T cells during primary HIV-1 infection. *Proceedings of the National Academy of Sciences* **1998,** *95* (15), 8869-8873.
81. Chun, T.-W.; Moir, S.; Fauci, A. S., HIV reservoirs as obstacles and opportunities for an HIV cure. *Nat Immunol* **2015,** *16* (6), 584-589.
82. Nishimura, Y.; Sadjadpour, R.; Mattapallil, J. J.; Igarashi, T.; Lee, W.; Buckler-White, A.; Roederer, M.; Chun, T.-W.; Martin, M. A., High frequencies of resting CD4+ T cells containing integrated viral DNA are found in rhesus macaques during acute lentivirus infections. *Proceedings of the National Academy of Sciences* **2009,** *106* (19), 8015-8020.
83. Whitney, J. B.; Hill, A. L.; Sanisetty, S.; Penaloza-MacMaster, P.; Liu, J.; Shetty, M.; Parenteau, L.; Cabral, C.; Shields, J.; Blackmore, S.; Smith, J. Y.; Brinkman, A. L.; Peter, L. E.; Mathew, S. I.; Smith, K. M.; Borducchi, E. N.; Rosenbloom, D. I. S.; Lewis, M. G.; Hattersley, J.; Li, B.; Hesselgesser, J.; Geleziunas, R.; Robb, M. L.; Kim, J. H.; Michael, N. L.; Barouch, D. H., Rapid Seeding of the Viral Reservoir Prior to SIV Viremia in Rhesus Monkeys. *Nature* **2014,** *512* (7512), 74-77.
84. Ananworanich, J.; Dubé, K.; Chomont, N., How does the timing of antiretroviral therapy initiation in acute infection affect HIV reservoirs? *Current opinion in HIV and AIDS* **2015,** *10* (1), 18-28.
85. Jain, V.; Hartogensis, W.; Bacchetti, P.; Hunt, P. W.; Hatano, H.; Sinclair, E.; Epling, L.; Lee, T.-H.; Busch, M. P.; McCune, J. M.; Pilcher, C. D.; Hecht, F. M.; Deeks, S. G., Antiretroviral Therapy Initiated Within 6 Months of HIV Infection Is Associated With Lower T-Cell Activation and Smaller HIV Reservoir Size. *The Journal of Infectious Diseases* **2013,** *208* (8), 1202-1211.
86. Hill, A. L.; Rosenbloom, D. I. S.; Goldstein, E.; Hanhauser, E.; Kuritzkes, D. R.; Siliciano, R. F.; Henrich, T. J., Real-Time Predictions of Reservoir Size and Rebound Time during Antiretroviral Therapy Interruption Trials for HIV. *PLoS Pathogens* **2016,** *12* (4), e1005535.
87. Li, J. Z.; Etemad, B.; Ahmed, H.; Aga, E.; Bosch, R. J.; Mellors, J. W.; Kuritzkes, D. R.; Lederman, M. M.; Para, M.; Gandhi, R. T., The Size of the Expressed HIV Reservoir Predicts Timing of Viral Rebound after Treatment Interruption. *AIDS (London, England)* **2016,** *30* (3), 343-353.
88. Persaud , D.; Gay , H.; Ziemniak , C.; Chen , Y. H.; Piatak , M. J.; Chun , T.-W.; Strain , M.; Richman , D.; Luzuriaga , K., Absence of Detectable HIV-1 Viremia after Treatment Cessation in an Infant. *New England Journal of Medicine* **2013,** *369* (19), 1828-1835.
89. Luzuriaga , K.; Gay , H.; Ziemniak , C.; Sanborn , K. B.; Somasundaran , M.; Rainwater-Lovett , K.; Mellors , J. W.; Rosenbloom , D.; Persaud , D., Viremic Relapse after HIV-1

Remission in a Perinatally Infected Child. *New England Journal of Medicine* **2015,** *372* (8), 786-788.
90. Schuetz, A.; Deleage, C.; Sereti, I.; Rerknimitr, R.; Phanuphak, N.; Phuang-Ngern, Y.; Estes, J. D.; Sandler, N. G.; Sukhumvittaya, S.; Marovich, M.; Jongrakthaitae, S.; Akapirat, S.; Fletscher, J. L. K.; Kroon, E.; Dewar, R.; Trichavaroj, R.; Chomchey, N.; Douek, D. C.; O′Connell, R. J.; Ngauy, V.; Robb, M. L.; Phanuphak, P.; Michael, N. L.; Excler, J.-L.; Kim, J. H.; de Souza, M. S.; Ananworanich, J.; on behalf of the, R. S.; Groups, R. S. S., Initiation of ART during Early Acute HIV Infection Preserves Mucosal Th17 Function and Reverses HIV-Related Immune Activation. *PLOS Pathogens* **2014,** *10* (12), e1004543.
91. Hong, J. J.; Silveira, E. L. d. V.; Amancha, P. K.; Byrareddy, S. N.; Gumber, S.; Chang, K.-T.; Ansari, A. A.; Villinger, F., Early initiation of antiretroviral treatment postSIV infection does not resolve lymphoid tissue activation. *AIDS* **2017,** *31* (13), 1819-1824.
92. Malzahn, J.; Shen, C.; Caruso, L.; Ghosh, P.; Sankapal, S. R.; Barratt-Boyes, S.; Gupta, P.; Chen, Y., Effect of early anti-retroviral therapy on the pathogenic changes in mucosal tissues of SIV infected rhesus macaques. *Virology Journal* **2012,** *9*, 269-269.
93. Davey, R. T.; Bhat, N.; Yoder, C.; Chun, T.-W.; Metcalf, J. A.; Dewar, R.; Natarajan, V.; Lempicki, R. A.; Adelsberger, J. W.; Miller, K. D.; Kovacs, J. A.; Polis, M. A.; Walker, R. E.; Falloon, J.; Masur, H.; Gee, D.; Baseler, M.; Dimitrov, D. S.; Fauci, A. S.; Lane, H. C., HIV-1 and T cell dynamics after interruption of highly active antiretroviral therapy (HAART) in patients with a history of sustained viral suppression. *Proceedings of the National Academy of Sciences of the United States of America* **1999,** *96* (26), 15109-15114.
94. Barouch, D. H.; Deeks, S. G., Immunologic strategies for HIV-1 remission and eradication. *Science* **2014,** *345* (6193), 169-174.
95. Barton, K. M.; Archin, N. M.; Keedy, K. S.; Espeseth, A. S.; Zhang, Y.-l.; Gale, J.; Wagner, F. F.; Holson, E. B.; Margolis, D. M., Selective HDAC Inhibition for the Disruption of Latent HIV-1 Infection. *PLOS ONE* **2014,** *9* (8), e102684.
96. Bannister, A. J.; Kouzarides, T., Regulation of chromatin by histone modifications. *Cell Research* **2011,** *21* (3), 381-395.
97. Bernhard, W.; Barreto, K.; Saunders, A.; Dahabieh, M. S.; Johnson, P.; Sadowski, I., The Suv39H1 methyltransferase inhibitor chaetocin causes induction of integrated HIV-1 without producing a T cell response. *FEBS Letters* **2011,** *585* (22), 3549-3554.
98. McKernan, L. N.; Momjian, D.; Kulkosky, J., Protein Kinase C: One Pathway towards the Eradication of Latent HIV-1 Reservoirs. *Adv Virol* **2012,** *2012*, 805347.
99. Jiang, G.; Mendes, E. A.; Kaiser, P.; Sankaran-Walters, S.; Tang, Y.; Weber, M. G.; Melcher, G. P.; Thompson, G. R.; Tanuri, A.; Pianowski, L. F.; Wong, J. K.; Dandekar, S., Reactivation of HIV latency by a newly modified Ingenol derivative via protein kinase Cδ–NF-κB signaling. *AIDS (London, England)* **2014,** *28* (11), 1555-1566.
100. Banerjee, C.; Archin, N.; Michaels, D.; Belkina, A. C.; Denis, G. V.; Bradner, J.; Sebastiani, P.; Margolis, D. M.; Montano, M., BET bromodomain inhibition as a novel strategy for reactivation of HIV-1. *Journal of leukocyte biology* **2012,** *92* (6), 1147-1154.
101. Kauder, S. E.; Bosque, A.; Lindqvist, A.; Planelles, V.; Verdin, E., Epigenetic Regulation of HIV-1 Latency by Cytosine Methylation. *PLOS Pathogens* **2009,** *5* (6), e1000495.
102. Contreras, X.; Schweneker, M.; Chen, C.-S.; McCune, J. M.; Deeks, S. G.; Martin, J.; Peterlin, B. M., Suberoylanilide hydroxamic acid reactivates HIV from latently infected cells. *The Journal of Biological Chemistry* **2009,** *284* (11), 6782-6789.

103. Das, B.; Dobrowolski, C.; Shahir, A.-M.; Feng, Z.; Yu, X.; Sha, J.; Bissada, N. F.; Weinberg, A.; Karn, J.; Ye, F., Short chain fatty acids potently induce latent HIV-1 in T-cells by activating P-TEFb and multiple histone modifications. *Virology* **2015,** *474*, 65-81.
104. Archin, N. M.; Liberty, A.; Kashuba, A. D.; Choudhary, S. K.; Kuruc, J.; Crooks, A.; Parker, D.; Anderson, E.; Kearney, M.; Strain, M., Administration of vorinostat disrupts HIV-1 latency in patients on antiretroviral therapy. *Nature* **2012,** *487* (7408), 482-485.
105. Archin, N. M.; Bateson, R.; Tripathy, M.; Crooks, A. M.; Yang, K.-H.; Dahl, N. P.; Kearney, M. F.; Anderson, E. M.; Coffin, J. M.; Strain, M. C., HIV-1 expression within resting CD4 T-cells following multiple doses of vorinostat. *Journal of Infectious Diseases* **2014**, jiu155.
106. Elliott, J. H.; Wightman, F.; Solomon, A.; Ghneim, K.; Ahlers, J.; Cameron, M. J.; Smith, M. Z.; Spelman, T.; McMahon, J.; Velayudham, P., Activation of HIV transcription with short-course vorinostat in HIV-infected patients on suppressive antiretroviral therapy. *PLoS Pathog* **2014,** *10* (11), e1004473.
107. Archin, N. M.; Kirchherr, J. L.; Sung, J. A. M.; Clutton, G.; Sholtis, K.; Xu, Y.; Allard, B.; Stuelke, E.; Kashuba, A. D.; Kuruc, J. D.; Eron, J.; Gay, C. L.; Goonetilleke, N.; Margolis, D. M., Interval dosing with the HDAC inhibitor vorinostat effectively reverses HIV latency. *The Journal of Clinical Investigation* **2017,** *127* (8), 3126-3135.
108. Rasmussen, T. A.; Tolstrup, M.; Brinkmann, C. R.; Olesen, R.; Erikstrup, C.; Solomon, A.; Winckelmann, A.; Palmer, S.; Dinarello, C.; Buzon, M., Panobinostat, a histone deacetylase inhibitor, for latent-virus reactivation in HIV-infected patients on suppressive antiretroviral therapy: a phase 1/2, single group, clinical trial. *The Lancet HIV* **2014,** *1* (1), e13-e21.
109. Archin, N. M.; Cheema, M.; Parker, D.; Wiegand, A.; Bosch, R. J.; Coffin, J. M.; Eron, J.; Cohen, M.; Margolis, D. M., Antiretroviral Intensification and Valproic Acid Lack Sustained Effect on Residual HIV-1 Viremia or Resting CD4+ Cell Infection. *PLoS ONE* **2010,** *5* (2), e9390.
110. Routy, J. P.; Tremblay, C. L.; Angel, J. B.; Trottier, B.; Rouleau, D.; Baril, J. G.; Harris, M.; Trottier, S.; Singer, J.; Chomont, N.; Sékaly, R. P.; Boulassel, M. R., Valproic acid in association with highly active antiretroviral therapy for reducing systemic HIV-1 reservoirs: results from a multicentre randomized clinical study. *HIV Medicine* **2012,** *13* (5), 291-296.
111. Søgaard, O. S.; Graversen, M. E.; Leth, S.; Olesen, R.; Brinkmann, C. R.; Nissen, S. K.; Kjaer, A. S.; Schleimann, M. H.; Denton, P. W.; Hey-Cunningham, W. J., The depsipeptide romidepsin reverses HIV-1 latency in vivo. *PLoS Pathog* **2015,** *11* (9), e1005142.
112. Policicchio, B. B.; Xu, C.; Brocca-Cofano, E.; Raehtz, K. D.; He, T.; Ma, D.; Li, H.; Sivanandham, R.; Haret-Richter, G. S.; Dunsmore, T.; Trichel, A.; Mellors, J. W.; Hahn, B. H.; Shaw, G. M.; Ribeiro, R. M.; Pandrea, I.; Apetrei, C., Multi-dose Romidepsin Reactivates Replication Competent SIV in Post-antiretroviral Rhesus Macaque Controllers. *PLoS Pathog* **2016,** *12* (9), e1005879.
113. Del Prete, G. Q.; Oswald, K.; Lara, A.; Shoemaker, R.; Smedley, J.; Macallister, R.; Coalter, V.; Wiles, A.; Wiles, R.; Li, Y.; Fast, R.; Kiser, R.; Lu, B.; Zheng, J.; Alvord, W. G.; Trubey, C. M.; Piatak, M.; Deleage, C.; Keele, B. F.; Estes, J. D.; Hesselgesser, J.; Geleziunas, R.; Lifson, J. D., Elevated Plasma Viral Loads in Romidepsin-Treated Simian Immunodeficiency Virus-Infected Rhesus Macaques on Suppressive Combination Antiretroviral Therapy. *Antimicrobial Agents and Chemotherapy* **2016,** *60* (3), 1560-1572.
114. Yang, W.; Sun, Z.; Hua, C.; Wang, Q.; Xu, W.; Deng, Q.; Pan, Y.; Lu, L.; Jiang, S., Chidamide, a histone deacetylase inhibitor-based anticancer drug, effectively reactivates latent HIV-1 provirus. *Microbes and Infection* **2017**.

115. Kashanchi, F.; Melpolder, J. C.; Epstein, J. S.; Sadaie, M. R., Rapid and sensitive detection of cell-associated HIV-1 in latently infected cell lines and in patient cells using sodium-n-butyrate induction and RT-PCR. *Journal of medical virology* **1997,** *52* (2), 179-189.
116. Imai, K.; Togami, H.; Okamoto, T., Involvement of histone H3 lysine 9 (H3K9) methyltransferase G9a in the maintenance of HIV-1 latency and its reactivation by BIX01294. *Journal of Biological Chemistry* **2010,** *285* (22), 16538-16545.
117. Williams, S. A.; Chen, L.-F.; Kwon, H.; Fenard, D.; Bisgrove, D.; Verdin, E.; Greene, W. C., Prostratin antagonizes HIV latency by activating NF-κB. *Journal of Biological Chemistry* **2004,** *279* (40), 42008-42017.
118. Kulkosky, J.; Culnan, D. M.; Roman, J.; Dornadula, G.; Schnell, M.; Boyd, M. R.; Pomerantz, R. J., Prostratin: activation of latent HIV-1 expression suggests a potential inductive adjuvant therapy for HAART. *Blood* **2001,** *98* (10), 3006-3015.
119. Gutiérrez, C.; Serrano-Villar, S.; Madrid-Elena, N.; Pérez-Elías, M. J.; Martín, M. E.; Barbas, C.; Ruipérez, J.; Muñoz, E.; Muñoz-Fernández, M. A.; Castor, T., Bryostatin-1 for latent virus reactivation in HIV-infected patients on antiretroviral therapy. *AIDS* **2016,** *30* (9), 1385-1392.
120. Mehla, R.; Bivalkar-Mehla, S.; Zhang, R.; Handy, I.; Albrecht, H.; Giri, S.; Nagarkatti, P.; Nagarkatti, M.; Chauhan, A., Bryostatin modulates latent HIV-1 infection via PKC and AMPK signaling but inhibits acute infection in a receptor independent manner. *PloS one* **2010,** *5* (6), e11160.
121. Jiang, G.; Mendes, E. A.; Kaiser, P.; Wong, D. P.; Tang, Y.; Cai, I.; Fenton, A.; Melcher, G. P.; Hildreth, J. E. K.; Thompson, G. R.; Wong, J. K.; Dandekar, S., Synergistic Reactivation of Latent HIV Expression by Ingenol-3-Angelate, PEP005, Targeted NF-kB Signaling in Combination with JQ1 Induced p-TEFb Activation. *PLOS Pathogens* **2015,** *11* (7), e1005066.
122. Wang, P.; Lu, P.; Qu, X.; Shen, Y.; Zeng, H.; Zhu, X.; Zhu, Y.; Li, X.; Wu, H.; Xu, J.; Lu, H.; Ma, Z.; Zhu, H., Reactivation of HIV-1 from Latency by an Ingenol Derivative from Euphorbia Kansui. *Scientific Reports* **2017,** *7* (1), 9451.
123. Contreras, X.; Barboric, M.; Lenasi, T.; Peterlin, B. M., HMBA releases P-TEFb from HEXIM1 and 7SK snRNA via PI3K/Akt and activates HIV transcription. *PLoS Pathog* **2007,** *3* (10), e146.
124. Fenaux, P., Inhibitors of DNA methylation: beyond myelodysplastic syndromes. *Nature Clinical Practice Oncology* **2005,** *2*, S36-S44.
125. Xing, S.; Bullen, C. K.; Shroff, N. S.; Shan, L.; Yang, H.-C.; Manucci, J. L.; Bhat, S.; Zhang, H.; Margolick, J. B.; Quinn, T. C., Disulfiram reactivates latent HIV-1 in a Bcl-2-transduced primary CD4+ T cell model without inducing global T cell activation. *Journal of virology* **2011,** *85* (12), 6060-6064.
126. Spivak, A. M.; Andrade, A.; Eisele, E.; Hoh, R.; Bacchetti, P.; Bumpus, N. N.; Emad, F.; Buckheit, R.; McCance-Katz, E. F.; Lai, J., A Pilot Study Assessing the Safety and Latency Reversing Activity of Disulfiram in HIV-1-Infected Adults on Antiretroviral Therapy. *Clinical infectious diseases* **2013**, cit813.
127. Elliott, J. H.; McMahon, J. H.; Chang, C. C.; Lee, S. A.; Hartogensis, W.; Bumpus, N.; Savic, R.; Roney, J.; Hoh, R.; Solomon, A., Short-term administration of disulfiram for reversal of latent HIV infection: a phase 2 dose-escalation study. *The Lancet HIV* **2015,** *2* (12), e520-e529.

128. Delagrèverie, H. M.; Delaugerre, C.; Lewin, S. R.; Deeks, S. G.; Li, J. Z., Ongoing Clinical Trials of Human Immunodeficiency Virus Latency-Reversing and Immunomodulatory Agents. *Open Forum Infectious Diseases* **2016,** *3* (4), ofw189-ofw189.
129. Rasmussen, T. A.; Tolstrup, M.; Søgaard, O. S., Reversal of Latency as Part of a Cure for HIV-1. *Trends in Microbiology* **2016,** *24* (2), 90-97.
130. Halper-Stromberg, A.; Lu, C.-L.; Klein, F.; Horwitz, J. A.; Bournazos, S.; Nogueira, L.; Eisenreich, T. R.; Liu, C.; Gazumyan, A.; Schaefer, U.; Furze, R. C.; Seaman, M. S.; Prinjha, R.; Tarakhovsky, A.; Ravetch, J. V.; Nussenzweig, M. C., Broadly Neutralizing Antibodies and Viral inducers decrease rebound from HIV-1 latent reservoirs in humanized mice. *Cell* **2014,** *158* (5), 989-999.
131. Laird, G. M.; Bullen, C. K.; Rosenbloom, D. I.; Martin, A. R.; Hill, A. L.; Durand, C. M.; Siliciano, J. D.; Siliciano, R. F., Ex vivo analysis identifies effective HIV-1 latency-reversing drug combinations. *J Clin Invest* **2015,** *125* (5), 1901-12.
132. Darcis, G.; Kula, A.; Bouchat, S.; Fujinaga, K.; Corazza, F.; Ait-Ammar, A.; Delacourt, N.; Melard, A.; Kabeya, K.; Vanhulle, C.; Van Driessche, B.; Gatot, J.-S.; Cherrier, T.; Pianowski, L. F.; Gama, L.; Schwartz, C.; Vila, J.; Burny, A.; Clumeck, N.; Moutschen, M.; De Wit, S.; Peterlin, B. M.; Rouzioux, C.; Rohr, O.; Van Lint, C., An In-Depth Comparison of Latency-Reversing Agent Combinations in Various In Vitro and Ex Vivo HIV-1 Latency Models Identified Bryostatin-1+JQ1 and Ingenol-B+JQ1 to Potently Reactivate Viral Gene Expression. *PLoS Pathogens* **2015,** *11* (7), e1005063.
133. Pérez, M.; de Vinuesa, A. G.; Sanchez-Duffhues, G.; Marquez, N.; Bellido, M. L.; Munoz-Fernandez, M.; Moreno, S.; Castor, T. P.; Calzado, M. A.; Muñoz, E., Bryostatin-1 synergizes with histone deacetylase inhibitors to reactivate HIV-1 from latency. *Current HIV research* **2010,** *8* (6), 418-429.
134. Reuse, S.; Calao, M.; Kabeya, K.; Guiguen, A.; Gatot, J.-S.; Quivy, V.; Vanhulle, C.; Lamine, A.; Vaira, D.; Demonte, D.; Martinelli, V.; Veithen, E.; Cherrier, T.; Avettand, V.; Poutrel, S.; Piette, J.; de Launoit, Y.; Moutschen, M.; Burny, A.; Rouzioux, C.; De Wit, S.; Herbein, G.; Rohr, O.; Collette, Y.; Lambotte, O.; Clumeck, N.; Van Lint, C., Synergistic Activation of HIV-1 Expression by Deacetylase Inhibitors and Prostratin: Implications for Treatment of Latent Infection. *PLOS ONE* **2009,** *4* (6), e6093.
135. Sarkar, I.; Hauber, I.; Hauber, J.; Buchholz, F., HIV-1 Proviral DNA Excision Using an Evolved Recombinase. *Science* **2007,** *316* (5833), 1912-1915.
136. Qu, X.; Wang, P.; Ding, D.; Li, L.; Wang, H.; Ma, L.; Zhou, X.; Liu, S.; Lin, S.; Wang, X.; Zhang, G.; Liu, S.; Liu, L.; Wang, J.; Zhang, F.; Lu, D.; Zhu, H., Zinc-finger-nucleases mediate specific and efficient excision of HIV-1 proviral DNA from infected and latently infected human T cells. *Nucleic Acids Research* **2013,** *41* (16), 7771-7782.
137. Ebina, H.; Kanemura, Y.; Misawa, N.; Sakuma, T.; Kobayashi, T.; Yamamoto, T.; Koyanagi, Y., A High Excision Potential of TALENs for Integrated DNA of HIV-Based Lentiviral Vector. *PLOS ONE* **2015,** *10* (3), e0120047.
138. Ebina, H.; Misawa, N.; Kanemura, Y.; Koyanagi, Y., Harnessing the CRISPR/Cas9 system to disrupt latent HIV-1 provirus. *Scientific Reports* **2013,** *3*, 2510.
139. Kaminski, R.; Bella, R.; Yin, C.; Otte, J.; Ferrante, P.; Gendelman, H. E.; Li, H.; Booze, R.; Gordon, J.; Hu, W.; Khalili, K., Excision of HIV-1 DNA by gene editing: a proof-of-concept in vivo study. *Gene Therapy* **2016,** *23*, 690.
140. Yin, C.; Zhang, T.; Qu, X.; Zhang, Y.; Putatunda, R.; Xiao, X.; Li, F.; Xiao, W.; Zhao, H.; Dai, S.; Qin, X.; Mo, X.; Young, W.-B.; Khalili, K.; Hu, W., In Vivo Excision of HIV-1 Provirus

by saCas9 and Multiplex Single-Guide RNAs in Animal Models. *Molecular Therapy* **2017,** *25* (5), 1168-1186.
141. Cannon, P.; June, C., CCR5 Knockout Strategies. *Current opinion in HIV and AIDS* **2011,** *6* (1), 74-79.
142. Tebas , P.; Stein , D.; Tang , W. W.; Frank , I.; Wang , S. Q.; Lee , G.; Spratt , S. K.; Surosky , R. T.; Giedlin , M. A.; Nichol , G.; Holmes , M. C.; Gregory , P. D.; Ando , D. G.; Kalos , M.; Collman , R. G.; Binder-Scholl , G.; Plesa , G.; Hwang , W.-T.; Levine , B. L.; June , C. H., Gene Editing of CCR5 in Autologous CD4 T Cells of Persons Infected with HIV. *New England Journal of Medicine* **2014,** *370* (10), 901-910.
143. Li, C.; Guan, X.; Du, T.; Jin, W.; Wu, B.; Liu, Y.; Wang, P.; Hu, B.; Griffin, G. E.; Shattock, R. J.; Hu, Q., Inhibition of HIV-1 infection of primary CD4+ T-cells by gene editing of CCR5 using adenovirus-delivered CRISPR/Cas9. *Journal of General Virology* **2015,** *96* (8), 2381-2393.
144. Hou, P.; Chen, S.; Wang, S.; Yu, X.; Chen, Y.; Jiang, M.; Zhuang, K.; Ho, W.; Hou, W.; Huang, J.; Guo, D., Genome editing of CXCR4 by CRISPR/cas9 confers cells resistant to HIV-1 infection. *Scientific Reports* **2015,** *5*, 15577.
145. Liu, Z.; Chen, S.; Jin, X.; Wang, Q.; Yang, K.; Li, C.; Xiao, Q.; Hou, P.; Liu, S.; Wu, S.; Hou, W.; Xiong, Y.; Kong, C.; Zhao, X.; Wu, L.; Li, C.; Sun, G.; Guo, D., Genome editing of the HIV co-receptors CCR5 and CXCR4 by CRISPR-Cas9 protects CD4(+) T cells from HIV-1 infection. *Cell & Bioscience* **2017,** *7*, 47.
146. Holt, N.; Wang, J.; Kim, K.; Friedman, G.; Wang, X.; Taupin, V.; Crooks, G. M.; Kohn, D. B.; Gregory, P. D.; Holmes, M. C.; Cannon, P. M., Zinc finger nuclease-mediated CCR5 knockout hematopoietic stem cell transplantation controls HIV-1 in vivo. *Nature biotechnology* **2010,** *28* (8), 839-847.
147. Xu, L.; Yang, H.; Gao, Y.; Chen, Z.; Xie, L.; Liu, Y.; Liu, Y.; Wang, X.; Li, H.; Lai, W.; He, Y.; Yao, A.; Ma, L.; Shao, Y.; Zhang, B.; Wang, C.; Chen, H.; Deng, H., CRISPR/Cas9-Mediated CCR5 Ablation in Human Hematopoietic Stem/Progenitor Cells Confers HIV-1 Resistance In Vivo. *Molecular Therapy 25* (8), 1782-1789.
148. DiGiusto, D. L.; Cannon, P. M.; Holmes, M. C.; Li, L.; Rao, A.; Wang, J.; Lee, G.; Gregory, P. D.; Kim, K. A.; Hayward, S. B.; Meyer, K.; Exline, C.; Lopez, E.; Henley, J.; Gonzalez, N.; Bedell, V.; Stan, R.; Zaia, J. A., Preclinical development and qualification of ZFN-mediated CCR5 disruption in human hematopoietic stem/progenitor cells. *Molecular Therapy. Methods & Clinical Development* **2016,** *3*, 16067.
149. Ye, L.; Wang, J.; Beyer, A. I.; Teque, F.; Cradick, T. J.; Qi, Z.; Chang, J. C.; Bao, G.; Muench, M. O.; Yu, J.; Levy, J. A.; Kan, Y. W., Seamless modification of wild-type induced pluripotent stem cells to the natural CCR5Δ32 mutation confers resistance to HIV infection. *Proceedings of the National Academy of Sciences* **2014,** *111* (26), 9591-9596.
150. Kang, H.; Minder, P.; Park, M. A.; Mesquitta, W.-T.; Torbett, B. E.; Slukvin, I. I., CCR5 Disruption in Induced Pluripotent Stem Cells Using CRISPR/Cas9 Provides Selective Resistance of Immune Cells to CCR5-tropic HIV-1 Virus. *Molecular Therapy - Nucleic Acids 4*.
151. Kambal, A.; Mitchell, G.; Cary, W.; Gruenloh, W.; Jung, Y.; Kalomoiris, S.; Nacey, C.; McGee, J.; Lindsey, M.; Fury, B.; Bauer, G.; Nolta, J. A.; Anderson, J. S., Generation of HIV-1 Resistant and Functional Macrophages From Hematopoietic Stem Cell–derived Induced Pluripotent Stem Cells. *Molecular Therapy* **2011,** *19* (3), 584-593.
152. Kitchen, S. G.; Levin, B. R.; Bristol, G.; Rezek, V.; Kim, S.; Aguilera-Sandoval, C.; Balamurugan, A.; Yang, O. O.; Zack, J. A., In Vivo Suppression of HIV by Antigen Specific T

Cells Derived from Engineered Hematopoietic Stem Cells. *PLoS Pathogens* **2012,** *8* (4), e1002649.
153. Kumar, P.; Ban, H.-S.; Kim, S.-S.; Wu, H.; Pearson, T.; Greiner, D. L.; Laouar, A.; Yao, J.; Haridas, V.; Habiro, K.; Yang, Y.-G.; Jeong, J.-H.; Lee, K.-Y.; Kim, Y.-H.; Kim, S. W.; Peipp, M.; Fey, G. H.; Manjunath, N.; Shultz, L. D.; Lee, S.-K.; Shankar, P., T Cell-Specific siRNA Delivery Suppresses HIV-1 Infection in Humanized Mice. *Cell* **2008,** *134* (4), 577-586.
154. Marsden, M. D.; Zack, J. A., Experimental Approaches for Eliminating Latent HIV. *Forum on immunopathological diseases and therapeutics* **2015,** *6* (1-2), 91-99.
155. Katlama, C.; Deeks, S. G.; Autran, B.; Martinez-Picado, J.; van Lunzen, J.; Rouzioux, C.; Miller, M.; Vella, S.; Schmitz, J. E.; Ahlers, J.; Richman, D. D.; Sekaly, R. P., Barriers to a Cure: New concepts in targeting and eradicating HIV-1 reservoirs. *Lancet* **2013,** *381* (9883), 10.1016/S0140-6736(13)60104-X.
156. Shan, L.; Deng, K.; Shroff, N. S.; Durand, C.; Rabi, S. A.; Yang, H.-C.; Zhang, H.; Margolick, J. B.; Blankson, J. N.; Siliciano, R. F., Stimulation of HIV-1-specific cytolytic T-lymphocytes facilitates elimination of latent viral reservoir after virus reactivation. *Immunity* **2012,** *36* (3), 491-501.
157. Schooley, R. T.; Spritzler, J.; Wang, H.; Lederman, M. M.; Havlir, D.; Kuritzkes, D. R.; Pollard, R.; Battaglia, C.; Robertson, M.; Mehrotra, D.; Casimiro, D.; Cox, K.; Schock, B.; Team, A. S., ACTG 5197: A Placebo Controlled Trial of Immunization of HIV-1 Infected Persons with a Replication Deficient Ad5 Vaccine Expressing the HIV-1 Core Protein. *The Journal of infectious diseases* **2010,** *202* (5), 705-716.
158. Gandhi, R. T.; O'Neill, D.; Bosch, R. J.; Chan, E. S.; Bucy, R. P.; Shopis, J.; Baglyos, L.; Adams, E.; Fox, L.; Purdue, L.; Marshak, A.; Flynn, T.; Masih, R.; Schock, B.; Mildvan, D.; Schlesinger, S. J.; Marovich, M. A.; Bhardwaj, N.; Jacobson, J. M., A randomized therapeutic vaccine trial of canarypox-HIV-pulsed dendritic cells vs. canarypox-HIV alone in HIV-1-infected patients on antiretroviral therapy. *Vaccine* **2009,** *27* (43), 6088.
159. Angel, J. B.; Routy, J.-P.; Tremblay, C.; Ayers, D.; Woods, R.; Singer, J.; Bernard, N.; Kovacs, C.; Smaill, F.; Gurunathan, S.; Sekaly, R.-P., A randomized controlled trial of HIV therapeutic vaccination using ALVAC with or without Remune. *AIDS* **2011,** *25* (6), 731-739.
160. Autran, B.; Murphy, R. L.; Costagliola, D.; Tubiana, R.; Clotet, B.; Gatell, J.; Staszewski, S.; Wincker, N.; Assoumou, L.; El-Habib, R.; Calvez, V.; Walker, B.; Katlama, C.; Group, a. t. O. S., Greater viral rebound and reduced time to resume antiretroviral therapy after therapeutic immunization with the ALVAC-HIV vaccine (vCP1452). *AIDS* **2008,** *22* (11), 1313-1322.
161. Hansen, S. G.; Ford, J. C.; Lewis, M. S.; Ventura, A. B.; Hughes, C. M.; Coyne-Johnson, L.; Whizin, N.; Oswald, K.; Shoemaker, R.; Swanson, T.; Legasse, A. W.; Chiuchiolo, M. J.; Parks, C. L.; Axthelm, M. K.; Nelson, J. A.; Jarvis, M. A.; Piatak, M.; Lifson, J. D.; Picker, L. J., Profound early control of highly pathogenic SIV by an effector-memory T cell vaccine. *Nature* **2011,** *473* (7348), 523-527.
162. Hansen, S. G.; Piatak, M.; Ventura, A. B.; Hughes, C. M.; Gilbride, R. M.; Ford, J. C.; Oswald, K.; Shoemaker, R.; Li, Y.; Lewis, M. S.; Gilliam, A. N.; Xu, G.; Whizin, N.; Burwitz, B. J.; Planer, S. L.; Turner, J. M.; Legasse, A. W.; Axthelm, M. K.; Nelson, J. A.; Früh, K.; Sacha, J. B.; Estes, J. D.; Keele, B. F.; Edlefsen, P. T.; Lifson, J. D.; Picker, L. J., Immune clearance of highly pathogenic SIV infection. *Nature* **2013,** *502* (7469), 100-104.
163. Barouch, D. H.; Whitney, J. B.; Moldt, B.; Klein, F.; Oliveira, T. Y.; Liu, J.; Stephenson, K. E.; Chang, H.-W.; Shekhar, K.; Gupta, S.; Nkolola, J. P.; Seaman, M. S.; Smith, K. M.; Borducchi, E. N.; Cabral, C.; Smith, J. Y.; Blackmore, S.; Sanisetty, S.; Perry, J. R.; Beck, M.;

Lewis, M. G.; Rinaldi, W.; Chakraborty, A. K.; Poignard, P.; Nussenzweig, M. C.; Burton, D. R., Therapeutic efficacy of potent neutralizing HIV-1-specific monoclonal antibodies in SHIV-infected rhesus monkeys. *Nature* **2013,** *503*, 224.
164. Williams, L. D.; Ofek, G.; Schätzle, S.; McDaniel, J. R.; Lu, X.; Nicely, N. I.; Wu, L.; Lougheed, C. S.; Bradley, T.; Louder, M. K.; McKee, K.; Bailer, R. T.; O'Dell, S.; Georgiev, I. S.; Seaman, M. S.; Parks, R. J.; Marshall, D. J.; Anasti, K.; Yang, G.; Nie, X.; Tumba, N. L.; Wiehe, K.; Wagh, K.; Korber, B.; Kepler, T. B.; Munir Alam, S.; Morris, L.; Kamanga, G.; Cohen, M. S.; Bonsignori, M.; Xia, S.-M.; Montefiori, D. C.; Kelsoe, G.; Gao, F.; Mascola, J. R.; Moody, M. A.; Saunders, K. O.; Liao, H.-X.; Tomaras, G. D.; Georgiou, G.; Haynes, B. F., Potent and broad HIV-neutralizing antibodies in memory B cells and plasma. *Science Immunology* **2017,** *2* (7).
165. Schoofs, T.; Klein, F.; Braunschweig, M.; Kreider, E. F.; Feldmann, A.; Nogueira, L.; Oliveira, T.; Lorenzi, J. C. C.; Parrish, E. H.; Learn, G. H.; West, A. P.; Bjorkman, P. J.; Schlesinger, S. J.; Seaman, M. S.; Czartoski, J.; McElrath, M. J.; Pfeifer, N.; Hahn, B. H.; Caskey, M.; Nussenzweig, M. C., HIV-1 therapy with monoclonal antibody 3BNC117 elicits host immune responses against HIV-1. *Science* **2016,** *352* (6288), 997-1001.
166. Liao, H.-X.; Lynch, R.; Zhou, T.; Gao, F.; Alam, S. M.; Boyd, S. D.; Fire, A. Z.; Roskin, K. M.; Schramm, C. A.; Zhang, Z.; Zhu, J.; Shapiro, L.; Mullikin, J. C.; Gnanakaran, S.; Hraber, P.; Wiehe, K.; Kelsoe, G.; Yang, G.; Xia, S.-M.; Montefiori, D. C.; Parks, R.; Lloyd, K. E.; Scearce, R. M.; Soderberg, K. A.; Cohen, M.; Kamanga, G.; Louder, M. K.; Tran, L. M.; Chen, Y.; Cai, F.; Chen, S.; Moquin, S.; Du, X.; Joyce, M. G.; Srivatsan, S.; Zhang, B.; Zheng, A.; Shaw, G. M.; Hahn, B. H.; Kepler, T. B.; Korber, B. T. M.; Kwong, P. D.; Mascola, J. R.; Haynes, B. F., Co-evolution of a broadly neutralizing HIV-1 antibody and founder virus. *Nature* **2013,** *496* (7446), 469-476.
167. Velu, V.; Shetty, R. D.; Larsson, M.; Shankar, E. M., Role of PD-1 co-inhibitory pathway in HIV infection and potential therapeutic options. *Retrovirology* **2015,** *12* (1), 14.
168. Topalian, S. L.; Hodi, F. S.; Brahmer, J. R.; Gettinger, S. N.; Smith, D. C.; McDermott, D. F.; Powderly, J. D.; Carvajal, R. D.; Sosman, J. A.; Atkins, M. B., Safety, activity, and immune correlates of anti–PD-1 antibody in cancer. *New England Journal of Medicine* **2012,** *366* (26), 2443-2454.
169. Gardiner, D.; Lalezari, J.; Lawitz, E.; DiMicco, M.; Ghalib, R.; Reddy, K. R.; Chang, K.-M.; Sulkowski, M.; Marro, S. O.; Anderson, J.; He, B.; Kansra, V.; McPhee, F.; Wind-Rotolo, M.; Grasela, D.; Selby, M.; Korman, A. J.; Lowy, I., A Randomized, Double-Blind, Placebo-Controlled Assessment of BMS-936558, a Fully Human Monoclonal Antibody to Programmed Death-1 (PD-1), in Patients with Chronic Hepatitis C Virus Infection. *PLoS ONE* **2013,** *8* (5), e63818.
170. Hatano, H.; Jain, V.; Hunt, P. W.; Lee, T.-H.; Sinclair, E.; Do, T. D.; Hoh, R.; Martin, J. N.; McCune, J. M.; Hecht, F.; Busch, M. P.; Deeks, S. G., Cell-Based Measures of Viral Persistence Are Associated With Immune Activation and Programmed Cell Death Protein 1 (PD-1)–Expressing CD4(+) T cells. *The Journal of Infectious Diseases* **2013,** *208* (1), 50-56.
171. Velu, V.; Titanji, K.; Zhu, B.; Husain, S.; Pladevega, A.; Lai, L.; Vanderford, T. H.; Chennareddi, L.; Silvestri, G.; Freeman, G. J.; Ahmed, R.; Amara, R. R., Enhancing SIV-Specific Immunity In Vivo by PD-1 Blockade. *Nature* **2009,** *458* (7235), 206-210.
172. Dyavar Shetty, R.; Velu, V.; Titanji, K.; Bosinger, S. E.; Freeman, G. J.; Silvestri, G.; Amara, R. R., PD-1 blockade during chronic SIV infection reduces hyperimmune activation and

microbial translocation in rhesus macaques. *The Journal of Clinical Investigation* **2012,** *122* (5), 1712-1716.
173. Maude, S. L.; Frey, N.; Shaw, P. A.; Aplenc, R.; Barrett, D. M.; Bunin, N. J.; Chew, A.; Gonzalez, V. E.; Zheng, Z.; Lacey, S. F.; Mahnke, Y. D.; Melenhorst, J. J.; Rheingold, S. R.; Shen, A.; Teachey, D. T.; Levine, B. L.; June, C. H.; Porter, D. L.; Grupp, S. A., Chimeric Antigen Receptor T Cells for Sustained Remissions in Leukemia. *New England Journal of Medicine* **2014,** *371* (16), 1507-1517.
174. Ye, B.; Stary, C. M.; Li, X.; Gao, Q.; Kang, C.; Xiong, X., Engineering chimeric antigen receptor-T cells for cancer treatment. *Molecular Cancer* **2018,** *17* (1), 32.
175. Yang, O. O.; Tran, A.-C.; Kalams, S. A.; Johnson, R. P.; Roberts, M. R.; Walker, B. D., Lysis of HIV-1-infected cells and inhibition of viral replication by universal receptor T cells. *Proceedings of the National Academy of Sciences of the United States of America* **1997,** *94* (21), 11478-11483.
176. Deeks, S. G.; Wagner, B.; Anton, P. A.; Mitsuyasu, R. T.; Scadden, D. T.; Huang, C.; Macken, C.; Richman, D. D.; Christopherson, C.; June, C. H.; Lazar, R.; Broad, D. F.; Jalali, S.; Hege, K. M., A Phase II Randomized Study of HIV-Specific T-Cell Gene Therapy in Subjects with Undetectable Plasma Viremia on Combination Antiretroviral Therapy. *Molecular Therapy* **2002,** *5* (6), 788-797.
177. Zhen, A.; Peterson, C. W.; Carrillo, M. A.; Reddy, S. S.; Youn, C. S.; Lam, B. B.; Chang, N. Y.; Martin, H. A.; Rick, J. W.; Kim, J.; Neel, N. C.; Rezek, V. K.; Kamata, M.; Chen, I. S. Y.; Zack, J. A.; Kiem, H.-P.; Kitchen, S. G., Long-term persistence and function of hematopoietic stem cell-derived chimeric antigen receptor T cells in a nonhuman primate model of HIV/AIDS. *PLOS Pathogens* **2017,** *13* (12), e1006753.
178. Gavegnano, C.; Detorio, M.; Montero, C.; Bosque, A.; Planelles, V.; Schinazi, R. F., Ruxolitinib and Tofacitinib Are Potent and Selective Inhibitors of HIV-1 Replication and Virus Reactivation In Vitro. *Antimicrobial Agents and Chemotherapy* **2014,** *58* (4), 1977-1986.
179. Gavegnano, C.; Brehm, J. H.; Dupuy, F. P.; Talla, A.; Ribeiro, S. P.; Kulpa, D. A.; Cameron, C.; Santos, S.; Hurwitz, S. J.; Marconi, V. C.; Routy, J.-P.; Sabbagh, L.; Schinazi, R. F.; Sékaly, R. P., Novel mechanisms to inhibit HIV reservoir seeding using Jak inhibitors. *PLOS Pathogens* **2017,** *13* (12), e1006740.
180. Mousseau, G.; Kessing, C. F.; Fromentin, R.; Trautmann, L.; Chomont, N.; Valente, S. T., The Tat Inhibitor Didehydro-Cortistatin A Prevents HIV-1 Reactivation from Latency. *mBio* **2015,** *6* (4), e00465-15.
181. Kessing, C. F.; Nixon, C. C.; Li, C.; Tsai, P.; Takata, H.; Mousseau, G.; Ho, P. T.; Honeycutt, J. B.; Fallahi, M.; Trautmann, L.; Garcia, J. V.; Valente, S. T., In Vivo Suppression of HIV Rebound by Didehydro-Cortistatin A, a "Block-and-Lock" Strategy for HIV-1 Treatment. *Cell Reports 21* (3), 600-611.
182. Byrareddy, S. N.; Kallam, B.; Arthos, J.; Cicala, C.; Nawaz, F.; Hiatt, J.; Kersh, E. N.; McNicholl, J. M.; Hanson, D.; Reimann, K. A.; Brameier, M.; Walter, L.; Rogers, K.; Mayne, A. E.; Dunbar, P.; Villinger, T.; Little, D.; Parslow, T. G.; Santangelo, P. J.; Villinger, F.; Fauci, A. S.; Ansari, A. A., Targeting α4β7 integrin reduces mucosal transmission of simian immunodeficiency virus and protects gut-associated lymphoid tissue from infection. *Nat Med* **2014,** *advance online publication*.
183. Byrareddy, S. N.; Arthos, J.; Cicala, C.; Villinger, F.; Ortiz, K. T.; Little, D.; Sidell, N.; Kane, M. A.; Yu, J.; Jones, J. W.; Santangelo, P. J.; Zurla, C.; McKinnon, L. R.; Arnold, K. B.; Woody, C. E.; Walter, L.; Roos, C.; Noll, A.; Van Ryk, D.; Jelicic, K.; Cimbro, R.; Gumber, S.;

Reid, M. D.; Adsay, V.; Amancha, P. K.; Mayne, A. E.; Parslow, T. G.; Fauci, A. S.; Ansari, A. A., Virologic control in SIV+ macaques after antiretroviral and α4β7 antibody therapy. *Science* **2016,** *354* (6309), 197-202.
184. Lu, X.; Li, Z.; Li, Q.; Jiao, Y.; Ji, Y.; Zhang, H.; Liu, Z.; Li, W.; Wu, H., Preferential loss of gut-homing α4β7 CD4(+) T cells and their circulating functional subsets in acute HIV-1 infection. *Cellular and Molecular Immunology* **2016,** *13* (6), 776-784.
185. Arthos, J.; Cicala, C.; Martinelli, E.; Macleod, K.; Van Ryk, D.; Wei, D.; Xiao, Z.; Veenstra, T. D.; Conrad, T. P.; Lempicki, R. A.; McLaughlin, S.; Pascuccio, M.; Gopaul, R.; McNally, J.; Cruz, C. C.; Censoplano, N.; Chung, E.; Reitano, K. N.; Kottilil, S.; Goode, D. J.; Fauci, A. S., HIV-1 envelope protein binds to and signals through integrin α4β7, the gut mucosal homing receptor for peripheral T cells. *Nat Immunol* **2008,** *9* (3), 301-309.
186. Hill, A. L.; Rosenbloom, D. I. S.; Fu, F.; Nowak, M. A.; Siliciano, R. F., Predicting the outcomes of treatment to eradicate the latent reservoir for HIV-1. *Proceedings of the National Academy of Sciences* **2014,** *111* (37), 13475-13480.
187. Mout, R.; Ray, M.; Lee, Y.-W.; Scaletti, F.; Rotello, V. M., In Vivo Delivery of CRISPR/Cas9 for Therapeutic Gene Editing: Progress and Challenges. *Bioconjugate Chemistry* **2017,** *28* (4), 880-884.
188. Martinez-Picado, J.; Deeks, S. G., Persistent HIV-1 replication during antiretroviral therapy. *Current Opinion in HIV and AIDS* **2016,** *11* (4), 417-423.
189. das Neves, J.; Amiji, M. M.; Bahia, M. F.; Sarmento, B., Nanotechnology-based systems for the treatment and prevention of HIV/AIDS. *Advanced Drug Delivery Reviews* **2010,** *62* (4–5), 458-477.
190. Gu, F. X.; Karnik, R.; Wang, A. Z.; Alexis, F.; Levy-Nissenbaum, E.; Hong, S.; Langer, R. S.; Farokhzad, O. C., Targeted nanoparticles for cancer therapy. *Nano Today* **2007,** *2* (3), 14-21.
191. Shao, J.; Kraft, J. C.; Li, B.; Yu, J.; Freeling, J.; Koehn, J.; Ho, R. J. Y., Nanodrug formulations to enhance HIV drug exposure in lymphoid tissues and cells: clinical significance and potential impact on treatment and eradication of HIV/AIDS. *Nanomedicine* **2016,** *11* (5), 545-564.
192. Zhou, T.; Su, H.; Dash, P.; Lin, Z.; Dyavar Shetty, B. L.; Kocher, T.; Szlachetka, A.; Lamberty, B.; Fox, H. S.; Poluektova, L.; Gorantla, S.; McMillan, J.; Gautam, N.; Mosley, R. L.; Alnouti, Y.; Edagwa, B.; Gendelman, H. E., Creation of a nanoformulated cabotegravir prodrug with improved antiretroviral profiles. *Biomaterials* **2018,** *151* (Supplement C), 53-65.
193. Wen, L.; Qian, W.; Yuan, L.; Fei, Y.; Qi, L.; Bingjie, Q.; Lan, X.; Lu, L.; Shibo, J., A Nanoparticle-Encapsulated Non-Nucleoside Reverse-Transcriptase Inhibitor with Enhanced Anti-HIV-1 Activity and Prolonged Circulation Time in Plasma. *Current Pharmaceutical Design* **2015,** *21* (7), 925-935.
194. Buehler, D. C.; Marsden, M. D.; Shen, S.; Toso, D. B.; Wu, X.; Loo, J. A.; Zhou, Z. H.; Kickhoefer, V. A.; Wender, P. A.; Zack, J. A.; Rome, L. H., Bioengineered Vaults: Self-Assembling Protein Shell–Lipophilic Core Nanoparticles for Drug Delivery. *ACS Nano* **2014,** *8* (8), 7723-7732.
195. Bae, Y.; Diezi, T. A.; Zhao, A.; Kwon, G. S., Mixed polymeric micelles for combination cancer chemotherapy through the concurrent delivery of multiple chemotherapeutic agents. *Journal of Controlled Release* **2007,** *122* (3), 324-330.
196. Freeling, J. P.; Koehn, J.; Shu, C.; Sun, J.; Ho, R. J. Y., Long-acting three-drug combination anti-HIV nanoparticles enhance drug exposure in primate plasma and cells within lymph nodes and blood. *AIDS* **2014,** *28* (17), 2625-2627. .

197. Freeling, J. P.; Koehn, J.; Shu, C.; Sun, J.; Ho, R. J., Anti-HIV drug-combination nanoparticles enhance plasma drug exposure duration as well as triple-drug combination levels in cells within lymph nodes and blood in primates. *AIDS research and human retroviruses* **2015,** *31* (1), 107-114.
198. Shibata, A.; McMullen, E.; Pham, A.; Belshan, M.; Sanford, B.; Zhou, Y.; Goede, M.; Date, A. A.; Destache, C. J., Polymeric Nanoparticles Containing Combination Antiretroviral Drugs for HIV Type 1 Treatment. *AIDS Research and Human Retroviruses* **2013,** *29* (5), 746-754.
199. Prathipati, P. K.; Mandal, S.; Pon, G.; Vivekanandan, R.; Destache, C. J., Pharmacokinetic and Tissue Distribution Profile of Long Acting Tenofovir Alafenamide and Elvitegravir Loaded Nanoparticles in Humanized Mice Model. *Pharm Res* **2017**.
200. Nowacek, A. S.; Miller, R. L.; McMillan, J.; Kanmogne, G.; Kanmogne, M.; Mosley, R. L.; Ma, Z.; Graham, S.; Chaubal, M.; Werling, J., NanoART synthesis, characterization, uptake, release and toxicology for human monocyte–macrophage drug delivery. *Nanomedicine* **2009,** *4* (8), 903-917.
201. Roy, U.; McMillan, J.; Alnouti, Y.; Gautum, N.; Smith, N.; Balkundi, S.; Dash, P.; Gorantla, S.; Martinez-Skinner, A.; Meza, J., Pharmacodynamic and antiretroviral activities of combination nanoformulated antiretrovirals in HIV-1–infected human peripheral blood lymphocyte–reconstituted mice. *The Journal of infectious diseases* **2012,** *206* (10), 1577-1588.
202. Chiodo, F.; Marradi, M.; Calvo, J.; Yuste, E.; Penadés, S., Glycosystems in nanotechnology: Gold glyconanoparticles as carrier for anti-HIV prodrugs. *Beilstein Journal of Organic Chemistry* **2014,** *10*, 1339-1346.
203. Kraft, J. C.; McConnachie, L. A.; Koehn, J.; Kinman, L.; Sun, J.; Collier, A. C.; Collins, C.; Shen, D. D.; Ho, R. J. Y., Mechanism-based pharmacokinetic (MBPK) models describe the complex plasma kinetics of three antiretrovirals delivered by a long-acting anti-HIV drug combination nanoparticle formulation. *Journal of Controlled Release* **2018,** *275*, 229-241.
204. Tang, X.; Liang, Y.; Liu, X.; Zhou, S.; Liu, L.; Zhang, F.; Xie, C.; Cai, S.; Wei, J.; Zhu, Y.; Hou, W., PLGA-PEG Nanoparticles Coated with Anti-CD45RO and Loaded with HDAC Plus Protease Inhibitors Activate Latent HIV and Inhibit Viral Spread. *Nanoscale Research Letters* **2015,** *10* (1), 413.
205. Li, W.; Yu, F.; Wang, Q.; Qi, Q.; Su, S.; Xie, L.; Lu, L.; Jiang, S., Co-delivery of HIV-1 entry inhibitor and nonnucleoside reverse transcriptase inhibitor shuttled by nanoparticles: cocktail therapeutic strategy for antiviral therapy. *AIDS* **2016,** *30* (6), 827-838.
206. Kumar, P.; Lakshmi, Y. S.; Kondapi, A. K., Triple Drug Combination of Zidovudine, Efavirenz and Lamivudine Loaded Lactoferrin Nanoparticles: an Effective Nano First-Line Regimen for HIV Therapy. *Pharm Res* **2017,** *34* (2), 257-268.
207. Jayant, R. D.; Atluri, V. S. R.; Tiwari, S.; Pilakka-Kanthikeel, S.; Kaushik, A.; Yndart, A.; Nair, M., Novel nanoformulation to mitigate co-effects of drugs of abuse and HIV-1 infection: towards the treatment of NeuroAIDS. *J. Neurovirol.* **2017,** *23* (4), 603-614.
208. Zhou, J.; Neff, C. P.; Liu, X.; Zhang, J.; Li, H.; Smith, D. D.; Swiderski, P.; Aboellail, T.; Huang, Y.; Du, Q.; Liang, Z.; Peng, L.; Akkina, R.; Rossi, J. J., Systemic Administration of Combinatorial dsiRNAs via Nanoparticles Efficiently Suppresses HIV-1 Infection in Humanized Mice. *Molecular Therapy* **2011,** *19* (12), 2228-2238.
209. Weber, N.; Ortega, P.; Clemente, M. I.; Shcharbin, D.; Bryszewska, M.; de la Mata, F. J.; Gómez, R.; Muñoz-Fernández, M. A., Characterization of carbosilane dendrimers as effective

carriers of siRNA to HIV-infected lymphocytes. *Journal of Controlled Release* **2008,** *132* (1), 55-64.
210. Zhou, J.; Shu, Y.; Guo, P.; Smith, D. D.; Rossi, J. J., Dual functional RNA nanoparticles containing phi29 motor pRNA and anti-gp120 aptamer for cell-type specific delivery and HIV-1 Inhibition. *Methods* **2011,** *54* (2), 284-294.
211. Neff, C. P.; Zhou, J.; Remling, L.; Kuruvilla, J.; Zhang, J.; Li, H.; Smith, D. D.; Swiderski, P.; Rossi, J. J.; Akkina, R., An Aptamer-siRNA Chimera Suppresses HIV-1 Viral Loads and Protects from Helper CD4+T Cell Decline in Humanized Mice. *Science Translational Medicine* **2011,** *3* (66), 66ra6.
212. Klein, F.; Halper-Stromberg, A.; Horwitz, J. A.; Gruell, H.; Scheid, J. F.; Bournazos, S.; Mouquet, H.; Spatz, L. A.; Diskin, R.; Abadir, A.; Zang, T.; Dorner, M.; Billerbeck, E.; Labitt, R. N.; Gaebler, C.; Marcovecchio, P.; Incesu, R.-B.; Eisenreich, T. R.; Bieniasz, P. D.; Seaman, M. S.; Bjorkman, P. J.; Ravetch, J. V.; Ploss, A.; Nussenzweig, M. C., HIV therapy by a combination of broadly neutralizing antibodies in humanized mice. *Nature* **2012,** *492* (7427), 10.1038/nature11604.
213. Freund, N. T.; Wang, H.; Scharf, L.; Nogueira, L.; Horwitz, J. A.; Bar-On, Y.; Golijanin, J.; Sievers, S. A.; Sok, D.; Cai, H.; Cesar Lorenzi, J. C.; Halper-Stromberg, A.; Toth, I.; Piechocka-Trocha, A.; Gristick, H. B.; van Gils, M. J.; Sanders, R. W.; Wang, L.-X.; Seaman, M. S.; Burton, D. R.; Gazumyan, A.; Walker, B. D.; West, A. P.; Bjorkman, P. J.; Nussenzweig, M. C., Coexistence of potent HIV-1 broadly neutralizing antibodies and antibody-sensitive viruses in a viremic controller. *Science Translational Medicine* **2017,** *9* (373).
214. Horwitz, J. A.; Halper-Stromberg, A.; Mouquet, H.; Gitlin, A. D.; Tretiakova, A.; Eisenreich, T. R.; Malbec, M.; Gravemann, S.; Billerbeck, E.; Dorner, M.; Büning, H.; Schwartz, O.; Knops, E.; Kaiser, R.; Seaman, M. S.; Wilson, J. M.; Rice, C. M.; Ploss, A.; Bjorkman, P. J.; Klein, F.; Nussenzweig, M. C., HIV-1 suppression and durable control by combining single broadly neutralizing antibodies and antiretroviral drugs in humanized mice. *Proceedings of the National Academy of Sciences of the United States of America* **2013,** *110* (41), 16538-16543.
215. Li, M.; Li, H.; Rossi, J. J., RNAi in Combination with a Ribozyme and TAR Decoy for Treatment of HIV Infection in Hematopoietic Cell Gene Therapy. *Annals of the New York Academy of Sciences* **2006,** *1082* (1), 172-179.
216. Lee, A. L. Z.; Wang, Y.; Cheng, H. Y.; Pervaiz, S.; Yang, Y. Y., The co-delivery of paclitaxel and Herceptin using cationic micellar nanoparticles. *Biomaterials* **2009,** *30* (5), 919-927.
217. Jang, M.; Han, H. D.; Ahn, H. J., A RNA nanotechnology platform for a simultaneous two-in-one siRNA delivery and its application in synergistic RNAi therapy. *Scientific Reports* **2016,** *6*, 32363.
218. Chen, Y.; Zhu, X.; Zhang, X.; Liu, B.; Huang, L., Nanoparticles Modified With Tumor-targeting scFv Deliver siRNA and miRNA for Cancer Therapy. *Molecular Therapy 18* (9), 1650-1656.
219. Kim, S.-S.; Peer, D.; Kumar, P.; Subramanya, S.; Wu, H.; Asthana, D.; Habiro, K.; Yang, Y.-G.; Manjunath, N.; Shimaoka, M.; Shankar, P., RNAi-mediated CCR5 Silencing by LFA-1-targeted Nanoparticles Prevents HIV Infection in BLT Mice. *Mol Ther* **2009,** *18* (2), 370-376.
220. Endsley, A. N.; Ho, R. J. Y., Design and Characterization of Novel Peptide-Coated Lipid Nanoparticles for Targeting Anti-HIV Drug to CD4 Expressing Cells. *The AAPS Journal* **2012,** *14* (2), 225-235.

221. Endsley, A. N.; Ho, R. J. Y., Enhanced anti-HIV efficacy of Indinavir after inclusion in CD4 targeted lipid nanoparticles. *Journal of acquired immune deficiency syndromes (1999)* **2012,** *61* (4), 417-424.
222. Puligujja, P.; McMillan, J.; Kendrick, L.; Li, T.; Balkundi, S.; Smith, N.; Veerubhotla, R. S.; Edagwa, B. J.; Kabanov, A. V.; Bronich, T.; Gendelman, H. E.; Liu, X.-M., Macrophage Folate Receptor-Targeted Antiretroviral Therapy Facilitates Drug Entry, Retention, Antiretroviral Activities and Biodistribution for Reduction of Human Immunodeficiency Virus Infections. *Nanomedicine : nanotechnology, biology, and medicine* **2013,** *9* (8), 1263-1273.
223. Puligujja, P.; Araínga, M.; Dash, P.; Palandri, D.; Mosley, R. L.; Gorantla, S.; Poluektova, L.; McMillan, J.; Gendelman, H. E., Pharmacodynamics of folic acid-receptor targeted antiretroviral nanotherapy in HIV-1-infected humanized mice. *Antiviral research* **2015,** *120*, 85-88.
224. Gu, J.; Al-Bayati, K.; Ho, E. A., Development of antibody-modified chitosan nanoparticles for the targeted delivery of siRNA across the blood-brain barrier as a strategy for inhibiting HIV replication in astrocytes. *Drug Delivery and Translational Research* **2017,** *7* (4), 497-506.
225. Kinman, L.; Brodie, S. J.; Tsai, C. C.; Bui, T.; Larsen, K.; Schmidt, A.; Anderson, D.; Morton, W. R.; Hu, S.-L.; Ho, R. J. Y., Lipid–Drug Association Enhanced HIV-1 Protease Inhibitor Indinavir Localization in Lymphoid Tissues and Viral Load Reduction: A Proof of Concept Study in HIV-2287-Infected Macaques. *JAIDS Journal of Acquired Immune Deficiency Syndromes* **2003,** *34* (4), 387-397.
226. Saiyed, Z. M.; Gandhi, N. H.; Nair, M., Magnetic nanoformulation of azidothymidine 5′-triphosphate for targeted delivery across the blood-brain barrier. *Int J Nanomedicine* **2010,** *5* (1), 157-66.
227. Chiappetta, D. A.; Hocht, C.; Opezzo, J. A. W.; Sosnik, A., Intranasal administration of antiretroviral-loaded micelles for anatomical targeting to the brain in HIV. *Nanomedicine* **2013,** *8* (2), 223-237.
228. Prabhakar, K.; Afzal, S. M.; Kumar, P. U.; Rajanna, A.; Kishan, V., Brain delivery of transferrin coupled indinavir submicron lipid emulsions—Pharmacokinetics and tissue distribution. *Colloids and Surfaces B: Biointerfaces* **2011,** *86* (2), 305-313.
229. Vyas, T. K.; Shahiwala, A.; Amiji, M. M., Improved oral bioavailability and brain transport of Saquinavir upon administration in novel nanoemulsion formulations. *International Journal of Pharmaceutics* **2008,** *347* (1), 93-101.
230. Gerson, T.; Makarov, E.; Senanayake, T. H.; Gorantla, S.; Poluektova, L. Y.; Vinogradov, S. V., Nano-NRTIs demonstrate low neurotoxicity and high antiviral activity against HIV infection in the brain. *Nanomedicine: Nanotechnology, Biology and Medicine* **2014,** *10* (1), 177-185.
231. Shegokar, R.; Singh, K. K., Surface modified nevirapine nanosuspensions for viral reservoir targeting: In vitro and in vivo evaluation. *International journal of pharmaceutics* **2011,** *421* (2), 341-352.
232. Kuo, Y.-C.; Kuo, C.-Y., Electromagnetic interference in the permeability of saquinavir across the blood–brain barrier using nanoparticulate carriers. *International journal of pharmaceutics* **2008,** *351* (1), 271-281.
233. Kuo, Y.-C.; Su, F.-L., Transport of stavudine, delavirdine, and saquinavir across the blood–brain barrier by polybutylcyanoacrylate, methylmethacrylate-sulfopropylmethacrylate, and solid lipid nanoparticles. *International journal of pharmaceutics* **2007,** *340* (1), 143-152.

234. Rao, K. S.; Reddy, M. K.; Horning, J. L.; Labhasetwar, V., TAT-conjugated nanoparticles for the CNS delivery of anti-HIV drugs. *Biomaterials* **2008,** *29* (33), 4429-4438.
235. Kanmogne, G. D.; Singh, S.; Roy, U.; Liu, X.; McMillan, J.; Gorantla, S.; Balkundi, S.; Smith, N.; Alnouti, Y.; Gautam, N.; Zhou, Y.; Poluektova, L.; Kabanov, A.; Bronich, T.; Gendelman, H. E., Mononuclear phagocyte intercellular crosstalk facilitates transmission of cell-targeted nanoformulated antiretroviral drugs to human brain endothelial cells. *International Journal of Nanomedicine* **2012,** *7*, 2373-2388.
236. Jiménez, J. L.; Clemente, M. I.; Weber, N. D.; Sanchez, J.; Ortega, P.; de la Mata, F. J.; Gómez, R.; García, D.; López-Fernández, L. A.; Muñoz-Fernández, M. Á., Carbosilane Dendrimers to Transfect Human Astrocytes with Small Interfering RNA Targeting Human Immunodeficiency Virus. *BioDrugs* **2010,** *24* (5), 331-343.
237. Serramía, M. J.; Álvarez, S.; Fuentes-Paniagua, E.; Clemente, M. I.; Sánchez-Nieves, J.; Gómez, R.; de la Mata, J.; Muñoz-Fernández, M. Á., In vivo delivery of siRNA to the brain by carbosilane dendrimer. *Journal of Controlled Release* **2015,** *200*, 60-70.
238. Ramishetti, S.; Kedmi, R.; Goldsmith, M.; Leonard, F.; Sprague, A. G.; Godin, B.; Gozin, M.; Cullis, P. R.; Dykxhoorn, D. M.; Peer, D., Systemic Gene Silencing in Primary T Lymphocytes Using Targeted Lipid Nanoparticles. *ACS Nano* **2015**.
239. Cao, S.; Jiang, Y.; Levy Claire, N.; Hughes Sean, M.; Zhang, H.; Hladik, F.; Woodrow Kim, A., Optimization and comparison of CD4-targeting lipid–polymer hybrid nanoparticles using different binding ligands. *Journal of Biomedical Materials Research Part A* **2017,** *106* (5), 1177-1188.
240. Hu, C.-M. J.; Kaushal, S.; Cao, H. S. T.; Aryal, S.; Sartor, M.; Esener, S.; Bouvet, M.; Zhang, L., Half-Antibody Functionalized Lipid−Polymer Hybrid Nanoparticles for Targeted Drug Delivery to Carcinoembryonic Antigen Presenting Pancreatic Cancer Cells. *Molecular Pharmaceutics* **2010,** *7* (3), 914-920.
241. Kaur, C. D.; Nahar, M.; Jain, N. K., Lymphatic targeting of zidovudine using surface-engineered liposomes. *Journal of drug targeting* **2008,** *16* (10), 798-805.
242. Kaminskas, L. M.; Kota, J.; McLeod, V. M.; Kelly, B. D.; Karellas, P.; Porter, C. J. H., PEGylation of polylysine dendrimers improves absorption and lymphatic targeting following SC administration in rats. *Journal of Controlled Release* **2009,** *140* (2), 108-116.
243. Richter, W. F.; Bhansali, S. G.; Morris, M. E., Mechanistic Determinants of Biotherapeutics Absorption Following SC Administration. *The AAPS Journal* **2012,** *14* (3), 559-570.
244. Kunisawa, J.; Kurashima, Y.; Kiyono, H., Gut-associated lymphoid tissues for the development of oral vaccines. *Advanced Drug Delivery Reviews* **2012,** *64* (6), 523-530.
245. Giannasca, P. J.; Giannasca, K. T.; Leichtner, A. M.; Neutra, M. R., Human Intestinal M Cells Display the Sialyl Lewis A Antigen. *Infection and Immunity* **1999,** *67* (2), 946-953.
246. Aungst, B. J., P-glycoprotein, secretory transport, and other barriers to the oral delivery of anti-HIV drugs. *Advanced Drug Delivery Reviews* **1999,** *39* (1–3), 105-116.
247. Nowacek, A.; Gendelman, H. E., NanoART, neuroAIDS and CNS drug delivery. *Nanomedicine* **2009,** *4* (5), 557-574.
248. Yin, H.; Kauffman, K. J.; Anderson, D. G., Delivery technologies for genome editing. *Nature Reviews Drug Discovery* **2017,** *16*, 387.
249. Yin, H.; Kanasty, R. L.; Eltoukhy, A. A.; Vegas, A. J.; Dorkin, J. R.; Anderson, D. G., Non-viral vectors for gene-based therapy. *Nature Reviews Genetics* **2014,** *15*, 541.

250. LaFountaine, J. S.; Fathe, K.; Smyth, H. D. C., Delivery and therapeutic applications of gene editing technologies ZFNs, TALENs, and CRISPR/Cas9. *International Journal of Pharmaceutics* **2015,** *494* (1), 180-194.
251. Mishra, V.; Kesharwani, P.; Jain, N. K., siRNA nanotherapeutics: a Trojan horse approach against HIV. *Drug Discovery Today* **2014,** *19* (12), 1913-1920.
252. Adesina, S. K.; Akala, E. O., Nanotechnology approaches for the delivery of exogenous siRNA for HIV therapy. *Molecular pharmaceutics* **2015,** *12* (12), 4175-4187.
253. Perisé-Barrios, A. J.; Jiménez, J. L.; Domínguez-Soto, A.; de la Mata, F. J.; Corbí, A. L.; Gomez, R.; Muñoz-Fernandez, M. Á., Carbosilane dendrimers as gene delivery agents for the treatment of HIV infection. *Journal of Controlled Release* **2014,** *184*, 51-57.
254. Shcharbin, D.; Pedziwiatr, E.; Nowacka, O.; Kumar, M.; Zaborski, M.; Ortega, P.; Javier de la Mata, F.; Gómez, R.; Muñoz-Fernandez, M. A.; Bryszewska, M., Carbosilane dendrimers NN8 and NN16 form a stable complex with siGAG1. *Colloids and Surfaces B: Biointerfaces* **2011,** *83* (2), 388-391.
255. Briz, V.; Serramia, M. J.; Madrid, R.; Hameau, A.; Anne-Marie, C.; Majoral, J. P.; Munoz-Fernandez, M. A., Validation of a Generation 4 Phosphorus-Containing Polycationic Dendrimer for Gene Delivery Against HIV-1. *Current Medicinal Chemistry* **2012,** *19* (29), 5044-5051.
256. Lee, K.; Conboy, M.; Park, H. M.; Jiang, F.; Kim, H. J.; Dewitt, M. A.; Mackley, V. A.; Chang, K.; Rao, A.; Skinner, C.; Shobha, T.; Mehdipour, M.; Liu, H.; Huang, W.-c.; Lan, F.; Bray, N. L.; Li, S.; Corn, J. E.; Kataoka, K.; Doudna, J. A.; Conboy, I.; Murthy, N., Nanoparticle delivery of Cas9 ribonucleoprotein and donor DNA in vivo induces homology-directed DNA repair. *Nature Biomedical Engineering* **2017,** *1* (11), 889-901.
257. Park, Y.-M.; Lee, S. J.; Kim, Y. S.; Lee, M. H.; Cha, G. S.; Jung, I. D.; Kang, T. H.; Han, H. D., Nanoparticle-Based Vaccine Delivery for Cancer Immunotherapy. *Immune Network* **2013,** *13* (5), 177-183.
258. Friedman, C. F.; Proverbs-Singh, T. A.; Postow, M. A., Treatment of the immune-related adverse effects of immune checkpoint inhibitors: A review. *JAMA Oncology* **2016,** *2* (10), 1346-1353.
259. Kosmides, A. K.; Sidhom, J.-W.; Fraser, A.; Bessell, C. A.; Schneck, J. P., Dual Targeting Nanoparticle Stimulates the Immune System To Inhibit Tumor Growth. *ACS Nano* **2017,** *11* (6), 5417-5429.
260. Schmid, D.; Park, C. G.; Hartl, C. A.; Subedi, N.; Cartwright, A. N.; Puerto, R. B.; Zheng, Y.; Maiarana, J.; Freeman, G. J.; Wucherpfennig, K. W.; Irvine, D. J.; Goldberg, M. S., T cell-targeting nanoparticles focus delivery of immunotherapy to improve antitumor immunity. *Nature Communications* **2017,** *8* (1), 1747.
261. Smith, T. T.; Stephan, S. B.; Moffett, H. F.; McKnight, L. E.; Ji, W.; Reiman, D.; Bonagofski, E.; Wohlfahrt, M. E.; Pillai, S. P. S.; Stephan, M. T., In situ programming of leukaemia-specific T cells using synthetic DNA nanocarriers. *Nat Nano* **2017,** *12* (8), 813-820.

Chapter 3. Core-shell nanoparticles for targeted and combination antiretroviral activity in gut-homing T cells

Adapted from: Cao S, Jiang Y, Zhang H, Kondza N, Woodrow KA. Core-shell nanoparticles for targeted and combination antiretroviral activity in gut-homing T cells. *Nanomedicine: Nanotechnology, Biology and Medicine.* 2018;14(7):2143-2153.

3.1 Abstract

A major sanctuary site for HIV infection is the gut-associated lymphoid tissue (GALT). The α4β7 integrin gut homing receptor is a promising therapeutic target for the virus reservoir because it leads to migration of infected cells to the GALT and facilitates HIV infection. Here, we developed a core-shell nanoparticle incorporating the α4β7 monoclonal antibody (mAb) as a dual-functional ligand for selectively targeting a protease inhibitor (PI) to gut-homing T cells in the GALT while simultaneously blocking HIV infection. Our nanoparticles significantly reduced cytotoxicity of the PI and enhanced its *in vitro* antiviral activity in combination with α4β7 mAb. We demonstrate targeting function of our nanocarriers in a human T cell line and primary cells isolated from macaque ileum, and observed higher *in vivo* biodistribution to the murine small intestines where they accumulate in α4β7+ cells. Our LCNP shows the potential to co-deliver ARVs and mAbs for eradicating HIV reservoirs.

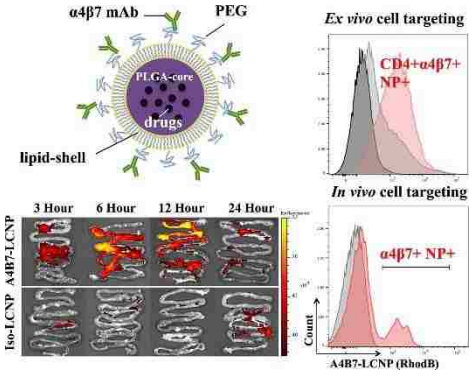

3.2 Introduction

Combination antiretroviral therapy (cART) achieves complete virus suppression to undetectable levels in peripheral blood but does not lead to complete eradication of HIV infection.[1] The existence of viral reservoirs is the main obstacle to HIV cure.[2-4] The gut-associated lymphoid tissue (GALT) is one of the largest lymphatic tissues in the human body where elevated levels of viral replication and depletion of CD4+ T cells occur in HIV-infected patients.[5-8] HIV reservoirs can be quickly established in the GALT, where the virus becomes resistant despite long-term cART.[9] Several mechanisms have been proposed to explain persistent HIV infection within the environment of the GALT. First, infected CD4+ T cells are able to traffic to the GALT from other parts of the body mediated by the α4β7 integrin gut homing receptor.[10] α4β7 mediates migration by binding to the mucosal vascular addressin cell adhesion molecule-1 (MAdCAM-1) expressed by endothelial cells of venules associated with the GALT.[11-12] Second, gut mucosal CD4+ lymphocytes are uniquely susceptible to HIV-1 infection,[7, 13-14] which may be explained by a higher expression of chemokine receptor CCR5 (a major coreceptor for HIV infection) and persistent activation and inflammation due to constant exposure to food and microbial antigens.[13, 15] In addition, studies have shown that α4β7 can serve as a receptor for the HIV-1 envelope protein gp120 and promote the upregulation of lymphocyte function-associated antigen-1 (LFA-1) to facilitate cell-to-cell spreading of HIV-1.[16] Resting central memory α4β7+ CD4+ T cells have been shown to be the predominant target of SIV during acute infection.[7, 17] These cells become latently infected and have the potential to traffic to and reside in the GALT because of the expression of α4β7. Lastly, concentrations of antiretroviral drugs (ARVs) in lymphatic tissues, including the GALT, are lower compared to those in the peripheral blood.[18] This may attribute to both early reservoir establishment and virus resistance in patients under

suppressive cART.[19] Thus, enhancement of ARV drug delivery to these α4β7-expressing gut-homing T cells and the GALT during the early phase of infection might be a strategy to reduce the reservoir size. Collectively, these findings suggest that the α4β7 cell marker is a promising therapeutic for HIV reservoir eradication by targeting gut-homing T cells.

Nanoparticle technology has been used with great promise in enhancing the efficacy of antiretroviral therapies.[20-21] We have previously shown that nanocarriers (NCs) formulated with physicochemically diverse ARVs delivered in combination result in higher intracellular drug concentrations, and lead to more synergistically potent inhibition of HIV-1 infection in cell and tissue cultures.[22] Nanoparticles surface conjugated with targeting ligand have been used to promote the accumulation of nanoparticles to specific cells or tissues.[23-24] A variety of nanocarrier-based delivery systems have been used to target anti-HIV drugs to cellular or anatomical viral reservoirs utilizing either peptides or antibodies as the ligands.[25-32] Immunoliposomes (antibody-coupled liposomes) have been the most widely investigated for this purpose and offer great flexibility for conjugating with targeted ligands.[33-35] However, liposomes lack structural integrity and consistent storage stability.[36] Lipid-polymer hybrid nanoparticles, that consist of a polymer core and a lipid shell, combine the advantageous properties of both polymeric nanoparticles and liposomes such as biocompatibility, biodegradability, multiple drug encapsulation, high drug loading, sustained drug-release profiles, high stability, functionalizable surfaces, *etc*.[37-41]

Here, we developed a nanocarrier-based delivery system using the α4β7 mAb for its dual function to target ARV drugs to gut-homing T cells and blocking HIV infection. We synthesized a core-shell nanoparticle consisting of a poly(lactic-*co*-glycolic) acid (PLGA) core and a phospholipid bilayer shell coated with an outer layer of polyethylene glycol (PEG) that was used

for direct conjugation of α4β7 mAbs (A4B7-LCNPs). Our LCNPs were designed such that the lipid shell, including the attached antibody, would delaminate from these nanoparticles and be available to block virus entry.[42] A protease inhibitor was also encapsulated in targeted LCNPs to prevent infected cells from producing new HIV virions in the GALT. Our *in vitro* and *ex vivo* data show that tipranavir (TPV) loaded A4B7-LCNPs exhibit the dual function of targeting CD4+α4β7+ cells and anti-HIV activity. We also found that A4B7-LCNPs accumulated with α4β7+ gut T cells of the small intestine after intravenous administration to mice. These data demonstrate that our LCNP delivery system has the potential to co-deliver ARV drugs and mAbs to anatomical and cellular HIV reservoirs for the purpose of reducing reservoir size and potentially eradicating the virus.

3.3 Materials and methods

3.3.1 *Materials*

PLGA (75:25 L:G; ester-terminated, inherent viscosity range: 0.55-0.75 dL/g in choloroform) was purchased from Lactel. All lipids for the nanoparticle synthesize were purchased from Avanti Polar Lipids, including DOPC, DOTAP, DSPE-PEG, DSPE-PEG-MAL, DOPC-NBD, and DSPE-PEG-CF. TPV was provided by NIH AIDS Reagent Program. Rhesus recombinant anti-α4β7 antibody, rhesus recombinant anti-α4β7 conjugated to APC (APC anti-α4β7), and rhesus recombinant IgG1 isotype control antibodies were purchased from NIH Nonhuman Primate Reagent Resource. FITC anti-human CD4 OKT4 clone, FITC anti-human CD4, APC anti-mouse LPAM-1 (integrin α4β7), APC Rat IgG2a isotype control and FITC Rat IgG2a isotype control antibodies were purchased from eBioscience. Anti-mouse LPAM-1(integrin α4β7) and mouse IgG2a isotype control antibodies were purchased from BioXCell. All anti-human and rhesus recombinant antibodies were used for *in vitro* human T cell lines and *ex vivo*

rhesus macaque ilieum studies, and anti-mouse antibodies were used for *in vivo* mice studies. RPMI 1640 containing 2mM L-glutamine and 25mM HEPES, DPBS, heat-inactivated fetal bovine serum (FBS), Penicillin-Streptomycin (10,000 U/mL), DiR dye, LIVE/DEAD® Fixable Violet Dead Cell Stain Kit, DyLight™633 and 680 amine-reactive dye were purchased from ThermoFisher. Human serum, Dispase II, Collagenase D, DNase I grade II from bovine pancreas and Percoll were purchased from Sigma. HIV-1 p24 ELISA kit was purchased from B-Bridge International. All other chemicals were purchased from Sigma-Aldrich and Fisher Scientific unless otherwise specified.

3.3.2 *Preparation of LCNPs*

LCNPs were prepared using a modified single emulsion solvent-evaporation method.[43] Briefly, the lipid mixtures (DOPC, DOTAP and DSPE-PEG-Mal at 4:4:1 molar ratio) in chloroform were dried under nitrogen, and left under high vacuum prior to usage. Lipid suspension was made by adding Milli-Q water into dried lipids and vortexing until lipids dispersed well in the water. PLGA was dissolved in ethyl acetate (10 mg/mL) and was added drop-wise to the lipid suspension at the volume ratio of 1:2 (v/v, PLGA:lipids) while vortexing. The mixture was then homogenized using a probe sonicator (500W, Ultrasonic Processor GEX500) and all residual organic solvent was evaporated by rotary evaporation (Rotavapor R-210, BUCHI). Nanoparticles were then washed by centrifugation at 14,000 rpm for 10 min at 4 °C and resuspended in water until use. For rhodamine-B fluorescent LCNPs, we first synthesized a rhodamine-PLGA conjugate using methods described by Costanitino *et al*.[44] Then rhodamine-B-PLGA conjugate (10 mg/mL, loading of 0.169% (w/w) rhodamine-B:PLGA) were used to fabricate LCNPs as described above. For DiR or DiD fluorescent LCNPs, 1 % (w/w, DiR or DiD/PLGA) DiR or DiD dissolved in ethyl acetate was added into PLGA/ethyl acetate solution right before the

synthesis as described above. For drug-loaded LCNPs, we dissolved TPV at 10% (w/w, TPV/PLGA) theoretical loading to the PLGA/ethyl acetate solution following LCNP synthesis.

3.3.3 *Preparation of liposomes*

Liposomes using same lipid composition were prepared to encapsulate TPV, as a comparison with our LCNPs. Liposomes were synthesized using the same amount and ratio of three lipids (DOPC, DOTAP, and DSPE-PEG-MAL). Total 5 mg lipids in chloroform and 2 mg TPV in ethyl acetate (same amount in TPV/LCNP synthesis) were mixed and dried under nitrogen and high vacuum. Lipids + TPV suspension was made by adding Milli-Q water into dried lipids and vortexing until lipids dispersed well in the water. Then the mixture was homogenized using a probe sonicator at 38% amplitude for three rounds at 20s per round. The lipid suspension was forced through a 2.0 μm filter to generate TPV loaded liposomes and to remove crystalized (unencapsulated) TPV.

3.3.4 *Conjugation of α4β7 mAb to LCNPs*

Thiolated α4β7 mAb was linked *via* maleimide-functionalized DSPE-PEG in the LCNP lipid layer shell. In brief, α4β7 mAb was thiolated using 10 molar excess of Traut's reagent in PBS buffer with ethylenediaminetetraacetic acid (EDTA) (5 mM, pH 8.0) for 1 hour. Thiolated α4β7 mAb was then purified and incubated with LCNPs in sodium phosphate buffer (50 mM, pH 7.5) at different molar ratios (100:1 ~ 2000:1, mAb:LCNP) for 2-3 hours. Final α4β7 mAb conjugated LCNPs (A4B7-LCNPs) were centrifuged at 4,700 rpm for 10 min or dialyzed against MilliQ water using a 300 kD cellulose ester dialysis tube (Spectrum) to remove unreacted antibodies and then resuspended in water at 4°C until further use. Isotype control IgG antibodies

were also thiolated and conjugated to the same LCNPs following the same process, and used as control in this study (Iso-LCNPs).

3.3.5 *Characterization of LCNP formulations*

The size, PDI and ζ-potential of all formulations (LCNPs, A4B7-LCNPs, TPV loaded LCNPs and TPV loaded A4B7-LCNPs) were measured by dynamic light scattering (DLS) using a Zetasizer Nano ZS90 (Malvern Instruments), and the size was also measured by NanoSight NS300 (Malvern instruments). Nanoparticles were suspended in Milli-Q water for size and PDI measurement or in NaCl buffer (10 mM, pH 7.4) for ζ-potential measurement. A drop of aqueous solution containing LCNPs or A4B7-LCNPs was dried on a sample grid and imaged using a FEI 200 kV Tecnai G2 TEM at the University of Washington Molecular Analysis Facility.

3.3.6 *Antibody conjugation efficiency*

The maximum amount of antibody that can be conjugated to the LCNP surface was measured by labeling α4β7 mAb with DyLight 633 dye and then conjugating it to LCNPs as previously described. After synthesis, A4B7-LCNPs were analyzed by flow cytometry (FACSCanto II) and mean fluorescent intensities from antibodies on the particles were detected and analyzed using FlowJo 10.0. The conjugation efficiency, which refers to the ratio of antibody conjugated to LCNPs to total input antibody, was determined by measuring amount of successfully conjugated fluorescent mAb after high-speed centrifuging of A4B7-LCNPs by a fluorescence plate reader (Infinite® 200 Pro, TECAN, Mañnedorf, Switzerland). The concentrations of A4B7-LCNPs were determined by Nanoparticle Tracking Analysis (NTA) using NanoSight NS300. To further measure the antibody loading, A4B7-LCNPs were lyophilized and weighted, followed by

measuring the antibody content using a Micro BCA Protein Assay Kit (Thermo Scientific). The loading was calculated as the ratio of the amount of α4β7 mAb to the total mass of A4B7-LCNPs.

3.3.7 *TPV loading analysis*

TPV loading was measured by dissolving a known mass of lyophilized TPV loaded LCNP, A4B7-LCNP, or liposomes in DMSO and analyzing the samples using an integrated reversed-phase high-performance liquid chromatography (HPLC) system. Briefly, the separation was made on a C18 column (5 µm, 250 × 4.6 mm, Phenomenex) at 30 °C using sodium acetate buffer (pH 5): methanol: acetonitrile (35:30:35, v/v/v) at the flow rate of 1 mL/min, based on a method previously established for detecting TPV.[45] Detections were performed at wavelengths of 245 nm and sample retention and run-time for TPV were 15/25 min. The drug loadings (DL) are calculated using Eq. (1):

$$\text{Drug Loading (DL, wt\%)} = \frac{\text{Mass of drug (mg)}}{\text{Mass of drug loaded LCNPs}} \times 100 \quad (1)$$

The encapsulation efficiencies are calculated using Eq. (2):

$$\text{Encapsulation Efficiency (\%)} = \frac{\text{Drug loading (wt\%)}}{\text{Feed TPV to LCNP ratio (wt\%)}} \times 100 \quad (2)$$

3.3.8 *Lipid and antibody delamination and TPV release analysis*

LCNPs were synthesized as described above, incorporating 2 mol % of DOPC-NBD or DSPE-PEG-CF. For characterization of the delamination of antibody, α4β7 mAb were labeled with a DyLight 680 amine-reactive dye and conjugated to LCNPs as described above. After synthesis, LCNPs were divided into individual microcentrifuge tubes for each time point/replicate, and incubated in a shaker at 4 °C or 37 °C. At each time point, tubes were centrifuged at 14,000 rpm

for 10 min, and the supernatants were collected, while the same amount of DMSO were added to dissolve pellets for measuring fluorescent lipids or mAb delamination from LCNPs. Delamination study of DiLight 680 labeled α4β7 mAb from LCNPs were also performed in human serum. TPV/A4B7-LCNPs were synthesized as described above and resuspended in PBS only, PBS containing BSA (50 mg/mL) or human serum, and were divided into individual microcentrifuge tubes for each time point/replicate. At each time point, replicate tubes were centrifuged at 14,000 rpm for 10 min. Supernatants were mixed with acetonitrile of 1:1 (v/v) and centrifuged to remove precipitated proteins. The TPV contents in the supernatant were measured by HPLC. The values were normalized to the total amount of TPV present.

3.3.9 *Storage stability of LCNPs*

We compared the stabilities of LCNPs with or without the PEG coating. For the LCNPs without PEG, DSPE-PEG-MAL was excluded from the lipid composition while other materials and the synthesis process remained same. LCNP formulations were suspended in MilliQ water at 1 mg/mL, and stored at 4 °C or 37 °C for storage stability study. Their diameters, PDI and ζ-potential were measured by DLS at day 0, 17 and 37. LCNPs (with or without PEG) were also suspended in PBS and characterized by DLS at different time points over 48 h to exam their stability in biological environment. Addition of cryo-protectant have been proven to stabilize NPs during lyophilization for longer storage.[40] Thus we also tested the effect of adding trehalose on PEG-LCNPs prior to lyophilization by measuring size, PDI and ζ-potential changes before and after lyophilization. The stability of TPV/A4B7-LCNP in human serum was documented by measuring its size using NanoSight after 10 days incubation at 37 °C.

3.3.10 *Cytotoxicity analysis*

HUT 78 cell lines were obtained from the NIH AIDS Research & Reference Reagent Program. Cells were maintained in RPMI 1640 cell culture media as described above, and were incubated at 37 °C in a humidified 5% CO_2 air environment. For cytotoxicity assay, HUT 78 cells were cultured in 96-well plates at the concentration of 25,000 cell/well in the absence or presence of various concentrations of TPV, TPV loaded LCNPs, TPV loaded A4B7-LCNPs, LCNPs only, or A4B7-LCNPs. After 2 days in culture, cell viability was assessed using CellTiter-Blue Cell Viability Assay (Promega) following the manufacturer's recommended procedures. Briefly, cells were incubated for 4 h with CellTiter-Blue reagent (20 μL/well), and fluorescence was recorded at 560/590 nm ex/em using a fluorescent plate reader.

3.3.11 *In vitro cell binding assay*

Firstly, we tested α4β7 integrin expression on several human T cell lines to select one with highest expression for cell binding study. HUT 78, PM-1, ACH-2, and CEMx174 cells obtained from the NIH AIDS Research & Reference Reagent Program, were incubated separately with α4β7-APC (obtained from NIH funded Nonhuman Primate Reagent Resource) for 30 min, followed by LIVE/DEAD® violet dead cell staining and were then analyzed by flow cytometry. HUT 78 cells showed significantly higher α4β7 integrin expression than other cell lines, and they were chosen for the following studies. The rhodamine B labeled LCNPs were synthesized as described above. HUT 78 cells were distributed into polystyrene tubes for each group/replicate at the concentration of 1×10^6 cell/tube. Cells were treated with 15 μg/mL bare LCNPs, A4B7-LCNPs or Iso-LCNPs for 30 min at 4 °C in culture medium, followed by two rounds of washing and LIVE/DEAD® violet dead cell staining. Another groups of cells were pretreated with 200 μg/mL soluble α4β7 mAb for a receptor blocking study following incubation with LCNP

formulations. HUT 78 cells were then washed, fixed in 2% PFA, and analyzed by flow cytometry.

3.3.12 *Anti-HIV-1 activities of TPV loaded A4B7-LCNPs*

HUT 78/HIV-1_{SF2} (ARV-2) were obtained from the NIH AIDS Research & Reference Reagent Program. These HIV-1_{SF2} infected HUT 78 cell lines were maintained in RPMI 1640 cell culture media. After two days incubation, HIV-1_{SF2} was harvested from supernatant of infected HUT 78 cells and used for antiviral activity studies using non-infected HUT 78 cells. HIV-1_{SF2} utilizes CCR5 and CXCR4 as coreceptors and it infects a variety of cell lines. Antiviral activity was measured as a reduction in HIV-1 production after infection of HUT 78 cells with HIV-1_{SF2}. Free TPV, α4β7 mAb, Iso mAb and the combination of TPV and α4β7 mAb or Iso mAb were dosed to achieve same concentrations of TPV or mAb in TPV-LCNPs or TPV-A4B7-LCNPs formulations where TPV was at 1.0 μg/mL, and this concentration of TPV doesn't cause cell apoptosis on cells based on published data. Briefly, HUT 78 cells were seeded at a concentration of 2.5×10^4 per well in 96-well microplates. HUT 78 cells were incubated with free TPV, α4β7 mAb, Iso mAb, free combination of TPV and α4β7 mAb or Iso mAb, TPV-LCNPs, A4B7-LCNPor TPV-A4B7-LCNPs at 37 °C for 1 h prior to virus exposure. Subsequently, HIV-1_{SF2} at a concentration equals to 300 pg/mL of p24 was added to the cultures and incubated for up to 10 days. At day 5, half of medium in each well was discarded and replaced with fresh medium containing same drug formulations with same concentrations. Untreated cells (100% infected) were used as a control. At day 10, HIV-1 concentrations in the supernatant of each well were measured by HIV-1 p24 Elisa Assay following the manufacturer's recommended procedures.

3.3.13 *Synergistic analysis*

Bliss independent model was used to analyze combined effects of multiple drugs (here are TPV and α4β7 mAb). The model is defined by the Eq. (3):

$$fa_{xy,P} = fa_x + fa_y - (fa_x)(fa_y) \quad (3)$$

$fa_{xy,P}$ is the predicted fraction (here is the percentage of HIV-1 inhibition) affected by a combination of TPV and α4β7 mAb, given the experimentally observed fraction affected by single drug fa_x or fa_y $individually$. Then the experimentally observed fraction affected by a combination of TPV and α4β7 mAb ($fa_{xy,O}$) will be compared with $fa_{xy,P}$ using the Eq. (4)

$$\Delta fa_{xy} = fa_{xy,O} - fa_{xy,P} \quad (4)$$

If $\Delta fa_{xy} > 0$ with statistical significance, the two drugs display synergy. If $\Delta fa_{xy} = 0$, the two drugs show independent action. If $\Delta fa_{xy} < 0$ with statistical significance, the two drugs display antagonism.

3.3.14 *Ex vivo rhesus macaque ileum cell targeting assay*

Pieces of rhesus macaque ileum were obtained from the tissue distribution program at Washington National Primate Research Center (WaNPRC), University of Washington. All macaques were confirmed to be serologically negative for simian type D retrovirus, SIV, and simian T-cell lymphotropic virus (STLV) prior to sample collection. LPLs were isolated from rhesus macaque ileum based on a protocol of isolation murine LPLs from colonic tissue, reported by Weigmann, *et al*.[46] In brief, rhesus macaque ileum was washed by ice-cold PBS to remove feces and residual mesenteric fat tissue, and then cut into 1 cm pieces and washed again. Afterwards, ileum pieces were incubated in 20 mL of pre-digestion solution, 1 × HBSS containing 5 mM EDTA and 1 mM dithiothreitol (DTT), for 20 min at 37 °C under slow

rotation. The solution containing ileum pieces was then passed through a 100 μm cell strainer and the pieces were collected and incubated in another fresh pre-digestion solution again for 20 min at the same condition. After passing through another 100 μm cell strainer, remaining tissues were cut into 1 mm pieces and washed by ice-cold PBS to remove remaining EDTA and DTT. Tissues were then transferred to 20 mL of digestion solution, which was 1 × PBS containing 0.5 mg/mL collagenase D, 0.5 mg/mL DNase I and 3 mg/mL dispase II, and incubated for 30 min at 37 °C placed in a shaker. Afterwards, the solution was vortexed intensely and passed through a 40 μm strainer. Remaining tissues were incubated with another fresh digestion solution for 40 min and then passed through cell strainer again. All cells (LPLs) passed through the strainer were combined and washed by PBS twice. Cells were also washed by MACS buffer to lyse red blood cells, and lymphocytes were further purified using lymphocyte separation medium, followed by centrifugation at 2,500 rpm at 15 min. Lymphocytes floated on the top of medium were collected for PBS washing. After last wash, cells were transferred to RPMI1640 cell culture media. For the particle targeting experiment, freshly isolated LPLs were divided into individual polystyrene tubes for each group/replicate at the concentration of 3×10^6 cell/tube. Cells were then incubated with APC anti-macaque α4β7 APC, FITC anti-human CD4, and A4B7-LCNPs or Iso-LCNPs for 30 min at 4 °C, followed by two rounds of washing and LIVE/DEAD® violet dead cell staining. LPLs were finally washed, fixed in 2% PFA buffer, and analyzed by flow cytometry.

3.3.15 *In vivo small intestine targeting*

Animal studies were approved by the Institutional Animal Care and Use Committee (IACUC) at the University of Washington (Protocol # 4260-01). All animals were obtained and cared for in accordance with the IACUC guidelines. 8~12 weeks old male C57BL6/J mice (The Jackson Laboratory, Bar Harbor, ME) were intravenously administered with PBS, DiR loaded A4B7-

LCNPs or Iso-LCNPs at a dose of 0.04 mg particles/1 g mouse, or 8×10^{-3} mL solution/1 g mouse by tail vein injection. At specified time points post-administration, mice were sacrificed by cardiac exsanguination under isoflurane overdose for terminal blood collection, followed by cervical dislocation. Necropsy was performed, and specified organs were harvested, including small intestine, liver, kidney, spleen, lung, and heart. Organs were washed in cold-PBS, dried on the tissue paper, and stored at -80 °C until processing. All organs were imaged and analyzed using Xenogen IVIS® Spectrum imaging system. Xenogen images were taken at 745/800 nm ex/em. Images were analyzed using Living Image® 4.0 software (Caliper Life Sciences, Inc.).

3.3.16 *Biodistribution of targeted LCNPs in major organs*

8~12 weeks old male C57BL6/J mice were administered with PBS, DiR loaded A4B7-LCNPs or Iso-LCNPs as described above. All the organs were harvested at 6 hours postinjection, and were homogenized in DMSO using a Precelleys homogenizer with beads according to the manufacturer's instructions. Fluorescent signals from A4B7-LCNP and Iso-LCNP groups was measured in the supernatant that was collected after homogenization and centrifugation. A calibrated standard of DiR/LCNP in the supernatant from respective homogenized tissues of untreated mice was used to determine the final dose, and fluorescence signal from PBS treated groups was subtracted from each organ.

3.3.17 *Histological analysis of mice major organs*

8~12 weeks old male C57BL6/J mice were administered with 0.2 mL PBS, 50 mg/kg A4B7-LCNPs or 50 mg/kg Iso-LCNPs. After two days, mice were sacrificed by cardiac exsanguination under isoflurane overdose for terminal blood collection, followed by cervical dislocation. Major organs including small intestine, heart, liver, spleen, lung, kidney were harvest and sectioned for

H&E staining by UW Pathology Research Service Laboratory. Stained issue slides were then examined under a Nikon Eclipse Ti microscope equipped with a Nikon Digital Sight DS-Fi2 camera (Nikon, Melville, NY). All H&E stain images were obtained using a 20X objective.

3.3.18 *In vivo gut-homing T cell targeting*

8~12 weeks old male C57BL6/J mice were intravenously administered with PBS, rhodamine B labeled A4B7-LCNPs or Iso-LCNPs by tail vein injection. At 12 hours post-administration, mice were sacrificed by cervical dislocation and small intestines were harvest. Immediately, we isolated LPLs from small intestines for A4B7-LCNPs cellular targeting experiments. The LPLs isolation process was similar to cell isolation from rhesus macaque ileum as described above with little changes. Briefly, small intestines were cleared of feces by flushing with a syringe filled with PBS and were opened longitudinally to be further washed. Intestine pieces were cut into 1 cm pieces and incubated in 10 ml of predigestion solution for 30 min at 37 °C under slow rotation. After passing through a 100 μm cell strainer, remaining tissues were cut into 1 mm pieces and were incubated in 5 ml of digestion solution for 20-30 min at 37 °C under slow rotation, followed by passing through a 40 μm cell strainer. This process was repeated and cells passing through were collected and combined for immunophenotyping. Immediately after cell isolation. LPLs were stained with APC anti-mouse α4β7 or APC isotype control antibody, followed by two rounds of washing and LIVE/DEAD® violet dead cell staining. LPLs were finally washed, fixed in 2% PFA and analyzed by flow cytometry.

3.3.19 *Statistical analysis*

Data were expressed mean ± SD unless otherwise indicated, with statistical significance defined as $p < 0.05$. Statistics were calculated using Prism 7.0 (GraphPad) and were performed by two-

sided student's *t* test (for two groups comparisons) or one-way ANOVA followed by Turkey's post hoc test (for multiple groups comparisons).

3.4 Results

3.4.1 *Synthesis and Characterization of Targeted LCNPs Loaded with Tipranavir*

We modified the commonly used single-emulsion evaporation method to fabricate nanoparticles with PLGA core that facilitate incorporation of a lipid bilayer shell (Figure 3.1A).[37, 43] We chose a lipid composition of neutral (1,2-Dioleoyl-sn-glycero-3-phosphocholine, DOPC), and cationic (1,2-dioleoyl-3-trimethylammonium-propane, DOTAP) lipids at equimolar content to obtain a positive net charge for stabilizing the negative PLGA core. In addition, we incorporated 1,2-distearoyl-*sn*-glycero-3-phosphoethanolamine-N-[maleimide(polyethylene glycol)-2000] (DSPE-PEG-MAL) at 11.1% molar ratio of total lipids. The DSPE-PEG-MAL has a maleimide end group for conjugating to antibodies, and a polyethylene glycol (PEG) chain that was expected to stabilize our nanoparticles. As expected, DSPE-PEG-MAL incorporation led to a significant increase in the LCNP diameter, and altered the surface charge from positive to neutral (Table 3.1). This change in surface charge is also beneficial for reducing non-specific binding to cells. Both LCNPs with or without PEG were stable when stored in MilliQ water at 4 °C or 37 °C (Figure S1A, Appendix II). However, LCNPs without PEG rapidly aggregated to sizes >1uM in PBS at 37 ºC whereas PEG-coated LCNPs maintained their original size over 2 days (Figure S1B, Appendix II). We observed aggregation of LCNPs after lyophilization during long-term storage, but this issue could be avoided by adding trehalose before freezing the LCNPs (Figure S1D, Appendix II).

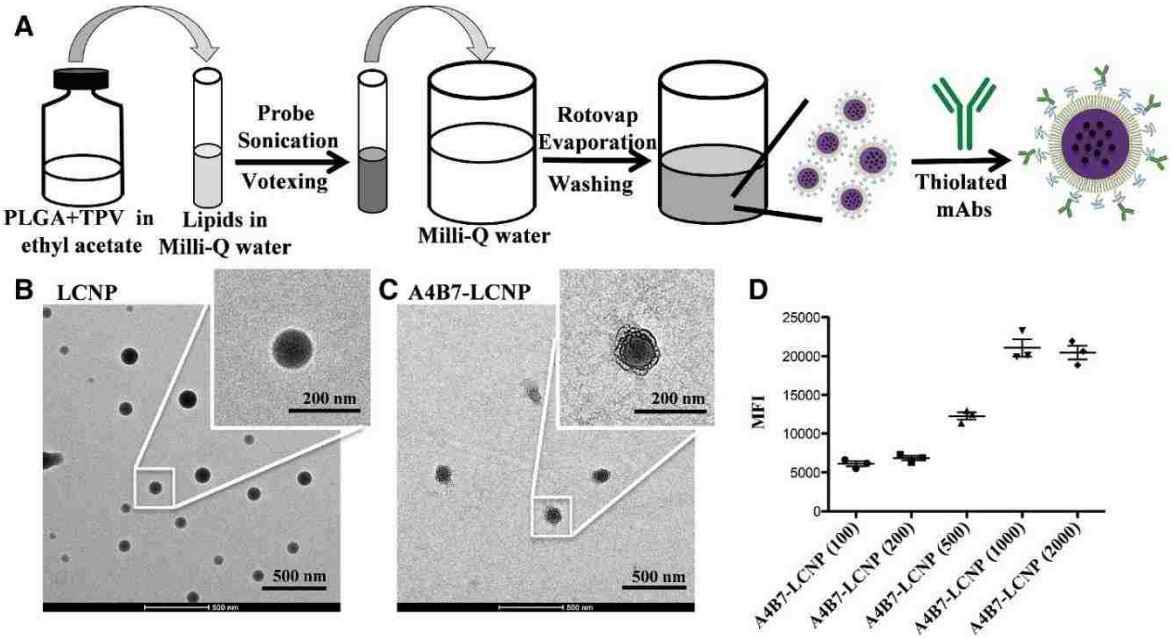

Figure 3.1. Preparation of LCNPs. (A) Schematic illustration of the A4B7-LCNP fabrication process using a modified single-emulsion evaporation method. (B, C) TEM images of LCNPs (B) and LCNPs surface conjugated with α4β7 mAb (A4B7-LCNPs) (C). (D) Mean fluorescence intensity (MFI) of LCNPs conjugated with fluorescent DyLight 633 labeled α4β7 mAb measured by flow cytometry. Data represents mean ± SD, n=3.

Table 3.1. Physical properties of LCNP formulations.*

Sample†	Size (d, nm)	PDI ‡	ζ-potential (mV)
LCNP (No PEG)	142 ± 5 §	0.10 ± 0.03	29.3 ± 1.2 #
LCNP	172 ± 2 §,‖	0.08 ± 0.02	1.2 ± 2.0
A4B7-LCNP ¶	204 ± 18 ‖	0.26 ± 0.10	2.1 ± 1.5
TPV/LCNP	178 ± 1	0.07 ± 0.01	4.4 ± 0.7
TPV/A4B7-LCNP ¶	233 ± 31	0.29 ± 0.05	2.1 ± 0.3

* Samples were diluted in Milli-Q water for size and PDI measurements and in 10 mM NaCl solution (pH = 7.0) for ζ-potential measurements. Data presents mean ± SD of at least three independent preparations. LCNP, lipid-coated PLGA nanoparticles.
† Lipids composition for LCNP is 4:4:1 DOPC/DOTAP/DSPE-PEG-MAL (mol/mol/mol), except for LCNP (No PEG), which omits the DSPE-PEG-MAL but retains the other lipids at the same amounts (4:4 DOPC/DOTAP).
‡ PDI: Polydispersity index.
§ Significant difference at the 0.001 probability level.
‖ Significant difference at the 0.05 probability level.
¶ NS, nonsignificant difference between A4B7-LCNP and TPV/A4B7-LCNP groups in size, PDI and ζ-potential.

Significant difference between LCNP (No PEG) and any of the other groups at the 0.0001 probability level.

We used α4β7 mAb conjugated to the lipid layer shell of LCNPs for the dual-function of targeting gut-homing T cells and inhibiting HIV transmission. The antibody was conjugated to the DSPE-PEG-MAL on the surface of LCNPs and led to a modest but significant increase in diameter (Table 3.1). Transmission electric microscope (TEM) showed a low contrast material associated with the A4B7-LCNPs surface (Figure 3.1B, C), which we attributed to be the lipid layer and antibodies surrounding the PLGA core. The surface density and efficiency of antibody conjugation to LCNPs was optimized using a Dylight 633-labeled α4β7 mAb. The fluorescently-labeled antibody was conjugated to LCNPs at molar ratios from 100:1 to 2000:1 and then analyzed by flow cytometry to quantify the amount of mAb that would saturate the fluorescent signal on the LCNP. We observed that the mean fluorescent intensity (MFI) saturated at a molar ratio of 1000:1 (Figure 3.1C). We used Nanoparticle Tracking Analysis (NTA) to obtain the number concentration of LCNPs and TECAN fluorescent plate reader to analyze the conjugation efficiency, which is the percentage of mAb conjugated to LCNPs relative to the input feed amount. Based on these values, we calculated the number of mAb per LCNP (Table 3.2). As expected, the efficiency of mAb conjugation was reduced as the input molar ratio of mAb to LCNPs was increased. We reached a conjugation efficiency of 30.8% for the 1000:1 input molar ratio of mAb to LCNPs. With this feed ratio, we achieved the highest surface density while maximizing conjugation efficiency since we expected to deliver α4β7 mAb not only as a targeting ligand for gut T cells but also as a blocking agent to prevent HIV-1 from binding to α4β7+ cells. The loading of α4β7 mAb on LCNPs at this feed ratio was 2.16 ± 0.10 wt% (w/w, weight of mAb relative to weight of LCNPs) measured by the micro bicinchoninic aicd (BCA) assay.

Table 3.2. Average content of antibody conjugated to the surface of LCNPs.

Sample*	Feed ratio of mAb to LCNP (mol/mol)	Conjugation efficiency†	Number of mAb per LCNP‡
A4B7-LCNP (100)	100	45%	45
A4B7-LCNP (200)	200	54%	108
A4B7-LCNP (500)	500	41.2%	206
A4B7-LCNP (1000)	1000	30.8%	308
A4B7-LCNP (2000)	2000	20.2%	405

*A4B7-LCNP, lipid-coated PLGA nanoparticles surface conjugated with α4β7 mAb at different molar ratios (100:1 ~ 2000:1, mAb to LCNP)

†Conjugation efficiency= $\frac{\text{amount of mAb associated with LCNPs}}{\text{total amound of mAbs added}}$

‡Number of conjugated mAb per LCNP= $\frac{\text{number concentration of total mAb conjugated to LCNP}}{\text{number concentration of total LCNPs}}$ =

$$\text{concentration of mAb} \times \frac{N_A}{\text{m.w. of mAb}} \times \frac{1}{\text{number concentration of LCNPs}}$$

N_A: the Avogadro constant.

m.w. of mAb: molecular weight of mAb, 15,000 g/mol.

A potential benefit of nanoparticles is the ability to incorporate physicochemically diverse drugs into the same delivery vehicle, which may increase drug potency through higher intracellular concentration and synergistic mechanisms.[22] We employed the α4β7 mAb to target gut-homing T cells and also used it to inhibit HIV transmission by blocking the α4β7 receptor on uninfected T cells. We also decided to incorporate a protease inhibitor into the same nanoparticle with the aim of increasing drug concentrations in the GALT as well as inhibiting viral production from HIV infected gut-homing T cells. We chose tipranavir (TPV) due to its high potency, low solubility and reported toxicity.[47-48] Nanoparticle-based delivery systems have the potential to improve solubility and bioavailability of poorly water-soluble drugs and may also improve the safety profile of TPV.[49-50] To this end, we incorporated TPV into the LCNPs with initial drug input of 10 wt% (w/w, weight of TPV relative to weight of PLGA and lipids) which led to 8.0 ± 0.1 wt% TPV loading in LCNPs.

Encapsulation of TPV did not significantly change the size, polydispersity index (PDI) or ζ-potential of the A4B7-LCNPs (Table 3.1). After conjugation, we obtained a measured drug loading of 4.7 ± 0.2 wt% of TPV-loaded A4B7-LCNPs (TPV/A4B7-LCNPs), which translated to an encapsulation efficiency of 45.7 ± 3.4 %. The observed decrease in TPV loading of A4B7-LCNPs was mainly due to burst release of TPV from LCNPs during the antibody conjugation process and was consistent with the TPV release kinetics as described below. We also measured drug loading in our LCNP and conventional liposomes, and found a two-fold higher TPV loading and a 9-fold higher encapsulation efficiency in untargeted LCNPs compared to untargeted liposomes (Figure S2, Appendix II). Our TPV/A4B7-LCNPs were stable in human serum over at least 14 days (Figure S1C, Appendix II).

3.4.2 *Release Kinetics of Lipids, α4β7 mAb and TPV from LCNPs*

Spontaneous delamination of the lipid shell from LCNPs has been previously documented and was used in our case to deliver the α4β7 mAb.[42] However, delamination could also lead to loss of targeting function. We characterized the delamination kinetics of our A4B7-LCNPs in PBS to ensure there would be sufficient antibodies remaining on the LCNPs to maintain nanoparticle targeting function over at least two days. We first characterized the delamination kinetics of DOPC and DSPE-PEG from LCNPs in PBS by using fluorescently-labeled versions of these lipids. We observed that DOPC and DSPE-PEG were stably associated with LCNPs at 4 °C but delaminated at 37°C, resulting in a 35% loss of both lipids after 48 hours (Figure S3, Appendix II). We also directly measured Dylight 688 dye labeled α4β7 mAb delamination and observed a faster delamination in human serum than in PBS (Figure 3.2A). Even after delamination, we measured that 60% of the α4β7 mAb remained associated with the nanoparticles in human serum over 2 days, which is sufficient for maintaining targeting properties. In our case, delaminated

antibodies that bind α4β7-expressing cells in the GALT was intended to further inhibit HIV transmission.

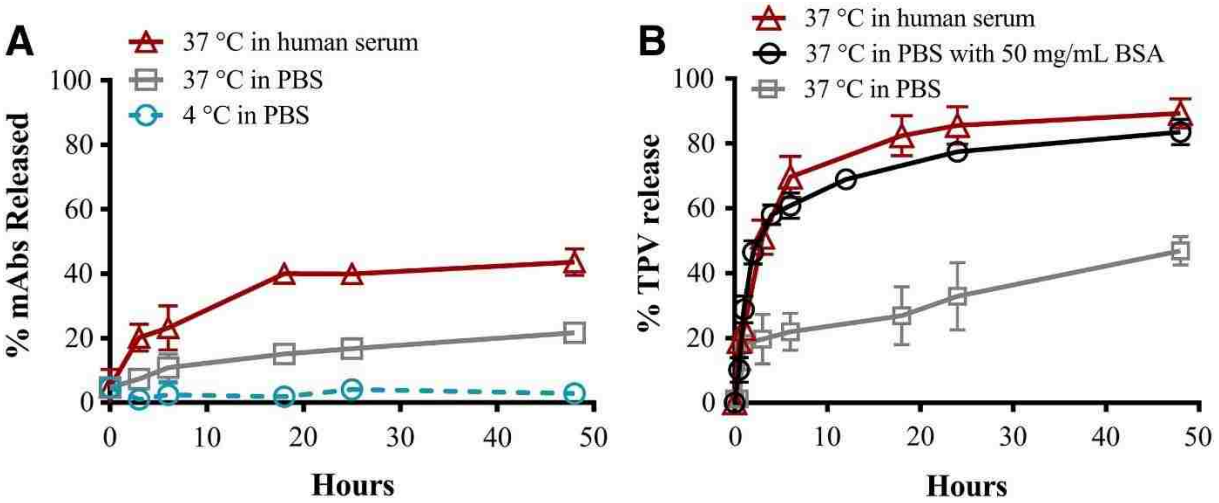

Figure 3.2. Release kinetics of mAb or TPV. (A) Delamination of DyLight 680 labeled α4β7 mAb from LCNPs in PBS at 37 °C or 4 °C, or in human serum at 37 °C over 48 hours. (B) Release kinetics of TPV from A4B7-LCNPs in PBS, PBS with 50 mg/mL BSA, or human serum at 37 °C over 48 hours. Data represents mean ± SD, n=3.

We also measured TPV release in sink conditions to inform potential drug bioavailability once dosed *in vivo*. Since TPV is rapidly bound to plasma proteins (>99%), including serum albumin and α_1-acid glycoprotein,[51] we expected that BSA could be used as a solubilizing agent in the release media. In fact, we found that 50 mg/mL BSA in PBS increased TPV solubility by nearly 2500-fold. Using *in vitro* sink-conditions established with 50 mg/mL BSA in PBS (pH 7.4) or human serum, we observed rapid TPV release from A4B7-LCNPs of up to 80% after 24 hours (Figure 3.2B). Since we observed that nanoparticles reach the gut by 6 hours following intravenous administration as described below, and 40% of TPV remained associated with our LCNP at this time. We expect that this amount of delivered TPV is sufficient for antiviral effectiveness due to its high potency. A single dose of 600 mg/kg TPV/A4B7-LCNPs every two

days would deliver a daily dose of ~800 mg TPV and ~140 mg α4β7 mAb based on their loading and release profiles, which is comparable to their currently prescribed or reported dosing.[52-53]

3.4.3 *A4B7-LCNPs Decrease Cytotoxicity of TPV*

Encapsulation of hydrophobic drugs in biodegradable and non-toxic nanoparticles can protect drugs from degradation, increase their circulation half-life and exhibit improved pharmacokinetics profiles thereby lowering toxicity.[54] Also, targeted nanoparticle-based delivery systems can increase the physiological concentration of drugs at target sites and minimize off-target binding. Here, we compared cytotoxicity of free TPV and LCNP-encapsulated TPV in the HUT-78 human T cell line. We chose HUT-78 cells for our *in vitro* studies since they exhibit high α4β7 integrin expression compared with other T cells lines we tested (Figure S4A, Appendix II), and their α4β7 expression has also been confirmed by others.[55] HUT-78 cells were treated with TPV, TPV/LCNPs or TPV/A4B7-LCNPs for two days and cell viability was measured by monitoring metabolic activity. Untargeted TPV/LCNPs and targeted TPV/A4B7-LCNPs were found to be less cytotoxic as measured by their higher half-maximal cytotoxic concentrations (CC_{50}), as 77.01 μg/mL (95% confidence interval (CI) = 66.10 to 89.73, TPV/LCNP) and 62.94 μg/mL (95% CI = 48.11 to 82.34, TPV/A4B7-LCNP) compared to that of free TPV as 32.01 μg/mL (95% CI = 30.06 to 34.07) (Figure 3.3A). No cytotoxicity was observed for either LCNPs or A4B7-LCNPs vehicle controls (Figure S5, Appendix II). Such reduced cytotoxicity might be explained by sustained release of TPV from LCNP formulations compared to the acute bolus of free drug.

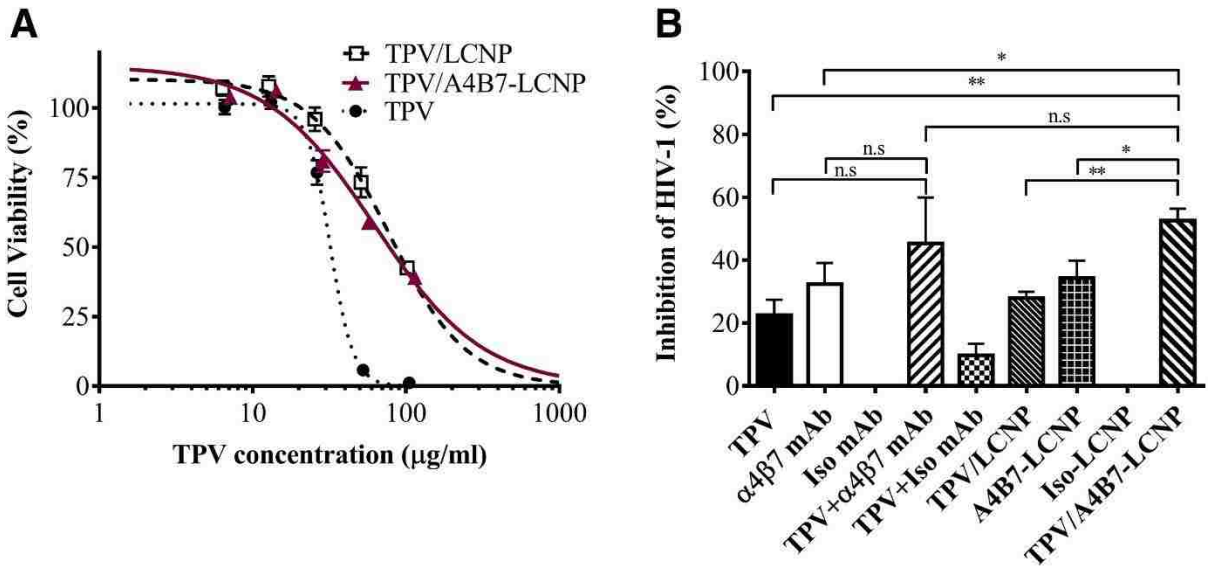

Figure 3.3. LCNPs reduce cytotoxicity of TPV and enhance antiviral activity of TPV in combination with α4β7 mAb. (A) Cell viability of HUT-78 cells after incubation with TPV, TPV/LCNP or TPV/A4B7-LCNPs at different concentrations for 2 days. (B) Anti-HIV activities of TPV, α4β7 mAb, Iso mAb, a combination of free TPV and α4β7 mAb, TPV and Iso mAb, TPV/LCNPs, A4B7-LCNPs or TPV/A4B7-LCNPs. HUT-78 cells were treated with free drugs or LCNP formulations for 1 hour followed by challenge with HIV-1SF2 for 10 days. HIV-1 p24 in the supernatant was measured by ELISA and percent inhibition was calculated as a reduction of HIV-1 production relative to untreated infected cell controls. Data represents mean ± SD, n=3, *p<0.05, ** p<0.005, ***p<0.0005, n.s., not statistically significant.

3.4.4 *Antiretroviral Activity of TPV Loaded A4B7-LCNPs In Vitro*

We performed an anti-HIV-1 assay in HUT-78 cells to evaluate the activity of LCNPs after TPV encapsulation or chemical conjugation with the targeting antibody. Cells were pre-treated for one hour before being challenged with HIV-1_{SF2}. After incubation for 10 days, culture supernatant was collected and tested for HIV-1 antigen production using HIV-1 p24 ELISA. We dosed TPV/LCNPs and TPV/A4B7-LCNPs based on total TPV loading and the free TPV, α4β7 mAb, and A4B7-LCNPs, were dosed at equivalent concentrations in all treatment groups. The potencies of TPV-LCNPs (27.9 ± 1.9% HIV-1 inhibition) or A4B7-LCNPs (34.3 ± 5.5% HIV-1 inhibition) were similar compared to free TPV (22.5 ± 4.9% HIV-1 inhibition) or α4β7 mAb (32.4 ± 6.7% HIV-1 inhibition), respectively (Figure 3.3B). When free TPV and α4β7 mAb are

delivered in combination, they showed higher HIV-1 inhibition (45.3 ± 14.6%) but the difference was not statistically significant. However, we found that combination of TPV and α4β7 mAb in our LCNPs (TPV/A4B7-LCNP, 52.5 ± 3.8% HIV-1 inhibition) led to a significantly higher potency than either free TPV or α4β7 mAb, as well as formulated TPV/LCNP or A4B7-LCNP. We used the Bliss independent model to quantitate combined effects of TPV and α4β7 mAb, and demonstrated that they displayed synergy in our TPV/A4B7-LCNPs ($\Delta fa_{xy} = 0.05 > 0$).

3.4.5 *Specific Targeting of A4B7-LCNPs to CD4+α4β7+ Cells from Rhesus Macaque Ileum*

Since α4β7 integrin mediates T cell migration to the GALT and also serves as a target of HIV, we were interested in investigating if our A4B7-LCNPs could specifically target these α4β7-expressing cells in the GALT. First, we used flow cytometry to analyze the binding of rhodamine B labeled A4B7-LCNPs to HUT 78 cells. Bare LCNPs without antibody or isotype IgG conjugated LCNPs (Iso-LCNPs) were used as the non-targeted control. To ensure that the rhodamine B remained conjugated with LCNPs, we performed *in vitro* release studies and found that less than 5% of rhodamine B released from A4B7-LCNPs over 24 hours in PBS at 37 °C. We observed that the association of A4B7-LCNPs to HUT-78 cells was significantly higher than bare LCNPs or Iso-LCNPs by comparing the MFI (Figure S4C, Appendix II). While all LCNP formulations had nonspecific bindings to HUT-78 cells, including bare LCNPs and Iso-LCNPs, the MFI of HUT-78 cells treated with A4B7-LCNPs was two-fold higher than the cells treated with control LCNPs, which we expect is due to specific antibody-α4β7 integrin interactions. We also performed a receptor blocking study to investigate the targeting specificity of our antibody-conjugated LCNPs, and observed significant but not a full reduction of cell binding after blocking with α4β7 mAb. This can partially be explained by our observation that binding of the antibody to HUT-78 cells was reversible (Figure S4D, Appendix II), which was indicated by a

decrease in MFI over time following 30 min incubation with fluorescently-labeled α4β7 mAb. We hypothesize that this could result in a competitive binding between A4B7-LCNP and free antibody.

Next, we tested the targeting function of A4B7-LCNPs for lamina propria lymphocytes (LPLs) isolated from the ileum of a rhesus macaque. Analysis of LPLs collected from the ileum showed a frequency of 36% CD4+ cells, 10% α4β7+ cells and 6% of cells that were both CD4+ and α4β7+ (Figure 3.4A). All cells were treated with either our A4B7-LCNPs or Iso-LCNPs control. LPLs treated with A4B7-LCNPs showed rhodamine B fluorescent was associated with most CD4+α4β7+ cells but not CD4-α4β7- cells (Figure 3.4B). Iso-LCNP control did not show any significant association with either CD4+ α4β7+ or CD4-α4β7- cells (Figure 3.4C). Comparison of the geometric mean fluorescent intensity (GMFI) showed that our A4B7-LCNPs had up to four-fold higher association with CD4+ α4β7+ cells compared to cells negative for both markers or cell populations treated with Iso-LCNPs (Figure 3.4D). These results demonstrated that A4B7-LCNPs targeted gut-homing T cells through a receptor-mediated process and could be used to potentially target CD4+α4β7+ cells in gut, thereby diminishing off-target effects and enhancing bioavailability in target cells.

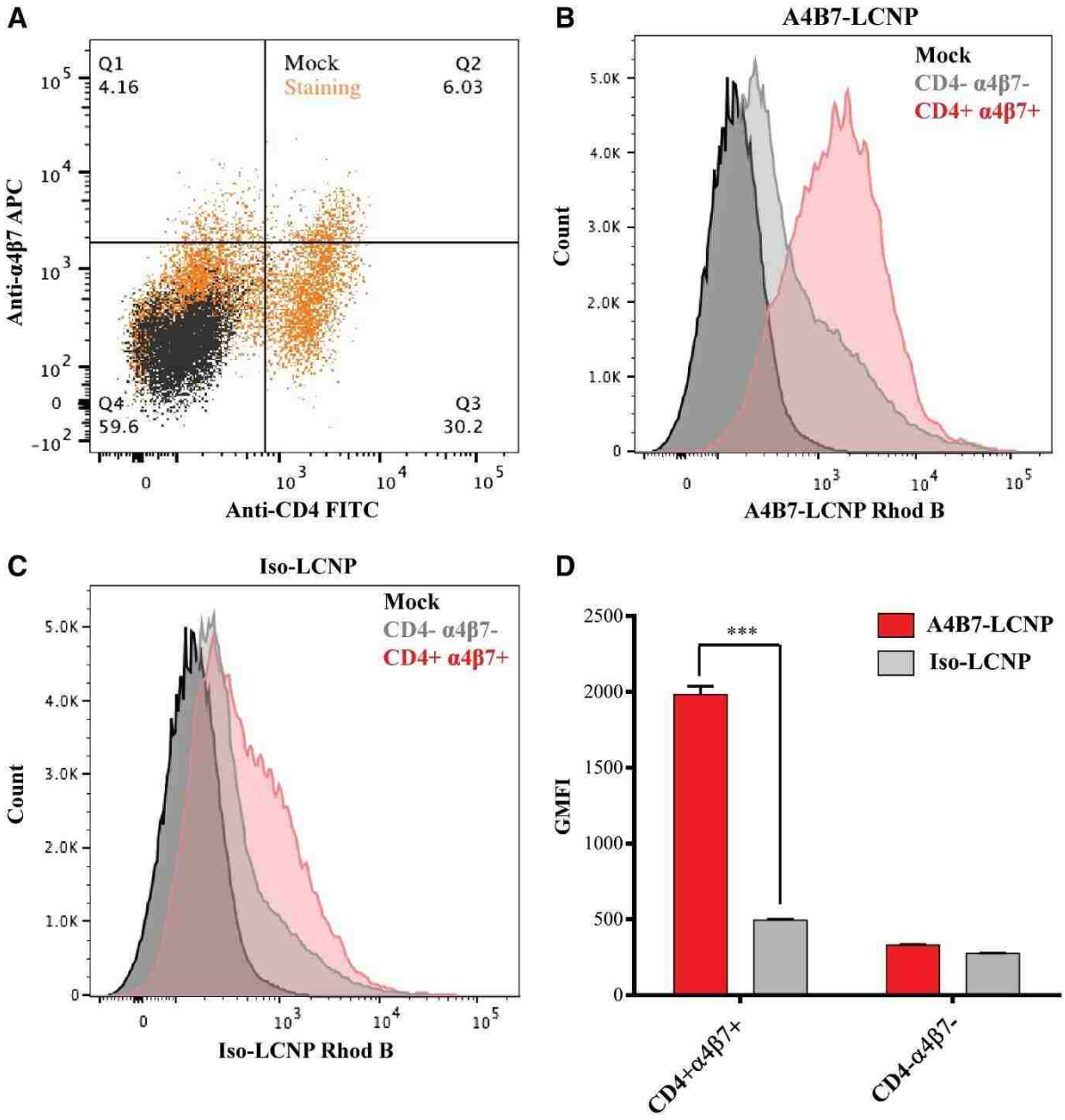

Figure 3.4. A4B7-LCNPs specifically bind to CD4+α4β7+ cells from lamina propria lymphocytes (LPLs) isolated from rhesus macaque ileum. (A) Flow cytometry dot plot analysis of isolated LPLs stained with anti-CD4 FITC and anti-α4β7 APC (orange dots) or their respective isotype controls (black dots), indicating CD4+ α4β7+ or CD4- α4β7- cell subsets. (B, C) LPLs were treated with rhodamine B (Rhod B) conjugated A4B7-LCNPs (B) or Iso-LCNPs (C), and labeled with anti-CD4 FITC and anti-α4β7 APC antibodies. Histogram curves represent Rhod B fluorescent signals from untreated LPLs (black), LCNP-treated CD4-α4β7- LPL subsets (gray), or LCNP-treated CD4+ α4β7+ LPL subsets. (D) Corresponding bar graphs of geometric mean fluorescence intensity (GMFI) are presented for A4B7-LCNPs or Iso-LCNPs binding to different subsets of LPLs. Data represents mean ± SD, n=3, ***p < 0.0005.

3.4.6 *A4B7-LCNPs Enhance Accumulation in Mouse Small Intestine and Target α4β7+ Cells*

In order to understand if α4β7 mAb could enhance LCNP accumulation in the gut by targeting α4β7+ cells, we administered fluorescently-labeled A4B7-LCNPs into mice by tail vein injection. To avoid autofluorescence, especially from the feces in the gut, we used a near-infrared dye, 1,1'-dioctadecyl-3,3,3',3'-tetramethylindotricarbocyanine iodide (DiR), encapsulated into LCNPs. We performed *in vitro* release studies to ensure that the DiR remained associated with A4B7-LCNPs, and found that less than 7% of DiR released from A4B7-LCNPs over 24 hours in PBS at 37 °C. Compared to treatment with Iso-LCNPs, mice treated with A4B7-LCNPs showed significantly higher distribution of fluorescent particles in small intestines at 6 hours after administration (Figure 3.5A, B). There were no significant differences in nanoparticle distribution to other organs between A4B7-LCNP and Iso-LCNPs groups (Figure 3.5C). We also found that nanoparticles quickly accumulated in the small intestine within 6 hours after administration but were eliminated by 24 hours (Figure 3.5A). We performed histological examination of major organs after administering 50 mg/kg A4B7-LCNPs, Iso-LCNPs or the same volume of PBS dosed intravenously to mice. All the organs from three treatment groups displayed no morphological difference, indicating LCNPs were well tolerated. (Figure S7, Appendix II).

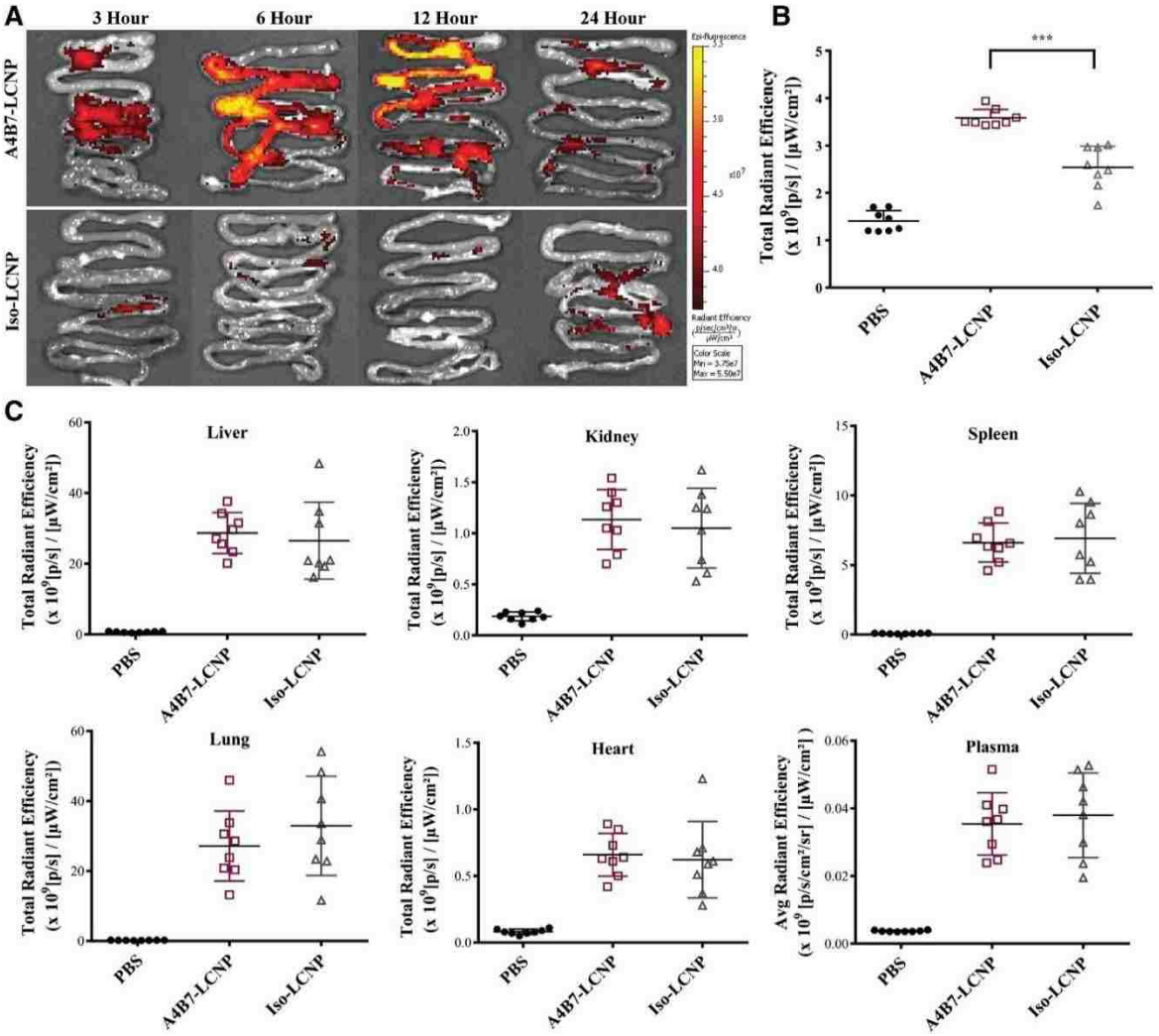

Figure 3.5. α4β7 mAb enhances LCNP accumulation in mouse small intestine compared to isotype control mAb. (A) Representative fluorescent images of mouse small intestines at 3, 6, 12, or 24 hours after intravenous administration of DiR loaded A4B7-LCNPs or Iso-LCNPs to mice. (B) Dot graph of total radiant efficiencies from Xenogen images of mouse small intestines at 6 hours post-administration of DiR loaded A4B7-LCNPs, Iso-LCNPs or PBS. (C) Dot graphs of total radiant efficiencies from Xenogen images of other organs (liver, kidney, spleen, lung and heart) and average radiant efficiencies from100 μL plasma. Data represents mean ± SD, ***p<0.0005. n=8 mice per group.

We also measured nanoparticle binding to LPLs isolated from small intestines of mice at 12 hours. We observed that 19% of α4β7+ cells but not α4β7- from isolated mouse LPLs were associated with A4B7-LCNPs. In the control groups, no nanoparticle association was observed for any cell populations, indicating cell-specific binding of A4B7-LCNPs to gut-homing T cells

when delivered to the small intestine (Figure 3.6). Such specific gut-homing T cell targeting *in vivo* might explain the observed higher accumulation of A4B7-LCNPs in the small intestine.

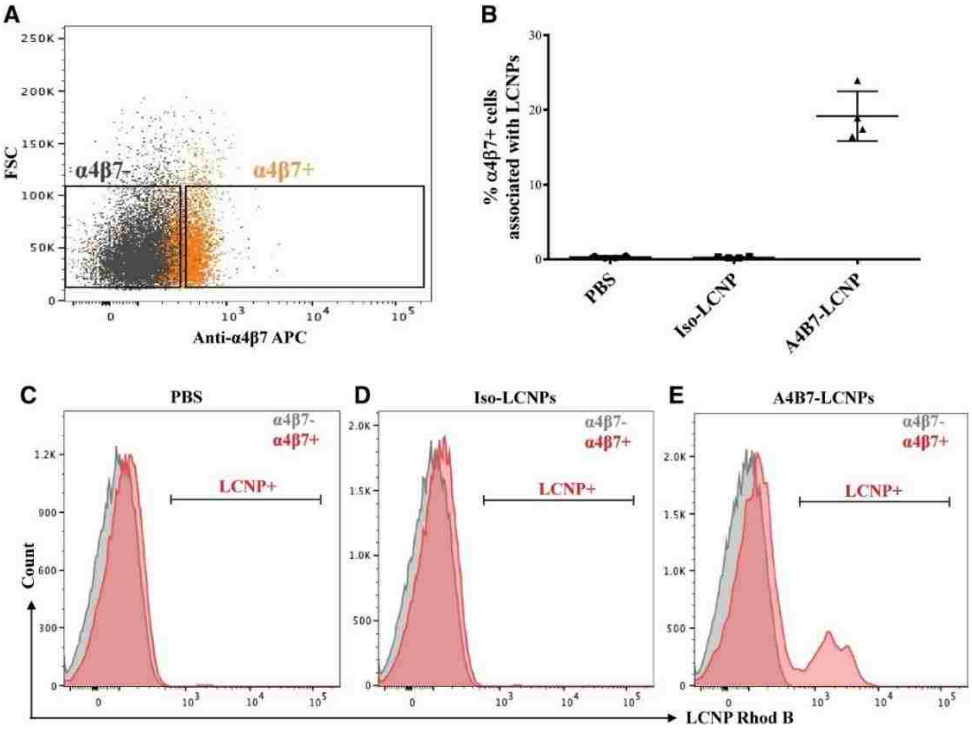

Figure 3.6. A4B7-LCNPs target α4β7+ cells among lamina propria lymphocytes (LPLs) from mouse small intestines at 12 hours post-administration. (A) Flow cytometry dot plot analysis of LPLs isolated from mouse small intestines indicating cells stained with anti-α4β7 APC (orange) or isotype control (gray). (B) Percentage of α4β7+ cells associated with rhodamine B conjugated A4B7-LCNP or Iso-LCNP analyzed by flow cytometry. (C-E) Representative histograms of flow cytometry analysis for α4β7+ (red) or α4β7- (gray) LPL subsets associated with LCNPs. Data represents mean ± SD, n=4 mice per group.

3.5 Discussion

Gut-homing T cells are attracting more attentions in the HIV field since they are actually infected at an early stage of infection and can traffic to the GALT within days of infection, leading to rapid virus replication, reservoir establishment and resistance to cART. Targeting these cells offers possible strategies to inhibit HIV transmission at specific reservoir sites and eradicate latent virus when combined with other therapeutics. In this work, we developed a core-shell nanoparticle surface modified with the α4β7 mAb for selectively targeting therapeutics to

gut-homing T cells, which are cells that play an important role in HIV infection and drug resistance. Our A4B7-LCNPs delivered TPV, a potent protease inhibitor, and used the α4β7 mAb for its known capacity to inhibit HIV transmission, reduce virus load, and sustain virologic control.[52-53, 56-57]

We designed and optimized our nanoparticles to meet the following criteria: (1) conjugation with antibodies for targeting gut-homing T cells, (2) encapsulation of hydrophobic drugs, (3) ability to release both antibody and drug from the nanoparticle, (4) stability in physiological and storage conditions, and (5) biodegradability and biocompatibility. Our nanoparticles decorated with targeting antibodies were expected to significantly improve therapeutic effectiveness while reducing toxicity.[58] Since we also aimed to deliver antibody and antiretroviral drugs as therapeutic agents to inhibit HIV transmission, achieving appropriate antibody and drug release kinetics from LCNPs for targeting was important.

TPV and α4β7 mAb co-delivered from our core-shell LCNPs retained and showed enhanced antiviral activity compared to the free drugs in preventing HIV-1_{SF2} infection of the HUT-78 human T cell line *in vitro*. While the mechanism for the antiviral activity of α4β7 mAb is not fully understood, the α4β7 integrin has been hypothesized to serve as a binding site for HIV-1 and facilitate cell-to-cell virus spreading through LFA-1.[16] Therefore, blocking α4β7 with a monoclonal antibody may inhibit the virus from binding and prevent infection. As described in our *in vitro* and *ex vivo* targeting studies, we hypothesize that this combined effect might enhance cell binding to A4B7-LCNPs and cause increased local concentrations of the drugs.

This work is significant because targeting gut-homing T cells with the α4β7 mAb also enhanced biodistribution of LCNPs to the small intestines when delivered intravenously to mice compared

to the isotype control mAb. Furthermore, we confirmed that A4B7-LCNPs accumulated in α4β7+ cells in the small intestines. Quantification of the dose that actually reached the major organs using DiR-labeled LCNPs also showed biodistribution of A4B7-LCNP in small intestines, liver and spleen. However, we observed specific accumulation of our A4B7-LCNP to the small intestine whereas the liver and spleen showed non-specific accumulation of the nanoparticles (Figure S8, Appendix II). Radiolabeled nanoparticles could be used in the future to obtain more accurate quantification of dose biodistribution since we observed that recovery efficiency using fluorescence was low and tissue- and dose-dependent. Other studies have also shown that liposomes, PLGA nanoparticles and silica nanoparticles accumulate in the liver and spleen and attribute this finding to clearance processes and the fact that these organs are highly vascular.[59-60] As such, future work will need to focus on increasing circulation half-life.

One of the biggest obstacles for curing HIV is the existence of HIV reservoirs, which cannot be cleared by current antiretroviral therapy. Targeting anti-HIV drugs to HIV reservoirs has been investigated for decades, but has focused mainly on targeting CD4+ T cells or macrophages, in the lymph nodes or brain.[25-26, 29-31, 61] Targeting gut-homing T cells has not been investigate although they are a major HIV reservoir.[14, 17] In addition, studies have demonstrated that ARV drug concentrations in gut-associated lymphatic tissues (GALT) is 99% lower than what is found in the blood and can lead to reservoir persistence.[18] Based on the TPV and α4β7 mAb loading in our LCNPs and their release data, we expect to improve the currently prescribed dosing of these therapeutics by only requiring a single dose once every two days to administer both drugs.[52-53] In addition, our data indicates that co-delivery of the α4β7 mAb and TPV together in a single LCNP had a modest but significant improvement in HIV inhibition compared to co-administration of the drugs separately. We also do not account for any improvement in efficacy

that might arise from the targeting function of our formulations. The rapid accumulation of our A4B7-LCNPs carrying both TPV and antibodies in the gut may provide a potential strategy to combat HIV-1 at an early stage and minimize HIV reservoir size. Moreover, our nanoparticles have the potential to target additional cellular or anatomical reservoirs when conjugated with other targeting ligands,[62] and deliver multiple agents such as latency reversing agents, HIV vaccines, neutralizing antibody, immune checkpoint inhibitors and gene-modifying oligonucleotide drugs for the eradication of HIV reservoirs.

3.6 References

1. Maldarelli, F.; Palmer, S.; King, M. S.; Wiegand, A.; Polis, M. A.; Mican, J.; Kovacs, J. A.; Davey, R. T.; Rock-Kress, D.; Dewar, R.; Liu, S.; Metcalf, J. A.; Rehm, C.; Brun, S. C.; Hanna, G. J.; Kempf, D. J.; Coffin, J. M.; Mellors, J. W., ART Suppresses Plasma HIV-1 RNA to a Stable Set Point Predicted by Pretherapy Viremia. *PLOS Pathogens* **2007,** *3* (4), e46.
2. Katlama, C.; Deeks, S. G.; Autran, B.; Martinez-Picado, J.; van Lunzen, J.; Rouzioux, C.; Miller, M.; Vella, S.; Schmitz, J. E.; Ahlers, J.; Richman, D. D.; Sekaly, R. P., Barriers to a cure for HIV: new ways to target and eradicate HIV-1 reservoirs. *The Lancet* **2013,** *381* (9883), 2109-2117.
3. Churchill, M. J.; Deeks, S. G.; Margolis, D. M.; Siliciano, R. F.; Swanstrom, R., HIV reservoirs: what, where and how to target them. *Nat Rev Micro* **2016,** *14* (1), 55-60.
4. Chun, T.-W.; Moir, S.; Fauci, A. S., HIV reservoirs as obstacles and opportunities for an HIV cure. *Nat Immunol* **2015,** *16* (6), 584-589.
5. Veazey, R. S.; DeMaria, M.; Chalifoux, L. V.; Shvetz, D. E.; Pauley, D. R.; Knight, H. L.; Rosenzweig, M.; Johnson, R. P.; Desrosiers, R. C.; Lackner, A. A., Gastrointestinal Tract as a Major Site of CD4+ T Cell Depletion and Viral Replication in SIV Infection. *Science* **1998,** *280* (5362), 427-431.
6. Guadalupe, M.; Reay, E.; Sankaran, S.; Prindiville, T.; Flamm, J.; McNeil, A.; Dandekar, S., Severe CD4+ T-Cell Depletion in Gut Lymphoid Tissue during Primary Human Immunodeficiency Virus Type 1 Infection and Substantial Delay in Restoration following Highly Active Antiretroviral Therapy. *Journal of Virology* **2003,** *77* (21), 11708-11717.
7. Li, Q.; Duan, L.; Estes, J. D.; Ma, Z.-M.; Rourke, T.; Wang, Y.; Reilly, C.; Carlis, J.; Miller, C. J.; Haase, A. T., Peak SIV replication in resting memory CD4+ T cells depletes gut lamina propria CD4+ T cells. *Nature* **2005,** *434* (7037), 1148-1152.
8. Mattapallil, J. J.; Douek, D. C.; Hill, B.; Nishimura, Y.; Martin, M.; Roederer, M., Massive infection and loss of memory CD4+ T cells in multiple tissues during acute SIV infection. *Nature* **2005,** *434* (7037), 1093-1097.
9. Chun, T.-W.; Nickle, D. C.; Justement, J. S.; Meyers, J. H.; Roby, G.; Hallahan, C. W.; Kottilil, S.; Moir, S.; Mican, J. M.; Mullins, J. I.; Ward, D. J.; Joseph A., K.; Mannon, P. J.;

Fauci, A. S., Persistence of HIV in Gut-Associated Lymphoid Tissue despite Long-Term Antiretroviral Therapy. *Journal of Infectious Diseases* **2008,** *197* (5), 714-720.
10. Wagner, N.; Löhler, J.; Kunkel, E. J.; Ley, K.; Leung, E.; Krissansen, G.; Rajewsky, K.; Müller, W., Critical role for β7 integrins in formation of the gut-associated lymphoid tissue. **1996**.
11. Arihiro, S.; Ohtani, H.; Suzuki, M.; Murata, M.; Ejima, C.; Oki, M.; Kinouchi, Y.; Fukushima, K.; Sasaki, I.; Nakamura, S., Differential expression of mucosal addressin cell adhesion molecule-1 (MAdCAM-1) in ulcerative colitis and Crohn's disease. *Pathology international* **2002,** *52* (5-6), 367-374.
12. Erle, D. J.; Briskin, M. J.; Butcher, E. C.; Garcia-Pardo, A.; Lazarovits, A. I.; Tidswell, M., Expression and function of the MAdCAM-1 receptor, integrin alpha 4 beta 7, on human leukocytes. *The Journal of Immunology* **1994,** *153* (2), 517-528.
13. Poles, M. A.; Elliott, J.; Taing, P.; Anton, P. A.; Chen, I. S., A preponderance of CCR5+ CXCR4+ mononuclear cells enhances gastrointestinal mucosal susceptibility to human immunodeficiency virus type 1 infection. *Journal of virology* **2001,** *75* (18), 8390-8399.
14. Cicala, C.; Martinelli, E.; McNally, J. P.; Goode, D. J.; Gopaul, R.; Hiatt, J.; Jelicic, K.; Kottilil, S.; Macleod, K.; O'Shea, A.; Patel, N.; Van Ryk, D.; Wei, D.; Pascuccio, M.; Yi, L.; McKinnon, L.; Izulla, P.; Kimani, J.; Kaul, R.; Fauci, A. S.; Arthos, J., The integrin α4β7 forms a complex with cell-surface CD4 and defines a T-cell subset that is highly susceptible to infection by HIV-1. *Proceedings of the National Academy of Sciences* **2009,** *106* (49), 20877-20882.
15. Izcue, A.; Coombes, J. L.; Powrie, F., Regulatory lymphocytes and intestinal inflammation. *Annual review of immunology* **2009,** *27*, 313-338.
16. Arthos, J.; Cicala, C.; Martinelli, E.; Macleod, K.; Van Ryk, D.; Wei, D.; Xiao, Z.; Veenstra, T. D.; Conrad, T. P.; Lempicki, R. A.; McLaughlin, S.; Pascuccio, M.; Gopaul, R.; McNally, J.; Cruz, C. C.; Censoplano, N.; Chung, E.; Reitano, K. N.; Kottilil, S.; Goode, D. J.; Fauci, A. S., HIV-1 envelope protein binds to and signals through integrin α4β7, the gut mucosal homing receptor for peripheral T cells. *Nat Immunol* **2008,** *9* (3), 301-309.
17. Kader, M.; Wang, X.; Piatak, M.; Lifson, J.; Roederer, M.; Veazey, R.; Mattapallil, J. J., α4+β7hiCD4+ memory T cells harbor most Th-17 cells and are preferentially infected during acute SIV infection. *Mucosal Immunol* **2009,** *2* (5), 439-449.
18. Fletcher, C. V.; Staskus, K.; Wietgrefe, S. W.; Rothenberger, M.; Reilly, C.; Chipman, J. G.; Beilman, G. J.; Khoruts, A.; Thorkelson, A.; Schmidt, T. E.; Anderson, J.; Perkey, K.; Stevenson, M.; Perelson, A. S.; Douek, D. C.; Haase, A. T.; Schacker, T. W., Persistent HIV-1 replication is associated with lower antiretroviral drug concentrations in lymphatic tissues. *Proceedings of the National Academy of Sciences* **2014,** *111* (6), 2307-2312.
19. Fletcher, C. V.; Staskus, K.; Wietgrefe, S. W.; Rothenberger, M.; Reilly, C.; Chipman, J. G.; Beilman, G. J.; Khoruts, A.; Thorkelson, A.; Schmidt, T. E.; Anderson, J.; Perkey, K.; Stevenson, M.; Perelson, A. S.; Douek, D. C.; Haase, A. T.; Schacker, T. W., Persistent HIV-1 replication is associated with lower antiretroviral drug concentrations in lymphatic tissues. *Proc Natl Acad Sci U S A* **2014,** *111* (6), 2307-12.
20. Gomes, M. J.; das Neves, J.; Sarmento, B., Nanoparticle-based drug delivery to improve the efficacy of antiretroviral therapy in the central nervous system. *International journal of nanomedicine* **2014,** *9*, 1757.
21. das Neves, J.; Nunes, R.; Rodrigues, F.; Sarmento, B., Nanomedicine in the development of anti-HIV microbicides. *Advanced Drug Delivery Reviews* **2016,** *103*, 57-75.

22. Jiang, Y.; Cao, S.; Bright, D. K.; Bever, A. M.; Blakney, A. K.; Suydam, I. T.; Woodrow, K. A., Nanoparticle-Based ARV Drug Combinations for Synergistic Inhibition of Cell-Free and Cell–Cell HIV Transmission. *Molecular pharmaceutics* **2015,** *12* (12), 4363-4374.
23. Kocbek, P.; Obermajer, N.; Cegnar, M.; Kos, J.; Kristl, J., Targeting cancer cells using PLGA nanoparticles surface modified with monoclonal antibody. *Journal of Controlled Release* **2007,** *120* (1–2), 18-26.
24. Gunaseelan, S.; Gunaseelan, K.; Deshmukh, M.; Zhang, X.; Sinko, P. J., Surface modifications of nanocarriers for effective intracellular delivery of anti-HIV drugs. *Advanced Drug Delivery Reviews* **2010,** *62* (4–5), 518-531.
25. Chiappetta, D. A.; Hocht, C.; Opezzo, J. A. W.; Sosnik, A., Intranasal administration of antiretroviral-loaded micelles for anatomical targeting to the brain in HIV. *Nanomedicine* **2013,** *8* (2), 223-237.
26. Gerson, T.; Makarov, E.; Senanayake, T. H.; Gorantla, S.; Poluektova, L. Y.; Vinogradov, S. V., Nano-NRTIs demonstrate low neurotoxicity and high antiviral activity against HIV infection in the brain. *Nanomedicine: Nanotechnology, Biology and Medicine* **2014,** *10* (1), 177-185.
27. Senanayake, T. H.; Gorantla, S.; Makarov, E.; Lu, Y.; Warren, G.; Vinogradov, S. V., Nanogel-Conjugated Reverse Transcriptase Inhibitors and Their Combinations as Novel Antiviral Agents with Increased Efficacy against HIV-1 Infection. *Molecular Pharmaceutics* **2015,** *12* (12), 4226-4236.
28. Tang, X.; Liang, Y.; Liu, X.; Zhou, S.; Liu, L.; Zhang, F.; Xie, C.; Cai, S.; Wei, J.; Zhu, Y.; Hou, W., PLGA-PEG Nanoparticles Coated with Anti-CD45RO and Loaded with HDAC Plus Protease Inhibitors Activate Latent HIV and Inhibit Viral Spread. *Nanoscale Research Letters* **2015,** *10* (1), 413.
29. Puligujja, P.; McMillan, J.; Kendrick, L.; Li, T.; Balkundi, S.; Smith, N.; Veerubhotla, R. S.; Edagwa, B. J.; Kabanov, A. V.; Bronich, T.; Gendelman, H. E.; Liu, X.-M., Macrophage Folate Receptor-Targeted Antiretroviral Therapy Facilitates Drug Entry, Retention, Antiretroviral Activities and Biodistribution for Reduction of Human Immunodeficiency Virus Infections. *Nanomedicine : nanotechnology, biology, and medicine* **2013,** *9* (8), 1263-1273.
30. Kovochich, M.; Marsden, M. D.; Zack, J. A., Activation of Latent HIV Using Drug-Loaded Nanoparticles. *PLoS ONE* **2011,** *6* (4), e18270.
31. Kraft, J. C.; McConnachie, L. A.; Koehn, J.; Kinman, L.; Collins, C.; Shen, D. D.; Collier, A. C.; Ho, R. J. Y., Long-acting combination anti-HIV drug suspension enhances and sustains higher drug levels in lymph node cells than in blood cells and plasma. *AIDS (London, England)* **2017,** *31* (6), 765-770.
32. Gautam, N.; Roy, U.; Balkundi, S.; Puligujja, P.; Guo, D.; Smith, N.; Liu, X.-M.; Lamberty, B.; Morsey, B.; Fox, H. S.; McMillan, J.; Gendelman, H. E.; Alnouti, Y., Preclinical Pharmacokinetics and Tissue Distribution of Long-Acting Nanoformulated Antiretroviral Therapy. *Antimicrobial Agents and Chemotherapy* **2013,** *57* (7), 3110-3120.
33. Leserman, L. D.; Barbet, J.; Kourilsky, F.; Weinstein, J. N., Targeting to cells of fluorescent liposomes covalently coupled with monoclonal antibody or protein A. **1980**.
34. Manjappa, A. S.; Chaudhari, K. R.; Venkataraju, M. P.; Dantuluri, P.; Nanda, B.; Sidda, C.; Sawant, K. K.; Ramachandra Murthy, R. S., Antibody derivatization and conjugation strategies: Application in preparation of stealth immunoliposome to target chemotherapeutics to tumor. *Journal of Controlled Release* **2011,** *150* (1), 2-22.

35. Béduneau, A.; Saulnier, P.; Hindré, F.; Clavreul, A.; Leroux, J.-C.; Benoit, J.-P., Design of targeted lipid nanocapsules by conjugation of whole antibodies and antibody Fab' fragments. *Biomaterials* **2007,** *28* (33), 4978-4990.
36. Cheow, W. S.; Hadinoto, K., Factors affecting drug encapsulation and stability of lipid–polymer hybrid nanoparticles. *Colloids and Surfaces B: Biointerfaces* **2011,** *85* (2), 214-220.
37. Mandal, B.; Bhattacharjee, H.; Mittal, N.; Sah, H.; Balabathula, P.; Thoma, L. A.; Wood, G. C., Core–shell-type lipid–polymer hybrid nanoparticles as a drug delivery platform. *Nanomedicine: Nanotechnology, Biology and Medicine* **2013,** *9* (4), 474-491.
38. Zhang, L.; Chan, J. M.; Gu, F. X.; Rhee, J.-W.; Wang, A. Z.; Radovic-Moreno, A. F.; Alexis, F.; Langer, R.; Farokhzad, O. C., Self-Assembled Lipid−Polymer Hybrid Nanoparticles: A Robust Drug Delivery Platform. *ACS Nano* **2008,** *2* (8), 1696-1702.
39. Moon, J. J.; Suh, H.; Polhemus, M. E.; Ockenhouse, C. F.; Yadava, A.; Irvine, D. J., Antigen-Displaying Lipid-Enveloped PLGA Nanoparticles as Delivery Agents for a Plasmodium vivax Malaria Vaccine. *PLoS ONE* **2012,** *7* (2), e31472.
40. Bershteyn, A.; Chaparro, J.; Yau, R.; Kim, M.; Reinherz, E.; Ferreira-Moita, L.; Irvine, D. J., Polymer-supported lipid shells, onions, and flowers. *Soft matter* **2008,** *4* (9), 1787-1791.
41. Hadinoto, K.; Sundaresan, A.; Cheow, W. S., Lipid–polymer hybrid nanoparticles as a new generation therapeutic delivery platform: A review. *European Journal of Pharmaceutics and Biopharmaceutics* **2013,** *85* (3, Part A), 427-443.
42. Hanson, M. C.; Bershteyn, A.; Crespo, M. P.; Irvine, D. J., Antigen Delivery by Lipid-Enveloped PLGA Microparticle Vaccines Mediated by in Situ Vesicle Shedding. *Biomacromolecules* **2014,** *15* (7), 2475-2481.
43. Cartiera, M. S.; Johnson, K. M.; Rajendran, V.; Caplan, M. J.; Saltzman, W. M., The uptake and intracellular fate of PLGA nanoparticles in epithelial cells. *Biomaterials* **2009,** *30* (14), 2790-2798.
44. Costantino, L.; Gandolfi, F.; Tosi, G.; Rivasi, F.; Vandelli, M. A.; Forni, F., Peptide-derivatized biodegradable nanoparticles able to cross the blood–brain barrier. *Journal of Controlled Release* **2005,** *108* (1), 84-96.
45. Giraud, E.; Rey, E.; Tréluyer, J.-M.; Pons, G.; Jullien, V., Quantification of tipranavir in human plasma by high-performance liquid chromatography with UV detection. *Journal of Chromatography B* **2006,** *830* (1), 86-90.
46. Weigmann, B.; Tubbe, I.; Seidel, D.; Nicolaev, A.; Becker, C.; Neurath, M. F., Isolation and subsequent analysis of murine lamina propria mononuclear cells from colonic tissue. *Nature protocols* **2007,** *2* (10), 2307-2311.
47. Muzammil, S.; Armstrong, A.; Kang, L.; Jakalian, A.; Bonneau, P.; Schmelmer, V.; Amzel, L.; Freire, E., Unique thermodynamic response of tipranavir to human immunodeficiency virus type 1 protease drug resistance mutations. *Journal of virology* **2007,** *81* (10), 5144-5154.
48. Boesecke, C.; Cooper, D. A., Toxicity of HIV protease inhibitors: clinical considerations. *Current Opinion in HIV and AIDS* **2008,** *3* (6), 653-659.
49. Merisko-Liversidge, E. M.; Liversidge, G. G., Drug nanoparticles: formulating poorly water-soluble compounds. *Toxicologic pathology* **2008,** *36* (1), 43-48.
50. Wang, H.; Yu, J.; Lu, X.; He, X., Nanoparticle systems reduce systemic toxicity in cancer treatment. Future Medicine: 2016.
51. King, J. R.; Acosta, E. P., Tipranavir. *Clinical Pharmacokinetics* **2006,** *45* (7), 665-682.
52. Byrareddy, S. N.; Kallam, B.; Arthos, J.; Cicala, C.; Nawaz, F.; Hiatt, J.; Kersh, E. N.; McNicholl, J. M.; Hanson, D.; Reimann, K. A.; Brameier, M.; Walter, L.; Rogers, K.; Mayne, A.

E.; Dunbar, P.; Villinger, T.; Little, D.; Parslow, T. G.; Santangelo, P. J.; Villinger, F.; Fauci, A. S.; Ansari, A. A., Targeting α4β7 integrin reduces mucosal transmission of simian immunodeficiency virus and protects gut-associated lymphoid tissue from infection. *Nat Med* **2014,** *advance online publication*.
53. Byrareddy, S. N.; Arthos, J.; Cicala, C.; Villinger, F.; Ortiz, K. T.; Little, D.; Sidell, N.; Kane, M. A.; Yu, J.; Jones, J. W.; Santangelo, P. J.; Zurla, C.; McKinnon, L. R.; Arnold, K. B.; Woody, C. E.; Walter, L.; Roos, C.; Noll, A.; Van Ryk, D.; Jelicic, K.; Cimbro, R.; Gumber, S.; Reid, M. D.; Adsay, V.; Amancha, P. K.; Mayne, A. E.; Parslow, T. G.; Fauci, A. S.; Ansari, A. A., Virologic control in SIV+ macaques after antiretroviral and α4β7 antibody therapy. *Science* **2016,** *354* (6309), 197-202.
54. Yildirimer, L.; Thanh, N. T. K.; Loizidou, M.; Seifalian, A. M., Toxicology and clinical potential of nanoparticles. *Nano Today* **2011,** *6* (6), 585-607.
55. Pan, W. J.; Hsu, H.; Rees, W. A.; Lear, S. P.; Lee, F.; Foltz, I. N.; Rathanaswami, P.; Manchulenko, K.; Chan, B. M.; Zhang, M.; Xia, X. Z.; Patel, S. K.; Prince, P. J.; Doherty, D. R.; Sheckler, C. M.; Reynhardt, K. O.; Krill, C. D.; Harder, B. J.; Wisler, J. A.; Brandvig, J. L.; Lynch, J. L.; Anderson, A. A.; Wienkers, L. C.; Borie, D. C., Pharmacology of AMG 181, a human anti-α(4)β(7) antibody that specifically alters trafficking of gut-homing T cells. *British Journal of Pharmacology* **2013,** *169* (1), 51-68.
56. Ansari, A. A.; Reimann, K. A.; Mayne, A. E.; Takahashi, Y.; Stephenson, S. T.; Wang, R.; Wang, X.; Li, J.; Price, A. A.; Little, D. M., Blocking of α4β7 gut-homing integrin during acute infection leads to decreased plasma and gastrointestinal tissue viral loads in simian immunodeficiency virus-infected rhesus macaques. *The Journal of Immunology* **2011,** *186* (2), 1044-1059.
57. Pereira, L. E.; Onlamoon, N.; Wang, X.; Wang, R.; Li, J.; Reimann, K. A.; Villinger, F.; Pattanapanyasat, K.; Mori, K.; Ansari, A. A., Preliminary in vivo efficacy studies of a recombinant rhesus anti-α4β7 monoclonal antibody. *Cellular Immunology* **2009,** *259* (2), 165-176.
58. Gao, J.; Feng, S.-S.; Guo, Y., Antibody engineering promotes nanomedicine for cancer treatment. *Nanomedicine* **2010,** *5* (8), 1141-1145.
59. Kumar, R.; Roy, I.; Ohulchanskky, T. Y.; Vathy, L. A.; Bergey, E. J.; Sajjad, M.; Prasad, P. N., In vivo biodistribution and clearance studies using multimodal organically modified silica nanoparticles. *ACS nano* **2010,** *4* (2), 699-708.
60. Alexis, F.; Pridgen, E.; Molnar, L. K.; Farokhzad, O. C., Factors Affecting the Clearance and Biodistribution of Polymeric Nanoparticles. *Molecular Pharmaceutics* **2008,** *5* (4), 505-515.
61. Buehler, D. C.; Marsden, M. D.; Shen, S.; Toso, D. B.; Wu, X.; Loo, J. A.; Zhou, Z. H.; Kickhoefer, V. A.; Wender, P. A.; Zack, J. A.; Rome, L. H., Bioengineered Vaults: Self-Assembling Protein Shell–Lipophilic Core Nanoparticles for Drug Delivery. *ACS Nano* **2014,** *8* (8), 7723-7732.
62. Cao, S.; Jiang, Y.; Levy Claire, N.; Hughes Sean, M.; Zhang, H.; Hladik, F.; Woodrow Kim, A., Optimization and comparison of CD4-targeting lipid–polymer hybrid nanoparticles using different binding ligands. *Journal of Biomedical Materials Research Part A* **2017,** *106* (5), 1177-1188.

Chapter 4. Optimization and comparison of CD4-targeting lipid-polymer hybrid nanoparticles

Adapted from: Cao S, Jiang Y, Levy CN, Hughes SM, Zhang H, Hladik F, and Woodrow KA. Optimization and comparison of CD4-targeting lipid-polymer hybrid nanoparticles using different binding ligands. *Journal of Biomedical Materials Research Part A.* 2018;106(5):1177-1188.

4.1 Abstract

Monoclonal antibodies and peptides are conjugated to the surface of nanocarriers (NCs) for targeting purposes in numerous applications. However, targeting efficacy may vary with their specificity, affinity or avidity when linked to NCs. The physicochemical properties of NCs may also affect targeting. We compared the targeting efficacy of the CD4 binding peptide BP4 and an anti-CD4 monoclonal antibody (CD4 mAb) and its fragments, when conjugated to lipid-coated poly(lactic-co-glycolic) acid nanoparticles (LCNPs). Negatively charged LCNPs with cholesteryl butyrate in the lipid layer (cbLCNPs) dramatically reduced nonspecific binding, leading to higher targeting specificity, compared to neutral or positively charged LCNPs with DOTAP (dtLCNP). cbLCNPs surface conjugated with a CD4 antibody (CD4-cbLCNPs) or its fragments (fCD4-cbLCNPs), but not BP4, showed high binding in vitro to the human T cell line 174xCEM, and preferential binding to CD3+CD14-CD8- cells from pigtail macaque peripheral blood mononuclear cells. CD4-cbLCNPs showed 10-fold higher binding specificity for CD4+ than CD8+ T cells, while fCD4-cbLCNPs demonstrated the highest binding level overall, but only three-fold higher binding specificity. This study demonstrates the importance of □-potential on NC targeting and indicates that CD4 mAb and its fragments are the best candidates for delivery of therapeutic agents to CD4+ T cells.

4.2 Introduction

Cell-targeted drug delivery has emerged as a solution to major challenges associated with conventional drug delivery systems. These challenges, including poor therapeutic index and off-target side effects, are largely due to the inability of the active pharmaceutical ingredients to act on target cells. Receptor-targeted NCs are designed to deliver therapeutics to cells through surface modification or functionalization with targeting molecules such as monoclonal antibodies,[1-3] peptides,[4] or aptamers[5] and have been used in various diagnostic,[6-7] therapeutic,[8-12] and vaccine applications.[13-14] NC-based therapies in conditions such as HIV,[15-18] cancer,[19-20] and autoimmune diseases[21-23] have attracted interest in targeting T lymphocytes. For example, CD4+ T cells are the major target for HIV infection, and resting memory CD4+ T cells are considered the primary reservoir of latent HIV-1 provirus that is ineradicable by current anti-HIV therapy.[24] NC delivery of antiretroviral drugs[15] and latency-reversing agents (LRAs)[25-28] to these CD4+ T cell may improve drug efficacy, and minimize toxicity and off-target effects.

Conventional monoclonal antibodies (mAb) against CD4 have been utilized for targeting nanoparticles to CD4+ T cells,[17, 29-30] but have some limitations such as immunogenicity,[31] nonspecific uptake by the reticuloendothelial system (RES) and a reduced circulation half-life.[32] Further, the binding sites of mAbs could be blocked due to random thiolation and the subsequent conjugation processes to NCs. Smaller antibody fragments, such as half-antibodies[33], single-chain variable fragments (svFc),[34-35] diabodies and minibodies[36-37] have been used to address some of these issues and could be promising alternatives to the full mAb. Additionally, several CD4 binding peptides have been reported to bind to CD4 molecules and have been used to target lipid nanoparticles to CD4+ T cells.[15, 38] These CD4 binding peptides could potentially reduce immunogenic responses caused by some antibodies and have improved shelf-life, lower cost and

offer scalable manufacturing.[39] Among the existing CD4 binding peptides,[40-43] we chose BP4 (peptide sequence: CARRPKFYRAPYVKNHPNVWGPWVAYGP, ST40 CD4 antibody mimetic) as it was previously reported to have the highest binding affinity and selective targeting to CD4 when conjugated to lipid nanoparticles.[38]

There are two key issues in choosing the best CD4 binding ligand for a particular adaptation. First, most CD4 binding ligands have not been tested head-to-head with other CD4 binding ligands on the same NCs. Second, although the role of ligands in delivering NCs to specific cells has long been recognized in many applications, relatively few studies have investigated the effects of physicochemical properties of nanocarriers on the ligand function. It is known that particle size and shape can affect the interactions of ligands with their targets,[44-47] but the effect of particle ζ-potential, another key parameter, has not been well investigated.

In this study, we selected several CD4 binding ligands including a rhesus recombinant CD4 mAb, the CD4 mAb fragments that are selectively reduced from this full mAb, and the BP4 binding peptide. These different CD4 binding ligands were each conjugated separately to lipid-coated PLGA nanoparticles (LCNP) in order to evaluate their targeting abilities (Figure 4.1). The LCNP, as an emerging drug delivery system, has advantages of both lipid and polymeric nanoparticles, such as encapsulation of both hydrophilic and hydrophobic drugs with high loading efficiency, tunable and sustained drug release profile, excellent colloidal stability, and ease of conjugation with a variety of ligands for targeting purposes.[48-54] We found that BP4 conjugated LCNP led to a high cell binding in general that was not specific to CD4+ T cells. The CD4 mAb slightly enhanced NC binding and specificity for CD4+ T cells. The CD4 antibody fragments had a higher conjugation efficiency to LCNPs, higher binding specificity for CD4 T cells and lower nonspecific binding than their parent full antibody. A surprising finding was that

negatively-charged LCNPs could dramatically reduce nonspecific binding and enhance CD4 targeting specificity, in comparison to neutral or positively charged LCNPs. To our knowledge, this is the first report investigating different CD4 targeting ligands on a single nanoparticle system, as well as the effect of ζ-potential on receptor-mediated nanocarrier targeting. By applying the results of these experiments, we developed an LCNP platform that can be widely utilized to target CD4+ T cells for a variety of applications.

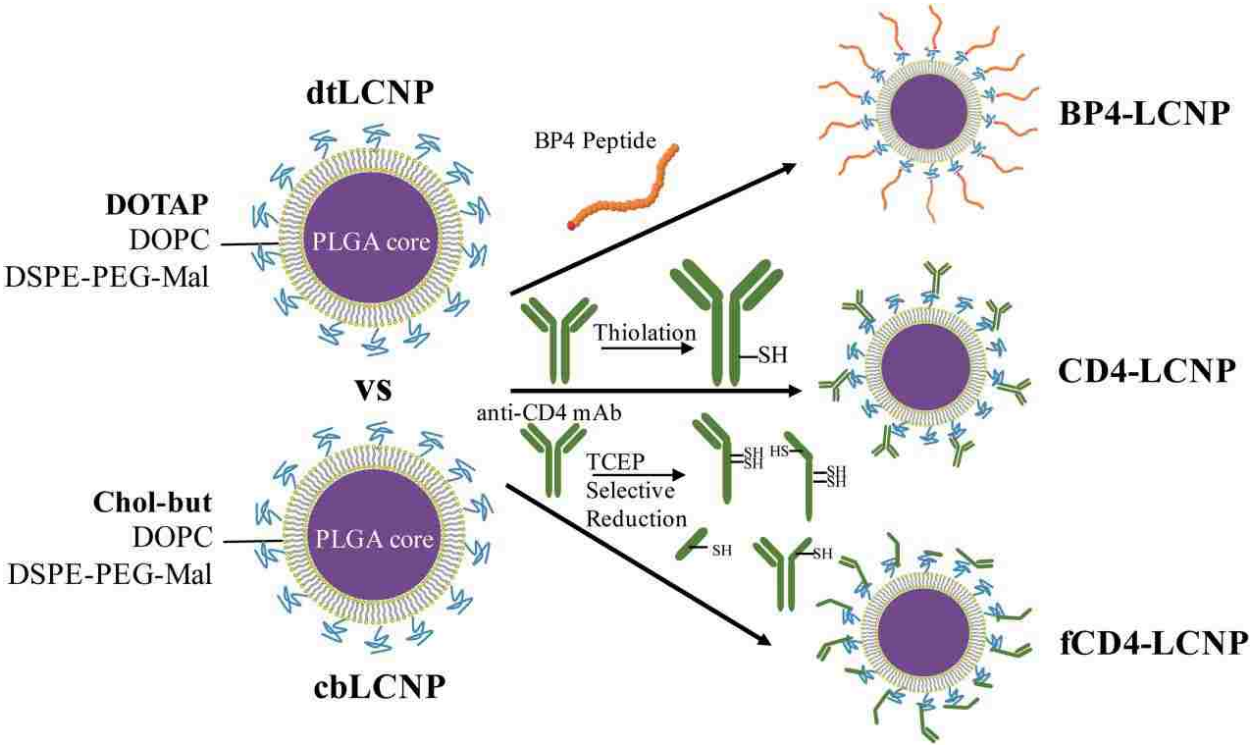

Figure 4.1. Schematic illustration of two LCNP formulations conjugated with different CD4 targeting ligands.

4.3 Materials and methods

4.3.1 *Materials*

PLGA (75:25 L:G; ester-terminated, inherent viscosity range: 0.55-0.75 dL/g in CHCl3) was purchased from Lactel. All lipids for the nanoparticle synthesize were purchased from Avanti

Polar Lipids, including 1,2-Dioleoyl-sn-glycero-3-phosphocholine (DOPC), 1,2-Dioleoyl-sn-glycero-3-phosphocholine (DOTAP), 1,2-distearoyl-*sn*-glycero-3-phosphoethanolamine-N-[maleimide(polyethylene glycol)-2000] (DSPE-PEG-MAL). Cholesteryl butyrate was purchased from Santa Cruz Biotechnology. Rhesus recombinant anti-CD4 antibody and rhesus recombinant IgG1 isotype control antibody were purchased from NIH Nonhuman Primate Reagent Resource. FITC mouse anti-human CD8, PE mouse anti-human CD14, PerCP mouse anti-human CD3 antibodies, FITC mouse anti-human CD4, and FITC mouse IgG1, PE mouse IgG2a, PerCP mouse IgG1 κ control antibodies were purchased from BD Biosciences. RPMI 1640 containing 2mM L-glutamine and 25mM HEPES, DPBS, heat-inactivated fetal bovine serum (FBS), Penicillin-Streptomycin (10,000 U/mL), 1,1'-Dioctadecyl-3,3,3',3'-Tetramethylindodicarbocyanine, 4-Chlorobenzenesulfonate Salt (DiD), LIVE/DEAD® Fixable Violet Dead Cell Stain Kit, Dylight 633 NHS Ester were purchased from ThermoFisher. All other chemicals were purchased from Sigma-Aldrich and Fisher Scientific unless otherwise specified.

4.3.2 *Peptide synthesis and characterization*

The BP4 peptide was synthesized at a 0.1 mmol scale with a CEM Liberty Blue automated microwave peptide synthesizer using standard Fmoc chemistry. Rink Amide MBHA resins (Novabiochem) were used to generate C-terminal peptides. Standard Fmoc amino acids (Chempep), N,N'-Diisopropylcarbodiimide (DIC), and ethyl(hydroxyimine)cyanoacetate were used all at 5 equiv. for coupling and 20% (v/v) piperidine in DMF was used for deprotection. The cleavage of peptides from the resin was done by an Accent peptide cleavage system (CEM) in the cleavage cocktail (trifluoroacetic acid (TFA)/triisopropylsilane/2,2′-(Ethylenedioxy)diethanethoil/water (9.25:0.25:0.25:0.25 by volume)) for 30 min. The peptides

were collected by the addition of cold diethyl ether and centrifugation, following purification by semi-preparative high performance liquid chromatography (HPLC) using a Prominence LC20AD HPLC (Shimadzu) with a Phenomenex Gemini C18 column (250 x 10 mm) eluting with water-acetonitrile (with 0.1% TFA) gradients. Purified BP4 peptide was analyzed by analytical HPLC with a Phenomenex Kinetex C18 column (250 x 4.6 mm), and matrix-assisted laser desorption/ionization time-of-flight (MALDI-TOF) mass spectrometer (MS) (Bruker AutoFlex II).

4.3.3 *Antibody thiolation, reduction and characterization.*

To prepare full antibody with free sulfhydryl groups, rhesus recombinant anti-CD4 antibody or rhesus recombinant IgG1 isotype control antibody was incubated with 10 molar excess of Traut's reagent in phosphate-buffered saline (PBS) with 5 mM ethylenediaminetetraacetic acid (EDTA) for 1 hour. Free Traut's reagent was removed using a Zeba spin-desalting column (7K MWCO, Life Technologies). The final concentration of mAb was measured using a Nanodrop 2000c spectrophotometer (Thermo Scientific). To prepare antibody fragments, the CD4 mAb or Isotype IgG control mAb was incubated with 3X molar excess of tris(2-carboxyethyl)phosphine (TCEP) in phosphate-buffered saline (PBS) with 5 mM ethylenediaminetetraacetic acid (EDTA) for 1 hour, followed by removal of TCEP by the Zeba spin-desalting column. The full mAb, thiolated mAb and cleaved mAb were run on a NuPAGE 4-12% Bis-Tris 10-well mini gel in MOPS SDS running buffer using XCell SureLock Mini-Cell Electrophoresis System (Invitrogen). The samples were run for 50 minutes at 200 V constant, and the resulting gel was stained in SimplyBlue following the manufacturer's recommended procedures. The sulfhydryl groups on thiolated CD4 mAb or reduced CD4 mAbs were measured using a Fluorometric Thiol Assay Kit (Sigma)

4.3.4 *Synthesis of LCNPs and conjugation of CD4 binding ligands to LCNPs*

LCNPs were synthesized using a modified single emulsion evaporation method. Briefly, the lipid mixture (DOPC, DOTAP, and DSPE-PEG-MAL, or DOPC, cholesteryl butyrate, and DSPE-PEG-MAL at 4:4:1 molar ratio) in chloroform were dried under nitrogen, and left under high vacuum prior to usage. Lipid suspension were prepared by adding Milli-Q water into dried lipids following votexing and bath sonication until lipids were dispersed well. PLGA was dissolved in ethyl acetate at 10 mg/mL and was added drop-wise to the lipid suspension at the mass ratio of 5:1 (PLGA : lipids) while votexing. The mixture was then homogenized using a probe sonicator (500 W, Ultrasonic Processor GEX500) with a 3 mm diameter microtip probe at 38% amplitude for three rounds at 30s per round. The sonicated emulsion was transferred to Milli-Q water and all residual organic solvent was evaporated by rotary evaporation (Rotavapor R-210, BUCHI). Nanoparticles were then washed by centrifugation at 14,000 rpm for 10 min at 4 °C and resuspended in water using alternating vortexing. LCNPs were stored in water at 4 °C until use.

BP4 was incubated with LCNPs at different feed ratios (6.2 wt% to 0.25 wt%, BP4 to LCNP) for 1 hour in PBS with 5 mM EDTA. Thiolated full mAb or reduced mAb fragments were incubated with LCNPs at a feed ratio of 10.2 wt% (mAb to LCNP), which approximately equals to 2000 mAb molecules per LCNP, for 1 hour in PBS with 5 mM EDTA. All ligands conjugated LCNPs were then centrifuged at 10,000 rpm for 5 min to remove unbound BP4, full mAbs or fragmented mAbs. Unthiolated full mAbs were also incubated with two LCNPs at the same ratios, followed by centrifugation, to investigate the amount of mAb that nonspecifically absorpted onto LCNPs and the ability of centrifugation to remove free mAbs.

4.3.5 *Ligands conjugation efficiency*

The surface loading of BP4, full mAbs and fragmented mAbs conjugation to LCNPs were measured after ligand conjugation and lyophilization of LCNPs. The ligand loading (LL) at the surface of LCNPs is calculated using Eq. (1):

$$\text{Ligand Loading (wt\%)} = \frac{\text{Mass of ligands (mg)}}{\text{Mass of ligands conjugated LCNPs}} \times 100 \quad (1)$$

The mass of LCNPs were measured after lyophilization of LCNPs. BP4-LCNPs were dissolved in DMSO, followed by at least 2-fold dilution in Milli-Q water, and BP4 contents were measured by Pierce Quantitative Fluorometric Peptide Assay (Thermo Scientific). The concentration of full mAb or fragmented mAb on the surface of LCNPs were measured after hydrolyzing CD4-LCNPs or fCD4-LCNPs in 1 M NaOH buffer and 20-fold dilution in Milli-Q water, following measurement with a Micro BCA Protein Asaay Kit (Thermo Scientific).

The number of ligands molecules per LCNP is calculated using Eq. (2):

$$\text{Ligand Molecules Per LCNP} = m_{LCNP} \times LL \times \frac{N_A}{MW(L)} \quad (2)$$

The mass per LCNP (m_{LCNP}) is calculated from the diameter of the LCNP (200 nm) and PLGA density (1.2 g/mL). Ligand loading (LL) is calculated as described above, N_A is the Avogadro constant (6.02×10^{23} mol^{-1}), and MW (L) is the molecular weight of BP4 (3371 Da) or mAb (~150,000 Da). The molecule number of fragmented CD4 mAbs on the surface of LCNPs was regarded as the number of their original full mAbs. The number of ligands per LCNPs can be further translated to the surface density of ligands using Eq. (3):

$$\text{Surface Density} = \frac{\text{Ligand molecules per LCNP}}{\text{Surface area of LCNP}} \quad (3)$$

The surface area is calculated using diameters of LCNPs (200nm).

The conjugation efficiency of ligands to LCNPs is calculated using Eq. (4):

$$\text{Conjugation Efficiency (\%)} = \frac{\text{Ligand loading (wt\%)}}{\text{Feed mass ratio (wt\%)}} \times 100 = \frac{\text{Actual ligand molecules per LCNP}}{\text{Feed ligand molecules per LCNP}} \times 100 \quad (4)$$

4.3.6 *Characterization and colloidal stability of LCNP formulations*

All LCNP formulations were resuspended in Milli-Q water and measured of their sizes by Nanoparticle Tracking Analysis (NTA) using a NanoSight NS300 instrument (Malvern Instruments). Their ζ-potentials were measured by a Zetsizer Nano ZS90 (Malvern Instruments) in 10-fold diluted PBS. The colloidal stability of all LCNP formulations was measured in a biological environment. LCNPs were resuspended in RPMI 1640 cell culture medium supplemented with heat-inactivated fetal bovine serum (FBS) (10%, v/v), penicillin (100 U/mL) and streptomycin (100 mg/mL) at 1 mg/ml and stored in a shaker at 37 °C. Their sizes were measured by NTA at day 0 and 14.

4.3.7 *Preparation of cell line and PBMCs for cytotoxicity analysis*

A human T cell line, 174xCEM, was obtained from the NIH AIDS Reagent Program. Cells were maintained in RPMI 1640 supplemented with heat-inactivated fetal bovine serum (FBS) (10%, v/v), penicillin (100 U/mL), streptomycin (100 mg/mL), L-glutamine (2mM) and HEPES (25mM), and were incubated at 37 °C in a humidified 5% CO_2 air environment. Cells were seeded at 1×10^6 cells/mL in a 96-well plate and incubated with all LCNP formulations at 1, 0.2, or 0.04 mg/mL. After 24 hours incubation, cell avability was assessed using CellTiter-Blue Cell Viability Assay (Promega) following the manufacturere's recommended procedures. Briefly, cells were incubated for 4 h with CellTiter-Blue reagent (20 μL/well), and fluorescent signals were recorded at 560/590 nm ex/em using a fluorescent plate reader.

Pigtailed macaque (*Macaca nemestrina*) blood was purchased from Washington National Primate Research Center (WaNPRC). Peripheral blood mononuclear cells (PBMCs) were isolated using lymphocyte separation medium (LSM, Mediatech, Inc). In brief, 10ml blood was carefully layered over 5ml LSM in a 15ml conical tube and centrifuged for 25 minutes at 800g. The mononuclear cell-rich band was removed, and resuspended in PBS and the cells pelleted by centrifugation for 10 minutes at 250g. Isolated PBMCs were maintained in the same RPMI 1640 cell culture medium as described above until usage. We used PBMCs from three pigtail macaques to measure cytotoxicity profiles of all LCNP formulations. PBMCs were seeded at the concentration of 1×10^6 cells/mL in a 24-well plate and incubated with different LCNP formulations at 0.5 mg/mL. After 24 hour incubation, cells were washed by PBS, and incubated with a Fixable Violet Live/Dead Cell Stain Kit(Invitrogen) at room temperature for 30 min, followed by another round wash with PBS and fixation in 2% paraformaldehyde (PFA). The percentage of live cells was then measured by flow cytometry (LSR II, BD Biosciences) and analyzed using FlowJo 10.8.

4.3.8 *In vitro cell binding assay*

First, the cross-reactivity of anti-macaque CD4 mAb on human CD4 was verified by staining 174xCEM with fluorescently-labeled mAbs. Rhesus recombinant anti-CD4 mAb or rhesus recombinant isotype IgG mAb was labeled by incubating with a DyLight 633 NHS Ester Amine-Reactive Dye (Thermo Scientific) for 1 hour at room temperature following desalting using a Zeba spin-desalting column. FITC mouse anti-human CD4 and FITC mouse IgG1 were used as the positive or negative control, respectively. These fluorescently-labeled mAbs were seperately incubated with 174xCEM cells for 30 min at 4 °C. Cells were then washed with PBS, stained

with the Live/Dead Kit, and fixed by 2% PFA. The fluorescent signals from cells were measured by flow cytometry.

DiD loaded LCNP formulations were synthesized as described above and used here for cell binding studies. 174xCEM cells were distributed into polystyrene tubes for each group/triplicate at the concentration of 1×10^6 cells/mL, and treated with 40 μg/mL bare LCNPs, BP4-LCNPs, CD4-LCNPs, Iso-LCNPs, fCD4-LCNPs, or Iso-LCNPs (dtLCNP or cbLCNP) for 30 min at 4 °C in the RPMI 1640 cell culture medium. After that, cells were washed and treated with Live/Dead staining following flow cytometry analysis.

4.3.9 *Ex vivo targeting assay from PBMCs of pigtail macaques*

PBMCs were isolated from pigtail macaque blood as described above. Cells were washed and resuspended in PBS, and divided into individual polystyrene tubes for each group/replicate at the concentration of 1×10^6 cells/mL. DiD loaded dtLCNP or cbLCNP formulations that conjugated with CD4 targeting ligands or their controls were added into each tube at the concentration of 40 μg/mL, and cells were incubated at 4 °C with gentle votexing every 10 minutes. FITC mouse anti-human CD8, PE mouse anti-human CD14, PerCP mouse anti-human CD3 antibodies were also added into cells for staining different cell populations. The FITC mouse IgG1, PE mouse IgG2a, PerCP mouse IgG1 κ control antibodies were used as the isotype control for gating CD3, CD8 or CD14 positive cells. After 30 min incubation, PBMCs were washed and treated with Live/Dead staining following flow cytometry analysis. CD4+ cells were gated by CD3+CD14-CD8- populations.

4.3.10 *Statistical analysis*

Data were expressed mean ± SD unless otherwise indicated, with statistical significance defined as $p < 0.05$. Statistics were calculated using Prism 7.0 (GraphPad Software, Inc.). Statistical analysis was performed using unpaired two-sided student's *t* test for most of experiments in this study, or paired two-sided student's *t* test for the *ex vivo* cell targeting assay when using PBMCs of three pigtail macaques.

4.4 Results

4.4.1 *Preparation of CD4 binding ligands.*

We evaluate targeting efficiency of the CD4 mAb and its fragment, as well as the BP4 peptide, conjugated to LCNPs. For the BP4 peptide, we added a cysteine at the N-terminus to provide a thiol for conjugation to the LCNP. We synthesized the peptide using a microwave synthesizer followed by HPLC purification, which yielded over 100 mg of the BP4 peptide that was >98% pure (Figure 4.2A). The peptide molecular weight (MW) was confirmed to be 3371 Da by mass spectrometry (MS) (Figure 4.2B). For the CD4 mAb, we modified the mAb with Traut's Reagent that incorporates a small cyclic spacer terminated by a free sulfhydryl group used for cross-linking to primary amines (e.g. lysine side chains).[55] We measured on average one sulfhydryl group per antibody molecule using a fluorometric thiol quantitation assay (Figure 4.2C).

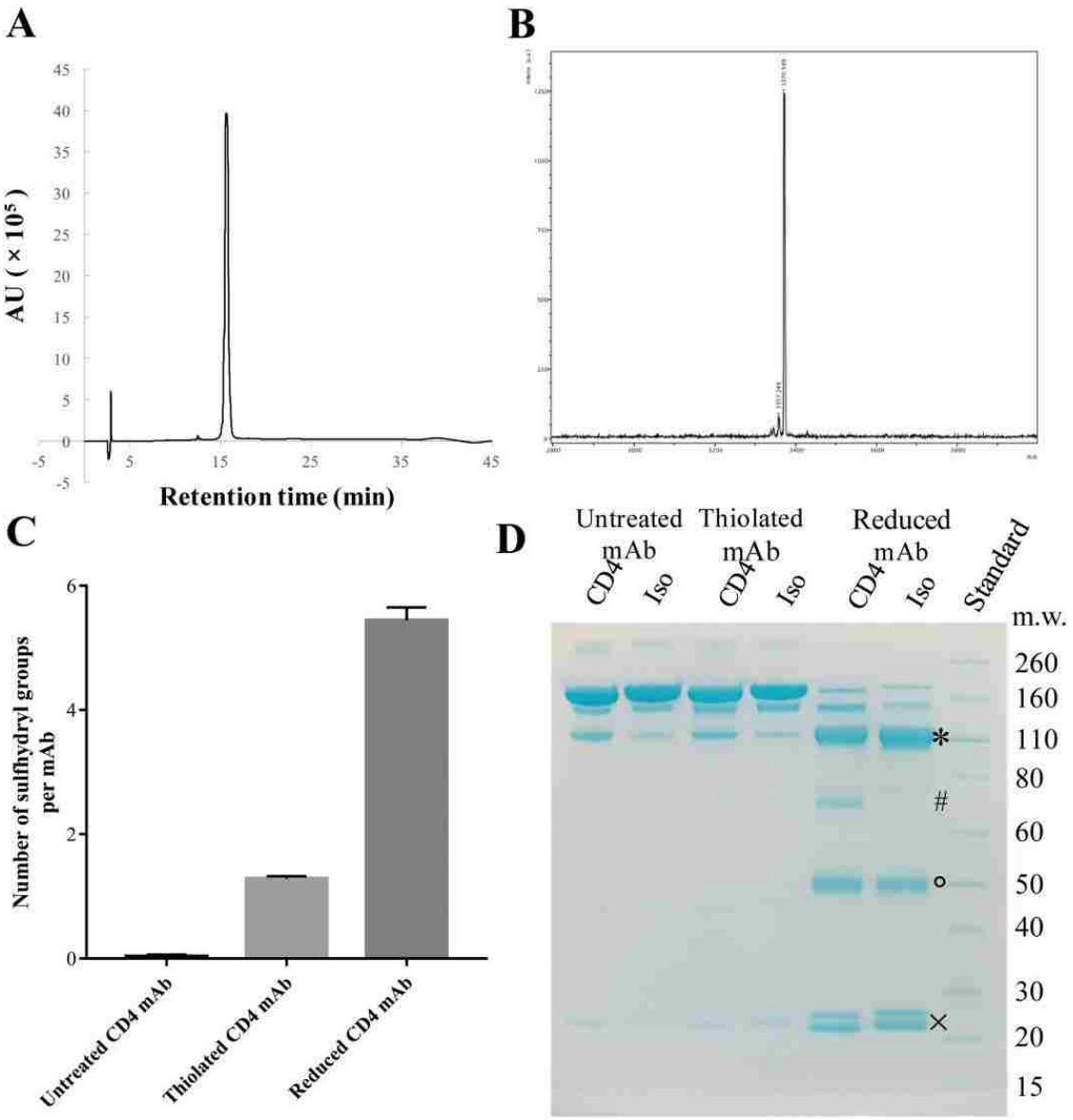

Figure 4.2. Characterization of different CD4 binding ligands. (A) Chromatograms for purified BP4 measured by HPLC. (B) Mass spectra for purified BP4. (C) Contents of free sulfhydryl groups on thiolated CD4 mAb or from the reduced CD4 mAb that generated fragments. Data represents mean ± SD, n=3. (D) SDS-PAGE results of anti-CD4 or isotype IgG antibody following thiolation or reduction. Full antibodies missing one single light chain (*), half antibodies (#) as well as the single heavy chain (°) and light chain (×) fragments were observed following TCEP reduction of CD4 mAB.

To generate the CD4 mAb fragments (fCD4), we used partial reduction with TCEP to selectively cleave the disulfide bonds between the antibody heavy chains or heavy and light chains. It has

been shown that 3-fold molar excess of TCEP maximizes the yield of a half antibody, which retains the binding affinity of the whole antibody.[33] At this ratio, we generated CD4 mAb fragments that were confirmed by SDS-PAGE, where we observed the full antibody missing one light chain and the half antibody, as well as the single heavy chain and light chain fragments following TCEP reduction (Figure 4.2D). The two heavy chains of the IgG1 antibody are connected by two disulfide bonds, and the light chain is connected to the heavy chain by one disulfide bonds.[56] Fluorometric thiol quantitation also showed that generation of CD4 mAb fragments by TCEP resulted in ~5 free sulfhydryl groups per one mAb molecule (Figure 4.2C), which confirmed the gel electrophoresis results and indicated that each mAb could generate 2-4 fragments.

4.4.2 *Synthesis and characterization of CD4-targeting LCNPs.*

We hypothesized that the targeting function of nanoparticles could be affected by the type of ligands conjugated to the surface or interference from physicochemical properties of the nanoparticle (e.g., size, charge). To investigate this hypothesis, we conjugated the three different CD4 binding ligands to LCNPs that were either neutral or negatively charged. The neutral LCNP (dtLCNP) contains a PLGA core and a lipid layer composed of the cationic lipid DOTAP, the neutral lipid DOPC, and the multifunctional lipid DSPE-PEG-MAL used for stabilization and providing the maleimide for conjugation to thiol-containing ligands. In contrast, the negatively charged LCNP (cbLCNP) replaced the DOTAP in the lipid bilayer shell with cholesteryl butyrate (chol-but). The chol-but has been reported to coat lipid solid nanoparticles that led to negative ζ-potentials,[57-59] and exhibits potential applications such as HIV latency reversal as a butyric acid prodrug.[60-61] We synthesized both LCNPs through modification of a commonly used single emulsion-solvent evaporation technique.[62]

We optimized the surface density and efficiency of BP4 conjugation to LCNPs by conjugating it at mass ratios from 0.25 wt% to 6.2 wt% (BP4 to LCNP), and quantified the amount of conjugated BP4 by a fluorometric peptide assay. We observed that BP4-LCNPs prepared at feed ratios above 1.24 wt% were difficult to reconstitute after washing and high-speed centrifugation. Thus, we chose the feed ratio of 1.24 wt% to ensure maximal BP4 density on the nanoparticles. The reaction between BP4 and either dtLCNPs or cbLCNPs led to over 98% conjugation efficiency and ~12 µg BP4 was successfully conjugated to 1 mg of LCNPs (Table 4.1), which translates to ~11,000 BP4 molecules per LCNP.

Table 4.1. Contents of CD4 binding ligands on LCNPs.

LCNP formulations	Feed mass ratio (wt%)	Feed ligand molecules per LCNP[a]	Ligand Loading (wt%)[b]	average ligand molecules per LCNP[a]	Conjugation efficiency (%)[b]
BP4-dtLCNP	1.24	11126	1.22 ± 0.01	10947	98.4 ± 0.2
CD4-dtLCNP	10.17	2053	4.17 ± 0.10	842	41.0 ± 1.0
fCD4-dtLCNP	10.17	2053	6.20 ± 0.07	1250	60.2 ± 0.7
BP4-cbLCNP	1.24	11126	1.23 ± 0.01	11070	99.5 ± 0.2
CD4-cbLCNP	10.17	2053	4.36 ± 0.10	881	42.9 ± 0.9
fCD4-cbLCNP	10.17	2053	6.28 ± 0.04	1268	61.0 ± 0.5

[a]The number of fCD4 molecules was regarded as the number of full antibodies that generated these fCD4 (one antibody could generate 2-4 fCD4 by TCEP reduction).
[b]Data represents mean ± SD from at least three samples.

To efficiently conjugate antibodies to LCNPs, we used a molar feed ratio of 2,000 mAb to one LCNP, which we have previously shown to effectively saturate the conjugation reaction to the LCNPs.[63] The amount of mAb retained with the LCNPs after centrifugation was 4.17 ± 0.10 wt% for CD4-dtLCNP (842 mAb per LCNP) and 4.36 ± 0.10 wt% for CD4-cbLCNP (881 mAb per LCNP) (Table 4.1). Conjugation of fCD4 mAb to LCNPs yielded 6.20 ± 0.07 wt%, on dtLCNPs and 6.28 ± 0.04 wt% on cbLCNP, which was about two-fold more efficient than conjugation of the full CD4 mAb. These values are equivalent to greater than 3,000 fCD4

molecules per LCNP as there were 2-4 fCD4 molecules generated from one full antibody. Taken together, these results indicate that smaller targeting ligands have higher conjugation efficiency and therefore can be conjugated at a higher density on LCNPs.

To confirm that the full and fragmented antibody conjugation was due to a specific thiol-maleimide linkage rather than nonspecific absorption, we mixed untreated mAb with cbLCNPs or dtLCNPs at the same ratio and concentrations. We found that less than 0.7 wt% or 0.5 wt% of the mAbs were retained with the cbLCNPs or dtLCNPs, respectively, and over 99% of the mAb was detected in the supernatant. These results indicate that washing and centrifugation are sufficient for removal of all free mAbs or their fragments, and there is only a negligible amount of mAb absorbed nonspecifically onto the LCNPs.

All the targeted LCNP formulations have particle diameters of ~200 nm in PBS, suggesting that the ligand conjugation or the lipid composition did not significantly affect the particle sizes (Figure 4.3A). However, the ζ-potential of dtLCNPs was altered from neutral to positive when linked to BP4, whereas the full antibody or fragmented antibody conjugation did not affect the ζ-potential of the dtLCNPs. As expected, replacing DOTAP with cholesteryl butyrate resulted in a negative ζ-potential for these LCNP formulations. (Figure 4.3B). These same formulations showed high colloidal stability (14 days), which we assessed by measuring the preservation of nanoparticle size in cell culture media (Figure 4.3C).

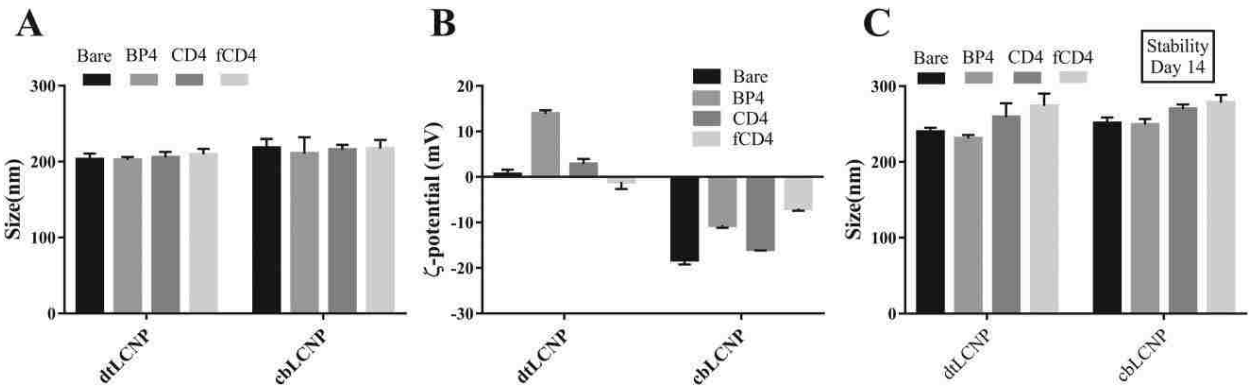

Figure 4.3. Properties of LCNPs conjugated with different CD4 binding ligands. (A) Sizes of CD4 targeted dtLCNPs or cbLCNPs measured by NanoSight. (B) ζ-potentials of CD4 targeted dtLCNPs or cbLCNPs measured by ZetaSizer. (C) Sizes of CD4 targeted dtLCNPs or cbLCNPs after incubation in RPMI 1640 cell culture medium for 14 days at 37 °C. Data represents mean ± SD from at least three samples.

4.4.3 *Comparison of cell binding in a 174xCEM human T cell line.*

We chose the 174xCEM human T cell line for our *in vitro* cell binding studies because these cells have been reported to express high densities of CD4,[64] and have also been used to test CD4 targeted nanoparticles by other groups.[38] We verified the cross-reactivity of a rhesus recombinant anti-CD4 antibody (labeled with DyLight 633) with these human CD4+ T cells (Figure 4.4A). We measured metabolic activity of 174xCEM after exposing the cells to the LCNP formulations for 24 hours and found that all LCNP formulations were not cytotoxic at LCNP concentrations up to 1 mg/mL (Figure 4.4B).

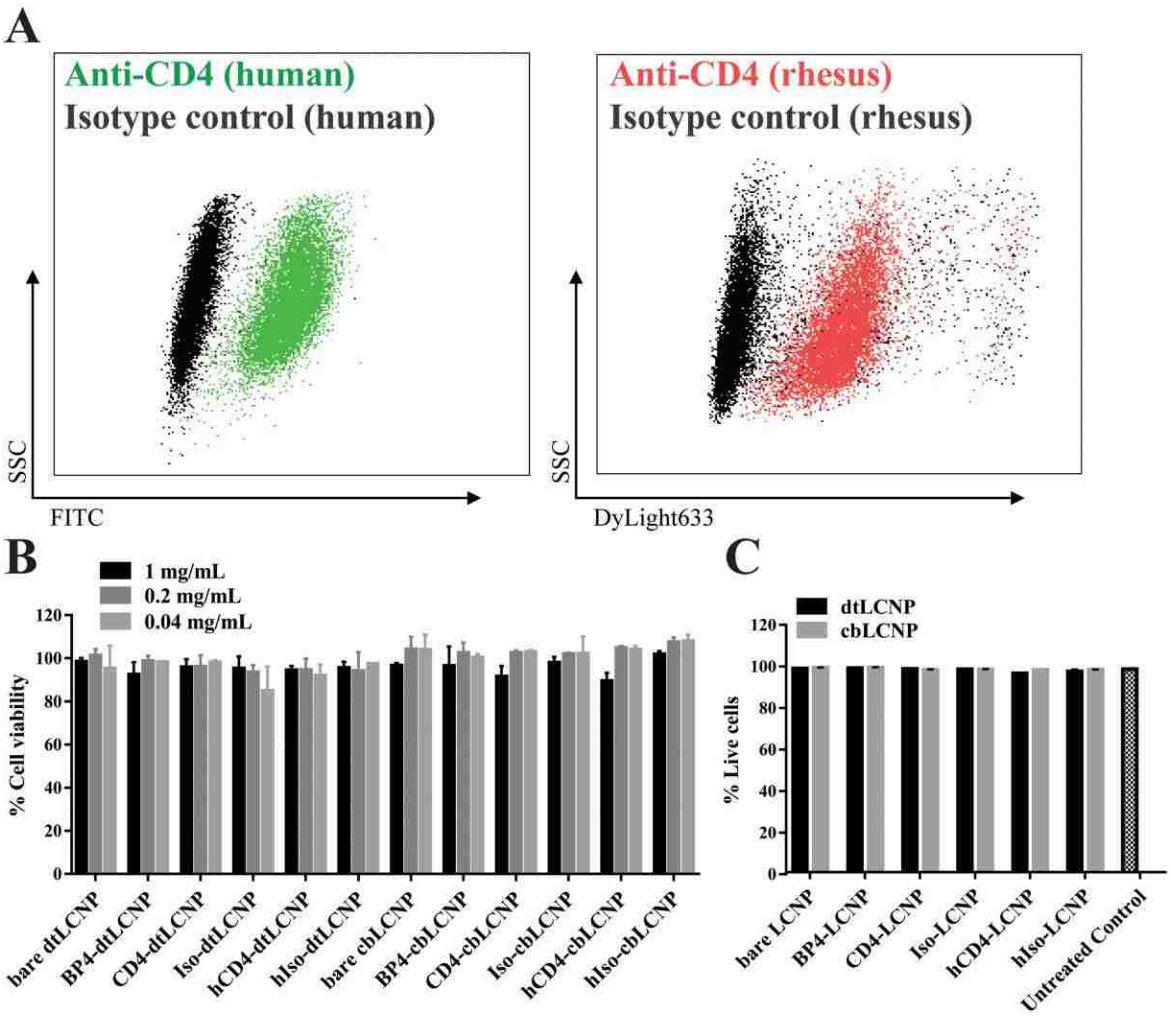

Figure 4.4. All LCNP formulations do not show cytotoxicity on human T cell line or primary cells. (A) Flow cytometry dot plot analysis of CD4 staining on a 174xCEM human T cell line. Left: 174xCEM cells treated with FITC anti-human CD4 antibody (green) or FITC isotype IgG antibody (gray). Right: 174xCEM cells treated with DyLight633 labeled rhesus recombinant anti-CD4 antibody (blue) or DyLight633 labeled rhesus recombinant isotype IgG antibody (gray). (B) dtLCNP or cbLCNP conjugated with different CD4 binding ligands showed no cytotoxicity to 174xCEM cells after treating cells with up to 1 mg/mL LCNPs for 24 hours, measured by CellTiter-Blue. Untreated cells were used as 100% viability control. (C) All LCNP formulations showed no cytotoxicity to PBMCs of pigtail macaques after incubation at 0.5 mg/mL LCNPs for 24 hours, following live/dead staining measured by flow cytometry. Data represents mean ± SD, n=3.

To evaluate the CD4-dependent binding of targeted and untargeted LCNP formulations to CD4-expressing cells, we exposed cells to a 0.05 wt% DiD loaded LCNP formulation and measured cellular fluorescence by flow cytometry. We found that free DiD released from LCNPs is

negligible since over 95% of DiD remained associated with the LCNPs after 24 hours incubation at 37 °C.

Our non-targeted controls included bare dtLCNPs without any ligands, isotype IgG-conjugated dtLCNPs (Iso-dtLCNPs), and fragmented isotype IgG conjugated dtLCNPs (fIso-dtLCNPs). BP4-dtLCNPs, CD4-dtLCNPs and Iso-dtLCNPs all bound to over 90% of live cells, and bare dtLCNPs bound to 45.2 ± 2.2% of cells, indicating high levels of nonspecific binding between cells and dtLCNPs. Interestingly, fIso-dtLCNPs only bound to 19.8 ± 1.3% of cells while fCD4-dtLCNPs showed 62.1 ± 1.2% cell binding (Figure 4.5A, B). While nonspecific binding was evident for the full mAb and peptide conjugated dtLCNP formulations, it was slightly reduced in the formulation conjugated with the fragmented antibodies.

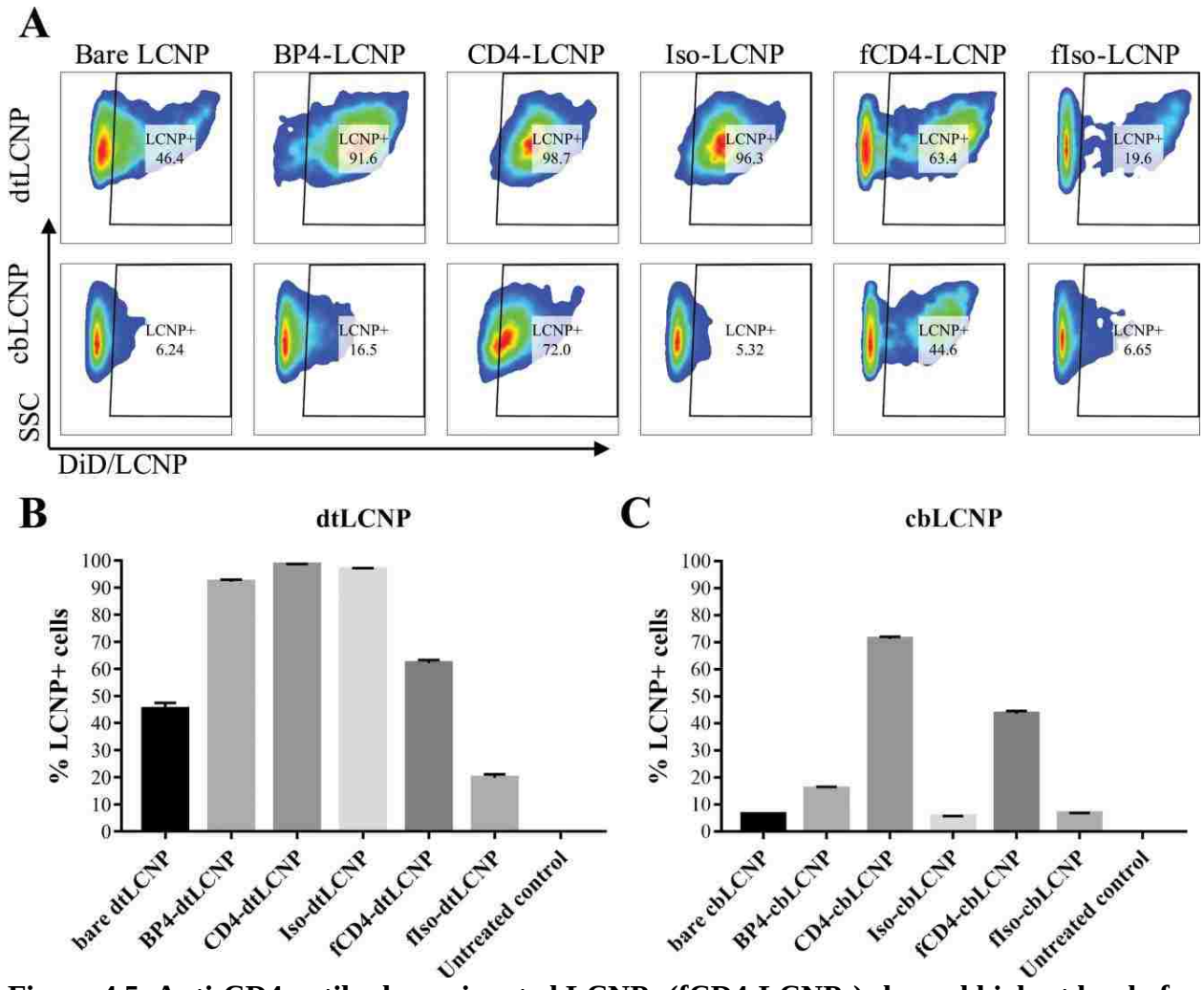

Figure 4.5. Anti-CD4 antibody conjugated LCNPs (fCD4-LCNPs) showed highest level of binding to 174xCEM human T cell line. Replacement of DOTAP with Chol-but in the lipid composition of LCNPs led to significant decrease of non-specific binding of LCNPs to cells. (A) Representative flow cytometry dot plots of 174xCEM bound with DiD loaded dtLCNPs or cbLCNPs conjugated with different CD4 targeting ligands. (B, C) The percentages of 174xCEM cells that associated with DiD/dtLCNPs (B) or DiD/cbLCNPs (C). Data represents mean ± SD, n=3.

Since most dtLCNP formulations revealed high levels of nonspecific binding, we evaluated whether replacing DOTAP with cholesteryl butyrate in the lipid composition of LCNPs (cbLCNP) could reduce non-specific binding and improve targeting specificity. Surprisingly, all control groups, including bare cbLCNP, Iso-cbLCNP, and fIso-cbLCNP showed less than 10% of cells associated with LCNPs. In contrast, CD4-cbLCNPs and fCD4-cbLCNPs bound to 71.2 ±

0.8% or 43.6 ± 0.9% cells, respectively (Figure 4.5A, C). cbLCNPs surface conjugated with the full antibody or its fragment, but not BP4 peptide, resulted in low non-specific cell binding and high receptor-mediated binding to 174xCEM cells *in vitro*.

4.4.4 *CD4-targeted LCNPs preferentially bind CD4+ T cells from pigtail macaque PBMCs.*

We used primary cells obtained from pigtail macaque PBMCs to further evaluate the targeting function of our LCNPs. We treated PBMCs with our DiD-loaded targeted LCNP formulations and measured LCNP binding to CD14-CD3+CD8- cells (mostly CD4+ T cells) compared to CD14-CD3+CD8+ cells (CD8+ T cells). All the formulations and their respective controls were tested for cytotoxicity to PBMCs and showed high cell viability at the two different concentrations (Figure 4.4C).

From the targeting studies using PBMCs with dtLCNPs (Figure 4.6A-C), we observed similar but relatively high DiD fluorescent signals from both CD4+ and CD8+ T cells from treatment with bare dtLCNPs and Iso-dtLCNPs. These results further confirm the high level of nonspecific binding of dtLCNPs to cells. Accounting for the non-specific binding, we found that CD4-dtLCNPs bound to more CD4+ cells (~40% LCNP-positive cells) than CD8+ cells (~20% LCNP-positive cells), which was also indicated by a 1.7-fold higher MFI in CD4+ cells over CD8+ cells. fCD4-dtLCNPs preferentially bound to CD4+ cells, demonstrated by a 2.5-fold higher MFI over CD8+ cells. The fIso-dtLCNP negative control did not bind well to either CD8+ or CD4+ cells, suggesting a much lower nonspecific association between cells and LCNPs compared with bare dtLCNPs and Iso-dtLCNPs. BP4-dtLCNPs showed high cell association to both CD8+ and CD4+ cells, indicating that BP4-dtLCNPs bound nonspecifically to cells and is not a useful ligand for targeting CD4+ cells from pigtail macaques.

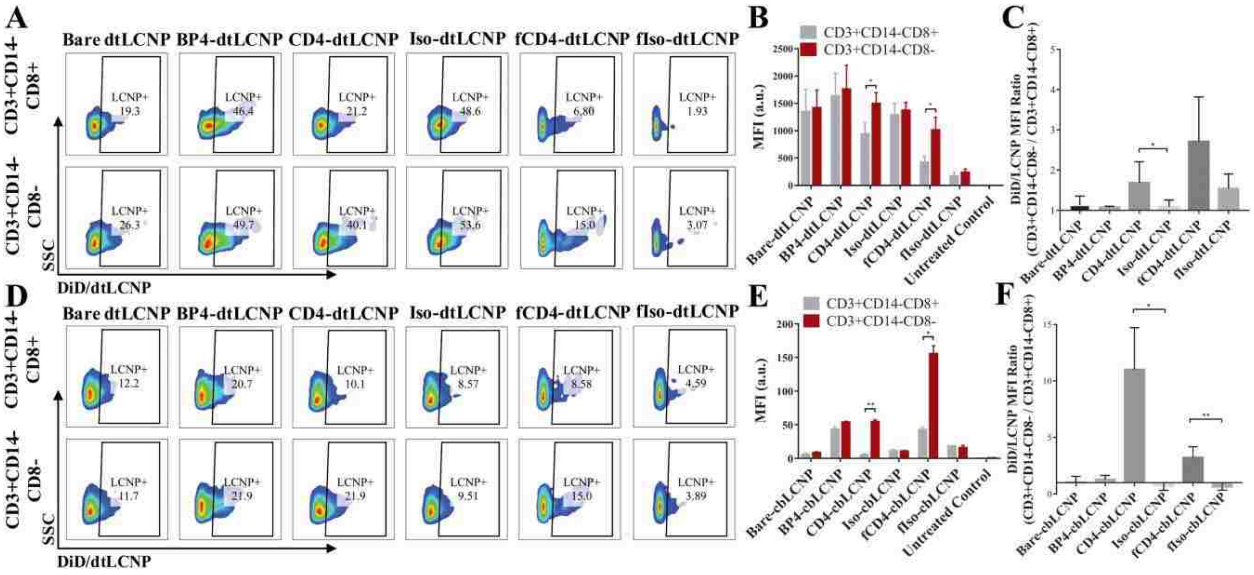

Figure 4.6. Both CD4-LCNPs and fCD4-LCNPs showed preferential binding to CD3+CD14-CD8- cells from macaque PBMCs. Replacement of DOTAP with chol-but in the LCNP lipid composition led to significant reduction of non-specific binding, and improved targeting functions of CD4-LCNPs. (A, D) Representative flow cytometry dot plots of PBMC populations (CD3+CD14-CD8- vs. CD3+CD14-CD8+) associated with DiD/dtLCNPs (A) or DiD/cbLCNPs (D) conjugated with different CD4 targeting ligands or their controls. (B, E) Mean fluorescent intensity (MFI) of DiD signals from CD3+CD14-CD8- or CD3+CD14-CD8+ cells after incubation of PBMCs with various CD4 targeted DiD/dtLCNPs (B) or DiD/cbLCNPs (E). (C, F) MFI ratio of DiD signals from CD3+CD14-CD8- cells to CD3+CD14-CD8+ cells after incubation of PBMCs with LCNPs accordingly. Data represents mean ± SD from PBMCs of three pigtail macaques. *p<0.05, **p<0.005. ***p<0.0005.

Since we observed that the nonspecific binding was significantly reduced using cbLCNP formulations in 174xCEM cell studies, we further tested the targeting of cbLCNPs in pigtail macaque PBMCs (Figure 4.6D-F). All control groups showed low levels of cell binding indicated by percentage of LCNP+ cells (<15%) and by MFI from both CD8+ and CD4+ cells (<50 a.u.). BP4-cbLCNPs still showed higher cell association compared to control groups, but there was no significant difference in MFI between CD8+ and CD4+ cells, indicating that these cell associations were most likely nonspecific and not CD4 receptor-mediated. The targeting function of anti-CD4 mAb was better revealed when linked to cbLCNPs compared to dtLCNPs, as it led to 10-fold higher MFI of DiD signal in CD4+ cells over CD8+ cells. fCD4-cbLCNPs

showed 3-fold higher MFI binding to CD4+ cell compared to CD4-cbLCNPs. However, there was also a relatively high level of CD8+ cell association with fCD4-LCNPs and only a 3-fold difference in MFI between CD4+ over CD8+ cells. These results indicate that targeted cbLCNP formulations using CD4 mAb or its fragmented mAb, performed better CD4 targeting than dtLCNP formulations.

4.5 Discussion

The results reported here show that targeting of functionalized LCNPs is dependent on ligands, but also affected by the LCNP lipid composition or its ζ-potential. The neutral or positively charged LCNPs had a high level of nonspecific binding to cells that hindered receptor-mediated targeting. The negatively charged LCNPs, however, showed negligible nonspecific binding and we were able to further determine the CD4 binding specificity between different CD4 binding ligands when conjugated to LCNPs.

Neutral control dtLCNPs that have DOTAP in the lipid composition, including bare dtLCNPs and Iso-dtLCNPs, showed high binding to the 174xCEM cell line, which might be a result of nonspecific binding interactions (e.g. the fusion of LCNPs with cellular membranes). We further confirmed such nonspecific binding in PBMCs isolated from pigtail macaques, where the two control dtLCNPs showed equally high binding to both CD4+ and CD8+ T cells. The BP4 binding peptide has a net charge of +5 at pH 7 with an isoelectric point at pH 10.61 (calculated based on its sequence) showing that the peptide is positively charged in the relevant physiological environment. As a consequence, the conjugation of positively charged BP4 caused the dtLCNP ζ-potential to change from neutral to positive. BP4-dtLCNPs showed higher binding to 174xCEM cells than bare dtLCNPs, but they did not reveal any preferential binding to CD4+

T cells in pigtail macaque PBMC studies. This suggested that BP4-dtLCNPs could lead to higher nonspecific binding to cells in comparison to other LCNP formulations. Because the cell membrane is negatively charged, these positively-charged BP4-dtLCNPs might fuse with cells through lipid interactions,[65] but could also have electrostatic interactions with the cell membrane. The dtLCNP conjugated with fragmented isotype IgG was an exception, as we observed a significantly reduced nonspecific binding of fIso-dtLCNPs to cells along with lower binding to both CD4+ and CD8+ cells from PBMCs. This might be due to the fact that the fragmented mAb had higher conjugation efficiency and loading on LCNPs, which would lead to greater surface area coverage of the lipid-shell layer and could impede interactions between the lipids and cell membrane. The fragmented antibody achieved a higher surface density up to 10,000 mAbs/um^2 (~1250 mAb per LCNP of ~200 nm diameter when accounting for the number of full mAb that generated these fragments, total number of fragments would be 2~4-fold more) compared to 6736 mAbs/um^2 for the full antibody conjugation (~ 842 mAbs per LCNP). Assuming the surface area projection of an antibody is 95 nm^2 (antibody radius ~5.5 nm),[66] approximately 64% of the spherical surface area is occupied by the full antibody and 95% is estimated to be occupied by fragmented antibodies. This calculation supports the hypothesis that the fragmented antibody could cover most of the surface of the LCNPs, thus hindering the nonspecific binding between the dtLCNPs and cells. In fact, we observed a high CD4 targeting specificity of fCD4-LCNPs both *in vitro* and *ex vivo*, while the CD4-LCNPs showed less preferential binding to CD4+ cells due to the obvious nonspecific binding.

When we replaced the lipid DOTAP with cholesteryl butyrate in the LCNP, the nonspecific binding was surprisingly low in all control groups, indicated by the low binding to 174xCEM cells and the similarity between CD4+ and CD8+ cell binding in PBMCs. This might be

explained by the negative ζ-potential of all cbLCNP formulations, which would lead to electrostatic repulsion to negatively-charged cell membranes. With the reduced nonspecific binding, we were able to better distinguish targeting functions of different CD4 binding ligands. BP4 peptides still caused nonspecific binding when conjugated with cbLCNPs, indicating that these peptides might not be the best candidate for CD4 targeting. However, this may be outweighed by the benefits of utilizing a CD4 binding peptide rather than an antibody and therefore it may be worthwhile to continue investigating other peptides with better binding affinity and lower nonspecific binding for the NC targeting. cbLCNPs surface conjugated with the full CD4 antibody or its fragment showed high binding *in vitro* to the 174xCEM cells, as well as preferential binding to CD3+CD14-CD8- cells from PBMCs. CD4-cbLCNPs showed 10-fold higher binding specificity for CD4+ T cells compared to CD8+ T cells, whereas fCD4-cbLCNP had a three-fold higher binding specificity for CD4+ T cells. In spite of this, fCD4-cbLCNP still had highest binding among all cbLCNP formulations to 174xCEM cells, as well as CD4+ T cells from PBMCs, which was probably due to the higher surface density of fragmented antibodies as explained above. A comparison of the CD4 mAb and its fragments on two LCNP formulations, cbLCNPs and dtLCNPs, showed significantly improved binding specificity of CD4-cbLCNP, but fCD4-cbLCNP remained similar to the dtLCNP formulation. This may be because the interaction of the LCNP lipid layer and cell membrane was already mostly inhibited for fCD4-dtLCNPs as shown in its low nonspecific binding.

4.6 Conclusion

In this study, we used a hybrid nanoparticle system to investigate the targeting of several CD4 binding ligands conjugate to NCs. The LCNPs can be conjugated with different kinds of ligands with high conjugation efficiencies, and their ζ-potential can be easily tuned to allow

investigation of both ligands and ζ-potential at the same time. We demonstrated that unlike neutral or positively charged LCNPs, a negative ζ-potential showed dramatically lower nonspecific binding and had preferential bindings to CD4+ T cells when conjugated with CD4 mAbs or its fragments. The BP4 peptide did not show any targeting effect and had high nonspecific binding when conjugated to one of LCNP formulations. Fragmented CD4 mAbs showed higher loading and better coverage on LCNP surfaces than the full mAbs, leading to a higher level of receptor-mediated cell binding. CD4-targeted LCNPs have great promise for delivery of anti-HIV cure agents, vaccines and gene-modifying oligonucleotide drugs that can be applied in a variety of biomedical areas.

4.7 Acknowledgements

The following reagents were obtained through the NIH AIDS Reagent Program, Division of AIDS, NIAID, NIH: 174xCEM cells from Dr. Peter Cresswell.[67] This work was supported by the Bringing Bioengineers to Cure HIV investment grant from amfAR (109541-61-RGRL) and the National Institute of Health (AI094412).

4.8 References

1. Arruebo, M.; Valladares, n.; Gonz, f.; lez-Fern; ndez, Antibody-conjugated nanoparticles for biomedical applications. *J. Nanomaterials* **2009,** *2009*, 1-24.
2. Shargh, V. H.; Hondermarck, H.; Liang, M., Antibody-targeted biodegradable nanoparticles for cancer therapy. *Nanomedicine* **2015,** *11* (1), 63-79.
3. Shi, J.; Kantoff, P. W.; Wooster, R.; Farokhzad, O. C., Cancer nanomedicine: progress, challenges and opportunities. *Nature reviews. Cancer* **2017,** *17* (1), 20-37.
4. Field, L. D.; Delehanty, J. B.; Chen, Y.; Medintz, I. L., Peptides for Specifically Targeting Nanoparticles to Cellular Organelles: Quo Vadis? *Accounts of Chemical Research* **2015,** *48* (5), 1380-1390.
5. Tan, K.; Danquah, M. K.; Sidhu, A.; Yon, L.; Ongkudon, C. M., Aptamer-mediated polymeric vehicles for enhanced cell-targeted drug delivery. *Current drug targets* **2016**.

6. Savla, R.; Minko, T., Nanoparticle design considerations for molecular imaging of apoptosis: Diagnostic, prognostic, and therapeutic value. *Advanced Drug Delivery Reviews* **2017,** *113* (Supplement C), 122-140.
7. Yang, J.; Lee, C.-H.; Park, J.; Seo, S.; Lim, E.-K.; Song, Y. J.; Suh, J.-S.; Yoon, H.-G.; Huh, Y.-M.; Haam, S., Antibody conjugated magnetic PLGA nanoparticles for diagnosis and treatment of breast cancer. *Journal of Materials Chemistry* **2007,** *17* (26), 2695-2699.
8. Ramana, L. N.; Anand, A. R.; Sethuraman, S.; Krishnan, U. M., Targeting strategies for delivery of anti-HIV drugs. *Journal of Controlled Release* **2014,** *192* (0), 271-283.
9. Yao, V. J.; D'Angelo, S.; Butler, K. S.; Theron, C.; Smith, T. L.; Marchiò, S.; Gelovani, J. G.; Sidman, R. L.; Dobroff, A. S.; Brinker, C. J.; Bradbury, A. R. M.; Arap, W.; Pasqualini, R., Ligand-targeted theranostic nanomedicines against cancer. *Journal of Controlled Release* **2016,** *240* (Supplement C), 267-286.
10. Kocbek, P.; Obermajer, N.; Cegnar, M.; Kos, J.; Kristl, J., Targeting cancer cells using PLGA nanoparticles surface modified with monoclonal antibody. *Journal of Controlled Release* **2007,** *120* (1–2), 18-26.
11. Look, J.; Wilhelm, N.; von Briesen, H.; Noske, N.; Günther, C.; Langer, K.; Gorjup, E., Ligand-Modified Human Serum Albumin Nanoparticles for Enhanced Gene Delivery. *Molecular Pharmaceutics* **2015,** *12* (9), 3202-3213.
12. Anhorn, M. G.; Wagner, S.; Kreuter, J.; Langer, K.; von Briesen, H., Specific Targeting of HER2 Overexpressing Breast Cancer Cells with Doxorubicin-Loaded Trastuzumab-Modified Human Serum Albumin Nanoparticles. *Bioconjugate Chemistry* **2008,** *19* (12), 2321-2331.
13. Du, J.; Zhang, Y. S.; Hobson, D.; Hydbring, P., Nanoparticles for immune system targeting. *Drug Discovery Today* **2017**.
14. Rincon-Restrepo, M.; Mayer, A.; Hauert, S.; Bonner, D. K.; Phelps, E. A.; Hubbell, J. A.; Swartz, M. A.; Hirosue, S., Vaccine nanocarriers: Coupling intracellular pathways and cellular biodistribution to control CD4 vs CD8 T cell responses. *Biomaterials* **2017,** *132*, 48-58.
15. Endsley, A. N.; Ho, R. J. Y., Enhanced anti-HIV efficacy of Indinavir after inclusion in CD4 targeted lipid nanoparticles. *Journal of acquired immune deficiency syndromes (1999)* **2012,** *61* (4), 417-424.
16. Kim, S.-S.; Peer, D.; Kumar, P.; Subramanya, S.; Wu, H.; Asthana, D.; Habiro, K.; Yang, Y.-G.; Manjunath, N.; Shimaoka, M.; Shankar, P., RNAi-mediated CCR5 Silencing by LFA-1-targeted Nanoparticles Prevents HIV Infection in BLT Mice. *Mol Ther* **2009,** *18* (2), 370-376.
17. Kovochich, M.; Marsden, M. D.; Zack, J. A., Activation of Latent HIV Using Drug-Loaded Nanoparticles. *PLoS ONE* **2011,** *6* (4), e18270.
18. Glass, J. J.; Yuen, D.; Rae, J.; Johnston, A. P. R.; Parton, R. G.; Kent, S. J.; De Rose, R., Human immune cell targeting of protein nanoparticles - caveospheres. *Nanoscale* **2016,** *8* (15), 8255-8265.
19. Dinauer, N.; Balthasar, S.; Weber, C.; Kreuter, J.; Langer, K.; von Briesen, H., Selective targeting of antibody-conjugated nanoparticles to leukemic cells and primary T-lymphocytes. *Biomaterials* **2005,** *26* (29), 5898-5906.
20. Smith, T. T.; Stephan, S. B.; Moffett, H. F.; McKnight, L. E.; Ji, W.; Reiman, D.; Bonagofski, E.; Wohlfahrt, M. E.; Pillai, S. P. S.; Stephan, M. T., In situ programming of leukaemia-specific T cells using synthetic DNA nanocarriers. *Nat Nano* **2017,** *12* (8), 813-820.
21. McHugh, M. D.; Park, J.; Uhrich, R.; Gao, W.; Horwitz, D. A.; Fahmy, T. M., Paracrine co-delivery of TGF-β and IL-2 using CD4-targeted nanoparticles for induction and maintenance of regulatory T cells. *Biomaterials* **2015,** *59*, 172-181.

22. Ramishetti, S.; Kedmi, R.; Goldsmith, M.; Leonard, F.; Sprague, A. G.; Godin, B.; Gozin, M.; Cullis, P. R.; Dykxhoorn, D. M.; Peer, D., Systemic Gene Silencing in Primary T Lymphocytes Using Targeted Lipid Nanoparticles. *ACS Nano* **2015**.
23. Peer, D.; Park, E. J.; Morishita, Y.; Carman, C. V.; Shimaoka, M., Systemic Leukocyte-Directed siRNA Delivery Revealing Cyclin D1 as an Anti-Inflammatory Target. *Science* **2008,** *319* (5863), 627-630.
24. Churchill, M. J.; Deeks, S. G.; Margolis, D. M.; Siliciano, R. F.; Swanstrom, R., HIV reservoirs: what, where and how to target them. *Nat Rev Micro* **2016,** *14* (1), 55-60.
25. Margolis, D. M.; Garcia, J. V.; Hazuda, D. J.; Haynes, B. F., Latency reversal and viral clearance to cure HIV-1. *Science* **2016,** *353* (6297).
26. Bullen, C. K.; Laird, G. M.; Durand, C. M.; Siliciano, J. D.; Siliciano, R. F., New ex vivo approaches distinguish effective and ineffective single agents for reversing HIV-1 latency in vivo. *Nat Med* **2014,** *20* (4), 425-9.
27. Freeling, J. P.; Ho, R. J. Y., Anti-HIV drug particles may overcome lymphatic drug insufficiency and associated HIV persistence. *Proceedings of the National Academy of Sciences of the United States of America* **2014,** *111* (25), E2512-E2513.
28. Buehler, D. C.; Marsden, M. D.; Shen, S.; Toso, D. B.; Wu, X.; Loo, J. A.; Zhou, Z. H.; Kickhoefer, V. A.; Wender, P. A.; Zack, J. A.; Rome, L. H., Bioengineered Vaults: Self-Assembling Protein Shell–Lipophilic Core Nanoparticles for Drug Delivery. *ACS Nano* **2014,** *8* (8), 7723-7732.
29. Eck, W.; Nicholson, A. I.; Zentgraf, H.; Semmler, W.; Bartling, S., Anti-CD4-targeted Gold Nanoparticles Induce Specific Contrast Enhancement of Peripheral Lymph Nodes in X-ray Computed Tomography of Live Mice. *Nano Letters* **2010,** *10* (7), 2318-2322.
30. Pimpha, N.; Chaleawlert-umpon, S.; Chruewkamlow, N.; Kasinrerk, W., Preparation of anti-CD4 monoclonal antibody-conjugated magnetic poly(glycidyl methacrylate) particles and their application on CD4+ lymphocyte separation. *Talanta* **2011,** *84* (1), 89-97.
31. Harding, F. A.; Stickler, M. M.; Razo, J.; DuBridge, R. B., The immunogenicity of humanized and fully human antibodies: Residual immunogenicity resides in the CDR regions. *mAbs* **2010,** *2* (3), 256-265.
32. Nie, S., Understanding and overcoming major barriers in cancer nanomedicine. *Nanomedicine (London, England)* **2010,** *5* (4), 523-528.
33. Hu, C.-M. J.; Kaushal, S.; Cao, H. S. T.; Aryal, S.; Sartor, M.; Esener, S.; Bouvet, M.; Zhang, L., Half-Antibody Functionalized Lipid−Polymer Hybrid Nanoparticles for Targeted Drug Delivery to Carcinoembryonic Antigen Presenting Pancreatic Cancer Cells. *Molecular Pharmaceutics* **2010,** *7* (3), 914-920.
34. Jackson, H.; Bacon, L.; Pedley, R. B.; Derbyshire, E.; Field, A.; Osbourn, J.; Allen, D., Antigen specificity and tumour targeting efficiency of a human carcinoembryonic antigen-specific scFv and affinity-matured derivatives. *British Journal of Cancer* **1998,** *78* (2), 181-188.
35. Richards, D. A.; Maruani, A.; Chudasama, V., Antibody fragments as nanoparticle targeting ligands: a step in the right direction. *Chemical Science* **2017,** *8* (1), 63-77.
36. Yazaki, P. J.; Shively, L.; Clark, C.; Cheung, C.-W.; Le, W.; Szpikowska, B.; Shively, J. E.; Raubitschek, A. A.; Wu, A. M., Mammalian expression and hollow fiber bioreactor production of recombinant anti-CEA diabody and minibody for clinical applications. *Journal of immunological methods* **2001,** *253* (1), 195-208.
37. Yazaki, P. J.; Wu, A. M.; Tsai, S.-W.; Williams, L. E.; Ikle', D. N.; Wong, J. Y.; Shively, J. E.; Raubitschek, A. A., Tumor targeting of radiometal labeled anti-CEA recombinant T84. 66

diabody and t84. 66 minibody: comparison to radioiodinated fragments. *Bioconjugate chemistry* **2001,** *12* (2), 220-228.
38. Endsley, A. N.; Ho, R. J. Y., Design and Characterization of Novel Peptide-Coated Lipid Nanoparticles for Targeting Anti-HIV Drug to CD4 Expressing Cells. *The AAPS Journal* **2012,** *14* (2), 225-235.
39. Fosgerau, K.; Hoffmann, T., Peptide therapeutics: current status and future directions. *Drug Discovery Today* **2015,** *20* (1), 122-128.
40. Casset, F.; Roux, F.; Mouchet, P.; Bes, C.; Chardes, T.; Granier, C.; Mani, J.-C.; Pugnière, M.; Laune, D.; Pau, B., A peptide mimetic of an anti-CD4 monoclonal antibody by rational design. *Biochemical and Biophysical Research Communications* **2003,** *307* (1), 198-205.
41. Zanotto, C.; Calderazzo, F.; Dettin, M.; Di Bello, C.; Autiero, M.; Guardiola, J.; Chieco-Bianchi, L.; De Rossi, A., Minimal Sequence Requirements for Synthetic Peptides Derived from the V3 Loop of the Human Immunodeficiency Virus Type 1 (HIV-1) to Enhance HIV-1 Binding to Cells and Infection. *Virology* **1995,** *206* (2), 807-816.
42. Monnet, C.; Laune, D.; Laroche-Traineau, J.; Biard-Piechaczyk, M.; Briant, L.; Bès, C.; Pugnière, M.; Mani, J.-C.; Pau, B.; Cerutti, M.; Devauchelle, G.; Devaux, C.; Granier, C.; Chardès, T., Synthetic Peptides Derived from the Variable Regions of an Anti-CD4 Monoclonal Antibody Bind to CD4 and Inhibit HIV-1 Promoter Activation in Virus-infected Cells. *Journal of Biological Chemistry* **1999,** *274* (6), 3789-3796.
43. Meier, J.; Kassler, K.; Sticht, H.; Eichler, J., Peptides presenting the binding site of human CD4 for the HIV-1 envelope glycoprotein gp120. *Beilstein Journal of Organic Chemistry* **2012,** *8*, 1858-1866.
44. Barua, S.; Yoo, J.-W.; Kolhar, P.; Wakankar, A.; Gokarn, Y. R.; Mitragotri, S., Particle shape enhances specificity of antibody-displaying nanoparticles. *Proceedings of the National Academy of Sciences of the United States of America* **2013,** *110* (9), 3270-3275.
45. Jiang, W.; KimBetty, Y. S.; Rutka, J. T.; ChanWarren, C. W., Nanoparticle-mediated cellular response is size-dependent. *Nat Nano* **2008,** *3* (3), 145-150.
46. Zhang, S.; Li, J.; Lykotrafitis, G.; Bao, G.; Suresh, S., Size-Dependent Endocytosis of Nanoparticles. *Advanced materials (Deerfield Beach, Fla.)* **2009,** *21*, 419-424.
47. Elias, D. R.; Poloukhtine, A.; Popik, V.; Tsourkas, A., Effect of ligand density, receptor density, and nanoparticle size on cell targeting. *Nanomedicine: Nanotechnology, Biology and Medicine* **2013,** *9* (2), 194-201.
48. Chan, J. M.; Zhang, L.; Yuet, K. P.; Liao, G.; Rhee, J.-W.; Langer, R.; Farokhzad, O. C., PLGA–lecithin–PEG core–shell nanoparticles for controlled drug delivery. *Biomaterials* **2009,** *30* (8), 1627-1634.
49. Zhang, L.; Chan, J. M.; Gu, F. X.; Rhee, J.-W.; Wang, A. Z.; Radovic-Moreno, A. F.; Alexis, F.; Langer, R.; Farokhzad, O. C., Self-Assembled Lipid−Polymer Hybrid Nanoparticles: A Robust Drug Delivery Platform. *ACS Nano* **2008,** *2* (8), 1696-1702.
50. Cheow, W. S.; Hadinoto, K., Factors affecting drug encapsulation and stability of lipid–polymer hybrid nanoparticles. *Colloids and Surfaces B: Biointerfaces* **2011,** *85* (2), 214-220.
51. Hu, Y.; Ehrich, M.; Fuhrman, K.; Zhang, C., In vitro performance of lipid-PLGA hybrid nanoparticles as an antigen delivery system: lipid composition matters. *Nanoscale research letters* **2014,** *9* (1), 1-10.
52. Bershteyn, A.; Hanson, M. C.; Crespo, M. P.; Moon, J. J.; Li, A. V.; Suh, H.; Irvine, D. J., Robust IgG responses to nanograms of antigen using a biomimetic lipid-coated particle vaccine. *Journal of Controlled Release* **2012,** *157* (3), 354-365.

53. Ma, T.; Wang, L.; Yang, T.; Ma, G.; Wang, S., M-cell targeted polymeric lipid nanoparticles containing a toll-like receptor agonist to boost oral immunity. *International Journal of Pharmaceutics* **2014,** *473* (1–2), 296-303.
54. Hadinoto, K.; Sundaresan, A.; Cheow, W. S., Lipid–polymer hybrid nanoparticles as a new generation therapeutic delivery platform: A review. *European Journal of Pharmaceutics and Biopharmaceutics* **2013,** *85* (3, Part A), 427-443.
55. Chan, L. W.; Wang, Y.-N.; Lin, L. Y.; Upton, M. P.; Hwang, J. H.; Pun, S. H., Synthesis and Characterization of Anti-EGFR Fluorescent Nanoparticles for Optical Molecular Imaging. *Bioconjugate Chemistry* **2013,** *24* (2), 167-175.
56. Liu, H.; May, K., Disulfide bond structures of IgG molecules: Structural variations, chemical modifications and possible impacts to stability and biological function. *mAbs* **2012,** *4* (1), 17-23.
57. Serpe, L.; Canaparo, R.; Daperno, M.; Sostegni, R.; Martinasso, G.; Muntoni, E.; Ippolito, L.; Vivenza, N.; Pera, A.; Eandi, M.; Gasco, M. R.; Zara, G. P., Solid lipid nanoparticles as anti-inflammatory drug delivery system in a human inflammatory bowel disease whole-blood model. *European Journal of Pharmaceutical Sciences* **2010,** *39* (5), 428-436.
58. Silva, E. L.; Lima, F. A.; Carneiro, G.; Ramos, J. P.; Gomes, D. A.; de Souza-Fagundes, E. M.; Miranda Ferreira, L. A., Improved In Vitro Antileukemic Activity of All-Trans Retinoic Acid Loaded in Cholesteryl Butyrate Solid Lipid Nanoparticles. *Journal of nanoscience and nanotechnology* **2016,** *16* (2), 1291-1300.
59. Brioschi, A.; Zara, G.; Calderoni, S.; Gasco, M.; Mauro, A., Cholesterylbutyrate Solid Lipid Nanoparticles as a Butyric Acid Prodrug. *Molecules* **2008,** *13* (2), 230.
60. Das, B.; Dobrowolski, C.; Shahir, A.-M.; Feng, Z.; Yu, X.; Sha, J.; Bissada, N. F.; Weinberg, A.; Karn, J.; Ye, F., Short chain fatty acids potently induce latent HIV-1 in T-cells by activating P-TEFb and multiple histone modifications. *Virology* **2015,** *474*, 65-81.
61. Park, J.; Kim, M.; Kang, S. G.; Jannasch, A. H.; Cooper, B.; Patterson, J.; Kim, C. H., Short-chain fatty acids induce both effector and regulatory T cells by suppression of histone deacetylases and regulation of the mTOR-S6K pathway. *Mucosal Immunol* **2015,** *8* (1), 80-93.
62. Cartiera, M. S.; Johnson, K. M.; Rajendran, V.; Caplan, M. J.; Saltzman, W. M., The uptake and intracellular fate of PLGA nanoparticles in epithelial cells. *Biomaterials* **2009,** *30* (14), 2790-2798.
63. Cao, S.; Jiang, Y.; Zhang, H.; Kondza, N.; Woodrow, K. A., Targeted Co-Delivery of Anti-HIV Drug and Dual-Function Monoclonal Antibody to Gut-Homing T Cells Using Lipid-Coated PLGA Nanoparticles. . **Submitted**.
64. Lee, B.; Sharron, M.; Montaner, L. J.; Weissman, D.; Doms, R. W., Quantification of CD4, CCR5, and CXCR4 levels on lymphocyte subsets, dendritic cells, and differentially conditioned monocyte-derived macrophages. *Proceedings of the National Academy of Sciences* **1999,** *96* (9), 5215-5220.
65. Gao, L.-Y.; Liu, X.-Y.; Chen, C.-J.; Wang, J.-C.; Feng, Q.; Yu, M.-Z.; Ma, X.-F.; Pei, X.-W.; Niu, Y.-J.; Qiu, C.; Pang, W.-H.; Zhang, Q., Core-Shell type lipid/rPAA-Chol polymer hybrid nanoparticles for in vivo siRNA delivery. *Biomaterials* **2014,** *35* (6), 2066-2078.
66. Thomas, G. D., Effect of dose, molecular size, and binding affinity on uptake of antibodies. *Drug Targeting: Strategies, Principles, and Applications* **2000**, 115-132.
67. Salter, R. D.; Howell, D. N.; Cresswell, P., Genes regulating HLA class I antigen expression in TB lymphoblast hybrids. *Immunogenetics* **1985,** *21* (3), 235-246.

Chapter 5. Hybrid nanocarriers incorporating mechanistic distinct drugs for lymphatic CD4+ T cell activation and HIV latency reversal

Adapted from: Cao S, Slack SD, Levy CN, Hughes SM, Jiang Y, Yogodzinski C, Roychoudhury P, Jerome KR, Schiffer JT, Hladik F, and Woodrow KA. Hybrid nanocarriers incorporating mechanistically distinct drugs for lymphatic CD4+ T cell activation and HIV latency reversal. *In revision.*

5.1 Abstract

A proposed strategy to cure HIV uses latency-reversing agents (LRAs) to reactivate latent proviruses for purging HIV reservoirs. A variety of LRAs have been identified, but none has yet proven effective in reducing the reservoir size in vivo. Nanocarriers (NCs) could address some major challenges by improving drug solubility and safety, providing sustained drug release, and simultaneously delivering multiple drugs to target tissues and cells. Here, we formulated hybrid NCs that incorporate physicochemically diverse LRAs and target lymphatic CD4+ T cells. We identified one LRA combination that displayed synergistic latency reversal and low cytotoxicity in a cell model of HIV and in CD4+ T cells from virologically suppressed patients. Furthermore, our targeted NCs selectively activated CD4+ T cells in non-human primate PBMCs as well as in murine lymph nodes, and significantly reduced local toxicity. This nanocarrier platform may enable new solutions for delivering anti-HIV agents for an HIV cure.

5.2 Introduction

Highly active antiretroviral therapy (HAART) has revolutionized the treatment of HIV-1 and transformed it into a chronic disease, but does not cure the infection. Long-term HIV infection is maintained by several factors including limited accessibility of antiretroviral drugs to certain

anatomical sites where viral replication may occur [1-3], and latent infection of resting cells where integrated provirus is invisible to drug treatment as well as the immune system [4-5]. The latent cell pool decays slowly despite suppressive HAART [6-7], requiring patients to take life-long antiretroviral drug regimens, associated with short- and long-term side effects [8].

Strategies to accelerate the decay of the HIV reservoir pool are being explored but none has yet proven effective in reducing reservoir size *in vivo*. One strategy, which has been studied extensively, including in clinical studies, is to induce HIV reactivation using latency-reversing agents (LRAs) while continuing suppressive HAART [9]. Upon reversal of the latent state, the reactivated cells can be eliminated by host immune responses or other killing strategies [10]. This "shock and kill" approach is still controversial based on recent safety issues and limited success in reducing reservoir sizes in clinical settings [11]. There are several hypotheses to explain the failures in clinical trials: First, these studies were restricted to individual LRAs from a single class [11-12], but recent evidence shows that combinations of multiple mechanistic classes may be needed to effectively overcome latency *in vivo* [13-15]. Second, some LRAs are associated with high toxicity [16-17], or nonspecific T cell activation that is unnecessary for latency reversal and causes off-target toxicity [14]. Finally, LRAs might not achieve sufficient concentrations in the lymphatic tissues including lymph nodes and gut-associated lymphoid tissue, where vast numbers of latently infected CD4+ T cells reside [1, 18]. Systemic administration of LRAs may work well on circulating CD4+ T cells, but those cells make up less than 2% of the body's CD4+ T cells [19-20].

Nanocarrier drug delivery systems provide a promising approach for overcoming these three challenges to using LRAs [21-23]. Specifically, nanocarrier drug delivery systems allow LRAs to be delivered specifically to target cells such as CD4+ T cells within organs of interest, thus achieving high concentrations at relevant sites, while minimizing off-target effects by keeping concentrations

low at other sites. However, few studies have reported on the use of nanocarriers for HIV cure and those studies used single LRAs [24-27]. Of these studies, none has investigated CD4-targeting or lymphatic tissue-targeting functions *in vivo.* Here, we developed lipid-coated poly lactic-co-glycolic acid (PLGA) nanoparticles (termed "LCNPs") to address the current barriers to LRA treatment. Through simple chemical synthesis and bio-conjugation processes, we successfully loaded a variety of LRAs into our LCNPs and formulated them to target CD4+ T cells in the lymph nodes. We demonstrate that these LCNPs can co-deliver multiple LRAs with varying release kinetics for synergistic latency reversal, and successfully traffic to lymph nodes after subcutaneous administration. More importantly, our CD4-targeted LCNPs incorporate a promising LRA candidate, ingenol-3-angelate (Ing3A), induced long-acting and specific CD4+ T cell activation in the complex lymphatic environment while significantly reducing local toxicity compared to free drug. Our approach is unique and potentially transformative because we investigate agents of multiple mechanistic classes and specifically target them to the cell types and tissues sustaining latency.

5.3 Materials and methods

5.3.1 *Study Design*

The objective of the study was to develop a nanocarrier-based drug delivery system that permits the loading of multiple diverse anti-HIV agents and specific targeting to HIV reservoir cells and tissues *in vivo*, to address the major clinical hurdles in the "shock and kill" strategy. We first developed several strategies to load different LRAs into our hybrid nanocarriers, and characterized the performance of every single formulation and determined the best drug combination in an HIV latency cell line model. We further confirmed their latency reversal in CD4+ T cells from virologically suppressed patient, a more clinically-relevant model. Then we evaluated CD4+ T cell

specific activation in non-human primate PBMCs *ex vivo*. We used C57BL6/J mice to evaluate the *in vivo* targeting properties of our optimized nanocarriers, especially the ability to target and activate CD4+ T cells in the mice lymph nodes after subcutaneous administration, and their toxicity profile. Sample sizes were chosen to demonstrate statistical significance. Statistical analysis was detailed in the section at the end.

5.3.2 *Materials*

PLGA B6013-2 (75:25 L:G; ester-terminated, inherent viscosity range: 0.55-0.75 dL/g in choloroform) was purchased from Lactel. All Resomer® PLGA polymers were purchased from Sigma-Aldrich. All lipids for the nanoparticle synthesize were purchased from Avanti Polar Lipids. Cholesteryl butyrate was purchased from Santa Cruz Biotechnology. LRAs were purchased from Cayman Chemical (Ing3A), LC Laboratories (prostratin and panobinostat), Active Biochem (romidepsin) or Sigma-Aldrich (disulfiram and JQ1). EasySep Human CD4+ T cell isolation kit was purchased from StemCell Technologies. Anti-human antibodies and anti-mouse antibodies including PE anti-CD14, PerCP/Cy5.5 anti-CD4, FITC anti-CD8, APC anti-CD69, and their isotype control antibodies were purchased from BD Biosciences. Rhesus recombinant anti-CD4 antibody and rhesus recombinant IgG1 isotype control antibody were purchased from NIH Nonhuman Primate Reagent Resource. Anti-mouse CD4 antibody and its isotype IgG2b control antibody were purchased from BioXCell. RPMI 1640 cell culture media containing 2 mM l-glutamine and 25 mM HEPES supplemented with heat-inactivated fetal bovine serum (FBS, 10%, v/v) and penicillin-streptomycin (100 U/mL), purchased from Thermo Fisher Scientific, were used for most of the in vivo and ex vivo studies. All other chemicals were purchased from Sigma-Aldrich and Thermo Fisher Scientific unless otherwise specified.

5.3.3 *PLGA-drug conjugation and LCNP fabrication.*

Ing3A and prostratin were conjugated to carboxyl-ended PLGA 503H using the Steglich esterification. Briefly, PLGA (1.29 x 10^{-5} mol) and Ing3A or prostratin (3.87 x 10^{-5} mol) were dissolved in 6 mL DCM. N,N'-diisopropylcarbodiimide (DIC) (1.16x 10^{-4} mol) and 4-(dimethylamino)pyridine (DMAP) (3.87 x 10^{-5} mol) were added and the mixture was incubated in room temperature (RT) for 24 hours. After that, 160 mL cold methanol was added to precipitate polymer-drug conjugates. The conjugates were then collected by centrifugation and dissolved in DCM for another washing. Final products were dissolved in DCM and lyophilized for future use. Panobinostat was conjugated to the same PLGA using the N-(3-dimethylaminopropyl)-N'-ethylcarbodiimide hydrochloride (EDC) chemistry. The process was similar to Ing3A or prostratin conjugation, except that EDC, 1-hydroxybenzotriazole hydrate (HoBt), and N,N-diisopropylethylamine (DIPEA) (all at 3.87 x 10^{-5} mol) were used as the catalyst.

These PLGA-LRA conjugates as well as PLGA and each LRAs were analyzed by H-NMR (Bruker AV500) after dissolving in deuterated DMSO. They were also verified by HPLC (Shimadzu) with a Phenomenex Kinetex C18 column (250 x 4.6 mm), eluting with water-acetonitrile (0.1% TFA) gradients (Figure S2a, Appendix III).

LCNP was synthesized using a modified single emulsion evaporation method as described previously[34]. In brief, the lipid mixture (DOPC, DOTAP, and DSPE-PEG-Mal, or DOPC, chol-but, DSPE-PEG-Mal at 4:4:1 molar ratio) in chloroform were dried under nitrogen and resuspended in Milli-Q water. PLGA (10 mg/mL in ethyl acetate) was added drop-wise to the lipid suspension while votexing. The mixture was then homogenized using a probe sonicator (500W, Ultrasonic Processor GEX500) for 30 sec x 3 times. The residual ethyl acetate in the

mixture was removed by rotary evaporation (Rotavapor R-210, BUCHI) for 10 min. LCNPs were then washed by high-speed centrifugation at 14,000 rpm for 10 min at 4 °C. To physically encapsulate LRAs into LCNPs, different LRAs are co-dissolved with PLGA B6013-2 in ethyl acetate following LCNP synthesis. PLGA-LRA conjugates were dissolved in ethyl acetate at 10 mg/mL following LCNP synthesis to make LRA conjugated LCNPs. For DiR or DiD fluorescent LCNPs, 1 % (w/w, DiR or DiD to PLGA) DiR or DiD dissolved in ethyl acetate was added into PLGA/ethyl acetate solution right before the LCNP synthesis. Anti-CD4 mAbs were conjugated to synthesize LCNPs *via* maleimide-functionalized DSPE-PEG in the lipid bilayer as described previously. In brief, the mAb was thiolated using Traut's reagents, and then incubated with LCNPs in PBS (containing 5 mM EDTA) for 2 hours. Final mAb conjugated LCNPs were centrifuged at 10,000 rpm for 5 min in a 50 mL falcon tube to remove unreacted antibodies.

5.3.4 *Characterization of LRA loaded LCNPs and their in vitro release kinetics.*

The size, PDI and ζ-potential of all LCNP formulations were measured by dynamic light scattering (DLS) using a Zetasizer Nano ZS90 (Malvern Instruments), and the size was also measured by NanoSight NS300 (Malvern instruments). Nanoparticles were suspended in Milli-Q water for size and PDI measurement or in NaCl buffer (10 mM, pH 7.4) for ζ-potential measurement. Drug loading was measured by dissolving pre-weighted lyophilized LRA loaded LCNPs in DMSO and analyzing the samples using HPLC. The separation was made on a C18 column. The gradient mobile phase described above was used to measure LRA content in conjugated LCNP formulations. For other LRAs, the mobile phase was isopropanol-acetonitrile (40:60, v/v) for chol-but[51], water-acetonitrile (30:70, v/v, with <0.045% TFA) for JQ1 and disulfiram, or water-acetonitrile (60:40, v/v, with <0.045% TFA) for prostratin and romidepsin. The drug loadings (DL) are calculated using Eq. (1):

$$\text{Drug Loading (DL, wt\%)} = \frac{\text{Mass of drug (mg)}}{\text{Mass of drug loaded LCNPs}} \times 100 \quad (1)$$

The encapsulation efficiencies are calculated using Eq. (2):

$$\text{Encapsulation Efficiency (\%)} = \frac{\text{Drug loading (wt\%)}}{\text{Feed drug to LCNP ratio (wt\%)}} \times 100 \quad (2)$$

The drug release studies were all performed in RPMI 1640 cell culture media as described above. After synthesis and centrifugation, LRA loaded LCNPs were resuspended in the cell culture media and divided into individual microcentrifuge tubes for each time point/replicate. At each time point, replicate tubes were centrifuged at 14,000 rpm for 10 min. Supernatants were taken out and mixed with acetonitrile or DMSO of 1:1 (v/v) and centrifuged to remove precipitated proteins. The LRA contents in the supernatant were measured by HPLC. The values were normalized to the total amount of LRA present. Release kinetics data were fitted in Eq. (3):

$$D(t) = Kt^n + K_0 \quad (3)$$

D(t) is the percentage of released drug, and *t* is the time (days).

5.3.5 *Efficacy and cytotoxicity of LRA loaded LCNPs in J-Lat A1 cells.*

J-Lat Tat-GFP (A1) cells were obtained from the NIH AIDS Research & Reference Reagent Program [45,46]. Cells were maintained in RPMI 1640 media as describe above and incubated at at 37 °C in a humidified 5% CO_2 air environment. Cells were seeded at a concentration of 1×10^6 per well in 24-well culture plates, and then treated with free LRAs or LCNP-formulated LRAs at different concentrations for 20 hours at 37 °C. Subsequently, cells were washed by PBS and incubated with LIVE/DEAD® violet dead cell stain for 30 min in RT. Cells were washed again and fixed in 2% paraformaldehyde (PFA) for flow cytometry analysis. The dose-response curves for each LRA formulations were fitted in Eq. (4):

$$f(x) = c + \frac{d-c}{1+e^{b(\log x - \log e)}} \quad (4)$$

x is the drug concentration, and *f(x)* is the percentage of GFP+ cells.

Cytotoxicity was measured simultaneously with the efficacy study using CellTiter-Blue Cell Viability Assay (Promega) following the manufacturer's recommended procedures. After cells being centrifuged and resuspened in PBS, 100 μL cells from each well were incubated with CellTiter-Blue reagent (20 μL) in a 96-well culture plate for 4 hours, and fluorescence was recorded at 560/590 nm ex/em using a fluorescent plate reader (Infinite® 200 Pro, TECAN, Mañnedorf, Switzerland).

LRA combination effects and cytotoxicity were assessed in J-Lat A1 cells using the same methods. Cells were incubated with single LRA at the concentrations that achieved approximately 20% GFP+ cell induction, as well as every pair of these LRAs for 20 hours, followed by flow cytometry analysis and CellTiter-Blue assay as described above. The Bliss independent model was used to analyze combined effects of LRAs. The model is defined by the Eq. (5):

$$fa_{xy,P} = fa_x + fa_y - (fa_x)(fa_y) \quad (5)$$

$fa_{xy,P}$ is the predicted fraction (here is the percentage of GFP+ A1 cells after treatment) affected by a combination of two LRAs, given the experimentally observed fraction affected by single drug fa_x or fa_y $individually$. Then the experimentally observed fraction affected by a combination of two LRAs ($fa_{xy,O}$) will be compared with $fa_{xy,P}$ using the Eq. (6)

$$\Delta fa_{xy} = fa_{xy,O} - fa_{xy,P} \quad (6)$$

If $\Delta fa_{xy} > 0$ with statistical significance, the two drugs display synergy. If $\Delta fa_{xy} = 0$, the two drugs show independent action. If $\Delta fa_{xy} < 0$ with statistical significance, the two drugs display antagonism.

5.3.6 *Measurement of intracellular HIV-1 mRNA levels in CD4+ T cells from infected individuals.*

We measured intracellular HIV-mRNA levels from CD4+ T cells isolated from three HIV+ PBMC donors from the HIV Vaccine Trials Network clinical cohort (IRB number: FH IR File #5567) in three independent experiments. CD4+ T cells were isolated by negative selection using the EasySep Human CD4+ T cell isolation kit (StemCell Technologies), and plated in a 24-well plate at 1x 10^6 cells/mL in 1mL R10 cell culture media as described above with 10 µM T20 (fusion inhibitor, from AIDS, NIAID) to prevent new infections. We exposed the cells to six experimental conditions, all performed in triplicate: 1) 3 µg/mL Ing3A/NP containing 50ng/mL Ing3A; 2) 60 µg/mL JQ1/NP containing 1020 ng/mL JQ1; 3) Both JQ1 and Ing3A nanoparticles in the same concentrations as the single drug/NP conditions; 4) 10ng/mL free Ing3A; 5) 4000ng/mL free JQ1; 6) Both free Ing3A and free JQ1 in the same concentrations as the single free drug conditions. As a positive control for cell stimulation and production of HIV mRNA, we stimulated the cells with 50 ng/mL phorbol myristate acetate (PMA) and 1 µM ionomycin. For a negative control, we added DMSO in an equal volume to the PMA/ionomycin. The cells were incubated with these treatments for 20-21 hrs at 37 °C and 5% CO2.

After incubation, the cells were harvested and an aliquot was taken for live/dead staining by flow cytometry. RNA was extracted from the remaining cells using the Qiagen RNeasy mini RNA extraction kit (Qiagen). cDNA was generated using the qScript cDNA synthesis kit (QuantaBio) starting with an equivalent input mass of RNA from each experimental replicate. After cDNA synthesis, the samples were diluted 1:1 with molecular grade water. For the ddPCR reaction, we combined 5µL of diluted cDNA, 11µL of ddPCR supermix (no dUTP) (Bio-Rad),1.1 µL of HIV mRNA primer/probe (Integrated DNA Technologies), and 4.9 µL of water. Droplet generation, thermal cycling and droplet reading were performed according to the Bio-Rad ddPCR supermix

protocol. All ddPCR reactions were performed in duplicate and wells with fewer than 10,000 droplets were excluded from analysis.

Primer and probe sequences for detecting HIV-1 mRNAs[52]:

Forward (5′→3′) CAGATGCTGCATATAAGCAGCTG (9501–9523)

Reverse (5′→3′) TTTTTTTTTTTTTTTTTTTTTTTTGAAGCAC (9629-poly A)

Probe (5′→3′) FAM-CCTGTACTGGGTCTCTCTGG-MGB (9531–9550)

The Bliss independent model, from Eq. (5) and (6) above, was used to analyze combined effects of JQ1 and Ing3A. However, here the *fa* is defined as percentage of intracellular HIV-1 mRNA induction compared to the PMA/I positive control group.

5.3.7 *Ex vivo reactivation study from pigtail macaque PBMCs.*

Pigtail macaque blood was obtained from the tissue distribution program at Washington National Primate Research Center (WaNPRC), University of Washington. All macaques were confirmed to be serologically negative for simian type D retrovirus, SIV, and simian T-cell lymphotropic virus (STLV) prior to sample collection. PBMCs were isolated from the blood using lymphocyte separation medium (LSM, Mediatech, Inc.), and maintained in the same RPMI 1640 cell culture media for the study. PBMCs were seeded at a concentration of 1× 106 per well in 24-well culture plates, and then treated with free Ing3A, Ing3A-cbLCNP, Ing3A-CD4-cbLCNP or Ing3A-Iso-cbLCNP for 20 hours at 37 °C. Subsequently, cells were washed and incubated with FITC anti-human CD8, PE anti-human CD14, PerCP/Cy5.5 anti-human CD3 antibodies and APC anti-human CD69 for 30 min at 4 °C. The FITC IgG1, PE IgG2a, PerCP IgG1, and APC IgG1 control antibodies were used as the isotype control for gating CD3, CD8, CD14, and CD69 positive cells. After incubation, cells were washed with PBS and then treated with LIVE/DEAD® violet dead cell stain for another 30 min at RT, followed by 2% PFA fixation and flow cytometry analysis.

5.3.8 *Biodistribution of CD4-targeted LCNPs in mice.*

Animal studies were approved by the Institutional Animal Care and Use Committee (IACUC) at the University of Washington (Protocol # 4260-01). All animals were obtained and cared for in accordance with the IACUC guidelines. 8-12 week old male C57BL6/J mice (The Jackson Laboratory) were subcutaneously administered with DiR loaded LCNP formulations to the left flank (Figure 5.5A). In our pilot animal studies, LCNPs with different lipid compositions (DOTAP vs chol-but) and sizes (100 nm vs 200 nm), as well as equivalent free DiR dye were administered into mice and the biodistribution in different organs was compared at different time points. In our scaled-up studies, selected CD4-cbLCNPs or control Iso-cbLCNPs were administered into mice. At 20 hours, 3 days, and 7 days post-administration, mice were sacrificed by cardiac exsanguination under isoflurane for terminal blood collection, followed by cervical dislocation. Major organs including inguinal lymph nodes, spleen, brain, heart, kidneys, lung, liver, and small intestine were harvested, and the fluorescence signal was quantified by a Xenogen IVIS Spectrum imaging system using ex/em = 745/800. Regions of interest were drawn across each organ for quantification, and total radiant efficiencies were normalized by tissue mass. 100 μL plasma from the blood was put in a 96-well plate for imaging and the signals were quantified the same way as other tissues.

5.3.9 *In vivo CD4+ T cell binding, activation and toxicity study.*

8~12 week old male C57BL6/J mice were injected subcutaneously with 0.3 mL PBS, free Ing3A, Ing3A-CD4-cbLCNPs or Ing3A-Iso-LCNPs at 0.48 mg/kg (Ing3A dose/body weight). 20-fold lower free Ing3A (0.024 mg/kg) was also injected because that concentration indicated similar potency compared to LCNP-formulated Ing3A in vitro. In addition, free Ing3A formulation at 0.48 mg/kg contained 0.64% DMSO in PBS buffer, thus a 0.64% DMSO in PBS

control was included to demonstrate the negligible effects by DMSO. After 20 hours, 3 days, and 7 days, mice were sacrificed, and left and right inguinal lymph nodes were harvested. Lymphocytes were then collected from those lymph nodes. In brief, the lymph nodes were incubated in the digestion media (RPMI 1640 cell culture media containing 1.5 mg/mL Collagenase D and 40 µg/mL DNase I) at 37 °C in the shaker. After 30 min incubation, 5 mM EDTA was added into the solution and incubated for another 5 min. Tissues and solutions were then smashed and passed through a 70 µm cell strainer. Collected cells were then washed and stained with FITC anti-mouse CD8, PE anti-mouse CD14, PerCP/Cy5.5 anti-mouse CD3 antibodies and APC anti-mouse CD69 or their isotype antibodies for 30 min at 4 °C. After incubation, cells were washed with PBS and then treated with LIVE/DEAD® violet dead cell stain for another 30 min in RT, followed by 2% PFA fixation and flow cytometry analysis.

For in vivo cell-specific biodistribution studies, mice were injected with. After 20 hours, mice were sacrificed, and left and right inguinal lymph nodes were harvested. Cells were isolated from those lymph nodes as described above and stained with fluorescent antibody (FITC anti-mouse CD8, PE anti-mouse CD14, PerCP/Cy5.5 anti-mouse CD3 antibodies) and LIVE/DEAD® stain, followed by 2% PFA fixation flow cytometry analysis.

For toxicity studies, at 3 days post-administration, inguinal lymph nodes and biopsy of subcutaneous tissue near the injection sites were collected and post-fixed in 4% PFA for 24 hours. Tissues were then processed and sectioned for H&E staining, performed by Pathology Research Services Laboratory at University of Washington. Tissue slides were then examined under a Nikon Eclipse Ti microscope equipped with a Nikon Digital Sight DS-Fi2 camera.

5.3.10 *Statistical analysis.*

Significant differences between control and treatment groups were determined by various statistical analyses. Student's t test was used for two groups comparison. One-way analysis of variance (ANOVA) with Bonferroni's test was used for multiple groups comparison. Two-way ANOVA with Bonferroni's test was used when there were subgroups in each group, for example, different lymph nodes or cells in those lymph nodes from different treatment groups. Data represent mean ± s.d. in each figure and table as indicated. Statistical analyses were performed using GraphPad Prism 7.0 software (Graphpad Software); * $p<0.05$, ** $p<0.005$, *** $p<0.0005$, **** $p<0.0001$.

5.4 Results

5.4.1 *Development of LCNPs loaded with mechanistically diverse LRAs.*

Combinations of LRAs have recently shown synergistically enhanced potency for latency reversal as compared to single LRAs in multiple ex vivo assays [13]. However, the varied physicochemical properties of different LRAs makes combined formulation difficult to achieve and administer. In addition, the low potency but high toxicity of some LRAs limits their tolerability when used in monotherapy. To improve LRA potency while minimizing toxicity, we co-formulated and targeted the drugs to CD4+ T cells using lipid-polymer hybrid nanoparticles (termed "LCNPs") surface modified with targeting antibodies and with LRA incorporated into both the lipid bilayer and the polymer core (Figure 5.1).

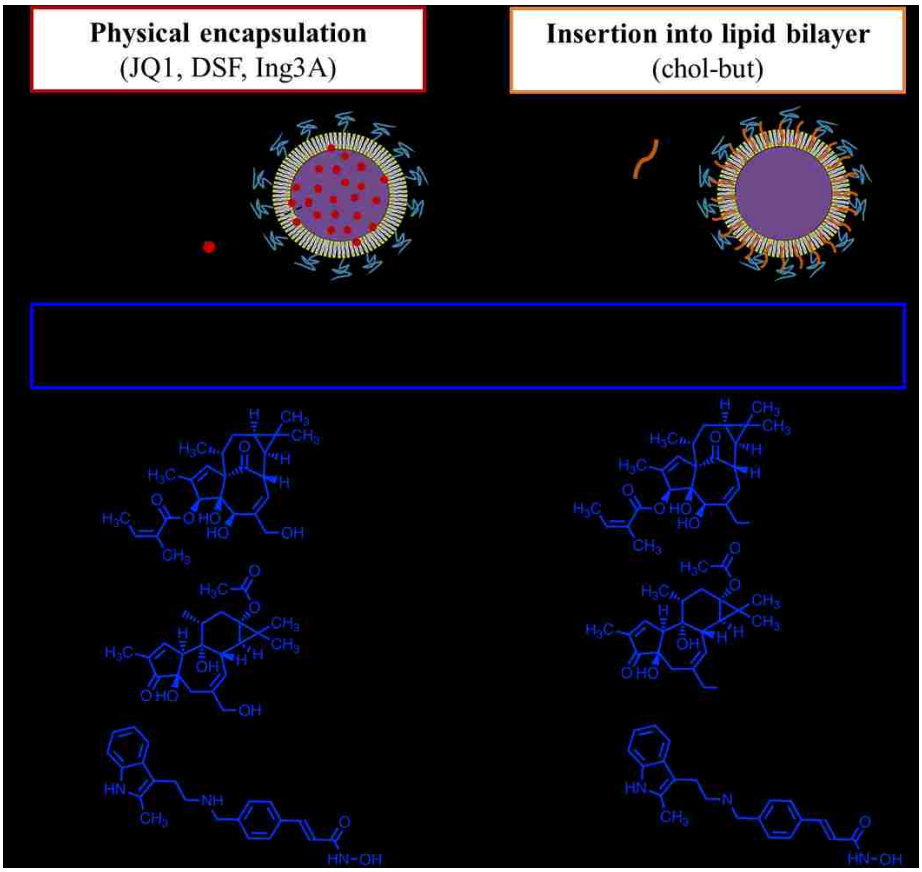

Figure 5.1. Strategies for loading LRAs into LCNPs. Hydrophobic LRAs were physically encapsulated into the PLGA core. Chol-but, as the prodrug of butyric acid, was inserted into lipid bilayer. LRAs with hydroxyl or amine groups were conjugated to the PLGA followed by LCNP synthesis. Abbreviations: DSF (disulfiram), Ing3A (ingenol-3-angelate), Prs (prostratin), PANO (panobinostat), chol-but (cholesteryl butyrate), PLGA (poly(lactic-co-glycolic acid)), DIC (N,N′-diisopropylcarbodiimide), DMAP (4-(dimethylamino)pyridine), DCM (dichloromethane), EDC (1-ethyl-3-(3-dimethylaminopropyl)carbodiimide), HoBt (1-Hydroxybenzotriazole), DIPEA (N,N-Diisopropylethylamine).

For ease of formulation, we first attempted to physically encapsulate all LRAs individually into LCNPs by co-dissolving each compound with PLGA in ethyl acetate, followed by a modified single-emulsion evaporation method as described previously [23]. An initial 6 wt% (ratio of LRA to PLGA) input of hydrophobic drugs JQ1, disulfiram, and Ing3A resulted in drug loadings of 1.70 ± 0.08 wt%, 2.54 ± 0.60 wt%, or 1.00 ± 0.04 wt%, respectively (Table 5.1). However, prostratin and romidepsin were encapsulated into LCNPs at less than 0.02 wt% (Table S1).

Physical encapsulation of panobinostat was also impractical due to its poor solubility in ethyl acetate and dichloromethane (DCM). We used DCM as an alternative solvent for romidepsin, which increased its drug loading to 0.2 wt%, but failed to improve the loading of either prostratin or panobisnostat. We were unable to encapsulate butyric acid, a short fatty acid that has shown potential in HIV latency reversal [28-29], into the PLGA core. Instead, we inserted its prodrug cholesteryl butyrate (chol-but) into the LCNP lipid bilayer [30], achieving a loading of 2.72 wt% (Figure 5.1).

Table 5.1. Physicochemical properties of LCNP formulated latency reversing agents (LRAs).

LRAs	JQ1	DSF	Ing3A	Ing3A-PLGA	Prs-PLGA	PANO-PLGA	Chol-but
Molecular Target	BET	NF-κβ	PKC	PKC	PKC	HDAC	HDAC
[a]Formulation Strategy	Single-emulsion			Steglich esterification		EDC	Lipid insertion
[b]Size (d, nm)	187.2 ± 4.0	183.7 ± 1.2	182.4 ± 1.7	164.6 ± 0.7	176.2 ± 1.3	169.9 ± 3.1	219.3 ± 2.6
[b]Polydispersity Index	0.09 ± 0.01	0.07 ± 0.02	0.05 ± 0.02	0.07 ± 0.03	0.09 ± 0.01	0.07 ± 0.01	0.06 ± 0.02
[b]ζ-potential (mV)	12.0 ± 3.8	15.7 ± 1.5	13.8 ± 5.9	15.2 ± 9.6	8.4 ± 8.0	9.41 ± 2.5	-10.4 ± 1.5
Drug Input (wt%)	5	5	5	1.7	1.2	0.4	4.3
[b]Drug Loading (wt%)	1.70 ± 0.08	2.54 ± 0.60	1.00 ± 0.04	1.62 ± 0.05	1.08 ± 0.03	0.31 ± 0.03	2.72 ± 0.03
[b,c]EE (%)	35.8 ± 1.6	53.3 ± 1.3	21.1 ± 0.8	93.3 ± 2.5	92.6 ± 2.2	70.6 ± 6.3	63.2 ± 7.7
[d]Colloidal Stability	≥10 days	≥10 days	≥10 days	≥10 days	≥10 days	≥10 days	≥10 days
[e]Time to Release 50%	<1h	14 h	1.6 days	25.7 days	24.0 days	1.4 days	n.d.

[a]Formulation was either by physical encapsulation in the PLGA core (single-emulsion), conjugation with PLGA (steglich esterification, EDC chemistry) or insertion into lipid bilayer surface coating;
[b]Data represent mean ± s.d. from three independently formulated batches;
[c]Encapsulation efficiency (EE) is the ratio of the actual loading (wt%) to the drug input (wt%) expressed as a percentage;
[d]Colloidal stability was measured in cell culture media;
[e]Drug-release curves were fit by nonlinear regression to estimate the time when 50% of the drug was released from the LCNP formulation (Figure 5.2A, Table S3, Appendix III).
Abbreviations: NF-κβ (nuclear factor kappa-light-chain-enhancer of activated B cells), BET (bromodomain and extra-terminal proteins), HDAC (histone deacetylase), PKC (protein kinase C), IMPDH (inosine monophosphate dehydrogenase). Others refer to Figure 5.1.

For Ing3A, prostratin and panobinostat, we also evaluated chemical conjugation into LCNPs (Figure 5.1). The ester or amide bond formed between PLGA and LRA is hydrolyzed to release free LRAs under physiological conditions by host esterases or the esterase-like activity of human

serum albumin [31]. Chemical conjugation was expected to decrease the release rate of LRAs compared to physical encapsulation. Drugs were conjugated in a 1:1 molar ratio with a low molecular weight PLGA to increase LRA content. However, we found that the LCNPs using PLGA of molecular weight less than 20 kDa led to poor particle size distribution and low stability (Table S2, Appendix III). Therefore, to maximize LCNP drug loading while minimizing polydispersity, we selected a 24-38 kDa carboxyl-terminated PLGA. We used proton-nuclear magnetic resonance (H-NMR) and high-performance liquid chromatography (HPLC) to verify the conjugation chemistry and efficiency. Both methods supported successful conjugation of each LRA with PLGA (Figure S1 and S2, Appendix III), with drug loading of 1.62 ± 0.05 wt% (Ing3A), 1.08 ± 0.03 wt% (prostratin), and 0.31 ± 0.03 wt% (panobinostat).

All LRA loaded LCNPs showed well-distributed sizes with diameters of 160-190 nm, and polydispersity index (PDI) < 0.1. Chol-but inserted LCNPs showed an increased size of ~220 nm in diameter and significant changes in ζ-potential going from positive to negative, as would be expected due to the replacement of the positively charged lipid DOTAP (Table 5.1). All LRA-loaded LCNPs were colloidally stable in physiological conditions for over 10 days in cell culture media supplemented with 10% fetal bovine serum (Figure S3, Appendix III).

5.4.2 *Efficacy of LRA-loaded LCNPs in an in vitro model of latent HIV-1 infection.*

LRA action requires release from LCNPs and subsequent binding to intracellular molecular targets. Previously, we and others have shown that physical encapsulation of drugs into LCNPs results in an intial burst release upon mixing with cell culture medium [23]. We hypothesized that the physically encapsulated LRAs would show similar burst release, while chemically conjugated LRAs would be released slowly. To test this hypothesis, we measured release kinetics of LRAs from LCNPs in cell culture media (Figure 5.2A). As expected, all physically

encapsulated LRAs (JQ1, disulfiram, Ing3A) showed burst release from LCNPs resulting in 50% of the drug released between 1 hour and 1.6 days as measured by nonlinear regression (Table 5.1, Figure 5.2A, and Table S3, Appendix III). In contrast, chemically conjugated LRAs showed slower release kinetics. For Ing3A and prostratin, which were conjugated by Steglich esterification, it took over one month to reach 50% release. Since Ing3A was both physically encapsulated and chemically conjugated, combining these separate formulations would provide both slow and fast release kinetics. For panobinostat conjugated by amide bond using EDC chemistry, 50% of the drug was released over 1.4 days.

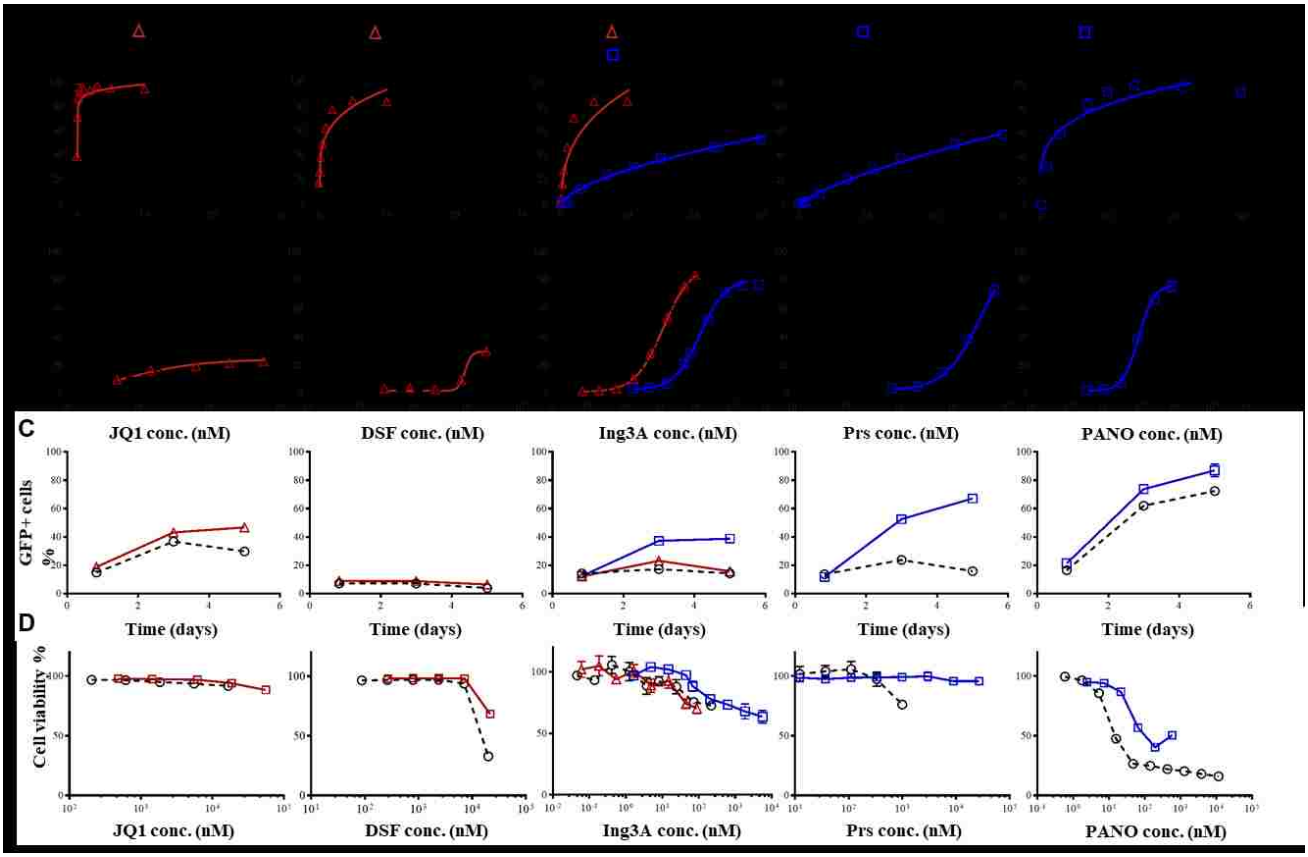

Figure 5.2. *In vitro* dose-response and time-dependent HIV-1 latency reversal correlates with LRA release kinetics from LCNPs. (A) Release kinetics of physically encapsulated LRAs (red triangle) and chemically conjugated LRAs (blue square) from LCNPs in cell culture media at 37 °C. Data were fit by nonlinear regression, detailed in table S3. (B) Dose-response curve for latent HIV reactivation (indicated as a percentage of GFP+ cells) on J-Lat A1 cells incubated

with single LRA formulations for 20 hours. Data were fit in the 4-parameter log-logistic model, detailed in table S4. (C) Time-dependent curve for latent HIV reactivation of J-Lat A1 cells incubated with single LRA formulations over 5 days. (D) Cell viability of J-Lat A1 cells after incubation with single free LRAs or LCNP formulated LRAs at different concentrations for 20 hours. Cell viability was measured by monitoring metabolic activity with the CellTiter-Blue Assay. Each experiment was performed once with n = 3 wells of each treatment. Data represent mean ± s.d. LRA/LCNP: LRA was physically encapsulated into LCNPs (red curve); LRA-LCNP: LRA was chemically conjugated to the PLGA (blue curve).

Next, we compared the HIV-1 latency reactivation potency of these LCNP-formulated LRAs with free LRAs on the J-Lat Tat-GFP (A1) cell line model, which expresses green fluorescent protein (GFP) upon reactivation of latent HIV-1 integrated into the cell genome [32-33]. The percentage of GFP-positive cells measured by flow cytometry was used to assess the potency of LRAs (Figure 5.2B and figure. S4, Appendix III). Physically encapsulated JQ1, disulfiram and Ing3A showed similar potency to the free drug used at the same concentrations after 20 hours of treatment. In contrast, all chemically conjugated LRAs (Ing3A, prostratin and panobinostat) showed lower potency than the free drug, likely due to their slower release from LCNPs (Table S3, Appendix III). To investigate whether the slow drug release kinetics could lead to delayed latency activation at later time points, we extended cell incubation with LRA formulations to 5 days, and observed that the conjugated LRAs (Ing3A-LCNP, Prs-LCNP, and PANO-LCNP) showed accumulated induction of GFP expression over time (Figure 5.2C). In contrast, the free LRAs (disulfiram, Ing3A, prostratin) and the physically encapsulated drugs (DSF/LCNP and Ing3A/LCNPs) exhibited constant activity over 5 days. Exceptions are physically encapsulated JQ1 and free panobinostat, which also showed accumulated effects. All the LCNP-formulated LRAs showed equal or lower cytotoxicity compared to free drug (Figure 5.2D), meaning that LCNPs could potentially deliver higher LRA doses required for efficacy while avoiding the high toxicity. Chol-but formulated LCNPs induced only ~5% GFP expression in this cell model at the

highest concentration we could achieve (Figure S5a, Appendix III). However, because chol-but reduces non-specific cell binding [34], we kept it in our formulations for the subsequent targeting and animal studies.

5.4.3 *Synergistic induction of HIV-1 mRNA levels by Ing3A and JQ1 loaded LCNPs in CD4+ T cells from infected individuals.*

Mechanistically distinct LRAs delivered in combination have shown synergistic interactions in ex vivo latent HIV-1 reactivation [13-14]. To identify the best LRA formulations to evaluate for HIV-1 latency reversal in human clinical samples, we first measured viral reactivation for every pairwise combination of LCNP-formulated LRA using J-Lat A1 cells. LRA concentrations were chosen to achieve similar induction of GFP expression (~20% GFP+ cells) when dosed individually, and this concentration was used to measure efficacy of the drug combination (Figure 5.3A, B). Most binary combinations showed higher GFP induction than the corresponding single drugs. We used the Bliss independence model to select LRAs with synergistic effects as measured by $\Delta faxy > 0$ (details in Methods). JQ1 in combination with any of the other four LRAs, and disulfiram in combination with Ing3A or prostratin, displayed synergy with $\Delta faxy$ above 0.1 (Figure 5.3C). Ing3A and panobinostat loaded LCNPs were the most potent, indicated by the lower dose necessary to achieve equivalent efficacy of ~20% GFP+ cells as well as their median effective dose or ED50 (Figure 5.2B, 5.3A, and Table S4, Appendix III). However, panobinostat demonstrated high cytotoxicity both individually and in combination with JQ1 (Figure 5.3D). A similar relationship between efficacy and cytotoxicity was observed for disulfiram. Disulfiram combined with prostratin in LCNPs led to the highest measured synergy and also high cell viability (Figure 5.3C, D). However, this LRA combination required use at 10-fold higher total dose (~18000 nM) compared to the combination of JQ1/LCNP and

Ing3A-LCNP (~1500 nM) (Figure 5.3A). The free drug combination of disulfiram and prostratin also showed low viability (Figure 5.3D). Finally, the combination of Ing3A and JQ1 was chosen as it showed equivalent and synergistic activity at a lower dose with significantly better viability (Figure 5.3A, B and D).

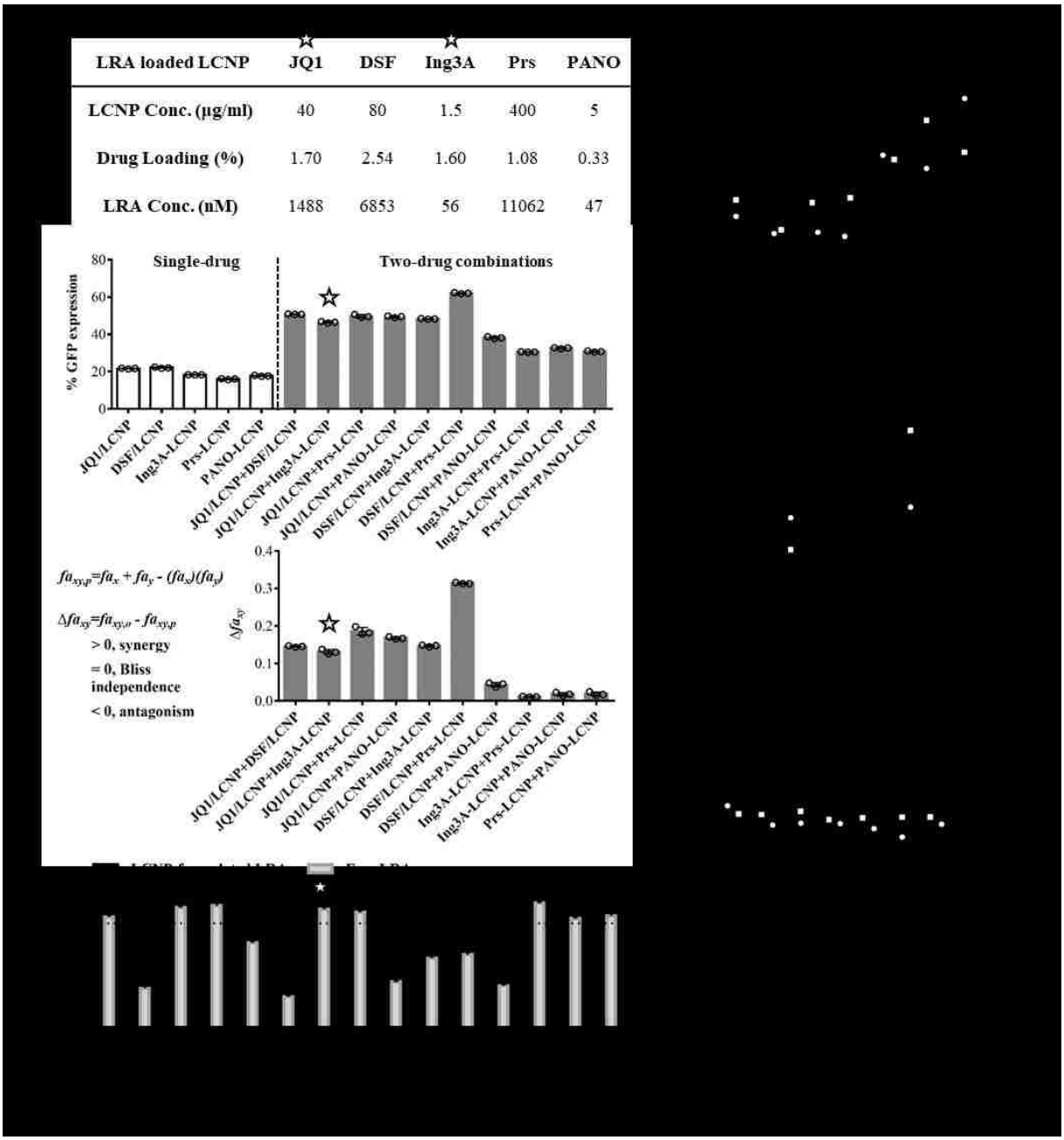

Figure 5.3. LCNP-formulated Ing3A and JQ1 enhance latent HIV reactivation and reduce cytotoxicity from J-Lat A1 cells, and synergistically increase HIV-1 mRNA expression in CD4+ T cells from infected individuals on suppressive ART. (A) Concentrations of single and

combination LCNP formulated LRAs. LRA concentrations were calculated as total LRA in LCNPs. (B) In vitro latent HIV reactivation using single or combination LCNP formulated LRAs on J-Lat A1 cells for 20 hours. (C) Calculation of synergy for LCNP formulated LRA combinations using the Bliss independence model. Data are presented as the difference between the observed and predicted percentage of GFP+ cells. fax or fay: % GFP expression by drug x or y; faxy,o : observed % GFP expression by a combination of drug x and y; faxy,p: predicted % GFP expression by a combination of drug x and y using the equation detailed in Methods. (D) Cell viability of J-Lat A1 cells after incubation with single or combination LRA formulations for 20 hours. Free or LCNP formulated LRAs were dosed at the concentrations that achieved similar latent HIV reactivation (JQ1 1488 nM, DSF 14840 nM, Ing3A 3.5 nM, Prs 251 nM and PANO 13.2 nM). The combination of JQ1 and Ing3A ( ) was chosen for high potency, synergy and low cytotoxicity. The experiment (A-D) was performed once with n = 3 wells of each treatment. Data represent mean ± s.d. (E) Intracellular HIV-1 mRNA levels in CD4+ T cells isolated from peripheral blood of infected individuals and treated with free Ing3A, Ing3A-LCNP, free JQ1, JQ1/LCNP, or their binary combinations. Data are presented as fold induction relative to DMSO control. Statistical analysis was performed using paired one-way ANOVA with Bonferroni's test comparing each group with the DMSO control. *p <0.05, ** p<0.005. (F) Calculation of synergy for Ing3A and JQ1 combinations using the Bliss independence model. Data are presented as the difference between the observed and predicted fractional effect by the LRAs compared to the PMA/I positive control (see Methods for details). Statistical analysis was performed using paired Student's t test. (G) Percentage of live cells after treatments, measured by live/dead staining following the FACS analysis. The experiments (E-G) were performed using peripheral blood from three different individuals, represented as a circle, square, or triangle. Each data point represents the mean fold induction of 3 replicate LRA treatments of 1x106 CD4+ T cells per individual. Error bars represent mean ± s.d. from three individuals.

CD4+ T cells isolated from HIV-1 infected individuals under suppressive ART were used to validate the activity of LCNP-formulated Ing3A and JQ1. Cells from three donors were used to test the induction of intracellular HIV-1 mRNA after treatment with Ing3A and JQ1 alone as well as their combination as free drugs and formulated in LCNPs. The single drugs in free or LCNP formulations increased intracellular HIV by 1-4 fold over DMSO control treatment, but the differences were not statistically significant (Figure 5.3E). Combining Ing3A and JQ1 significantly increased intracellular HIV-1 mRNA expression 6.1- (free Ing3A + JQ1) and 6.4-fold (LCNP formulated Ing3A + JQ1), which was similar to the positive control of phorbol myristate acetate plus ionomycin (PMA/I, 8.1-fold induction). Because Ing3A and JQ1 act through different mechanisms, we compared the experimentally observed synergistic effect to

the predicted effect by the Bliss independence model. We found that the combined effects from both free and LCNP formulated Ing3A and JQ1 significantly exceeded the Bliss model prediction resulting in a calculated Δfaxy of 0.44 and 0.56 (Figure 5.3F), respectively, validating that the combination synergistically induces intracellular HIV-1 mRNA from clinical samples. None of these LRA formulations caused significant cytotoxicity in comparison to the DMSO control (Figure 5.3G).

5.4.4 *CD4-targeted LCNPs selectively activate CD4+ T cells from pigtail macaque PBMCs.*

We have previously shown that conjugating an anti-CD4 monoclonal antibody (CD4 mAb) to our optimized chol-but inserted LCNPs led to high specificity for CD4+ T cells[34]. Here, we conjugated an anti-CD4 mAb to our Ing3A-cbLCNPs (Figure 5.4A). We chose conjugated Ing3A as the model drug because our screening showed that it is the most potent LRA and the chemically conjugated formulation provides sustained release which is especially beneficial for targeting. To facilitate a higher-level of passive targeting to the draining lymph nodes [3, 35], we synthesized smaller LCNPs by optimizing the single-emulsion process with a different lipid to PLGA ratio (Table S5, Appendix III). After conjugation with anti-CD4 mAb, the diameter of LCNPs remained less than 150 nm (Figure 5.4A). We confirmed the activity of these smaller Ing3A-LCNPs in J-Lat A1 cells and observed slightly higher latency reversal compared to the larger particle (Figure S6a, Appendix III). To evaluate reactivation of the targeted formulations, we used primary cells obtained from pigtail macaque PBMCs and compared CD69 expression between CD4+ (CD3+CD14-CD8-) and CD8+ (CD3+CD14-CD8+) T cells (Figure S7, Appendix III). CD69 is a marker for T cell activation and positively correlates with HIV-1 latency reversal [25, 36]. PBMCs were treated with free drug, bare LCNPs, anti-CD4 LCNPs and isotype LCNPs. The targeted Ing3A-CD4-cbLCNPs showed 2-fold increased CD69 expression

in CD4+ T cells compared with CD8+ T cells (Figure 5.4B), demonstrating the ability of our targeted LCNPs to specifically activate CD4+ T cells.

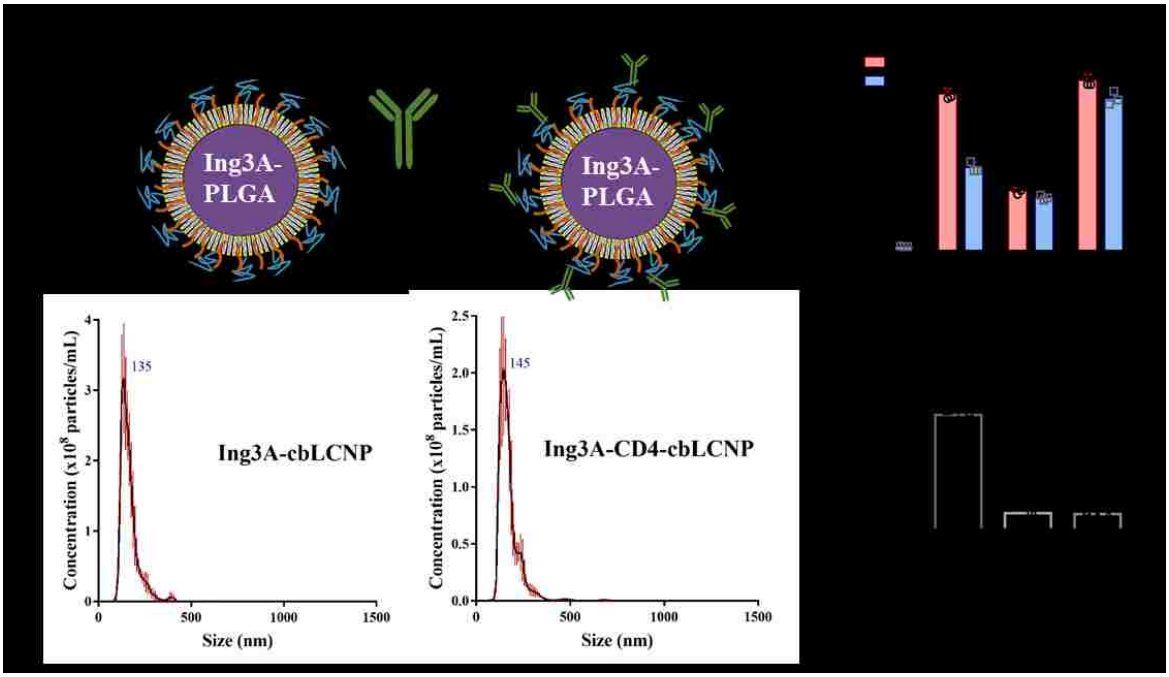

Figure 5.4. CD4-targeted LCNP formulating Ing3A selectively reactivates CD4+ T cells from PBMCs isolated from pigtail macaque blood. (A) Ing3A-LCNP (<150 nm) conjugated with anti-CD4 monoclonal antibody. Resulting size distribution measured by NanoSight. (B) CD69 median fluorescence intensity (MFI) of CD4+ (CD14-CD3+CD8-) cells and CD8+ (CD14-CD3+CD8+) cells (top figure), and their respective MFI ratio (bottom figure) from PBMCs isolated from pigtail macaque blood and treated with free Ing3A, bare LCNPs, CD4-targeted LCNPs and isotype LCNPs for 20 hours. The experiment was performed once with blood samples from three pigtail macaques (n = 3). Statistical significance was calculated using two-way (top figure) or one-way (bottom figure) ANOVA with Bonferroni's test. *** $p<0.0005$. **** $p<0.0001$. Data represent mean ± s.d.

5.4.5 *CD4-LCNP biodistribution in mice over 7 days.*

Most of the latent HIV reservoir is harbored in lymphatic tissues such as lymph nodes, making it inaccessible to many anti-HIV-1 agents [2-3, 21]. Nanocarriers have been developed to target ARVs to anatomical HIV reservoirs including lymph nodes, the central nervous system, and gut-associated lymphoid tissues [21, 23]. However, none of those nanocarriers have been used to deliver LRAs to lymphatic tissues. We hypothesized that our nanocarriers could traffic to draining

lymph nodes after subcutaneous administration and enter the lymphatic system to deliver LRAs to resident CD4+ T cells. To test this hypothesis, we labeled our LCNPs with DiR dye, subcutaneously injected them into the left flank of C57BL/6J mice, and tracked the LCNPs by imaging the draining and non-draining inguinal lymph nodes, as well as other major tissues and organs (spleen, lung, liver, gut, kidney, heart, brain and plasma). First, we surprisingly found that LCNPs with DOTAP in the lipid bilayer (dtLCNPs) showed little accumulation to lymph nodes after subcutaneous injection (Figure S8a, Appendix III). In contrast, negatively charged LCNPs, formulated with chol-but (cbLCNPs) in the lipid bilayer, resulted in dramatically increased lymph node accumulation (Figure S8b, Appendix III). We assumed the difference was due to non-specific cell binding of neutrally to positively charged dtLCNPs at the injection site that hindered lymph node trafficking. Next, we found that the smaller-size optimized cbLCNPs (<150 nm) containing chol-but enhanced lymph node accumulation compared to the larger particle (Figure S8c, Appendix III). This was consistent with other reported studies that bigger nanoparticles might be more easily trapped at the injection site instead of efficiently draining to the lymph node [3, 35]. Because of their desirable trafficking properties, as well as the increased targeting specificity reported previously [34], we moved forward with smaller CD4-targeted cbLCNPs for all animal studies.

We selected 20 hours, 3 days, and 7 days as time points for investigating the biodistribution of CD4-cbLCNPs in mice (Figure 5.5). For all three time points, both targeted and non-targeted cbLCNPs exhibited preferential accumulation in the left draining inguinal lymph node (LN) compared to other organs. The second highest fluorescent signal among all major organs was observed in the right inguinal LN. Comparing the targeted and non-targeted cbLCNPs, CD4-cbLCNPs showed 2.1-fold and 2.2-fold increased left LN accumulation over the Iso-cbLCNPs at

20 hours and 3 days, respectively, suggesting that CD4 targeting also led to higher LN accumulation and retention.

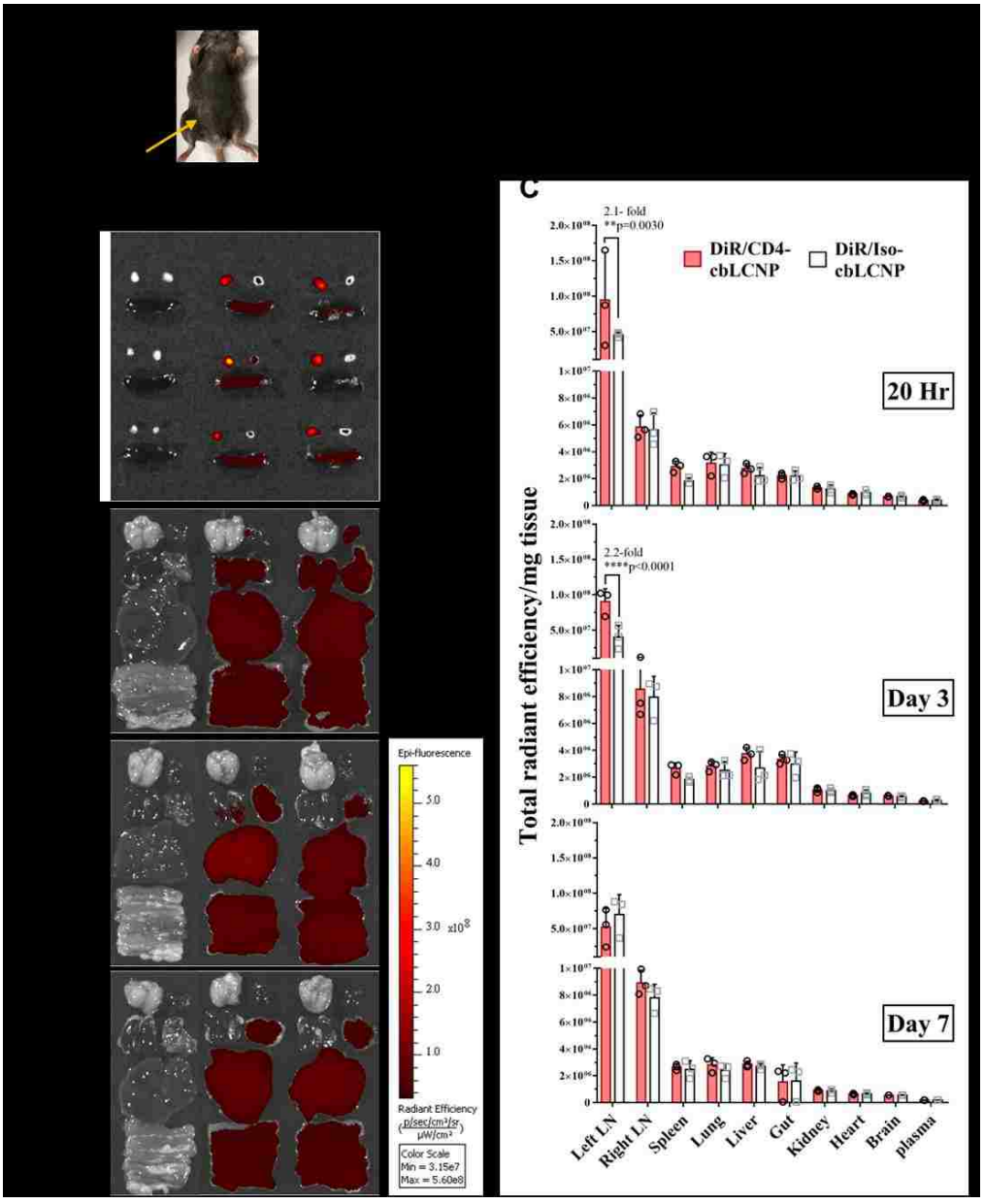

Figure 5.5. Biodistribution of fluorescently-labeled CD4-targeting LCNPs at 20 hours, 3 days and 7 days after subcutaneous injection to mouse left flank. (A) Schedule of injection and tissue harvest. C57BL/6J mice were injected with PBS, DiR loaded CD4-cbLCNPs, and Iso-cbLCNPs subcutaneously at left flank and sacrificed at 20 hours, 3 days, and 7 days for analysis. (B) Representative fluorescent images of inguinal lymph nodes (LNs), spleen (top figure), and other major organs at 20 hours, 3 days and 7 days. (C) Region of interest quantification of tissue fluorescence normalized by tissue mass. Statistical significance was calculated using paired two-way ANOVA with Bonferroni's test. ** $p<0.005$, **** $p<0.0001$. Data represent mean ± s.d.; *n* = 3 mice per group.

5.4.6 *CD4-LCNPs selectively activate lymphatic CD4+ T cells and protect tissues from drug toxicity over 7 days.*

Having shown that our LCNPs target and reactivate CD4+ T cells ex vivo and accumulate in LNs in vivo, we investigated in vivo lymphatic CD4+ T cell activation using our targeted Ing3A-cbLCNPs. We performed this in vivo study following similar procedures as in the biodistribution study, but instead injected mice with free Ing3A, Ing3A-CD4-cbLCNPs and Ing3A-Iso-cbLCNPs containing equal amounts of drug. We also injected mice with 20-fold lower free Ing3A, because our previous in vitro and ex vivo studies (Figure 5.2A and 5.3E) show this concentration demonstrated similar or equivalent efficacy to our Ing3A-LCNPs (due to the slow release nature of the LCNPs). We isolated cells from the left and right inguinal LNs and evaluated CD4+ and CD8+ T cell activation at all time points by measuring CD69 expression (Figure S9, Appendix III). At 20 hours, free Ing3A induced the highest activation of both CD4+ and CD8+ T cells from left LNs, without any significant difference between the two cell populations as expected (Figure. 5.6A). In contrast, our targeted Ing3A-CD4-cbLCNPs selectively activated CD4+ T cells, while CD8+ T cells were not activated. Surprisingly, the induction in the right LN was as high as that in the left LN, even though the left LN showed higher LCNP accumulation in the biodistribution study. Ing3A-CD4-cbLCNP induced less CD69 expression than free Ing3A, which was expected due to the slower drug release from these chemically-conjugated LCNP formulations. We did not observe statistically significant activation of T cells from any other treatment groups. At day 3 and day 7 post-administration, treatment groups with free Ing3A showed a ~10-fold reduction in T cell activation from the levels seen at 20 hours down to levels indistinguishable from the untreated controls. In contrast, the Ing3A-CD4-cbLCNP treated mice resulted in sustained CD69 expression on CD4+ T cells in both lymph nodes out to day 3 and, to a lesser extent, day 7. These results are the first investigation of Ing3A delivered subcutaneously in vivo for T cell activation.

To further investigate the targeting effect of our LCNP formulations, we measured the cell-specific biodistribution of DiD fluorescently-labeled LCNP formulations in primary cells isolated from the left and right inguinal lymph nodes at 20 hours after subcutaneous dosing (Figure 5.6C). We observed that mice treated with CD4-cbLCNPs showed 3-fold higher signal in CD4+ compared to CD8+ cells from the left draining lymph node, indicating preferential targeting to CD4+ T cells (Figure 5.6C) and is consistent with our CD69 activation studies (Figure 5.6A). In addition, the CD14+ monocytes from those lymph nodes also showed significant DiD signals, indicating uptake or binding by monocytes. In the right non-draining lymph node, we were unable to measure cell-specific biodistribution above the PBS control (Figure 5.6C), which is consistent with our biodistribution studies showing a ~10-fold lower accumulation of DiR/LCNP in the right lymph node (Figure 5.5). Finally, the isotype control LCNPs showed no significant uptake by either CD4+ or CD8+ T cells, but was taken up or bound by monocytes, possibly via FcR binding.

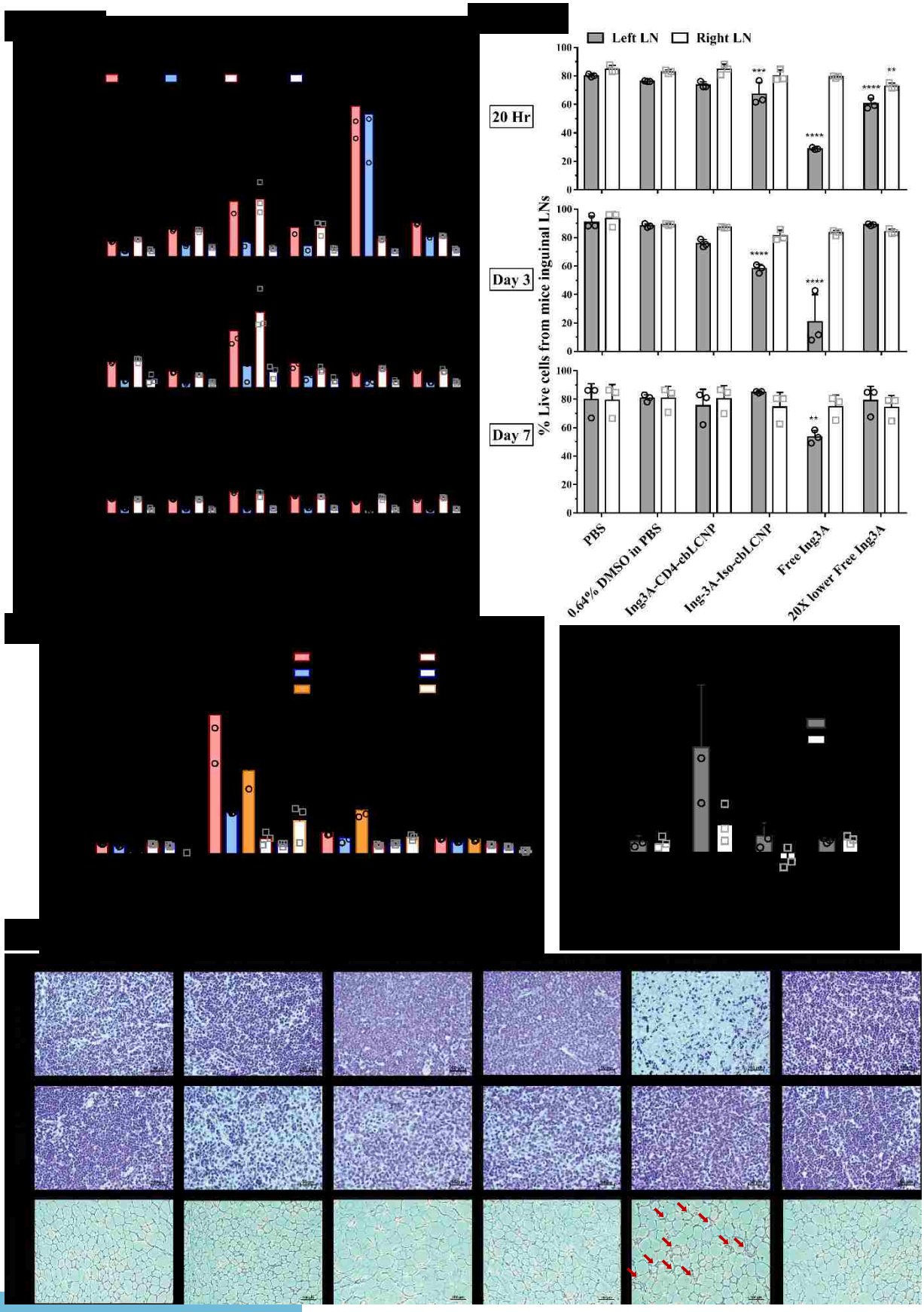

Figure 5.6. CD4-targeted LCNPs selectively activate CD4+ T cells in inguinal lymph nodes after subcutaneous injection to mouse left flank and protects local tissues from toxicity. (A) Mean fluorescent intensity (MFI) of CD69 expression on CD4+ (CD14-CD3+CD8-) and CD8+ (CD14-CD3+CD8+) cells from mice left and right inguinal lymph nodes. Mice were injected with 0.3 mL PBS, 0.64% DMSO, Ing3A-CD4-cbLCNP (0.48 mg/kg, Ing3A dose/body weight), Ing3A-Iso-cbLCNP (0.48 mg/kg), free Ing3A at 0.48 mg/kg or at 0.024 mg/kg, and were sacrificed after 20 hours, 3 days, and 7 days for analysis. **(B)** Percent live cells from all cell populations in the left and right inguinal lymph nodes after treatment. **(C)** Left: MFI of DiD fluorescent signal from CD4+, CD8+, and CD14+ cells from mice left or right inguinal lymph nodes. Mice were injected subcutaneously at left flank with 0.3 mL PBS, DiD/CD4-cbLCNP, DiD/Iso-cbLCNP, or equivalent amount of free DiD in PBS, and were sacrificed after 20 hours for analysis. Right: MFI ratio of DiD fluorescent signal between CD4+ and CD8+ T cells. Statistical significance was calculated using paired two-way ANOVA with Bonferroni's test comparing each treatment group with PBS. * $p<0.05$, ** $p<0.005$, *** $p<0.0005$, **** $p<0.0001$. Data represent mean ± s.d.; $n = 3$ mice per group. **(D)** H&E staining of tissue slides (left and right inguinal lymph nodes, subcutaneous tissues near the injection site) from mice at day 3. From free Ing3A treatment group, condensed cell nucleus in the left LN that indicated cell death, and immune cell infiltration into the adipose tissue near the injection site (red arrows) were observed.

From our efficacy studies, we noticed that free Ing3A induced severe inflammation-like toxicity in the tissues near the injection sites at all time points (Figure S10, Appendix III). To test for toxicity at a cellular level, we isolated cells from the inguinal LNs and found that most cells (>70%) in the left LNs were dead after treatment with free Ing3A at the 20 hour and 3 days time points, while less than 30% of cells were dead from Ing3A-CD4-cbLCNP treatments (Figure 5.6B). Importantly, our Ing3A-CD4-cbLCNPs did not show significant toxicity even though they had better CD4 specific activation at day 3. In addition, while our targeted LCNPs showed preferential accumulation to CD4+ T cells in the draining lymph nodes, the CD4+ T cells retained high viability (Figure S11, Appendix III). To further understand the injection site toxicity that resulted from free Ing3A, we performed histological examination of the LNs and tissue at the injection site (Figure 5.6D). The free Ing3A treatment group was the only group with obvious morphological changes in the draining LN and subcutaneous tissue. Free Ing3A caused cell apoptosis as indicated by condensed cell nucleus from the left inguinal LN near the

injection site, but no effect on the right LN. Additionally, we observed inflammatory cell infiltration into the adipose tissue near the injection site from the mice treated with free Ing3A. These data suggest that, although free Ing3A exhibits high T cell activation efficacy, its activation is not CD4-specific and causes severe cell apoptosis in the draining lymph nodes as well as inflammatory-like toxicity in vivo near the injection site. In contrast, our Ing3A-CD4-cbLCNPs induce specific CD4+ T cell activation for at least 7 days without toxicity.

5.5 Discussion

The major challenges for the current "shock and kill" approach to HIV cure include: insufficient potency of single LRAs, low LRA concentration in the lymphatic tissues that harbor the majority of latent reservoirs, and toxicity. Nanocarriers have shown great promise in delivering combination therapeutics to specific sites or cells and therefore could address these challenges. However, nanocarriers have not been tested in a rigorous fashion as a strategy to deliver LRAs for HIV cure. In a few reported studies, LRAs were evaluated in vitro [24, 26-27], or in vivo through systemic administration without specific targeting [25]. In addition, no studies have investigated delivery of combination LRAs, which may be necessary to sufficiently stimulate HIV reactivation [13]. In this study, we focused on using targeted nanocarriers to deliver mechanistically distinct LRAs in combination, and to specifically act on CD4+ T cells in the lymph nodes.

Our approach shows many advantages over conventional drug delivery systems and existing nanocarrier platforms to deliver LRAs. One of the biggest advantages is the ability of nanocarriers to passively traffic to LNs and actively target CD4+ T cells. We optimized our LCNPs to achieve a high level of LN accumulation by altering lipid composition and reducing their size (Table S5, Appendix III). Our CD4-targeted Ing3A-LCNPs selectively reactivate

CD4+ T cells from both NHP PBMCs ex vivo and mouse LNs in vivo. Together, the high accumulation and long-term retention of targeted LCNPs in the LNs, along with sustained release of conjugated Ing3A, result in up to 7 days of specific CD4+ T cells activation in the LNs. Notably, significantly more CD4-targeted LCNPs accumulated in draining LNs and bound to CD4+ T cells compared to control Iso-LCNPs at 20 hours and 3 days post-administration, demonstrating that the targeted LCNPs preferentially traffic to and remain in the LNs. As we observed non-specific particle binding to or uptake by monocytes in vivo, it will be needed to determine whether some entry of LCNP-formulated Ing3A into monocytes can cause any side effects. Further studies are also necessary to investigate why we saw similar levels of CD4+ T cell activation in the left and right LN despite the observed lower biodistribution of LCNPs in the right LN, opposite the injection site. To achieve CD4+ T cell activation and eventually reservoir eradication throughout the body, it will be necessary to assess T cell activation in other lymph nodes and lymphatic tissues such as the GALT. The impact of multiple subcutaneous injection sites on drug efficacy, as well as alternative administration routes on systemic activity also warrants further investigation.

The CD4 targeting effect also allows LRAs to only reactivate lymphatic CD4+ T cells without affecting other cells such as CD8+ T cells. This avoids inducing aberrant autoimmune responses and focuses drug activity on HIV-1 latency reversal. Indeed, we found that free Ing3A caused severe cell apoptosis and inflammation-like toxicity near the injection sites in mice (Figure 5.6B&D, and Figure S10, Appendix III), even though it caused little cytotoxicity in cell line and primary cell studies (Figure 5.2D, 3D, and Figure S7d, Appendix III). In contrast, Ing3A in our targeted LCNP formulation did not cause severe inflammation in local tissues or cell apoptosis in the draining lymph nodes. In addition to the targeting effects, we also hypothesize that the lack

of toxicity is due to the sustained release of Ing3A from LCNPs which results in consistent low-level exposure over time in contrast to exposure to brief, high levels of free drug exposure. Ing3A is approved by U.S. Food and Drug Administration for topical treatment of actinic keratosis [37], but has not been studied for HIV cure research until recently, and then only in an ex vivo model of latency reversal [13-15]. Our approach is the first to deliver Ing3A to mice subcutaneously, and demonstrate its T cell activation and toxicity profiles in vivo.

Some other advantages of our LCNPs include the capability to incorporate multiple physicochemically diverse LRAs and to improve drug solubility. LRAs vary in their solubility and bioavailability, and it may therefore be difficult to achieve the expected efficacy when dosed in combination with conventional delivery approaches. Our LCNPs deliver multiple LRAs with fixed dose ratios to the target sites that may be more easily translated from in vitro to in vivo studies. Furthermore, our LCNPs can be dosed at concentrations up to 10 mg/mL in saline, which could significantly increase the solubility of hydrophobic LRAs.

In summary, we have developed hybrid nanocarriers that can deliver multiple types of LRA and determined an LCNP-formulated JQ1 and Ing3A combination that induces robust and synergistic HIV-1 latent reactivation with low toxicity. Our targeted formulations provide long-term and specific activation of CD4+ T cells in LNs, while reducing local drug toxicity in vivo. These nanocarriers will be tested in an NHP model for reactivation of latent SIV. This robust platform for targeting CD4+ T cells in the lymph nodes has potential for delivery of other types of anti-HIV agents, vaccines, immunomodulating agents, and gene-modifying oligonucleotide drugs for many biomedical applications.

5.6 Acknowledgement

The following reagent was obtained through the NIH AIDS Reagent Program, Division of AIDS, NIAID, NIH: J-Lat Tat-GFP cells (A1) from Dr. Eric Verdin[32-33]. T20, Fusion inhibitor from AIDS, NIAID. This work was supported by the National Institute of Health [grant number AI094412], amfAR (The Foundation for AIDS Research) [109541-61-RGRL], and CFAR award 2037020 [Prime P30 AI064518-13].

5.7 References

1. Lorenzo-Redondo, R.; Fryer, H. R.; Bedford, T.; Kim, E.-Y.; Archer, J.; Pond, S. L. K.; Chung, Y.-S.; Penugonda, S.; Chipman, J.; Fletcher, C. V.; Schacker, T. W.; Malim, M. H.; Rambaut, A.; Haase, A. T.; McLean, A. R.; Wolinsky, S. M., Persistent HIV-1 replication maintains the tissue reservoir during therapy. *Nature* **2016,** *530* (7588), 51-56.
2. Fletcher, C. V.; Staskus, K.; Wietgrefe, S. W.; Rothenberger, M.; Reilly, C.; Chipman, J. G.; Beilman, G. J.; Khoruts, A.; Thorkelson, A.; Schmidt, T. E.; Anderson, J.; Perkey, K.; Stevenson, M.; Perelson, A. S.; Douek, D. C.; Haase, A. T.; Schacker, T. W., Persistent HIV-1 replication is associated with lower antiretroviral drug concentrations in lymphatic tissues. *Proceedings of the National Academy of Sciences* **2014,** *111* (6), 2307-2312.
3. Freeling, J. P.; Ho, R. J. Y., Anti-HIV drug particles may overcome lymphatic drug insufficiency and associated HIV persistence. *Proceedings of the National Academy of Sciences of the United States of America* **2014,** *111* (25), E2512-E2513.
4. Eisele, E.; Siliciano, Robert F., Redefining the Viral Reservoirs that Prevent HIV-1 Eradication. *Immunity* **2012,** *37* (3), 377-388.
5. Barton, K.; Winckelmann, A.; Palmer, S., HIV-1 Reservoirs During Suppressive Therapy. *Trends in microbiology* **2016,** *24* (5), 345-355.
6. Siliciano, J. D.; Kajdas, J.; Finzi, D.; Quinn, T. C.; Chadwick, K.; Margolick, J. B.; Kovacs, C.; Gange, S. J.; Siliciano, R. F., Long-term follow-up studies confirm the stability of the latent reservoir for HIV-1 in resting CD4+ T cells. *Nature Medicine* **2003,** *9*, 727.
7. Crooks, A. M.; Bateson, R.; Cope, A. B.; Dahl, N. P.; Griggs, M. K.; Kuruc, J. D.; Gay, C. L.; Eron, J. J.; Margolis, D. M.; Bosch, R. J., Precise quantitation of the latent HIV-1 reservoir: implications for eradication strategies. *Journal of Infectious Diseases* **2015,** *212* (9), 1361-1365.
8. Carr, A.; Cooper, D. A., Adverse effects of antiretroviral therapy. *The Lancet* **2000,** *356* (9239), 1423-1430.
9. Margolis, D. M.; Garcia, J. V.; Hazuda, D. J.; Haynes, B. F., Latency reversal and viral clearance to cure HIV-1. *Science* **2016,** *353* (6297).
10. Barouch, D. H.; Deeks, S. G., Immunologic strategies for HIV-1 remission and eradication. *Science* **2014,** *345* (6193), 169-174.
11. Rasmussen, T. A.; Lewin, S. R., Shocking HIV out of hiding: where are we with clinical trials of latency reversing agents? *Current Opinion in HIV and AIDS* **2016,** *11* (4), 394-401.

12. Delagrèverie, H. M.; Delaugerre, C.; Lewin, S. R.; Deeks, S. G.; Li, J. Z., Ongoing Clinical Trials of Human Immunodeficiency Virus Latency-Reversing and Immunomodulatory Agents. *Open Forum Infectious Diseases* **2016,** *3* (4), ofw189-ofw189.
13. Laird, G. M.; Bullen, C. K.; Rosenbloom, D. I.; Martin, A. R.; Hill, A. L.; Durand, C. M.; Siliciano, J. D.; Siliciano, R. F., Ex vivo analysis identifies effective HIV-1 latency-reversing drug combinations. *J Clin Invest* **2015,** *125* (5), 1901-12.
14. Darcis, G.; Kula, A.; Bouchat, S.; Fujinaga, K.; Corazza, F.; Ait-Ammar, A.; Delacourt, N.; Melard, A.; Kabeya, K.; Vanhulle, C.; Van Driessche, B.; Gatot, J.-S.; Cherrier, T.; Pianowski, L. F.; Gama, L.; Schwartz, C.; Vila, J.; Burny, A.; Clumeck, N.; Moutschen, M.; De Wit, S.; Peterlin, B. M.; Rouzioux, C.; Rohr, O.; Van Lint, C., An In-Depth Comparison of Latency-Reversing Agent Combinations in Various In Vitro and Ex Vivo HIV-1 Latency Models Identified Bryostatin-1+JQ1 and Ingenol-B+JQ1 to Potently Reactivate Viral Gene Expression. *PLoS Pathogens* **2015,** *11* (7), e1005063.
15. Jiang, G.; Mendes, E. A.; Kaiser, P.; Wong, D. P.; Tang, Y.; Cai, I.; Fenton, A.; Melcher, G. P.; Hildreth, J. E. K.; Thompson, G. R.; Wong, J. K.; Dandekar, S., Synergistic Reactivation of Latent HIV Expression by Ingenol-3-Angelate, PEP005, Targeted NF-kB Signaling in Combination with JQ1 Induced p-TEFb Activation. *PLOS Pathogens* **2015,** *11* (7), e1005066.
16. Gray, L. R.; On, H.; Roberts, E.; Lu, H. K.; Moso, M. A.; Raison, J. A.; Papaioannou, C.; Cheng, W.-J.; Ellett, A. M.; Jacobson, J. C.; Purcell, D. F. J.; Wesselingh, S. L.; Gorry, P. R.; Lewin, S. R.; Churchill, M. J., Toxicity and in vitro activity of HIV-1 latency-reversing agents in primary CNS cells. *J. Neurovirol.* **2016,** *22* (4), 455-463.
17. Wong, V. C.; Fong, L. E.; Adams, N. M.; Xue, Q.; Dey, S. S.; Miller-Jensen, K., Quantitative evaluation and optimization of co-drugging to improve anti-HIV latency therapy. *Cellular and molecular bioengineering* **2014,** *7* (3), 320-333.
18. Estes, J. D.; Kityo, C.; Ssali, F.; Swainson, L.; Makamdop, K. N.; Del Prete, G. Q.; Deeks, S. G.; Luciw, P. A.; Chipman, J. G.; Beilman, G. J.; Hoskuldsson, T.; Khoruts, A.; Anderson, J.; Deleage, C.; Jasurda, J.; Schmidt, T. E.; Hafertepe, M.; Callisto, S. P.; Pearson, H.; Reimann, T.; Schuster, J.; Schoephoerster, J.; Southern, P.; Perkey, K.; Shang, L.; Wietgrefe, S. W.; Fletcher, C. V.; Lifson, J. D.; Douek, D. C.; McCune, J. M.; Haase, A. T.; Schacker, T. W., Defining total-body AIDS-virus burden with implications for curative strategies. *Nature Medicine* **2017,** *23*, 1271.
19. Di Mascio, M.; Paik, C. H.; Carrasquillo, J. A.; Maeng, J.-S.; Jang, B.-S.; Shin, I. S.; Srinivasula, S.; Byrum, R.; Neria, A.; Kopp, W.; Catalfamo, M.; Nishimura, Y.; Reimann, K.; Martin, M.; Lane, H. C., Noninvasive in vivo imaging of CD4 cells in simian-human immunodeficiency virus (SHIV)–infected nonhuman primates. *Blood* **2009,** *114* (2), 328-337.
20. Westermann, J.; Pabst, R., Distribution of lymphocyte subsets and natural killer cells in the human body. *The clinical investigator* **1992,** *70* (7), 539-544.
21. Cao, S.; Woodrow, K. A., Nanotechnology approaches to eradicating HIV reservoirs. *European Journal of Pharmaceutics and Biopharmaceutics* **2018**.
22. Freeling, J. P.; Koehn, J.; Shu, C.; Sun, J.; Ho, R. J., Anti-HIV drug-combination nanoparticles enhance plasma drug exposure duration as well as triple-drug combination levels in cells within lymph nodes and blood in primates. *AIDS research and human retroviruses* **2015,** *31* (1), 107-114.
23. Cao, S.; Jiang, Y.; Zhang, H.; Kondza, N.; Woodrow, K. A., Core-shell nanoparticles for targeted and combination antiretroviral activity in gut-homing T cells. *Nanomedicine: Nanotechnology, Biology and Medicine* **2018,** *14* (7), 2143-2153.

24. Kovochich, M.; Marsden, M. D.; Zack, J. A., Activation of Latent HIV Using Drug-Loaded Nanoparticles. *PLoS ONE* **2011,** *6* (4), e18270.
25. Buehler, D. C.; Marsden, M. D.; Shen, S.; Toso, D. B.; Wu, X.; Loo, J. A.; Zhou, Z. H.; Kickhoefer, V. A.; Wender, P. A.; Zack, J. A.; Rome, L. H., Bioengineered Vaults: Self-Assembling Protein Shell–Lipophilic Core Nanoparticles for Drug Delivery. *ACS Nano* **2014,** *8* (8), 7723-7732.
26. Tang, X.; Liang, Y.; Liu, X.; Zhou, S.; Liu, L.; Zhang, F.; Xie, C.; Cai, S.; Wei, J.; Zhu, Y.; Hou, W., PLGA-PEG Nanoparticles Coated with Anti-CD45RO and Loaded with HDAC Plus Protease Inhibitors Activate Latent HIV and Inhibit Viral Spread. *Nanoscale Research Letters* **2015,** *10* (1), 413.
27. Jayant, R. D.; Atluri, V. S. R.; Agudelo, M.; Sagar, V.; Kaushik, A.; Nair, M., Sustained-release nanoART formulation for the treatment of neuroAIDS. *International Journal of Nanomedicine* **2015,** *10*, 1077-1093.
28. Das, B.; Dobrowolski, C.; Shahir, A.-M.; Feng, Z.; Yu, X.; Sha, J.; Bissada, N. F.; Weinberg, A.; Karn, J.; Ye, F., Short chain fatty acids potently induce latent HIV-1 in T-cells by activating P-TEFb and multiple histone modifications. *Virology* **2015,** *474*, 65-81.
29. Park, J.; Kim, M.; Kang, S. G.; Jannasch, A. H.; Cooper, B.; Patterson, J.; Kim, C. H., Short-chain fatty acids induce both effector and regulatory T cells by suppression of histone deacetylases and regulation of the mTOR-S6K pathway. *Mucosal Immunol* **2015,** *8* (1), 80-93.
30. Brioschi, A.; Zara, G.; Calderoni, S.; Gasco, M.; Mauro, A., Cholesterylbutyrate Solid Lipid Nanoparticles as a Butyric Acid Prodrug. *Molecules* **2008,** *13* (2), 230.
31. Yang, F.; Bian, C.; Zhu, L.; Zhao, G.; Huang, Z.; Huang, M., Effect of human serum albumin on drug metabolism: Structural evidence of esterase activity of human serum albumin. *Journal of Structural Biology* **2007,** *157* (2), 348-355.
32. Jordan, A.; Bisgrove, D.; Verdin, E., HIV reproducibly establishes a latent infection after acute infection of T cells in vitro. *The EMBO Journal* **2003,** *22* (8), 1868-1877.
33. Jordan, A.; Defechereux, P.; Verdin, E., The site of HIV-1 integration in the human genome determines basal transcriptional activity and response to Tat transactivation. *The EMBO Journal* **2001,** *20* (7), 1726-1738.
34. Cao, S.; Jiang, Y.; Levy Claire, N.; Hughes Sean, M.; Zhang, H.; Hladik, F.; Woodrow Kim, A., Optimization and comparison of CD4-targeting lipid–polymer hybrid nanoparticles using different binding ligands. *Journal of Biomedical Materials Research Part A* **2017,** *106* (5), 1177-1188.
35. Jiang, H.; Wang, Q.; Sun, X., Lymph node targeting strategies to improve vaccination efficacy. *Journal of Controlled Release* **2017**.
36. Beans, E. J.; Fournogerakis, D.; Gauntlett, C.; Heumann, L. V.; Kramer, R.; Marsden, M. D.; Murray, D.; Chun, T.-W.; Zack, J. A.; Wender, P. A., Highly potent, synthetically accessible prostratin analogs induce latent HIV expression in vitro and ex vivo. *Proceedings of the National Academy of Sciences* **2013,** *110* (29), 11698-11703.
37. Gupta, A. K.; Paquet, M., Ingenol Mebutate: A Promising Treatment for Actinic Keratoses and Nonmelanoma Skin Cancers. *Journal of Cutaneous Medicine and Surgery* **2013,** *17* (3), 173-179.
38. Duncan, I. W.; Culbreth, P. H.; Burtis, C. A., Determination of free, total, and esterified cholesterol by high-performance liquid chromatography. *Journal of Chromatography B: Biomedical Sciences and Applications* **1979,** *162* (3), 281-292.

39. Ritz, C.; Baty, F.; Streibig, J. C.; Gerhard, D., Dose-Response Analysis Using R. *PLOS ONE* **2016,** *10* (12), e0146021.
40. Bullen, C. K.; Laird, G. M.; Durand, C. M.; Siliciano, J. D.; Siliciano, R. F., New ex vivo approaches distinguish effective and ineffective single agents for reversing HIV-1 latency in vivo. *Nat Med* **2014,** *20* (4), 425-9.

Chapter 6. Summary and future perspectives

6.1 Overall summary and discussion

In this dissertation, we investigated targeted nanocarriers (NCs) for the delivery of anti-HIV drugs to specific HIV reservoir cells and tissues. Combination antiretroviral therapy (cART) has revolutionized the treatment of HIV-1 infection, but does not completely eradicate the virus due to the existence of HIV reservoirs. Gut-associated lymphoid tissue (GALT) and lymph nodes (LNs) are the two largest lymphoid tissues that harbor the majority of latently-infected cells, but only limited access by anti-HIV drugs occurs, contributing to viral persistence and reservoir expansion. We developed NCs to target and deliver drugs to the GALT and LNs, specifically to gut-homing T cells and CD4+ T cells in those tissues. Such cell-targeting was achieved by linking targeting ligands such as anti-α4β7 monoclonal antibodies (mAbs) or anti-CD4 antibody, respectively, to the NC surface. Our NCs are composed of a lipid bilayer shell and a polymer core, and are able to load physicochemically diverse anti-HIV agents, including antiretroviral drugs (ARVs), monoclonal antibodies (mAbs), and latency reversing agents (LRAs). With these capabilities, we were able to use our NC platform to deliver combination anti-HIV therapeutics to the reservoir cells and tissues.

In Chapter 3, we developed a lipid-coated poly(lactic-co-glycolic) acid nanoparticles (LCNPs) incorporating the anti-α4β7 mAb as a dual-functional ligand for selectively targeting antiretroviral drugs to gut-homing T cells in the GALT while simultaneously blocking HIV infection. LCNPs were used to physically encapsulate a protease inhibitor in the nanoparticle-core and chemically conjugate anti-α4β7 mAb to the lipid layer shell. We demonstrated that these LCNPs reduce cytotoxicity and enhance antiviral activities of the PI and α4β7 mAb in combination. The targeted

LCNPs could specifically bind to CD4+ and α4β7+ T cells from lamina propria lymphocytes isolated from rhesus macaque ileum, and enhanced accumulation to murine small intestine and bound to α4β7+ cells in the GALT when administered intravenously. This is the first report of delivering antiretroviral drugs and mAbs simultaneously in nanoparticles for HIV treatment, where the α4β7 mAb serves both a targeting function as well as inhibits HIV infection. We used the protease inhibitor as a model drug here, but also expect this platform to load and deliver other types of therapeutics to the GALT.

In Chapter 4, we further utilized our NC and optimize it to target CD4+ T cells, which are the major HIV targets and reservoir cells. Monoclonal antibodies (mAbs) against CD4 and CD4 binding peptides have been developed and conjugated to the surface of NCs for targeting. However, targeting efficacy of different ligands varies with their specificity, affinity or avidity when linked to NCs. In addition, the physicochemical properties of NCs could also affect the ligand function but have been relatively less studied. Here, we selected several CD4 binding ligands and conjugated them separately to two types of LCNPs with neutral or negative ζ-potentials in order to evaluate their targeting abilities. The targeting ligands evaluated include the CD4 binding peptide (BP4), and rhesus recombinant anti-CD4 mAb (CD4 mAb) and its fragments (fCD4). First, we demonstrate that negatively charged LCNPs (termed cbLCNPs) dramatically reduced nonspecific binding, leading to a higher targeting specificity, compared to neutral or positively charged LCNPs (termed dtLCNPs) in a human CD4+ T cell line. Second, we show that cbLCNPs surface conjugated with CD4 mAbs (CD4-cbLCNPs) preferentially bound to CD4+ cells from pigtail macaque peripheral blood mononuclear cells, indicated by 10-fold binding specificity for CD4+ than CD8+ T cells. This study demonstrates the importance of surface charge on NC targeting and indicates that CD4 mAb is the best candidate for delivering therapeutic agents

to CD4+ T cells. CD4+ T cells in the lymph nodes are major target of HIV and also contribute to viral persistence and reservoir maintenance, we proposed that our CD4-targeted NCs could be applied to deliver anti-HIV agents to lymphatic CD4+ T cells after subcutaneous administration followed by passive trafficking to the lymphatic system.

In Chapter 5, we used the optimized CD4-targeted LCNPs to deliver combination LRAs to the CD4+ T cells in the lymph nodes. A proposed strategy uses LRAs to accelerate the purge of integrated HIV, but has not yet been proven effective in reducing the reservoir size in clinical trials. We hypothesized that our targeted NCs could overcome some of the major challenges for this strategy, including insufficient potency from single LRAs, low concentration in the lymphatic tissues that harbor the majority of latent reservoirs, and toxicity. First, we were able to load a variety of LRAs into our nanocarrier system through different strategies and identified several combinations that displayed synergistically high potency and low cytotoxicity. Second, our LCNPs could passively traffic to the lymph nodes after subcutaneous administration to mice, and selectively activate CD4+ T cells in the lymph nodes. Lastly, we show that our nanocarriers reduced cytotoxicity of most LRAs in both single and combination formulations. In particular, the targeted nanocarriers avoided inflammatory-like toxicity from free LRA in vivo through CD4 specific targeting and sustained release of LRAs. To our knowledge, these studies are the first report of delivering combination LRAs in nanocarriers that successfully target CD4+ T cells in the complex lymph node environment.

In this work, we loaded ARVs and mAbs into our NCs to target the GALT, and on the other hand, we delivered combination LRAs to the CD4+ T cells in the lymph node. Accordingly, we expect that our NCs could also be used to deliver LRAs to the GALT, or ARVs and mAbs to the lymph nodes, or other types of therapeutics to those reservoir tissues. Our core-shell nanoparticles could

serve as a universal platform to be surface-conjugated with different targeting ligands, and loaded with diverse therapeutic agents inside the polymer core or into the lipid bilayer. Through different loading strategies such as physical encapsulation, chemical conjugation and lipid insertion, we were able to achieve different drug releasing kinetics to accommodate various applications.

Several limitations have been discovered from this work. In Chapter 3, we observed high fluorescent signal from murine liver, lung and spleen when injected fluorescently-labeled LCNPs intravenously to mice, indicating the non-specific accumulation of the nanoparticles in these tissues. Radiolabeled nanoparticles could be used in the future to obtain more accurate quantification of dose biodistribution since we observed that recovery efficiency using fluorescence was low and tissue- and dose-dependent. Some other limitations from Chapter 3 include non-specific cell binding of LCNPs from our *in vitro* and *ex vivo* studies, and burst release of tipranavir from LCNPs. We have addressed the non-specific issue in Chapter 4 by changing the LCNP surface charge from neutral to negative, which could cause electrostatic repulsion to cells that are also negatively-charged. We also made polymer-drug conjugates to achieve sustained drug release in Chapter 5. In Chapter 4, we only compared three CD4-binding ligands on two LCNP formulations. Future studies are being directed to investigate more binding ligands such as the antigen-binding (Fab) fragment of anti-CD4 mAbs, or other CD4-binding peptides that might be discovered using novel techniques (e.g., Next-Generation Sequencing). In Chapter 5, we have achieved either burst drug release (less than 2 days to achieve 50% drug release) by physical encapsulation or slow drug release (nearly 30 days to achieve 50% drug release) by chemical conjugation. Other conjugation strategies or linkers for the polymer-drug conjugates might be studied in the future to generate moderate drug release kinetics. In addition, the drug loading using PLGA-drug conjugates was low (<5 wt%) due to the fact that we were only able to conjugate drug

to PLGA at 1:1 molar ratio. Thus, alternative biodegradable polymers that have reactive branches can be used to conjugate more drugs to one molecule of polymer in order to increase the drug loading. From the biodistribution studies, we observed that 100 nm LCNPs had higher accumulation to the draining lymph nodes than 200 nm LCNPs, indicating the size of LCNPs could affect the passive lymph node targeting. LCNPs might be further optimized to reach even smallr size (e.g. 50 nm) and tested for their lymph node targeting properties. Further studies are necessary to investigate why we saw similar levels of CD4+ T cell activation in draining and non-draining inguinal lymph nodes, despite the lower biodistribution of LCNPs in the non-draining lymph nodes. To achieve CD4+ T cell activation and eventually reservoir eradication throughout the body, it will be essential to assess T cell activation in many other lymph nodes and lymphatic tissues such as the GALT. The impact of multiple subcutaneous injection sites on drug efficacy, as well as alternative administration routes on systemic activity also warrants further investigation.

Most of our *in vivo* studies were done in mice which are still in the early stage towards the clinical translation. For the potential clinical studies, there are still obstacles for assessing pharmacokinetics (PK) profile and measuring reservoir sizes in organs or tissues such as mesenteric lymph nodes or many other lymph nodes from patients. Thus, more clinically relevant animal models are necessary to assess the PK, safety and efficacy of these targeted NCs before clinical trials. Currently, the wildly used HIV-1 animal models include humanized mice and non-human primates. In the next section, we proposed to evaluate our CD4-targeted NCs delivering lead LRA combination in a non-human primate model.

6.2 Future studies towards clinical translation

Our long-term goal is to address the complex molecular mechanisms determining HIV reservoir dynamics in tissue compartments and cells that present physiological barriers to therapeutic

delivery *in vivo*. Here, we used nano-sized drug delivery systems to increase drug solubility, decrease toxicity, and expand the drug combinations that can be used for HIV cure. The modular design of nanocarriers has the potential to penetrate sanctuary sites harboring latently infected cells and to deliver therapies that will work synergistically to deplete the reservoir. Eliminating the need for lifelong therapy will be of significant impact for people living with HIV.

In the future, we will conduct PK analyses that identify the optimal dose, dosing interval and drug combinations for the lead LRA agents formulated into CD4-targeted NCs that maximize safety and efficacy in our non-human primate (NHP) mode (6.2.1). To measure efficacy, we will employ a well-established NHP model that recapitulates HIV-1 infection in humans on suppressive cART, and complimentary assays to measure the latent reservoir (6.2.2). We expect these PK, safety and efficacy studies in the NHP model would provide valuable data towards clinical translation.

6.2.1 *PK and safety in NHPs.*

Rationale: Most PK studies of LRAs conducted in humans[1-3], monkeys[4-5], or rodents[6-9] use i.v. doses in the range of 5 mg/kg to 30 mg/kg. Two exceptions are bryostatin 1, dosed at 25 ug/m^2 (<~1 mg/kg)[2] in a phase Ib trail, and romidepsin, dosed up to 3.75 mg/m^2 (~45 mg/kg) in rhesus macaques[5]. Based on these findings, and that NC formulations are expected to extend drug half-life, we anticipate obtaining all relevant PK dynamics within one week and emphasize tissue sampling at early time points, to better capture C_{max} in gut and LN biopsies. We will evaluate a high and low dose range that is comparable to previous studies, but will ultimately determine dose based on the specific HIV cure agents in our lead formulations JQ1+ Ing3A .

Experimental plan: Free LRAs or CD4-targeted NCs formulated with LRAs will be administered subcutaneously at two doses to maximize biodistribution to reservoir tissues and cells in naive pigtailed macaques (Table 6.1). Drug concentrations in blood, gut and lymph node compartments

will be measured by LC/MS-MS to obtain all relevant PK parameters (C_{max}, t_{max}, AUC, $t_{0.5z}$). NC targeting function will be measured by sorting CD4 T cells and quantifying intracellular drug concentration. Animals will be monitored throughout the study for signs of toxicity by serum chemistry, CBC and leucocyte phenotype analyses.

Table 6.1. Dose optimization and PK/safety of targeted-NC compared to free-drug controls.

Weekno.	Expt. #ID	Group	Animal no.	SC route x 2 doses	Sampling Time (hours)[1]		
Stage 1: NP-LRA combinations (cLRA)			**Total=12**		**Blood**	**Gut biopsy**	**LN biopsy, fine needle**
1	6.2.1A	Free-JQ1	2	0.085 mg/kg	0, 0.5, 2, 4, 6,12, 24, 48, 72, 96, 168	4, 12, 24, 72	4, 12, 24
1	6.2.1B	Free-Ing3A	2	0.075 mg/kg	0, 0.5, 2, 4, 6,12, 24, 48, 72, 96, 168	4, 12, 24, 72	4, 12, 24
1	6.2.1C	Free-JQ1	2	0.85 mg/kg	0, 0.5, 2, 4, 6,12, 24, 48, 72, 96, 168	4, 12, 24, 72	4, 12, 24
1	6.2.1D	Free-Ing3A	2	0.75 mg/kg	0, 0.5, 2, 4, 6,12, 24, 48, 72, 96, 168	4, 12, 24, 72	4, 12, 24
1	6.2.1E	Vehicle control	2	25 mg/kg	0, 0.5, 2, 4, 6,12, 24, 48, 72, 96, 168	4, 12, 24, 72	4, 12, 24
1	6.2.1F	Vehicle control	2	50 mg/kg	0, 0.5, 2, 4, 6,12, 24, 48, 72, 96, 168	4, 12, 24, 72	4, 12, 24
2	**Washout/Rest**						
3	6.2.1F	NP-JQ1	3	5 mg/kg (0.085 mg/kg JQ1)	0, 0.5, 2, 4, 6,12, 24, 48, 72, 96, 168	4, 12, 24, 72	4, 12, 24
3	6.2.1G	NP-Ing3A	3	5 mg/kg (0.075 mg/kg Ing3A)	0, 0.5, 2, 4, 6,12, 24, 48, 72, 96, 168	4, 12, 24, 72	4, 12, 24
3	6.2.1H	NP-JQ1	3	50 mg/kg (0.85 mg/kg JQ1)	0, 0.5, 2 ,4, 6,12, 24, 48, 72, 96, 168	4, 12, 24, 72	4, 12, 24
3	6.2.1I	NP-Ing3A	3	50 mg/kg (0.75 mg/kg Ing3A)	0, 0.5, 2, 4, 6,12, 24, 48, 72, 96, 168	4, 12, 24, 72	4, 12, 24
4-6	**Washout/Rest**						

[1]Drug concentration: blood, tissue biopsies; Targeting: CD4+ intracellular drug concentration; Safety: blood chemistry, general health (body weight, temperature, food intake).

Criteria *for success:* Targeted NCs show selective drug delivery to CD4 T cells and have minimal toxicity compared to equivalently dosed unformulated (free) drug combinations.

6.2.2 *Demonstrate that CD4-targeted NC cure formulations reduce the latent pool in an NHP efficacy model.*

Rationale: We will reuse the 12 NHPs from our previous PK/safety study and conduct an efficacy study to measure reduction of the latent reservoir size in infected but virally-suppressed animals. NHPs will be infected with SHIV-C for 16 weeks and plasma viral load will be monitored to confirm steady-state viremia. Animals will then be treated with cART for 6 months, at which time

we expect no plasma viremia will be detected. The clearance rate of HIV DNA will be measured between months 4 and 6 of cART as most HIV DNA at this stage in human ART treatment is slowly decaying and likely to be of reservoir origin[10]. These clearance rates will be used as comparators to clearance rates on NC-formulated LRA in each NHP. In this sense, each NHP serves as its own control with respect to measuring change in reservoir size before and after cure treatment. Reduction in reservoir size will be measured by comparing the quantity of cell-associated HIV DNA and mRNA in blood and tissues (lymph node and gut). Cell-associated HIV DNA and mRNA will be measured by droplet digital PCR (ddPCR)[11-13].

Experimental plan: Each NHP will receive weekly LRA dosing for 2 months at doses which are optimized from Phase II (Table 6.2). NHPs will be divided evenly into free (n=6) and NC formulated dosing arms (n=6).

Table 6.2. HIV cure efficacy study.

(A) Establish latent reservoir in NHPs				**Animal No. = 12 NHPs (reuse)**	[1]Monitoring (cell-associated viral DNA: caDNA)	
					Blood	**Gut/LN biopsy**
1-4 (4 mo)	**Infection phase: SHIV1157ipd3N4 (SHIV C)**				Weekly: Plasma viremia	-
5-10 (6 mo)	**cART treatment phase: PMPA (20 mg/kg, SC), FTC (40 mg/kg, SC), Raltegravir (150 mg, oral bid)**				Weekly: Plasma viremia	Gut: week 32, 40 LN: week 40
(B) [2]cLRA Cure Treatment: free cLRA vs NP-cLRA					[1]Monitoring (cell-associated viral DNA: caDNA)	
Month no.	**Expt. #ID**	**Group**	**[3]Route/Dose**	**Animal no.**	**Blood**	**Gut/LN biopsy**
11-12 (2 mo)	6.2.2B1	**Free cLRA**	SC, once/weekly	6 NHPs (a,b,c,d,e,f)	Weekly	Gut: week 44, 48 LN: week 48
11-12 (2 mo)	6.2.2B2	**NP-cLRA**	SC, once/weekly	6 NHPs (g,h,i,j,k,l)	Weekly	Gut: week 44, 48 LN: week 48

[1]Droplet-digital PCR (ddPCR) (TILDA, Q-VOA as needed)
[2]Combination of LRA to be determined.
[3]Frequency of LRA dosing to be determined.

Criteria for success: Primary evidence of an enhanced therapeutic effect due to NC formulation will be an increase in the proportion of blips (plasma viral loads >40 SHIV RNA copies /ml) 3

days following the once-weekly NC-LRA doses relative to free-LRA. Plasma blips indicate viral reactivation and replication in a sufficient number of cells for detection in plasma and are therefore the most relevant currently available metric for measuring LRA potency.

6.3 Future directions

Cell or tissue-targeted drug delivery has emerged as a solution to major challenges associated with conventional drug delivery systems, such as poor therapeutic index and off-target side effects. This dissertation has focused on the targeted delivery of anti-HIV agents, such as ARVs and LRAs to the HIV reservoir cells and tissues using targeted NCs. However, there is much left to be explored for targeting T lymphocytes, or lymphatic tissues, in conditions such as HIV, cancer and autoimmune diseases.

Recognizing that HIV reservoirs are major barriers to HIV cure, several therapeutic strategies have focused on finding and diminishing latently infected cells. These cure strategies include early cART, "shock and kill", gene-editing approaches and immunotherapy[14]. Our NCs demonstrate the ability to load a variety of agents including small molecules (ARVs and LRAs), peptides, and macromolecules (mAbs), and to deliver these agents to the cell or tissue of interest. Therefore, future studies are being directed towards using NCs to deliver more agents that currently have limited access to the target cells and tissues or have issues associated with off-target effects, such as HIV therapeutic vaccines, broadly neutralizing antibodies, PD-1 blockades, and exogenous nucleic acids. It is also likely that a synergistic approach combining multiple strategies will be needed to establish an HIV cure. For example, in Chapter 5, we investigated the NCs for delivering LRAs to reverse HIV latency, but it may be also necessary to deliver agents such as broadly neutralizing mAbs or therapeutic vaccines to boost the killing of reactivated cells, and to deliver ARVs at the same time to control viral spreading. Thus, NCs are a promising tool that can be

applied to deliver multiple diverse agents simultaneously to achieve the eradication of HIV reservoirs.

There are still many obstacles that remain in the challenging process of translating the NCs from the laboratory to the clinic[15]. First, an investigational new drug (IND) application to the Food and Drug Administration (FDA) requires robust preclinical studies to demonstrate the safety and efficacy of the new drug. Once the IND application is approved, the therapeutic will be evaluated in a phase I clinical trial in humans to determine its safety and pharmacology profiles. A successful phase I trial will be followed by a phase II trial to examine the effectiveness of the drug as well as its toxicity and tolerability. If the drug demonstrates efficacy in phase II, a phase III clinical trial will be performed to compare with the "gold standard" treatment, although in some cases conditional FDA approval can be given based on phase II data or interim phase III data. Every step towards FDA approval requires careful and thorough design of the study and successful completion of each trial. There is a "short-cut" for agents that have already been approved in other applications; however, for nanomedicine, both the exact nanoparticle system and the drug being delivered would need to be previously approved. So far, there are more than 200 nanomedicine products that have been approved or are under clinical investigation[16], but none has been designed for HIV therapy. Interdisciplinary collaborations on nanocarrier development and evaluation, as well as appropriate *in vitro*, *ex vivo* and *in vivo* models are the best way to ensure rapid translation of nanomedicine for the cure of HIV.

6.4 References

1. Pavlick, A. C.; Wu, J.; Roberts, J.; Rosenthal, M. A.; Hamilton, A.; Wadler, S.; Farrell, K.; Carr, M.; Fry, D.; Murgo, A. J.; Oratz, R.; Hochster, H.; Liebes, L.; Muggia, F., Phase I Study of Bryostatin 1, a Protein Kinase C Modulator, Preceding Cisplatin in Patients with Refractory Non-hematologic Tumors. *Cancer chemotherapy and pharmacology* **2009,** *64* (4), 803-810.

2. Grant, S.; Roberts, J.; Poplin, E.; Tombes, M. B.; Kyle, B.; Welch, D.; Carr, M.; Bear, H. D., Phase Ib trial of bryostatin 1 in patients with refractory malignancies. *Clinical Cancer Research* **1998,** *4* (3), 611-618.
3. Elliott, J. H.; McMahon, J. H.; Chang, C. C.; Lee, S. A.; Hartogensis, W.; Bumpus, N.; Savic, R.; Roney, J.; Hoh, R.; Solomon, A., Short-term administration of disulfiram for reversal of latent HIV infection: a phase 2 dose-escalation study. *The Lancet HIV* **2015,** *2* (12), e520-e529.
4. Kinman, L.; Bui, T.; Larsen, K.; Tsai, C.-C.; Anderson, D.; Morton, W. R.; Hu, S.-L.; Ho, R. J., Optimization of lipid-indinavir complexes for localization in lymphoid tissues of HIV-infected macaques. *JAIDS Journal of Acquired Immune Deficiency Syndromes* **2006,** *42* (2), 155-161.
5. Del Prete, G. Q.; Oswald, K.; Lara, A.; Shoemaker, R.; Smedley, J.; Macallister, R.; Coalter, V.; Wiles, A.; Wiles, R.; Li, Y.; Fast, R.; Kiser, R.; Lu, B.; Zheng, J.; Alvord, W. G.; Trubey, C. M.; Piatak, M.; Deleage, C.; Keele, B. F.; Estes, J. D.; Hesselgesser, J.; Geleziunas, R.; Lifson, J. D., Elevated Plasma Viral Loads in Romidepsin-Treated Simian Immunodeficiency Virus-Infected Rhesus Macaques on Suppressive Combination Antiretroviral Therapy. *Antimicrobial Agents and Chemotherapy* **2016,** *60* (3), 1560-1572.
6. Zhang, X.; Zhang, R.; Zhao, H.; Cai, H.; Gush, K. A.; Kerr, R. G.; Pettit, G. R.; Kraft, A. S., Preclinical Pharmacology of the Natural Product Anticancer Agent Bryostatin 1, an Activator of Protein Kinase C. *Cancer Research* **1996,** *56* (4), 802-808.
7. Filippakopoulos, P.; Qi, J.; Picaud, S.; Shen, Y.; Smith, W. B.; Fedorov, O.; Morse, E. M.; Keates, T.; Hickman, T. T.; Felletar, I.; Philpott, M.; Munro, S.; McKeown, M. R.; Wang, Y.; Christie, A. L.; West, N.; Cameron, M. J.; Schwartz, B.; Heightman, T. D.; La Thangue, N.; French, C. A.; Wiest, O.; Kung, A. L.; Knapp, S.; Bradner, J. E., Selective inhibition of BET bromodomains. *Nature* **2010,** *468* (7327), 1067-1073.
8. Song, W.; Tang, Z.; Lei, T.; Wen, X.; Wang, G.; Zhang, D.; Deng, M.; Tang, X.; Chen, X., Stable loading and delivery of disulfiram with mPEG-PLGA/PCL mixed nanoparticles for tumor therapy. *Nanomedicine: Nanotechnology, Biology and Medicine* **2016,** *12* (2), 377-386.
9. Lin, F.; Wang, S.; Zhou, Y.; Wu, C.; Zou, H.; Geng, P.; Zhang, Q.; Zhang, X., Pharmacokinetic Interaction Study Combining Lapatinib with Vorinostat in Rats. *Pharmacology* **2015,** *95* (3-4), 160-165.
10. Besson, G. J.; Lalama, C. M.; Bosch, R. J.; Gandhi, R. T.; Bedison, M. A.; Aga, E.; Riddler, S. A.; McMahon, D. K.; Hong, F.; Mellors, J. W., HIV-1 DNA Decay Dynamics in Blood During More Than a Decade of Suppressive Antiretroviral Therapy. *Clinical Infectious Diseases* **2014,** *59* (9), 1312-1321.
11. Matrajt, L.; Younan, P. M.; Kiem, H.-P.; Schiffer, J. T., The Majority of CD4(+) T-Cell Depletion during Acute Simian-Human Immunodeficiency Virus SHIV89.6P Infection Occurs in Uninfected Cells. *Journal of Virology* **2014,** *88* (6), 3202-3212.
12. Strain, M. C.; Lada, S. M.; Luong, T.; Rought, S. E.; Gianella, S.; Terry, V. H.; Spina, C. A.; Woelk, C. H.; Richman, D. D., Highly Precise Measurement of HIV DNA by Droplet Digital PCR. *PLOS ONE* **2013,** *8* (4), e55943.
13. Sedlak, R. H.; Liang, S.; Niyonzima, N.; De Silva Feelixge, H. S.; Roychoudhury, P.; Greninger, A. L.; Weber, N. D.; Boissel, S.; Scharenberg, A. M.; Cheng, A.; Magaret, A.; Bumgarner, R.; Stone, D.; Jerome, K. R., Digital detection of endonuclease mediated gene disruption in the HIV provirus. *Scientific Reports* **2016,** *6*, 20064.
14. Cao, S.; Woodrow, K. A., Nanotechnology approaches to eradicating HIV reservoirs. *European Journal of Pharmaceutics and Biopharmaceutics* **2018**.

15. Min, Y.; Caster, J. M.; Eblan, M. J.; Wang, A. Z., Clinical Translation of Nanomedicine. *Chemical Reviews* **2015,** *115* (19), 11147-11190.
16. Etheridge, M. L.; Campbell, S. A.; Erdman, A. G.; Haynes, C. L.; Wolf, S. M.; McCullough, J., The big picture on nanomedicine: the state of investigational and approved nanomedicine products. *Nanomedicine : nanotechnology, biology, and medicine* **2013,** *9* (1), 1-14.

Appendix I: Nanoparticle-based ARV drug combinations for synergistic inhibition of cell-free and cell-cell HIV transmission

Adapted from: Jiang Y, Cao S, Bright DK, Bever AM, Blakney AK, Suydam IT, Woodrow KA. Nanoparticle-Based ARV Drug Combinations for Synergistic Inhibition of Cell-Free and Cell–Cell HIV Transmission. Molecular pharmaceutics. *Molecular pharmaceutics.* 2015;12(12):4363-74.

AI.1 Abstract

Nanocarrier-based drug delivery systems are playing an emerging role in *human immunodeficiency virus* HIV chemoprophylaxis and treatment for their ability to alter the pharmacokinetics and improve the therapeutic index of various antiretroviral (ARV) drug compounds used alone and in combination. Although several nanocarriers have been described for combination delivery of ARV drugs, measurement of drug-drug activities facilitated by the use of these nanotechnology platforms has not been fully investigated for topical prevention. Here, we show that physicochemically diverse ARV drugs can be encapsulated within polymeric nanoparticles to deliver multidrug combinations that provide potent HIV chemoprophylaxis in relevant models of cell-free, cell-cell and mucosal tissue infection. In contrast to existing approaches that co-formulate ARV drug combinations together in a single nanocarrier, we prepared single-drug loaded nanoparticles that were subsequently combined upon administration. ARV drug-nanoparticles were prepared using emulsion-solvent evaporation techniques to incorporate maraviroc (MVC), etravirine (ETR), and raltegravir (RAL) into poly(lactic-co-glycolic acid) (PLGA) nanoparticles. We compared the antiviral potency of the free and formulated drug combinations for all pairwise and triple drug combinations against both cell-free and cell-associated HIV-1 infection *in vitro*. The efficacy of ARV-drug nanoparticle combinations was also

assessed in a macaque cervicovaginal explant model using a chimeric *simian-human immunodeficiency virus* (SHIV) containing the reverse transcriptase (RT) of HIV-1. We observed that our ARV-NPs maintained potent HIV inhibition and were more effective when used in combinations. In particular, ARV-NP combinations involving ETR-NP exhibited significantly higher antiviral potency and dose-reduction against both cell free and cell-associated HIV-1 BaL infection *in vitro*. Furthermore, ARV-NP combinations that showed large dose-reduction were identified to be synergistic whereas the equivalent free drug combinations were observed to be strictly additive. Higher intracellular drug concentration was measured for cells dosed with the triple ARV-NP combination compared to the equivalent unformulated drugs. Finally, as a first step toward evaluating challenge studies in animal models, we also show that our ARV-NP combinations inhibit RT-SHIV virus propagation in macaque cervicovaginal tissue and block virus transmission by migratory cells emigrating from the tissue. Our results demonstrate that ARV-NP combinations control HIV-1 transmission more efficiently than free drug combinations. These studies provide a rationale to better understand the role of nanocarrier systems in facilitating multidrug effects in relevant cells and tissues associated with HIV infection.

AI.2 Introduction

The delivery of drug combinations is a paradigm for treatment of cancer and infectious diseases, including HIV/AIDS. Although the use of drug combinations is standard for the treatment of HIV, topical delivery of combination ARV drugs for pre-exposure prophylaxis has only been recently investigated. However, the physicochemical diversity of ARV drugs may prohibit their co-formulation in conventional vaginal dosage forms[1]. Clinical implementation of combination microbicides requires co-formulating drugs with different physicochemical properties and engineering the delivery of these drug combinations to have optimal inhibitory activity against

both cell-free and cell-cell virus transmission. Therefore, the development of drug delivery systems that formulate multiple ARVs into a single platform has the potential to enhance the efficacy of current ARV-based prevention strategies. The design of these systems should be flexible enough to harness drug combinations with demonstrated synergistic activity against various modes of HIV infection associated with sexual transmission[2-3].

A number of nanotechnology-based systems have been developed to deliver incompatible drug combinations for the purpose of enhancing potency, reducing toxicity and prolonging drug residence time to reduce dosing frequency[4-5]. For example, a lipid-drug nanoparticle formulation containing lopinavir/ritonavir and tenofovir produced intracellular drug concentrations in lymph nodes that were 50-fold higher than those obtained with the unformulated drugs[6]. In a related study, HIV-1 infected cells treated with biodegradable nanoparticles containing efavirenz combined with lopinavir/ritonavir produced significantly higher nuclear, cytoskeleton, and membrane antiretroviral drug levels compared to cells treated with unformulated drugs[7]. These examples demonstrate that nanocarriers can overcome challenges with co-formulating drugs. However, in these cases and others, drug combinations are typically co-formulated together, which makes it challenging to control the drug ratios and bioavailability needed to achieve optimal antiviral potency. For example, lipid-drug nanoparticles entrapped 10-fold higher amounts of lopinovir/ritonavir compared to tenofovir even though a different ratio was identified as having the greatest potency[6]. Formulating drugs separately and combining them upon administration is an alternative approach that is both modular and may provide better control over bioavailability of individual drugs.

Although several antiretroviral agents have been successfully incorporated in diverse nanocarriers[8-9], the use of these systems for identifying unique drug-drug activities for topical prevention has not been fully investigated. To fully understand the potential of these platforms to address critical gaps for HIV prevention, a comparison of safety and efficacy between the unformulated and nanoparticle formulated drug combinations is needed in relevant models of cell-free, cell-cell and mucosal tissue infection. In the current study, we measured the antiviral potency emerging from nanoparticle co-delivery of etravirine (ETR), maraviroc (MVC) and raltegravir (RAL) in these various models of HIV infection. ETR is a non-nucleoside reverse transcriptase inhibitor (NNRTI) with high intrinsic antiviral potency against wild-type as well as various resistant HIV variants[10]. ETR exhibits interesting nonlinear dose-effect responses at high concentrations, which may reflect a particular form of set-point intermolecular cooperativity controlling virus replication[11-12]. However, it is unclear what contribution these dose-effect properties contribute to its synergistic activity when combined with other ARV drugs. MVC is an entry inhibitor that blocks binding of HIV gp120 to CCR5, an essential co-receptor for HIV to enter host cells during infection[13-14]. RAL is an integrase inhibitor that inhibits insertion of the proviral DNA into host cell genome. Since integration is a critical step in the HIV life cycle, it represents one of the most promising targets for therapeutic intervention[15-17]. MVC and RAL have been highly effective in combination therapy although both have significantly lower intrinsic antiviral potency compared to ETR. Despite the fact that MVC acts on an extracellular receptor, we formulated all of the ARV drugs to compare with the delivery of unformulated compounds. Nanoparticle formulation of drugs with extracellular targets may also be advantageous for modulating bioavailability, targeting, and preventing drug degradation or metabolism. The purpose of this study was to demonstrate that physicochemically diverse APIs, which may be

difficult to co-formulate in conventional vaginal dosage forms, could be individually formulated in nanoparticles and co-delivered to study their combination effects.

Here, we present data on poly(lactic-*co*-glycolic acid) (PLGA) nanoparticles individually encapsulating ETR, MVC and RAL. All pairwise combinations of the unformulated and NP-formulated ARVs were tested for antiviral potency against both cell-free and cell-associated HIV-1 infection *in vitro*. Our results show that unformulated and ARV-loaded nanoparticles (ARV-NP) have similar inhibitory activity, but that the drug-loaded nanoparticle combinations exhibited greater antiviral potency against both cell-free and cell-associated HIV-1 BaL infection *in vitro*. We observed a significant dose-reduction of up to 10-fold when using ARV-NP combinations compared to the free drug combinations or individual ARV-NP. The dose-reduction appeared to arise from synergistic activity from drug combinations involving ARV-NP but not the unformulated drugs. ARV-NP combinations also resulted in higher intracellular drug concentrations in specific subcellular fractions. The antiviral potency of combined nanoparticle ARV drugs was also measured in a macaque cervicovaginal explant model against challenge with RT-SHIV. This is the first demonstration of dose-reduction and synergy using combination ARV-NPs of ETR, MVC and RAL across relevant models for mucosal HIV transmission. Our findings support a rationale and need for understanding drug-drug interactions mediated by polymeric nanomaterials, and may support a new paradigm for topical delivery of combination ARVs to enhance potency and long-acting efficacy of current microbicides.

AI.3 Materials and methods

Chemicals and ARV Drugs.

Reagents for nanoparticle fabrication and characterization were purchased from Sigma-Aldrich and Fisher Scientific unless otherwise specified. PLGA (50:50 ester terminated, MW 52-54 kDa, inherent viscosity 0.55-0.75dL/g) was purchased from Lactel. ETR, MVC and RAL were isolated from their pharmaceutical formulations using standard techniques consisting of (i) solubilization and extraction of ARVs from their commercial formulations, (ii) isolation of crude ARVs from excipients, and (iii) large-scale secondary purifications. Secondary purifications consisted of acid-base extractions, silica gel chromatography and recrystallization and were adapted from the published syntheses[18-20]. Purified ARVs were characterized by ^{1}H NMR (400 MHz), ^{13}C NMR (100 MHz), LC-MS and UV-HPLC (Supporting information Figures AI.S1-5). The spectroscopic and spectrometric data for ETR and MVC were identical to those obtained with standards provided by the NIH AIDS Research and Reference Reagent Program. Both RAL and MVC were isolated as the neutral compounds, which are highly soluble in dichloromethane. Because the neutral form of RAL was unavailable through the NIH AIDS Research and Reference Reagent Program the spectroscopic and spectrometric data for RAL were compared to literature values and were identical to those reported by Summa et. al[20]. All purified ARVs produced inhibition curves identical to those obtained with reagent standards using the cell free HIV infection assay described below.

Fabrication of ARV Loaded Nanoparticles.

ARV loaded nanoparticles and blank nanoparticles (vehicle control) were formulated individually such that only a single drug was encapsulated in an individual nanoparticle formulation.

Nanoparticles were fabricated using a single emulsion/solvent evaporation method. A theoretical drug loading of 10wt% ETR, MVC or RAL (w/w, weight of ARV relative to weight of PLGA polymer) was combined with PLGA (5% w/v) in a volatile organic solvent to generate the "oil"-phase. MVC and RAL were dissolved together with PLGA in DCM whereas ETR was dissolved together with PLGA in ethyl acetate[21].This mixture was added drop-wise into 2.5% w/v aqueous polyvinyl alcohol (PVA) solution while vortexing. The solution was emulsified using a probe sonicator (500W, Ultrasonic Processor GEX 500) with a 3 mm diameter microtip probe (Sonics & Materials) for intervals of 20 second at 50% amplitude for three rounds with vortexing between intervals. The sonicated emulsion was transferred to a continuously stirred aqueous solution of PVA (0.25% w/v) for 3-5 h to evaporate all residual organic solvent. Nanoparticles were washed with Milli-Q water three times by centrifugation at 14,000 rpm for 10 min at 4^0C in order to remove any residual PVA surfactant and unencapsulated drug. Following these wash steps the nanoparticles were suspended in water, frozen at -80^0C and lyophilized (24 h, 0.133 mbarr at -87^0C). Lyophilized nanoparticles were stored at -80°C until use.

Characterizations of ARV Loaded Nanoparticles (ARV-NPs)

ARV-NP size, polydispersity (PDI) and zeta (ζ)-potential were measured by dynamic light scattering (DLS) in Milli-Q water using a Zetasizer Nano ZS90 (Malvern Instruments). HPLC was used to measure drug loading, which is defined as the measured mass of ARV drug per mass of PLGA-NP, and encapsulation efficiency, which is defined as the ratio of the drug loaded to the total drug used for fabricating the nanoparticles (see equations, Table AI.1). A direct measure of drug loading was determined by dissolving a known mass of lyophilized ARV drug-NP in DMSO and analyzing the samples using an integrated reversed-phase high-pressure liquid chromatography (HPLC) system. In brief, separations were made on a C18 column (5µm, 250 x

4.6 mm, Phenomenex) at either 25^{0}C (MVC) or 30^{0}C (RAL and ETR) and based on methods previously established for detecting ETR, RAL and MVC[22-23]. Detections were performed at wavelengths of 300nm (RAL), 193nm (MVC), and 234nm (ETR). Sample retention and run-times for RAL, MVC and ETR were: 4/10 min, 9/15 min, and 5/22 min, respectively. Long-term storage stability of blank and ARV-NPs was assessed after lyophilization in the presence or absence of trehalose (1:1 by mass). Stability was monitored by measuring the ARV-NP size, PDI and ζ-potential at day 0, 1, 3, 5, 7, 14 and 21 during incubation at 25^{0}C, 39^{0}C and 60^{0}C. Transmission electron microscopy (TEM) images were obtained on a FEI Tecnai F20 transmission electron microscope operating at 200 kV at Molecular Analysis *Facility* (MAF), University of Washington.

In vitro Drug Release from ARV-NP Formulations.

ARV drug release kinetics from our PLGA nanoparticle formulations were measured under sink conditions. Sink conditions are defined as concentrations ≥10-fold the drug solubility, which was achieved for MVC and RAL by using PBS and for ETR by using 2 wt% solutol (Sigma Aldrich, Kolliphor HS 15, Cat#: 42966-1KG) in PBS. Lyopholized ARV-NPs were individually re-suspended in their respective release media at sink conditions, aliquoted into individual tubes for each time point to quantify drug release, and incubated at room temperature. At various times up to 215 h, the aliquots were centrifuged to remove nanoparticles and the supernatant was analyzed by HPLC to quantify released drug. Percent release was measured in triplicate from three independent samples and was based on loading data obtained for the identical nanoparticle formulations.

Cell Lines and Viruses.

TZM-bL (JC53-BL), PM-1 and CEMx174 cell lines and HIV-1 BaL virus were obtained from the NIH AIDS Research & Reference Reagent Program. TZM-bL cells are a genetically engineered HeLa cell clone that expresses CD4, CXCR4, and CCR5 and contains Tat-responsive reporter genes for firefly luciferase (Luc) and *Escherichia coli* β-galactosidase under regulatory control of an HIV-1 long terminal repeat, which permits sensitive and accurate measurements of HIV infection. TZM-bL cells were maintained in Dulbecco's Modified Eagle's Medium (DMEM) supplemented with 10% heat-inactivated fetal bovine serum (FBS), 100 U/mL penicillin, 100 mg/mL streptomycin and 2mM L-glutamine and 25mM HEPES. PM-1 is a human T cell line while CEMx174 cell line is a human T/B-lymphocyte hybrid. Both cell lines were grown in RPMI1640 medium supplemented as above. All cell lines were incubated at 37^0C in a humidified 5% CO_2 air environment.

HIV-1 BaL is a CCR5 tropic virus, which uses CCR5 as a co-receptor to enter target cells and is dominant in HIV mucosal transmission[24]. HIV-1 BaL stock was propagated in PM-1 cells and titrated in both PM-1 and TZM-bL cell lines. RT-SHIV, a chimeric SHIV where the reverse transcriptase (RT) of the backbone SIV_{mac239} is replaced with that of HIV-1HXB2 was originally provided by L. Alexander at Yale University and was propagated in CEMx174 cells.

Evaluation of ARV Particle Drugs Against Cell Free HIV Infection.

Antiviral activity was measured as a reduction in luciferase reporter gene expression after infection of TZM-bL cells with HIV-1 BaL. All single ARV drugs and ARV-NPs were dosed based on molar concentrations of the drug. Drug combinations were dosed to achieve a total drug concentration that combined the drugs at an equimolar ratio. Briefly, TZM-bL cells were seeded at a concentration of $1x10^4$ per well in 96-well microplates (~30,000 cells/cm^2). After 24h culture,

TZM-bL cells were incubated with various concentrations of either free drugs or NP-formulated drugs at 37^0C for 1h prior to virus exposure. At this time, cell free HIV-1 BaL at 200 TCID50 (50% tissue culture infective dose) was added to the cultures and incubated for an additional 48 h. Untreated cells (100% infected) were used as a control. Antiviral activity was measured by luciferase expression using the Promega™ Luciferase Assay System. Antiviral activity was plotted as a percent inhibition relative to virus control (no drug treatment, 100% infected) and cell control (no virus exposure, 0% infected) Nonlinear regression was used to fit the data to an inhibition model with a constant Hill coefficient to determine the slope parameter and IC50 value, which is the sample concentration giving 50% of relative luminescence units (RLUs) compared to the virus control after subtraction of background RLUs.

For drug combinations that showed significant dose-reduction, we used the model of Bliss independence with variable Hill coefficients to quantitatively analyze the combination effect as synergistic, additive or antagonistic. For this analysis, dose-response data for the combination and single ARV assays were plotted as median-effect plots with the response transformed to $\log(f_a/f_u)$, where f_a is the fraction of infection events affected by drug and f_u is the fraction of infection events unaffected by drug ($f_u = 1 - f_a$). To calculate the Bliss independence prediction for combinations of ARVs exhibiting variable Hill slopes we followed the method of Jilek et al[11], restricting the analysis to combination data within the dynamic range of our assay ($-2 < \log(f_a/f_u) < 3$). Bliss independence predictions were calculated using Eq. 1, where D is the concentration of each drug present in the combination and m is the slope of the median-effect plot for each drug at a given concentration (local Hill coefficient). Variable Hill coefficients and IC_{50} values were determined via linear regression centered at the concentration of interest. The magnitude of the combined effect was quantified by measuring the difference between the

observed and predicted fraction affected following the approach of Laird et al[25]. Synergy, additivity and antagonism as defined by the Bliss models occur for values of $0<\Delta f_{axy}\leq 1$, $\Delta f_{axy}=0$, and $-1\leq\Delta f_{axy}<0$, respectively (see Figure AI.3e).

$$f_{u1+2} = \frac{1}{1+\left(\frac{D_1}{IC_{50_1}}\right)^{m_1}} \times \frac{1}{1+\left(\frac{D_2}{IC_{50_2}}\right)^{m_2}} \quad (0.1)$$

Cell-to-Cell Transmission Assay.

For cell-cell transmission assays, TZM-bL cells were seeded at a concentration of $1x10^4$ per well in 96-well microplates (~30,000 cells/cm^2). The following day, TZM-bL cells were incubated with various concentrations of either free drugs or ARV-loaded nanoparticles in combination at equimolar ratio at 37^0C for 1h prior to exposure to chronically infected PM-1 cells. Infected PM-1 cells were produced by infecting with HIV-1 BaL and culturing these cells for three days. These cells were washed twice with phosphate-buffered saline (PBS) to remove cell free virus before they were added to TZM-bL cell culture ($5x10^3$ cells/well). After 1h of incubation, PM-1 cells were removed by washing wells twice with PBS. TZM-bL cells were then incubated in the presence of drug for an additional 48h. Cells were lysed and the luciferase activity of the cell lysate was measured using the luciferase assay system (Promega). Antiviral activity was expressed as described above.

Culture of Macaque Cervicovaginal Tissue Explants and RT-SHIV Infection.

Macaque reproductive tracts were purchased from the tissue distribution program at Washington National Primate Research Center (WaNPRC), University of Washington. All macaques were confirmed to be serologically negative for simian type D retrovirus, SIV, and simian T-cell lymphotropic virus (STLV) prior to sample collection. Cervical and vaginal explants, comprising

both epithelial and stromal tissue, were obtained using a 3-mm-diameter biopsy punch(Miltex Medical Instruments, Cat# 33-32). Intact explants (3mm) were pre-treated with combined ARV-NPs containing ETR, MVC and RAL with equimolar ratios of the three drugs (EMR-NP, 1:1:1 molar ratio) at 37^0C for 1h prior to exposure to RT-SHIV (10^5 TCID50) for 2 h at 37^0C. Explants were then washed three times with PBS and were cultured individually in 300µl of complete RPMI1640 in a 96-well plate in a humidified atmosphere containing 5% CO_2. Following overnight culture, explants were transferred to fresh culture plates and cultured for an additional 14 days, with two-thirds of the medium exchanged every 2 to 3 days. Cells that spontaneously migrated out of the tissue explants during overnight culture were washed twice with PBS, transferred to fresh plates, and co-cultured with $5x10^3$ CEMx174 cells/well to assess the blockade of virus transfer by migrating cells. Co-cultures were examined daily for cytopathic effect (CPE). RT-SHIV infection was determined by the measurement of SIV p27 in culture supernatants by ELISA (ZeptoMetrix Corporation RETROtek SIV p27 Antigen ELISA Kit).

Quantification of ARV Drug Uptake and Subcellular Distribtuion.

Intracellular uptake was investigated in TZM-bL cells for the triple ARV-NP combination and the equivalent free drug combination. Cells were cultured at 37°C, 5% CO_2 for 48 h in the presence of 1 µM total drug at equimolar ratio for each drug. After removing culture medium, cells were detached with 1 ml ice-cold PBS and collected by centrifuged at 500×g for 10 min at 4°C. Cells were processed using used the Subcellular Protein Fraction Kit (Thermo Scientific, Cat#78840) following the manufacture's guidelines to isolate cytoplasmic, membrane and nuclear/chromatin-bound and cytoskeletal subcellular fractions.

Drug concentration in the different subcellular compartments was analyzed by LC-MS/MS at the University of Washington Mass Spectrometry Center. A Chromolith Performance RP-18e 100-3mm column was used for LC analysis, with a gradient method of 10 mM formic acid in H_2O and 10 mM formic acid in 80:20 ACN:MeOH. Etravirine-$^{13}C_6$, maraviroc-d_6 and raltegravir-d_6 (Alsachim, Strasbourg, France) were used as internal standards and combined prior to spiking into samples. All subcellular fraction samples were aliquoted at a volume of 50 µL and spiked with 5 µL of a 10 ng mL^{-1} solution of the combined internal standard mix (50 pg per sample). A standard curve ranging from 0.01-100 ng mL^{-1} was prepared in MeOH and run before and after unknown sample sets. Samples were analyzed using a single LC-MS/MS method for detection of ETR, MVC and RAL on a Waters Xevo TQ-S couple with an I-Class Acquity UPLC (Waters Corporation, Milford, MA, USA). All analytes were acquired in electrospray positive mode and the drugs and internal standards were analyzed at the following m/z transitions: 435.22 to 162.98 (ETR), 441.20 to 162.98 (ETR-$^{13}C_6$), 445.35 to 109.10 (RAL), 451.35 to 115.10 (RAL-d_6), 514.48 to 290.22 (MVC), and 520.48 to 280.22 (MVC-d_6). All species were analyzed at a cone voltage of 50 kV and collision energy of 28 (ETR and MVC) or 30V (RAL) (full list of parameters can be found at Blakney et al.- publication in process).

Cytotoxicity Assay.

TZM-bL cells were cultured in 96-well plates in the absence or presence of various concentrations of ARV-loaded nanoparticles. After three days in culture, cell viability was assessed using CellTiter-Blue® Cell Viability Assay (Promega) following the *manufacturer's recommended* procedures. Cells were incubated for 4h with 20µl/well of CellTiter-Blue®Reagent and fluorescence was recorded at 560/590nm.

AI.4 Results

PLGA Nanoparticles Successfully Formulate Mechanistically and Physicochemically Distinct ARV Drugs and Are Non-cytotoxic.

ARV-loaded nanoparticles were prepared using emulsion-solvent evaporation techniques to incorporate ETR, RAL and MVC into separate PLGA nanoparticles. Irrespective of the specific drugs, all of our ARV-NPs showed an average diameter of ~340 nm, PDI of ~0.2 and an average negative ζ-potential of -23mV (Table AI.1). Size estimates obtained from *TEM images* are consistent with the size of the ARV-NPs reported by DLS measurements (Supporting Information, Figure AI.S6). Nanoparticles of this size range (200-500 nm) have been reported by others to transport through mucus and penetrate the vaginal epithelium after topical delivery to the mucosa [26-28]. We used a nominal initial drug loading of 10 wt%, which resulted in formulated ARV-NPs with measured drug loadings of 8.1± 0.8 wt% , 2.4±0.2 wt% and 1.2± 0.1 wt% for ETR-NP, RAL-NP, and MVC-NP, respectively (Table AI.1). These respective drug loadings translated to encapsulation efficiencies of 91%, 17% and 12%. As expected, encapsulation efficiency and drug loading were much greater for the hydrophobic ETR compared to the ionizable and more water-soluble RAL and MVC.

We observed that our ARV-NPs were stable during storage at room temperature for 21 d and showed minimal change to their originally measured value of size, PDI and ζ-potential (Supporting Information, Figure AI.S7). However, addition of trehalose during lyophilization was required to maintain the stability of PLGA NPs at elevated temperatures of 39^0C and 60^0C (Supporting Information, Figure AI.S8). We also measured ARV drug release kinetics for each of the NP-formulated drugs under sink conditions *in vitro*. We observe that ETR, RAL and MVC all exhibit

a burst-phase of release that is likely due to surface associated drug (Supporting Information, Figure AI.S9). In particular, MVC, which acts extracellularly with the host CCR5 cell-surface receptor, shows complete drug release in <15 min under sink conditions. In contrast, ETR and RAL exhibit a burst phase of release within the first 15-60 min followed by a slower pseudo-linear release up to 150 h (~6 d) of the remaining 20% and 40% of the entrapped drugs, respectively. In summary, we have successfully fabricated three physicochemically and mechanistically distinct ARV drugs into PLGA nanoparticles that allow their modular combination.

Table AI.1. Properties of ARV drug-loaded PLGA nanoparticles

[1]Measured Properties	**Etravirine** NNRTI	**Raltegravir** Integrase	**Maraviroc** CCR5 inhibitor
Molecular weight	435.3	444.5	513.7
Size (diameter, nm)	371.4 ± 71.6	311.2 ± 9.3	331.6 ± 27.4
Polydispersity Index	0.36 ± 0.11	0.09 ± 0.03	0.2 ± 0.1
Zeta-potential (mV, pH 6)	-21.0 ± 1.8	-22.5 ± 3.0	-26.5 ± 2.5
[2]Loading (wt%)	8.1 ± 0.8	2.4 ± 0.2	1.2 ± 0.1
[3]Encapsulation Efficiency (%)	91.0 ± 9.9	16.8 ± 2.6	12.0 ± 0.6
[4]Polymer Yield (%)	66.7 ± 9.3	64.2 ± 7.8	91.7 ± 2.9
[5]IC50 (nM) [95% CI]	1.4 [1.2, 1.6]	6.9 [5.2, 9.2]	17.4 [9.2, 32.7]

1. Measured properties are reported as the mean ± s.d. from n≥3 independent nanoparticle fabrications.

2. $\text{Drug loading \%} = \frac{mass\ of\ drug\ in\ nanoparticles}{mass\ of\ nanoparticles\ recovered} * 100$

3. $\text{Encapsulation efficiency \%} = \frac{mass\ of\ drug\ in\ nanoparticles}{mass\ of\ drug\ used\ in\ formulation} * 100$

4. $\text{Polymer Yield \%} = \frac{mass\ of\ nanoparticles\ recovered}{mass\ of\ all\ excipient\ used\ in\ formulation} * 100$

5. Antiviral activity is reported for HIV-1 BaL infection of TZM-bL cells. The value represents the mean of triplicate measurements obtained from ≥3 independent nanoparticle fabrications for each ARV drug.

The ARV-NPs were tested for cytoxicity in the cell line used to measure HIV infection. No significant reduction in cell viability was observed in TZM-bL cells treated with ARV-NPs compared to blank NPs or untreated control groups (Supporting Information, Figure AI.S10). The data indicates that blank PLGA nanoparticles cause no reduction of cell viability at concentrations below 2.5mg/mL. At this maximum concentration of ARV-NPs, the corresponding drug concentrations would be $6.6x10^5$nM ETR, $1.2x10^5$ nM RAL and $5.8x10^4$ nM MVC. All of the antiviral assays involving ARV-NPs in this study were conducted at concentrations well below these limits. For this reason cytotoxicity from the nanoparticles themselves is unlikely to confound the antiviral activity results.

ARV-NP Combinations that Include ETR Exhibit Significant Antiviral Potency and Dose-reduction Against HIV-1 BaL Infection in vitro.

The ARV drug loading for all of our ARV-NP formulations were sufficient to measure antiviral potency against HIV-1 BaL infection *in vitro*. We dosed the ARV-NPs based on their total drug loading and observed a dose-dependent inhibition of TZM-bL infection by HIV-1 BaL (Figure AI.1). The measured IC50 of the individual ARV-NPs was in the low nanomolar range and similar to the anti-HIV activity measured for the equivalent unformulated drugs. We also performed the antiviral assay with blank NPs (vehicle control) dosed at the same polymer concentrations as the ARV-NPs to control for the possibility that NP sedimentation resulting from aggregation could cause non-specific antiviral activity from steric hindrance (data not shown). No HIV inhibition was observed, which indicates that PLGA NPs alone do not contribute to any measurable antiviral efficacy seen with the ARV-NPs. Based on these viral inhibition results, the individual ARV-NPs were evaluated in all three pairwise combinations using the same assay for HIV-1 BaL virus transmission. We first measured the antiviral potency of different molar ratios of the three ARV

drugs and identified that equimolar concentrations of ETR, RAL and MVC resulted in the greatest antiviral potency (Supporting Information, Table AI.S1). Therefore, we used this ratio to compare the antiviral potency of the free and ARV-NP drug combinations. We observed that combinations involving ETR-NP exhibited significant dose-reduction compared to the equivalent free drug combinations (Figure AI.2a,b) and compared to the antiviral potency of the single ARV drug-NP (Figure AI.1). In contrast, drug combinations of free and NP-formulated MVC and RAL showed similar IC50s and no dose-reduction compared to the potency of only the single ARV drugs (Figure AI.2c). For example, ETR-NP combined with MVC-NP or RAL-NP showed an approximately 10-fold dose reduction in the IC50 compared to the same combinations using unformulated drugs (Figure AI.2a,b). The drug combinations that included ETR-NPs also showed a 2-40 fold dose-reduction compared to the IC50 measured for the single ARV drug-NP (Figure AI.1 and Table AI.1). The unformulated drug combinations of free ETR combined with either free RAL or MVC did not show a dose-reduction relative to the most active component present. Instead, these free drug combinations had a measured IC50 that was of median value between the IC50 for the single ARV drugs. The triple drug combination of either the free or NP-formulated drugs also did not show an enhanced potency compared to the two-drug combinations (Figure AI.2d). In summary, we observed that ARV-NP combinations including ETR-NP show significant dose reductions relative to all unformulated drug combinations tested against HIV infection *in vitro.*

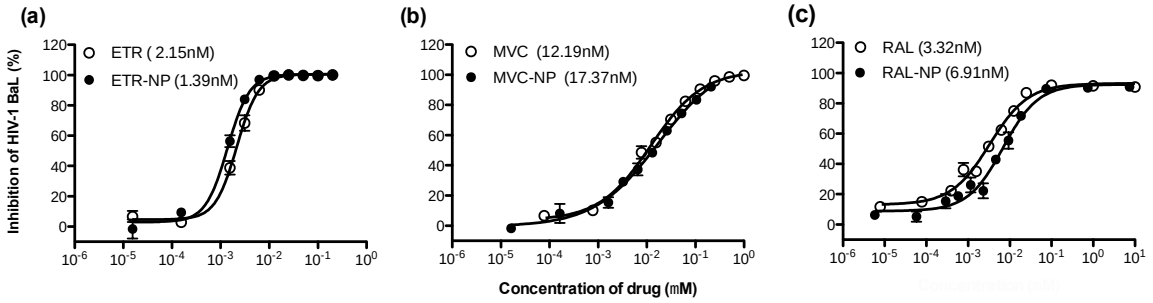

Figure AI.1. Antiviral activity of single ARV and ARV-NP drug against cell free HIV-1 BaL in TZM-bL cells. TZM-bL cells were pretreated with ARV and ARV-NP drugs individually for 1 h prior to HIV-1 BaL exposure (200TCID50). Luciferase activity was measured 48 h after virus infection. Dose-response curves show the mean and standard deviation of the percent inhibition of cell-free HIV-1 BaL virus for free drug (o) and nanoparticle drug (□) of (a) ETR-NP, (b) MVC-NP, and (c) RAL-NP. The numbers in brackets indicate the 50% inhibitory concentration (IC50). Data was analyzed by GraphPad Prism 5.0 and presented as the means ± standard deviations from three separate experiments; each condition was tested in duplicate.

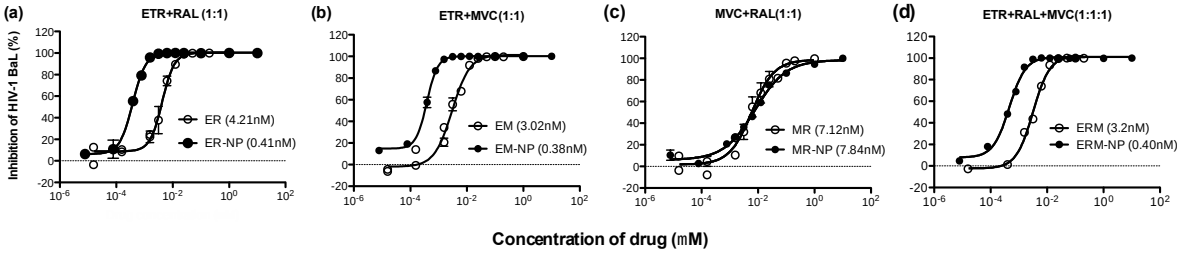

Figure AI.2. Antiviral ARV-NP combinations show potent antiviral activity and dose-reduction compared to the analogous free-drug combinations against HIV-1 BaL transmission. TZM-bL cells were pretreated with free ARV drug and ARV-NP drug combinations at equimolar ratio for 1h prior to HIV-1 BaL exposure (200TCID50). Luciferase activity was measured 48 h after virus infection. Dose-response curves show the mean and standard deviation of the percent inhibition of cell-free HIV-1 BaL virus for free drug (o) and nanoparticle drug (□) combinations of (a) ETR-NP and MVC-NP, (b) ETR-NP and RAL-NP, (c) MVC-NP and RAL-NP, and (d) ETR-NP, RAL-NP and MVC-NP. The numbers in brackets indicate the 50% inhibitory concentration (IC50). Data was analyzed by GraphPad Prism 5.0. Graphs show values of the means ± standard deviations from three separate experiments.

For the ARV-NP combinations that showed significant dose-reduction compared to the equivalent unformulated drug combinations, we used the model of Bliss independence to identify if the observed combination effects were synergistic. The Bliss independence model can be used to

predict the additive effect arising from combinations of multiple drugs that have independent mechanisms of action, as in the case with ETR, MVC and RAL. We observed steep upward inflections in the median-effect plots of ETR (free and nanoparticle loaded), which is consistent with previous findings[11] (Figure AI.3). Because we combined ETR in an equimolar ratio with MVC or RAL (1:1), the Bliss independence prediction is expected to be dominated by the response observed for ETR alone due to the large Hill coefficients observed for ETR at high concentration[11]. Drug combinations involving ETR-NP with MVC-NP or RAL-NP resulted in higher antiviral activity than would be predicted by the Bliss model if the combination effect were strictly additive (Figure AI.3b,d). The combination effect was dose-dependent such that the greatest deviation from the Bliss prediction was observed at concentrations much higher than the IC50 (Figure AI.3e). In contrast to the two drug combinations that included ETR-NP, the antiviral effect measured for the equivalent unformulated drug combinations was within error of the Bliss model for additivity. Therefore, the combined effects from these ARV-NP combinations but not the free drug combinations appear to be acting synergistically.

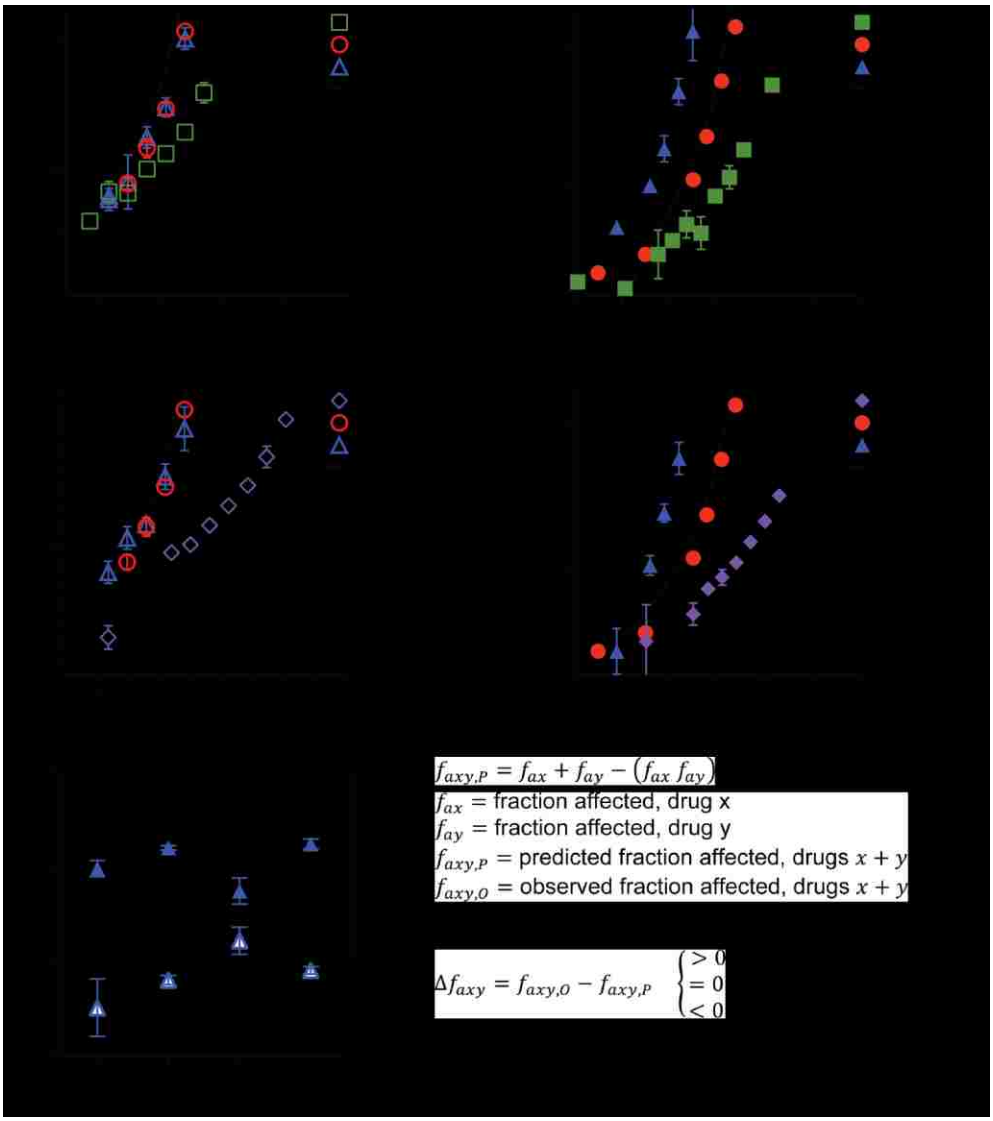

Figure AI.3. Median-effect plots for ARV drug combinations compared to the Bliss independence prediction. Median-effect plots for (a) RAL/ETR, (b) RAL-NP/ETR-NP, (c) MVC/ETR and (d) MVC-NP/ETR-NP. The combination and single ARV concentrations have been adjusted to a log dilution scale to allow a comparison to the activity observed for single ARVs at the concentrations present in the combination experiment. The activity predicted by the Bliss independence model is shown (dashed line). This prediction incorporates the variable Hill slopes observed in the single ARV median-effect plots. The Bliss independence prediction tracks closely with the effect observed with ETR alone in all combination experiments because the median-effect plot for ETR exhibits large Hill slopes at high concentrations. Combination experiments using ARV loaded nanoparticles containing ETR exhibit drug synergy with the observed response exceeding that predicted by the Bliss independence model. Free drugs and their combinations (a, c) are shown as open shapes whereas ARV-NP and their combinations (b, d) are shown as filled shapes. The Bliss prediction (dashed line) is compared to the observed data for the different combinations (diamonds). (e) Data are plotted as the difference between the observed fraction affected ($f_{axy,o}$) and predicted fraction affected ($f_{axy,p}$) at concentration values

near the IC50 and IC90 for the ARV-NP combinations (closed triangle) or free drug combinations (open triangle). Drug combinations that exhibit synergistic activity as defined by the Bliss model have values of $0<\Delta f_{axy} \leq 1$.

ARV-NP Combinations Show Enhanced Cell-associated Drug Content.

We used LC-MS/MS to measure the concentration of ETR, RAL and MVC in subcellular fractions after dosing to TZM-bL cells. Since ETR-NP showed a dose-reduction with both MVC- and RAL-NP, we hypothesized that the triple ARV-NP combination would allow us to capture the intracellular drug concentration of both binary combinations in a single study. TZM-bL cells were cultured in similar conditions used in the antiviral assay and the cells were dosed with 1 μM of the triple ARV drug combination either as NP-formulated or free drug combinations. We selected a dose where the difference between the triple ARV-NP and free drug combinations was the largest on the median-effect plot but still within the dynamic range of our antiviral assay. A commercial kit with specific extraction buffers was used to isolate cytoplasmic, membrane and nuclear/chromatin-bound and cytoskeletal cell fractions. LC-MS/MS was used to quantify the concentration of each drug in these separate fractions. In general, we observed higher cell-associated drug concentration for ETR, RAL and MVC when dosed as the triple drug ARV-NP formulations compared to the equivalent free drug combination (Figure AI.4). The triple ARV-NP combinations resulted in the highest measured cell-associated total drug content for ETR when dosed as a NP combination (~350 ng per 10^6 cells) compared to the free drug combination (~94 ng per 10^6 cells), of which there was almost a 10-fold difference in the measured cytoplasmic drug content (ETR-NP=20 ng versus ETR-free=2.8 ng per 10^6 cells). The data indicate that a greater fraction of RAL partitioned to the cytoplasm (80%) compared to the membrane (10%), whereas MVC showed almost equivalent partitioning into these same cellular fractions (44% versus 42%, respectively). Despite being dosed at equimolar ratios in both the triple ARV-NP combinations

and free drug, we measured ~100-fold less MVC and RAL associated with the cells compared to ETR. This may be a result of variable solubility of the drugs within the different buffers extraction leading to different extraction efficiencies, which were not accounted for in our measurements. In addition, for the cells treated with ARV-NPs, we are unable to distinguish between released drug and drug that is still entrapped in the nanoparticles. These results suggest that ARV-NPs achieve better intracellular uptake over free drug combinations.

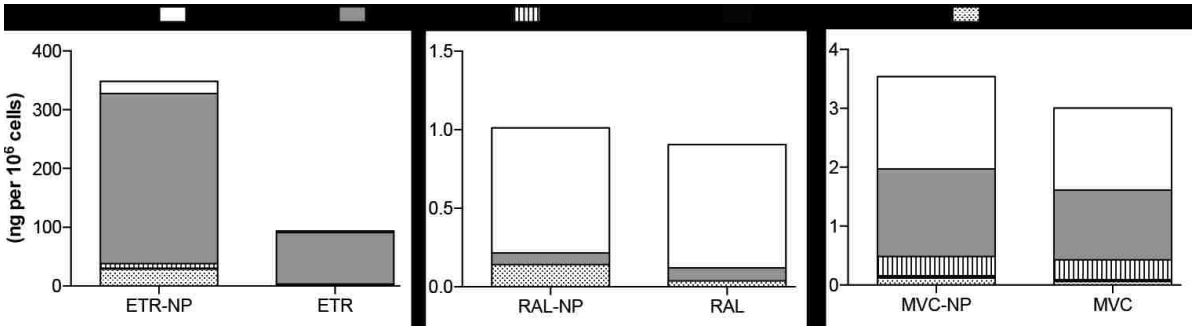

Figure AI.4. Antiviral Subcellular distribution of ARV drug combinations delivered from nanoparticles. TZM-bL cells were dosed with the triple drug combinations formulated in NPs or delivered as the free-drugs. The amount of cell-associated ETR, RAL and MVC content (ng per 10^6 cell) resulting from the drug combinations were measured in subcellular fractions collected for the cytoplasm, membrane, nuclear/chromatin-bound and cystokeleton. Data are plotted for the individual ARV drugs and show the cumulative drug amount that is cell-associated from the different subcellular fractions.

ARV-NP Combinations Are Effective Against Cell-associated HIV-1 Infection in vitro.

We tested the efficacy of our ARV drug-loaded nanoparticles to inhibit cell-to-cell HIV-1 transmission between HIV-1 BaL infected PM-1 cells and TZM-bL cells. The target TZM-bL cells were pre-treated with all three pairwise combinations of unformulated and NP-formulated ETR, RAL and MVC delivered at equimolar ratios and then exposed to infected PM-1 cells but not free virus. We observed that higher ARV drug dosing is required to prevent the direct infection of

TZM-bL cells by PM-1 cells for all combinations tested (Figure AI.5). This observation is consistent with previous findings that show cell-cell virus transmission is much more efficient than infection from cell free virus[3, 29]. Drug combinations that included ETR (Figure AI.5a,b) resulted in at least a 10-fold higher inhibition of cell-cell virus transmission compared to two drug combinations of MVC and RAL (Figure AI.5c). ETR-NP combined with MVC-NP or RAL-NP also showed an approximately three-fold higher potency compared to the unformulated combinations of the same ARV drugs (Figure AI.5a,b). In contrast, the free combinations of MVC and RAL showed an approximately two-fold higher potency compared to the equivalent ARV-NP combinations, a decrease in potency not observed in the cell-free assay (Figure AI.2c). In summary, combinations of ARV-NPs that include ETR show improved inhibition of cell-cell transmission compared to the equivalent free drug combinations.

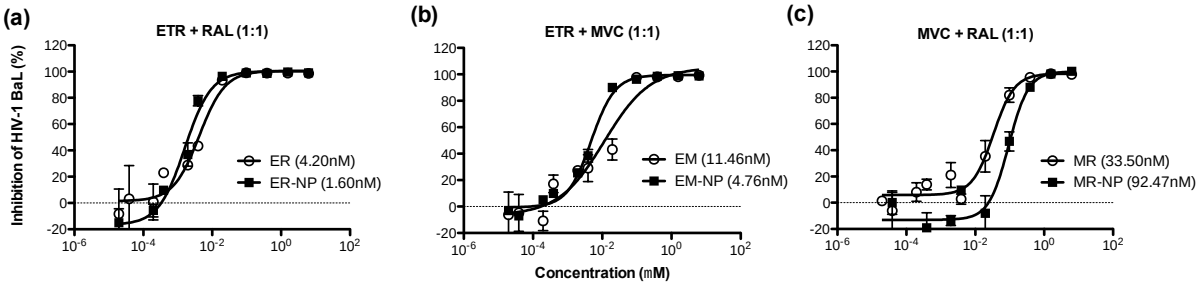

Figure AI.5. ARV-NP combinations show potent antiviral activity and dose-reduction compared to the analogous free-drug combinations against cell-cell HIV-1 BaL transmission. TZM-bL cells were exposed to different free ARV drug and ARV-NP drug combinations in the presence of PM-1 cells infected with HIV-1BaL. Dots indicate the drug concentration giving 50% inhibition(IC50) of cell-cell HIV-1 BaL transmission from infected PM-1 cells to TZM-bL report cells for free drug (o) and nanoparticle drug (□) combinations of (a) ETR-NP and MVC-NP, (b) ETR-NP and RAL-NP, and (c) MVC-NP and RAL-NP. Data was analyzed by GraphPad Prism 5.0 and represent the mean±SD of three independent experiments; each condition was tested in duplicate.

ARV-NP Combination Inhibits RT-SHIV Transmission in Nonhuman Cervicovaginal Explants and Blocks Virus Propagation by Migratory Cells.

Motivated by the antiviral activity of ARV-NP in our cell culture infection assays, we investigated a triple combination of ARV-NP to prevent RT-SHIV infection of nonhuman primate cervicovaginal explant tissue. RT-SHIV virus replication in infected tissue was measured to evaluate the pre-exposure prophylaxis of EMR-NP. The EMR-NP combinations were dosed at 5 μM in culture with the explant biopsy (~25 mg), and the biopsies were challenged with 10^5 TCID50 RT-SHIV. The tissue explants were cultured for 9 days and culture supernatant was removed every 3 days to monitor for SIV p27 concentration by ELISA. Compared to tissue biopsy controls that were untreated, ARV-NP combinations show protection of the explant tissue from RT-SHIV infection (Figure AI.6a). In particular, after 9 days in culture, the untreated tissue biopsy showed measurable SIV p27 of ~1200 pg/mL in the supernatant whereas the combination ARV-NP treatment groups were similar to the media control measured at the start of the study (day 0) and had no detectable virus replication.

We also assessed the same ERM-NP combinations for its ability to inhibit virus dissemination by infected migratory cells emigrating out of the cervicovaginal tissue explants. Cells that had migrated from the tissue explants after overnight culture were collected and co-cultured with permissive CEMx174 cells. At day 6, CEMx174 cells co-cultured with migratory cells from untreated explants showed SIV p27 levels of 11,600 pg/mL. In contrast, migratory cells from EMR-NP treated explants co-cultured with CEMx174 cells showed SIV p27 levels of 700pg/mL (Figure AI.6b). Infection in migratory cells was also confirmed by co-culture with CEMx174 cells and monitoring for CPE, which refers to morphological changes in the host cells that are caused

by viral infection including rounding of the infected cell, fusion with adjacent cells to form multinucleated cells. For the EMR-NP treated co-culture, CPE was not observed until day 5 whereas the untreated co-culture showed CPE at day 1 (Figure AI.6c). Together, these results indicate that EMR-NPs also delays infection against viral dissemination by migratory cells.

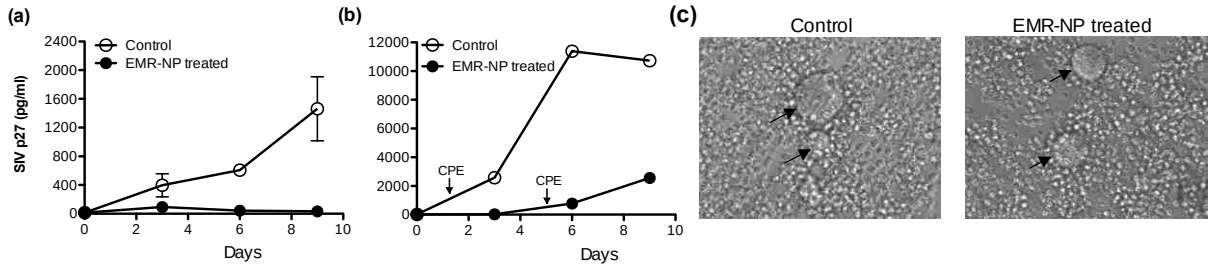

Figure AI.6. ARV drug-NP combinations inhibit RT-SHIV infection of cervicovaginal tissue explants. Pigtailed macaque cervicovaginal tissues were pretreated with 5μM etravirine/maraviroc/raltegravir nanoparticle combinations (EMR-NP) at equimolar ratio prior to exposure with 10^5 TCID50 RT-SHIV. (a) Infection of tissue explants was monitored by detection of SIV p27 antigen in the tissue culture supernatants. Untreated tissue biopsy controls (o) showed a trend towards increasing p27 concentration in culture over the course of 9 d. In contrast, tissue biopsies treated with ARV drug-NP combinations (□) showed no significant change in p27 concentration during the same time course. (b) Migratory cells were co-cultured with CEMx174 cells, and infection was monitored by p27 ELISA at the same time points. Virus dissemination by migratory cells from cervicovaginal tissues was also blocked by ARV drug-NP combinations treatment (□) compared to untreated tissues (o). (c) Migratory cells co-cultured with CEMx174 cells were examined by light microcopy for CPE. Virus-induced giant cells (indicated with arrows) were observed in the co-culture of the untreated control group at day 1. Whereas, CPE was first observed at day 5 for the EMR-NP treatment group. Each condition was tested in duplicate or triplicate. Data represent the mean ± SD.

AI.5 Discussion

Here, we investigated the role of nanoparticles to enhance the antiviral potency of ARV drug combinations in models of *in vitro* cell-free and cell-cell HIV infection as well as in an *ex vivo* tissue organ system. We focused on delivering nanoparticles containing MVC, ETR and RAL because the inhibitory potential of this triple combination is predicted to be sufficiently large to halt viral replication[10-11]. In addition, this triple drug combination is one of many promising ARV

drug combinations that would be difficult to formulate in a single topical microbicide due to low intrinsic aqueous solubility and incompatible drug physicochemical properties[30]. The combination of MVC, ETR and RAL is also promising due to its documented antiviral activity against drug resistant HIV viral isolates, its demonstrated efficacy when used in salvage therapy, and the absence of identified adverse drug-drug interactions[30-32]. In addition, clinical studies of highly treatment-experienced patients show that this combination is associated with good long-term efficacy and safety profiles[33].

In contrast to existing approaches that co-formulate ARV drug combinations together in a single liposome or nanoparticle[6-7], we chose to prepare single-drug loaded nanoparticles that were subsequently combined upon administration. Our data for drug loading in PLGA nanoparticles indicate that ETR, a hydrophobic drug, shows greater loading and encapsulation efficiency than either MVC or RAL, which are both ionizable at neutral pH. As such, these particular drugs are interesting not only for their mechanism of action and potency when used alone and in combination, but also because they represent a challenge for co-delivery in current vaginal dosage forms. If co-formulated together in a single NP, these drugs would be likely to combine at a ratio near 8:2:1, which is the ratio observed for the individual loading of ETR, RAL and MVC, respectively (Table AI.1). However, there are many applications where combining drugs at ratios that differ from their loading capacity may be beneficial. The molar ratio of drug combinations is known to be a significant factor in determining if the combined effect will be additive, synergistic or antagonistic[34-37]. While formulating drugs together in the same carrier may ensure that they will be in fixed ratios when delivered intracellularly, most clinical applications require high inhibition (f_a>>90%) and, in this limit, the dosing of multiple drugs either separately or combined in a single

carrier may be similar. Our data provide a rationale for formulating the drugs separately in order to understand and maximize beneficial drug ratios for increased antiviral potency.

We observed that the ARV-NPs used in this study maintained potent HIV inhibition and were more effective when used in combinations. In particular, ARV-NP combinations with ETR exhibited significantly higher antiviral potency and dose-reduction against cell-free HIV-1 BaL infection despite no enhanced potency observed for the single ARV-NP. Based on the *in vitro* releases kinetics, we expect that MVC instantaneously releases from the NP once dosed to the cells and would behave similarly to free MVC by interacting with its extracellular receptor. This may explain the similar dose-effect response observed for free MVC and MVC-NP. ETR and RAL exhibited both a burst and significant sustained release phase. We anticipate that under physiological conditions, in the absence of a solubilizing agents such as solutol, ETR would show significantly slower release kinetics. Coupling the observed release kinetics with knowledge of the cellular uptake kinetics of nanoparticles should help clarify the mechanisms responsible for observed dose-reductions. Although NP internalization by cells can occur within minutes to hours, the kinetics of internalization is likely to depend on cell type/cycle as well as nanoparticle size, shape, and colloidal stability[38-41].

ARV-NP combinations that showed large dose-reduction compared to their single drug components and the equivalent unformulated drug combinations, were identified as synergistic based on the model of Bliss independence. For these ARV-NP combinations, deviation from the modified Bliss prediction for additivity was dose-dependent and showed the greatest difference at effect levels that were much higher than the IC50 (fa>>90%). In contrast, the combination effect

of free ETR and RAL appeared to be strictly additive. A previous study with similar two-drug combination but using a single-round infection assay with PBMCs showed that free ETR and RAL are additive in combination, which is consistent with our observed data, whereas free ETR and MVC were strongly synergistic[11]. It is possible that the lack of synergy observed for the unformulated ETR/MVC combination in our study originates from differences in the assay employed, including sensitivity and the choice of viral isolate. We used the model of Bliss independence with a variable slope to predict the additive effect from our drug combinations, which provides a more stringent criterion for synergy than existing approaches[42]. An alternative approach that is more widely used to describe the effect of multidrug combinations is the Loew additivity model, which is based on the widely used isobolograms to describe an interaction index[42-44]. However, based on binding mechanism alone, the Loew additivity model is only applicable to drugs that have the same mechanism of action and therefore compete for the same binding site. In addition, existing models are only valid when the Hill coefficient is constant and not applicable for drugs that exhibit non-linear dose-effects as is seen with ETR and many other ARV drugs[10]. It is interesting that the combination effect we observed from the free drugs differed from the ARV-NP combinations, but our result is consistent with other studies showing unique combination effects from nanoparticles used for combination chemotherapy[45].

Although most studies on HIV transmission have focused on cell free viral infection, an effective prophylaxis strategy including microbicides must also block the direct transmission of virus from cell-cell contact with infected cells such as seminal macrophages and T cells. It is now well established that both cell free-virus and cell-associated virus play important roles in initiating mucosal infection by HIV-1[46-48]. In general, cell-cell HIV transmission is more difficult to inhibit

than cell-free virus infection[2-3, 29, 49-50]. We observed that cell-cell HIV-1 BaL transmission was inhibited at least 10-fold more effectively with drug combinations that included ETR-NP. Nanoparticle combinations of ETR and MVC showed the greatest dose-reduction in cell-cell HIV transmission compared to all other free- or formulated-drug combinations that were tested. Our observation that ARV-loaded nanoparticle combinations effectively inhibit cell-to-cell HIV transmission demonstrates their potential in this important aspect of HIV prophylaxis and should be further investigated. Finally, as a first step toward evaluating challenge studies in animal models, we also measured the activity of ARV-loaded nanoparticles in a virus infection assay using a macaque cervicovaginal explant model. We observed that ARV-NP combinations inhibit RT-SHIV virus propagation in tissue and also block virus transmission by migratory cells emigrating out of the tissue. Together, these results indicate that ARV-loaded nanoparticles can inhibit both cell free and cell associated HIV transmission in relevant model systems. Our results also demonstrate that ARV-NP combinations control HIV-1 transmission more efficiently than free drug combinations in both cell-free and cell-associated HIV infection assays.

The underlying mechanism behind the dose-reduction observed with ARV-NP combinations involving ETR-NP is unclear but appears to be dependent on the formulation of the drugs in nanoparticles. Drug-loaded nanoparticles can improve intracellular drug uptake and biodistribution in tissues and cells due to a combination of tissue penetration and trafficking properties[5]. The bioavailability of ARV drugs delivered in NPs is associated with both the intracellular uptake of the nanocarriers as well as the dissolution of the drug from these polymeric solid dispersions. Although we observe higher intracellular drug concentration in cells dosed with the triple ARV-NP combination compared to the equivalent unformulated drugs, this does not

prove that the higher intracellular concentration underlies the mechanism that drives synergy. That is, higher intracellular drug concentrations are sufficient but not necessary to explain the dose-reduction from synergistic combinations. Although some synergistic combinations can be correlated to changes in intracellular drug concentrations (e.g., saquinavir boosted ritonavir), dose reduction due to synergy can also arise without changes in intracellular drug concentration (e.g., allosteric effects). Numerous ARV drug combinations exhibit synergy when dosed clinically but the underlying mechanism for enhanced potency is not known for the vast majority of these combinations [11]. Although measuring the intracellular PK of drugs dosed in combinations is a first step, alternative approaches are likely needed to fully understand the complex mechanisms underlying synergy and other combination effects[51].

We envision that these combination NP drug cocktails can be administered topically to the vaginal mucosa using a conventional dosage form such as a gel where they can be incorporated as a suspension. In this case, nanoparticles may benefit the formulation of hydrophobic drugs into these water-based gels. Nanoparticles may also be incorporated in quick-dissolving films and intravaginal rings. However, these solid dosage forms have processing requirements such as hot-melt extrusion or solvent-cast evaporation that are likely to alter the integrity of the nanoparticles. Electrospun fibers, which are an emerging solid dosage form for vaginal delivery[52] could also be used for nanoparticle delivery. While the current nanoparticle drug delivery system is being considered for use as a topical microbicide, we expect it will have other applications including parenteral administration. While the PLGA nanocarriers used in our studies were effective at inhibiting HIV transmission across three different models of virus infection (cell-free, cell-cell, and tissue), the low loading observed for ionizable and water-soluble drugs may limit this

platform's utility to study highly soluble drugs at high doses in other interesting combinations. Evaluating other nanocarrier systems that may be more amenable to loading highly soluble drugs, or developing pro-drugs that allow better loading into PLGA nanoparticles, could overcome these limitations. These and other strategies are needed to fully understand the role of nanocarrier systems in facilitating multidrug effects in relevant cells and tissue associated with HIV infection.

AI.6 Conclusions

We have developed ARV-loaded nanoparticles for ETR, RAL and MVC and tested them in combination for *prophylaxis* against both cell-free and cell-associated HIV-1 BaL infection. We have also evaluated the protective efficacy of ARV-NP combinations in a nonhuman primate cervicovaginal tissue explant model against RT-SHIV infection. We observe that the ARV-NP combinations used in this study exhibit non-linear and steep dose-effect responses at lower concentrations than the equivalent free drug combinations. Combined with the ability to extend the half-life of the drugs by providing sustained release, this increased potency could enable an extended dosing interval. Identifying drug combination regiments that exceed the antiviral potency needed to achieve complete virus replication may allow for less frequent dosing as well as decreased dosing, which may depend on the modular ability to deliver and tune the release of different drug combinations. We expect that the versatility of nanoparticle delivery platforms, particularly their ability to deliver high concentrations of physicochemical diverse agents, will result in broad applications for HIV chemoprophylaxis and treatment.

AI.7 Supplementary information

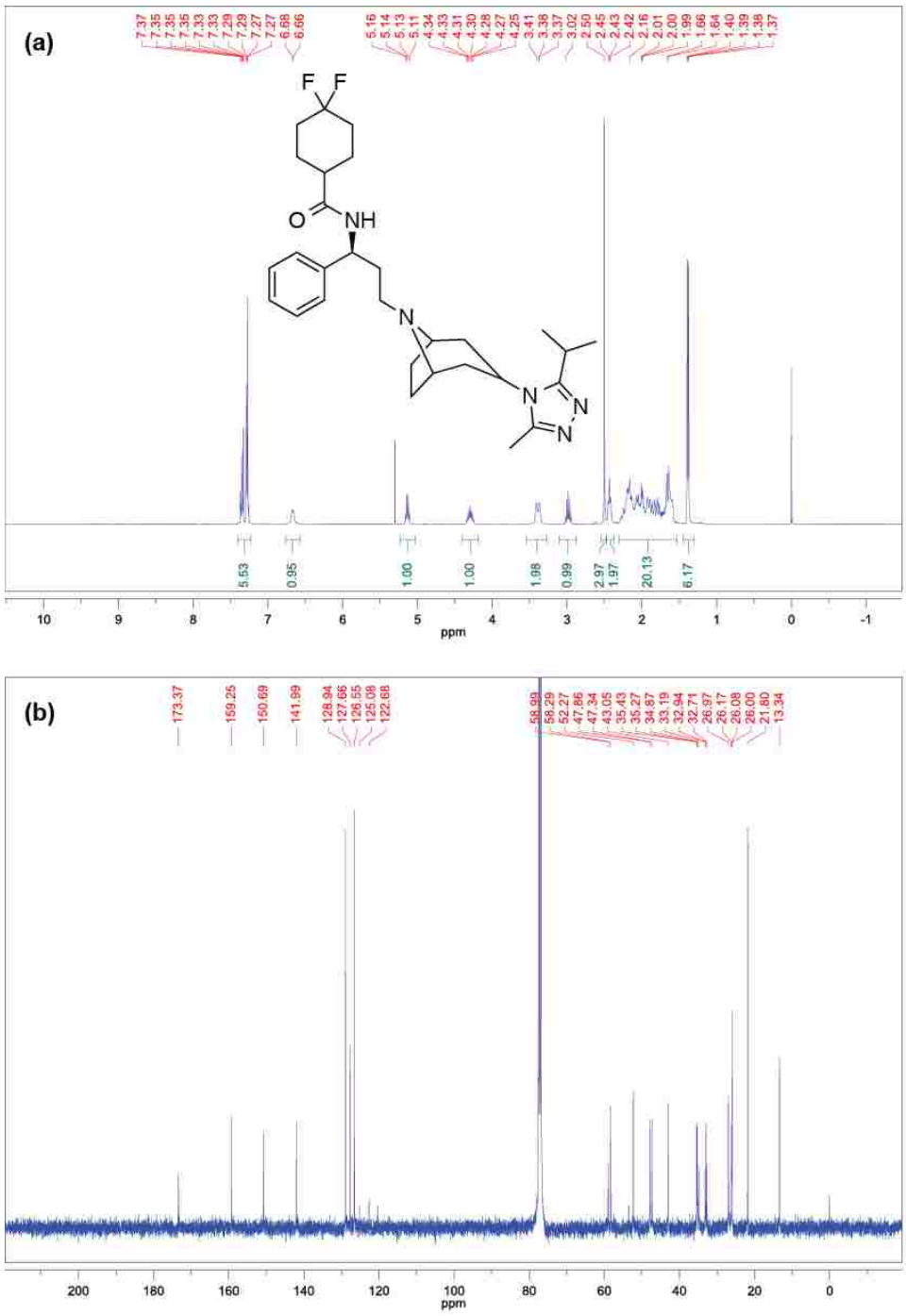

Figure AI.S1. **(a)** ^{1}H NMR ($CDCl_3$, 400 MHz) spectrum of isolated maraviroc. **(b)** ^{13}C NMR ($CDCl_3$, 100 MHz) spectrum of isolated maraviroc.

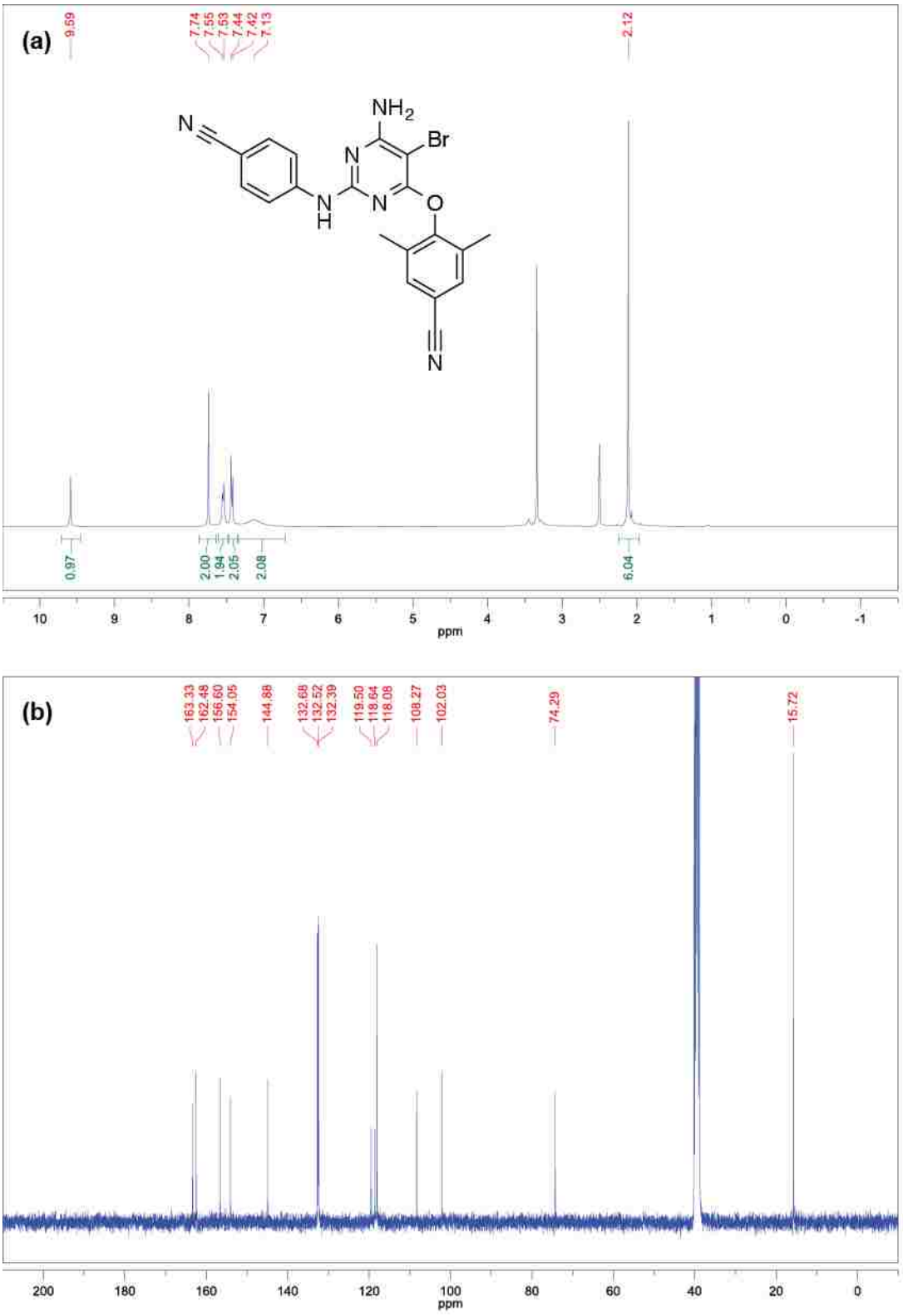

Figure AI.S2. (a) ^{1}H NMR (d_6-DMSO, 400 MHz) spectrum of isolated etravirine. **(b)** ^{13}C NMR (d_6-DMSO, 100 MHz) spectrum of isolated etravirine.

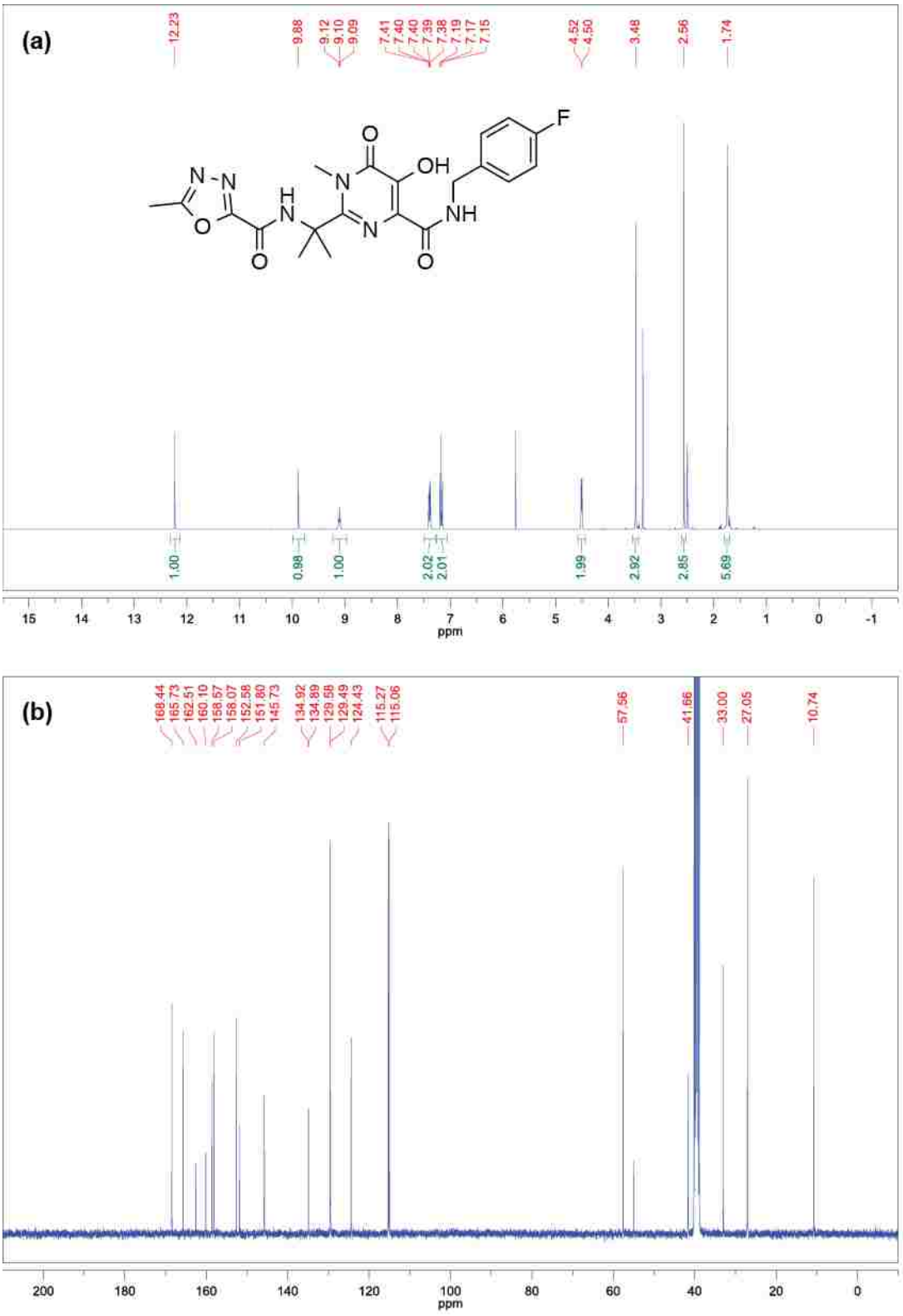

Figure AI.S3. **(a)** ^{1}H NMR (d_6-DMSO, 400 MHz) spectrum of isolated raltegravir. **(b)** ^{13}C NMR (d_6-DMSO, 100 MHz) spectrum of isolated raltegravir.

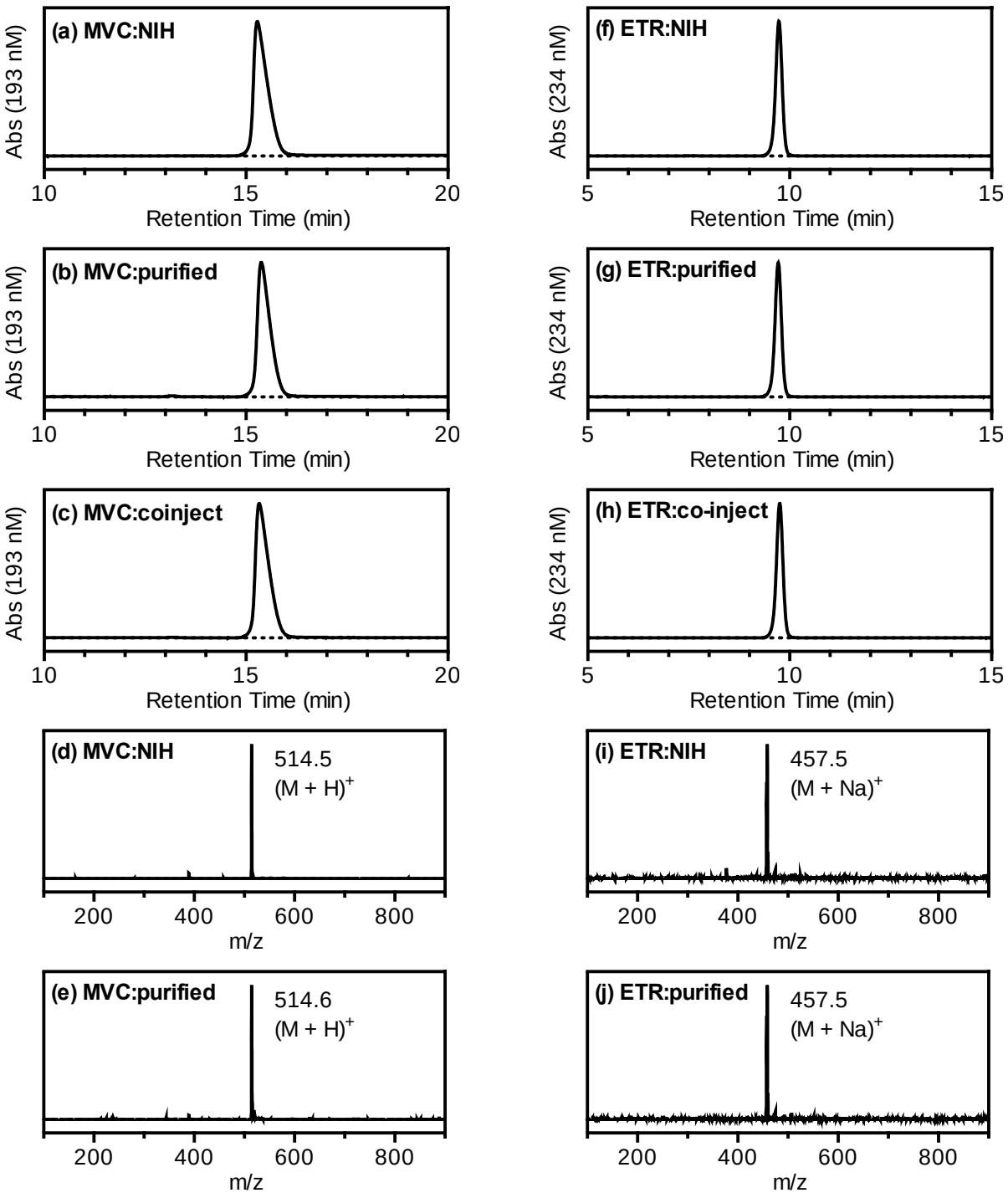

Figure AI.S4. LC-MS data for maraviroc (**a-e**) and etravirine (**f-j**). LC chromatographs obtained from reference standards (**a,f**) ARVs purified from pharmaceutical formulations (**b,g**) and co-injections (**c,h**). Mass spectra obtained from reference standards (**d,i**) and ARVs purified from pharmaceutical formulations (**e,j**).

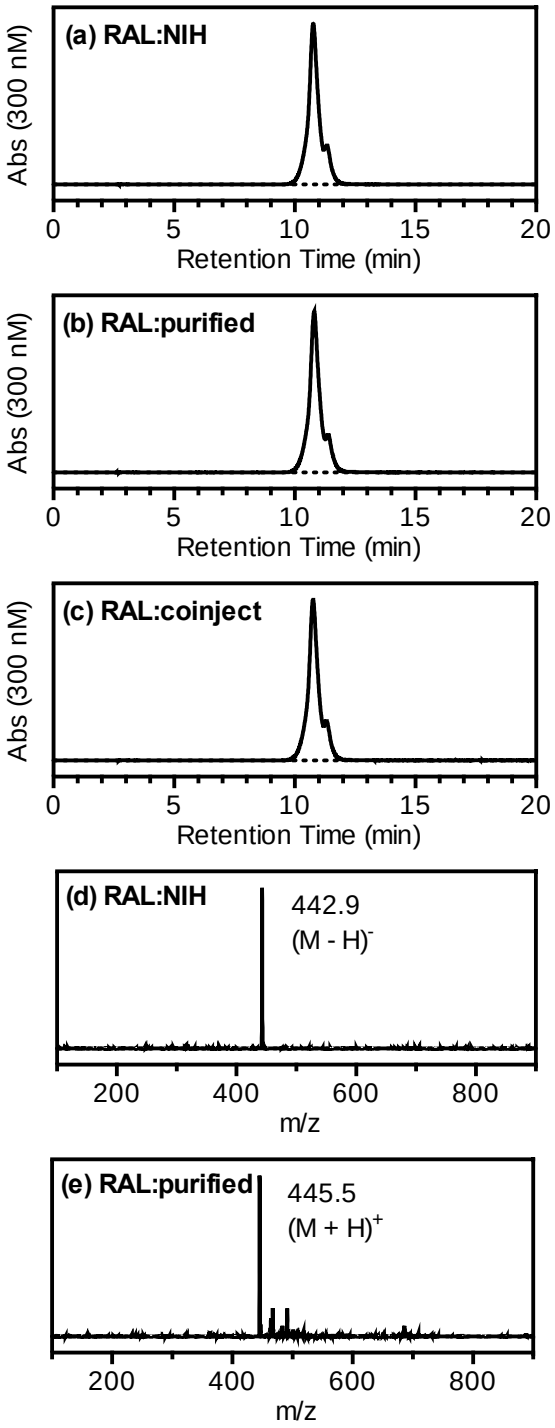

Figure AI.S5. LC-MS data for raltegravir (**a-e**). LC chromatographs obtained from reference standards (**a**) ARVs purified from pharmaceutical formulations (**b**) and co-injections (**c**). Mass spectra obtained from reference standards (**d**) and ARVs purified from pharmaceutical formulations (**e**).

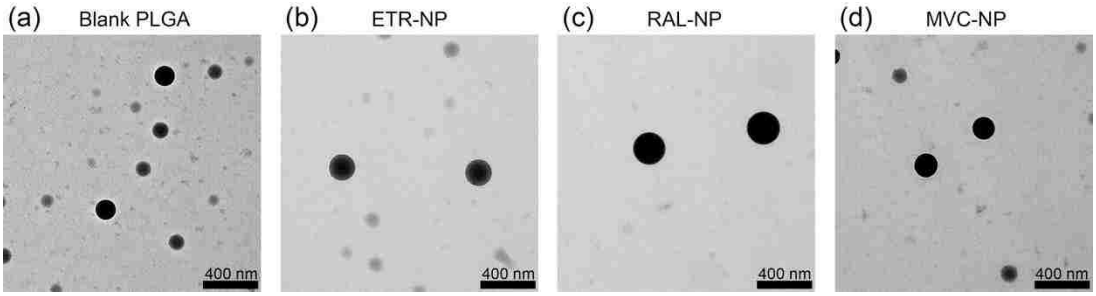

Figure AI.S6. Transmission electron microscopy (TEM) images of ARV drug nanoparticles. (a). Blank PLGA, (b). ETR-NP, (c). RAL-NP, (d). MVC-NP. Scale bar (400nm) was shown in (d).

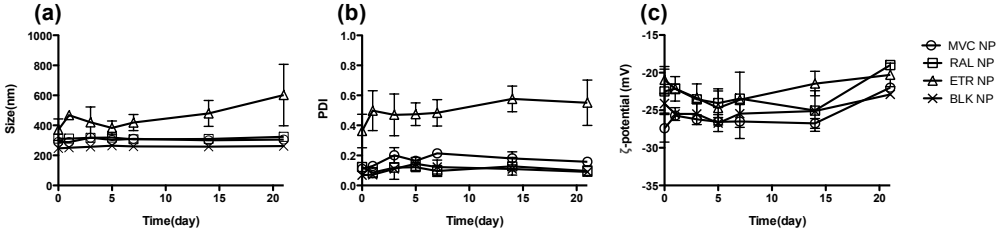

Figure AI.S7. Storage stability of ARV drug nanoparticles. ARV drug- and blank NPs were stored at room temperature (25°C) after lyophilisation and changes in nanoparticle (a) diameter, (b) PDI and (c) ζ-potential were measured by DLS at day 0, 1, 3, 5, 7, 14 and 21. Values are the means ± standard deviation (n=3).

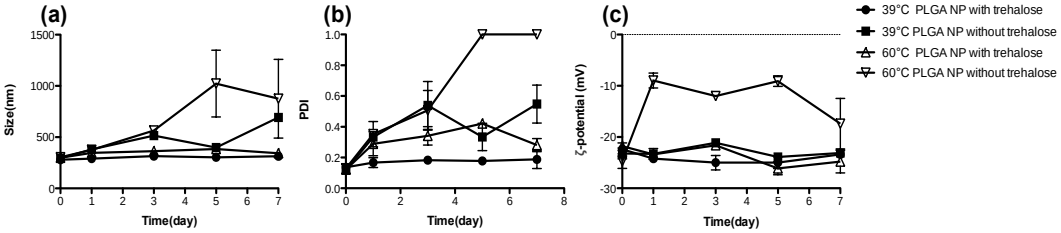

Figure AI.S8. Effect of treahalose on storage stability of nanoparticles. Change of diameters, polydispersity index (PdI) and zeta potential of Blank NPs with or without trehalose added within 7 days of storage at 39°C and 60°C after lyophilisation. Trehalose was added to blank NPs at a 1:1 weight ratio before lyophilisation. Lyophilized NPs were subsequently stored at 39°C or 60°C and changes in nanoparticle (a) diameter, (b) PDI and (c) ζ-potential were measured by DLS at day 0, 1, 3, 5, and 7. Values are the means ± standard deviation (n=3).

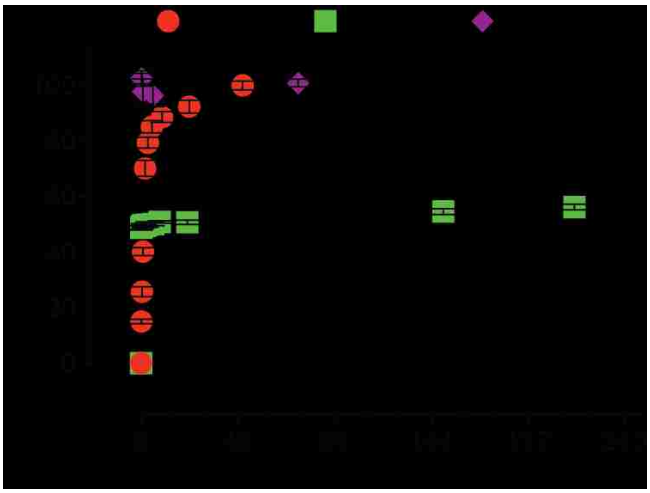

Figure AI.S9. *In vitro* release of ETR, RAL or MVC from PLGA-based nanoparticles. The kinetic of drug release from ARV-NPs was measured by resuspending lyophilized ARV-NPs in PBS and incubated at 37°C on a shaker. A small amount of supernatant was collected between 0.25 - 215h, and the concentration of drug in each sample was determined by HPLC.

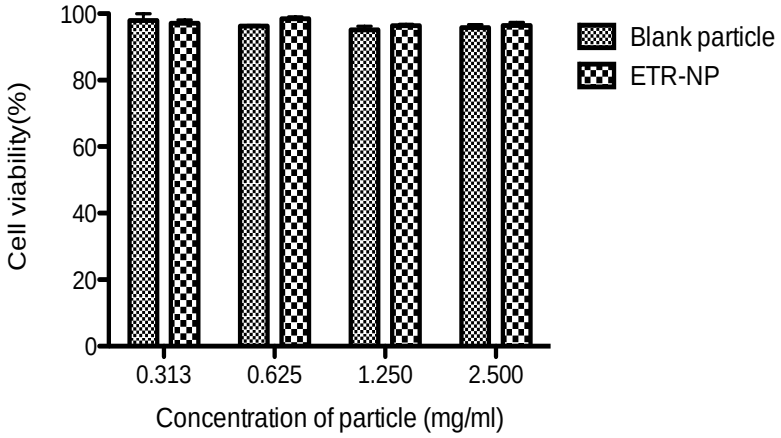

Figure AI.S10. Cytotoxicity of blank PLGA and ETR-NPs were evaluated using Cell Titer blue assay. TZM-bL cells were cocultured with particles for three days before cell viability was examined. Similar results were obtained in MVC-NP and RAL-NP treated cell cultures (data not shown).

Table AI.S1. Comparison of the antiviral activity of drug combinations with different ratios*

ETR:RAL:MVC (molar ratio)	IC50 (nM)
1:1:1	3.20
1:5:7	7.56
2:1:5	4.49
1:5:33	6.63
1:1:6	5.99
1:3:5	7.98

*The antiviral activity of ARV-NP combinations was assessed in TZM-bL cells with HIV-1 BaL. IC_{50} value indicates the sample concentration giving 50% of relative luminescence units (RLUs) compared with those of virus control after subtraction of background RLUs

AI.8 References

1. Pirrone, V.; Thakkar, N.; Jacobson, J. M.; Wigdahl, B.; Krebs, F. C., Combinatorial Approaches to the Prevention and Treatment of HIV-1 Infection. *Antimicrobial Agents and Chemotherapy* **2011,** *55* (5), 1831-1842.
2. Zhong, P.; Agosto, L. M.; Ilinskaya, A.; Dorjbal, B.; Truong, R.; Derse, D.; Uchil, P. D.; Heidecker, G.; Mothes, W., Cell-to-Cell Transmission Can Overcome Multiple Donor and Target Cell Barriers Imposed on Cell-Free HIV. *PLoS ONE* **2013,** *8* (1), e53138.
3. Kolodkin-Gal, D.; Hulot, S. L.; Korioth-Schmitz, B.; Gombos, R. B.; Zheng, Y.; Owuor, J.; Lifton, M. A.; Ayeni, C.; Najarian, R. M.; Yeh, W. W.; Asmal, M.; Zamir, G.; Letvin, N. L., Efficiency of Cell-Free and Cell-Associated Virus in Mucosal Transmission of Human Immunodeficiency Virus Type 1 and Simian Immunodeficiency Virus. *Journal of Virology* **2013,** *87* (24), 13589-13597.
4. Shahiwala, A.; Amiji, M. M., Nanotechnology-based delivery systems in HIV/AIDS therapy. *Future HIV Therapy* **2007,** *1* (1), 49-59.
5. das Neves, J.; Amiji, M. M.; Bahia, M. F.; Sarmento, B., Nanotechnology-based systems for the treatment and prevention of HIV/AIDS. *Advanced Drug Delivery Reviews* **2010,** *62* (4–5), 458-477.

6. Freeling, J. P.; Koehn, J.; Shu, C.; Sun, J.; Ho, R. J. Y., Long-acting three-drug combination anti-HIV nanoparticles enhance drug exposure in primate plasma and cells within lymph nodes and blood. *AIDS* **2014,** *28* (17), 2625-2627. .
7. Shibata, A.; McMullen, E.; Pham, A.; Belshan, M.; Sanford, B.; Zhou, Y.; Goede, M.; Date, A. A.; Destache, C. J., Polymeric Nanoparticles Containing Combination Antiretroviral Drugs for HIV Type 1 Treatment. *AIDS Research and Human Retroviruses* **2013,** *29* (5), 746-754.
8. Lisziewicz, J.; Tőke, E. R., Nanomedicine applications towards the cure of HIV. *Nanomedicine: Nanotechnology, Biology and Medicine* **2013,** *9* (1), 28-38.
9. Makadia, H. K.; Siegel, S. J., Poly Lactic-co-Glycolic Acid (PLGA) as Biodegradable Controlled Drug Delivery Carrier. *Polymers* **2011,** *3* (3), 1377-1397.
10. Shen, L.; Peterson, S.; Sedaghat, A. R.; McMahon, M. A.; Callender, M.; Zhang, H.; Zhou, Y.; Pitt, E.; Anderson, K. S.; Acosta, E. P.; Siliciano, R. F., Dose-response curve slope sets class-specific limits on inhibitory potential of anti-HIV drugs. *Nat Med* **2008,** *14* (7), 762-766.
11. Jilek, B. L.; Zarr, M.; Sampah, M. E.; Rabi, S. A.; Bullen, C. K.; Lai, J.; Shen, L.; Siliciano, R. F., A quantitative basis for antiretroviral therapy for HIV-1 infection. *Nat Med* **2012,** *18* (3), 446-451.
12. Sampah, M. E. S.; Shen, L.; Jilek, B. L.; Siliciano, R. F., Dose–response curve slope is a missing dimension in the analysis of HIV-1 drug resistance. *Proceedings of the National Academy of Sciences of the United States of America* **2011,** *108* (18), 7613-7618.
13. Van Der Ryst, E., Maraviroc – A CCR5 Antagonist for the Treatment of HIV-1 Infection. *Frontiers in Immunology* **2015,** *6*, 277.
14. Malcolm, R. K.; Forbes, C. J.; Geer, L.; Veazey, R. S.; Goldman, L.; Johan Klasse, P.; Moore, J. P., Pharmacokinetics and efficacy of a vaginally administered maraviroc gel in rhesus macaques. *Journal of Antimicrobial Chemotherapy* **2013,** *68* (3), 678-683.
15. Blanco, J. L.; Whitlock, G.; Milinkovic, A.; Moyle, G., HIV integrase inhibitors: a new era in the treatment of HIV. *Expert Opinion on Pharmacotherapy* **2015,** *16* (9), 1313-1324.
16. Emery, S.; Winston, A., Raltegravir: a new choice in HIV and new chances for research. *The Lancet 374* (9692), 764-766.
17. Dobard, C.; Sharma, S.; Parikh, U. M.; West, R.; Taylor, A.; Martin, A.; Pau, C.-P.; Hanson, D. L.; Lipscomb, J.; Smith, J.; Novembre, F.; Hazuda, D.; Garcia-Lerma, J. G.; Heneine, W., *Postexposure Protection of Macaques from Vaginal SHIV Infection by Topical Integrase Inhibitors*. 2014; Vol. 6, p 227ra35-227ra35.
18. Joshi, S.; Maikap, G. C.; Titirmare, S.; Chaudhari, A.; Gurjar, M. K., An Improved Synthesis of Etravirine. *Organic Process Research & Development* **2010,** *14* (3), 657-660.
19. Zhao, G.-L.; Lin, S.; Korotvička, A.; Deiana, L.; Kullberg, M.; Córdova, A., Asymmetric Synthesis of Maraviroc (UK-427,857). *Advanced Synthesis & Catalysis* **2010,** *352* (13), 2291-2298.
20. Summa, V.; Petrocchi, A.; Bonelli, F.; Crescenzi, B.; Donghi, M.; Ferrara, M.; Fiore, F.; Gardelli, C.; Gonzalez Paz, O.; Hazuda, D. J.; Jones, P.; Kinzel, O.; Laufer, R.; Monteagudo, E.; Muraglia, E.; Nizi, E.; Orvieto, F.; Pace, P.; Pescatore, G.; Scarpelli, R.; Stillmock, K.; Witmer, M. V.; Rowley, M., Discovery of Raltegravir, a Potent, Selective Orally Bioavailable HIV-Integrase Inhibitor for the Treatment of HIV-AIDS Infection. *Journal of Medicinal Chemistry* **2008,** *51* (18), 5843-5855.
21. Rao, K. S.; Reddy, M. K.; Horning, J. L.; Labhasetwar, V., TAT-conjugated nanoparticles for the CNS delivery of anti-HIV drugs. *Biomaterials* **2008,** *29* (33), 4429-4438.

22. Notari, S.; Tommasi, C.; Nicastri, E.; Bellagamba, R.; Tempestilli, M.; Pucillo, L. P.; Narciso, P.; Ascenzi, P., Simultaneous determination of maraviroc and raltegravir in human plasma by HPLC-UV. *IUBMB Life* **2009,** *61* (4), 470-475.
23. Hirano, A.; Takahashi, M.; Kinoshita, E.; Shibata, M.; Nomura, T.; Yokomaku, Y.; Hamaguchi, M.; Sugiura, W., High Performance Liquid Chromatography Using UV Detection for the Simultaneous Quantification of the New Non-nucleoside Reverse Transcriptase Inhibitor Etravirine (TMC-125), and 4 Protease Inhibitors in Human Plasma. *Biological and Pharmaceutical Bulletin* **2010,** *33* (8), 1426-1429.
24. Margolis, L.; Shattock, R., Selective transmission of CCR5-utilizing HIV-1: the 'gatekeeper' problem resolved? *Nat Rev Micro* **2006,** *4* (4), 312-317.
25. Laird, G. M.; Bullen, C. K.; Rosenbloom, D. I. S.; Martin, A. R.; Hill, A. L.; Durand, C. M.; Siliciano, J. D.; Siliciano, R. F., Ex vivo analysis identifies effective HIV-1 latency–reversing drug combinations. *The Journal of Clinical Investigation* **2015,** *125* (5), 1901-1912.
26. Lai, S. K.; Wang, Y.-Y.; Hida, K.; Cone, R.; Hanes, J., Nanoparticles reveal that human cervicovaginal mucus is riddled with pores larger than viruses. *Proceedings of the National Academy of Sciences* **2010,** *107* (2), 598-603.
27. Ensign, L. M.; Tang, B. C.; Wang, Y.-Y.; Tse, T. A.; Hoen, T.; Cone, R.; Hanes, J., Mucus-Penetrating Nanoparticles for Vaginal Drug Delivery Protect Against Herpes Simplex Virus. *Science Translational Medicine* **2012,** *4* (138), 138ra79-138ra79.
28. das Neves, J.; Araújo, F.; Andrade, F.; Amiji, M.; Bahia, M.; Sarmento, B., Biodistribution and Pharmacokinetics of Dapivirine-Loaded Nanoparticles after Vaginal Delivery in Mice. *Pharm Res* **2014,** *31* (7), 1834-1845.
29. Schiffner, T.; Sattentau, Q. J.; Duncan, C. J. A., Cell-to-cell spread of HIV-1 and evasion of neutralizing antibodies. *Vaccine* **2013,** *31* (49), 5789-5797.
30. Calcagno, A.; Nozza, S.; Bonora, S.; Castagna, A.; Gonzalez de Requena, D.; D'Avolio, A.; Lazzarin, A.; Di Perri, G., Pharmacokinetics of the raltegravir/maraviroc/etravirine combination. *Journal of Antimicrobial Chemotherapy* **2011**.
31. Nozza, S.; Galli, L.; Bigoloni, A.; Nicola, G.; Pogliaghi, M.; Cossarini, F.; Salpietro, S.; Galli, A.; Torre, L. D.; Tambussi, G.; Lazzarin, A.; Castagna, A., Durability and Safety of a Novel Salvage Therapy in R5-Tropic HIV-Infected Patients: Maraviroc, Raltegravir, Etravirine. *JAIDS Journal of Acquired Immune Deficiency Syndromes* **2011,** *56* (4), e113-e115. .
32. Khanlou, H.; Sayana, S., Efficacy and Tolerability of RAL, MVC and ETV used in combination in the treatment of highly treatment experienced HIV infected patients. *Retrovirology* **2010,** *7* (Suppl 1), P48-P48.
33. Achhra, A. C.; Boyd, M. A., Antiretroviral regimens sparing agents from the nucleoside(tide) reverse transcriptase inhibitor class: a review of the recent literature. *AIDS Research and Therapy* **2013,** *10*, 33-33.
34. Pavillard, V.; Kherfellah, D.; Richard, S.; Robert, J.; Montaudon, D., Effects of the combination of camptothecin and doxorubicin or etoposide on rat glioma cells and camptothecin-resistant variants. *British Journal of Cancer* **2001,** *85* (7), 1077-1083.
35. Tardi, P.; Johnstone, S.; Harasym, N.; Xie, S.; Harasym, T.; Zisman, N.; Harvie, P.; Bermudes, D.; Mayer, L., In vivo maintenance of synergistic cytarabine:daunorubicin ratios greatly enhances therapeutic efficacy. *Leukemia Research* **2009,** *33* (1), 129-139.
36. Meng, H.; Wang, M.; Liu, H.; Liu, X.; Situ, A.; Wu, B.; Ji, Z.; Chang, C. H.; Nel, A. E., Use of a Lipid-Coated Mesoporous Silica Nanoparticle Platform for Synergistic Gemcitabine and Paclitaxel Delivery to Human Pancreatic Cancer in Mice. *ACS Nano* **2015,** *9* (4), 3540-3557.

37. Blanco, E.; Sangai, T.; Wu, S.; Hsiao, A.; Ruiz-Esparza, G. U.; Gonzalez-Delgado, C. A.; Cara, F. E.; Granados-Principal, S.; Evans, K. W.; Akcakanat, A.; Wang, Y.; Do, K.-A.; Meric-Bernstam, F.; Ferrari, M., Colocalized Delivery of Rapamycin and Paclitaxel to Tumors Enhances Synergistic Targeting of the PI3K/Akt/mTOR Pathway. *Mol Ther* **2014,** *22* (7), 1310-1319.
38. Nowacek, A.; McMillan, J.; Miller, R.; Anderson, A.; Rabinow, B.; Gendelman, H., Nanoformulated Antiretroviral Drug Combinations Extend Drug Release and Antiretroviral Responses in HIV-1-Infected Macrophages: Implications for NeuroAIDS Therapeutics. *J Neuroimmune Pharmacol* **2010,** *5* (4), 592-601.
39. Nowacek, A. S.; Balkundi, S.; McMillan, J.; Roy, U.; Martinez-Skinner, A.; Mosley, R. L.; Kanmogne, G.; Kabanov, A. V.; Bronich, T.; Gendelman, H. E., Analyses of Nanoformulated Antiretroviral Drug Charge, Size, Shape and Content for Uptake, Drug Release and Antiviral Activities in Human Monocyte-Derived Macrophages. *Journal of controlled release : official journal of the Controlled Release Society* **2011,** *150* (2), 204-211.
40. Chono, S.; Tanino, T.; Seki, T.; Morimoto, K., Uptake characteristics of liposomes by rat alveolar macrophages: influence of particle size and surface mannose modification. *Journal of Pharmacy and Pharmacology* **2007,** *59* (1), 75-80.
41. Kim, J. A.; Aberg, C.; Salvati, A.; Dawson, K. A., Role of cell cycle on the cellular uptake and dilution of nanoparticles in a cell population. *Nat Nano* **2012,** *7* (1), 62-68.
42. Chou, T. C., Theoretical basis, experimental design, and computerized simulation of synergism and antagonism in drug combination studies. *Pharmacological Reviews* **2006,** *58* (3), 621-681.
43. Loewe, S. M., H, Effect of combinations: mathematical basis of problem. *Arch. Exp. Pathol. Pharmakol.* **1926,** *114*, 313-326.
44. Greco, W. R.; Bravo, G.; Parsons, J. C., The Search for Synergy - a Critical-Review from a Response-Surface Perspective. *Pharmacological Reviews* **1995,** *47* (2), 331-385.
45. Federico, C.; Morittu, V. M.; Britti, D.; Trapasso, E.; Cosco, D., Gemcitabine-loaded liposomes: rationale, potentialities and future perspectives. *International Journal of Nanomedicine* **2012,** *7*, 5423-5436.
46. Barreto-de-Souza, V.; Arakelyan, A.; Margolis, L.; Vanpouille, C., HIV-1 Vaginal Transmission: Cell-Free or Cell-Associated Virus? *American Journal of Reproductive Immunology* **2014,** *71* (6), 589-599.
47. Shattock, R.; Moore, J., Inhibiting sexual transmission of HIV-1 infection. *Nat Rev Microbiol* **2003,** *1* (1), 25 - 34.
48. Barre-Sinoussi, F., Cell-Associated Mucosal HIV Transmission. *Journal of Infectious Diseases* **2014,** *210* (suppl 3), S605.
49. Costiniuk, C. T.; Jenabian, M.-A., Cell-to-cell transfer of HIV infection: implications for HIV viral persistence. *Journal of General Virology* **2014,** *95* (Pt 11), 2346-2355.
50. Whaley, K. J.; Mayer, K. H., Strategies for Preventing Mucosal Cell-Associated HIV Transmission. *Journal of Infectious Diseases* **2014,** *210* (suppl 3), S674-S680.
51. Pritchard, J. R.; Bruno, P. M.; Gilbert, L. A.; Capron, K. L.; Lauffenburger, D. A.; Hemann, M. T., Defining principles of combination drug mechanisms of action. *Proceedings of the National Academy of Sciences* **2013,** *110* (2), E170–E179.
52. Ball, C.; Krogstad, E.; Chaowanachan, T.; Woodrow, K. A., Drug-Eluting Fibers for HIV-1 Inhibition and Contraception. *PLoS ONE* **2012,** *7* (11), e49792.

Appendix II: Supplementary information for Chapter 3

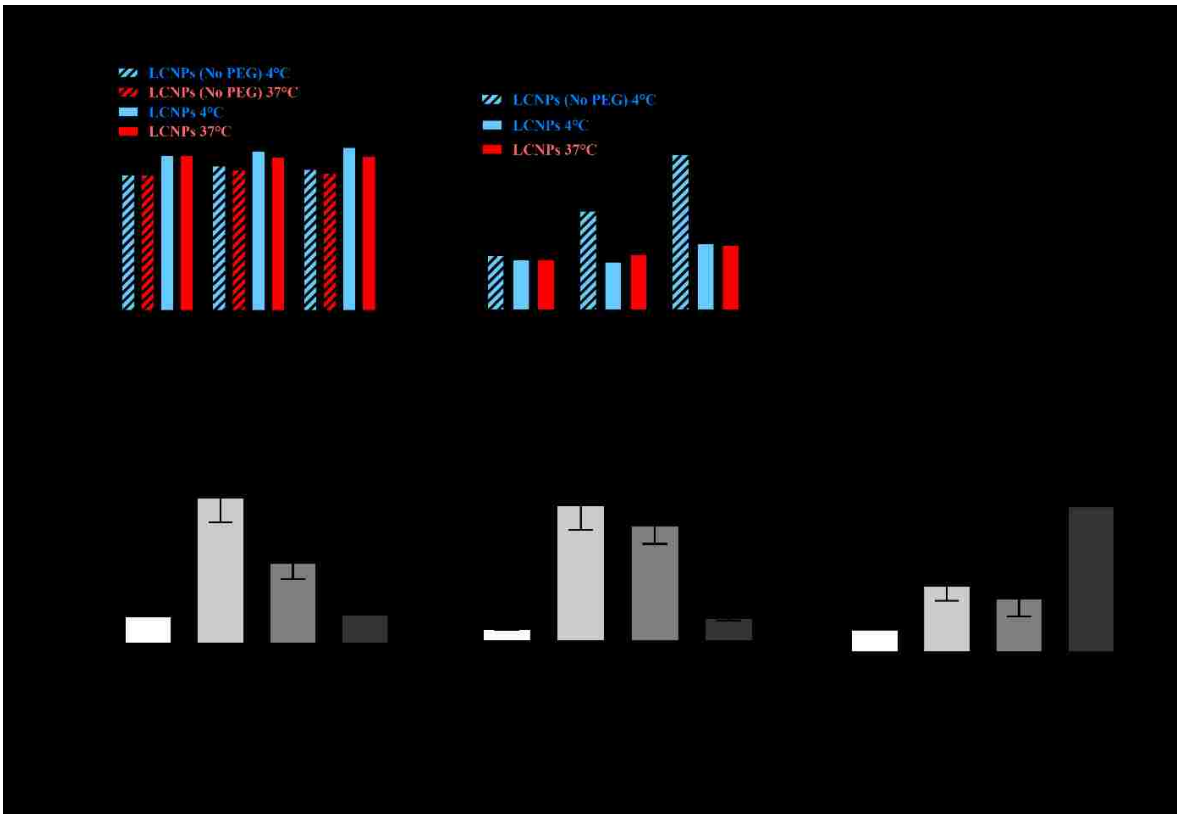

Figure S1. Stability of lipid-coated PLGA nanoparticles (LCNPs). LCNP formulations were incubated in water (A) or PBS (B) at 4°C or 37 °C and size measurements were taken by dynamic light scattering (DLS) at the indicated time points. LCNPs without the PEG surface modification (LCNP (No PEG)) aggregated immediately in PBS at 37°C and the size was above the instrument detection limit. (C) Tipranavir (TPV) loaded LCNPs surface conjugated with α4β7 mAb were incubated in human serum for 14 days at 37 °C, and the size was measured by NanoSight. (D) Effect of trehalose (1 mg/mL or 2 mg/mL) on stability of size (left), PDI (middle) and ζ-potential (right) of lyophilized LCNPs. Data represents mean ± SD, n=3. * $p < 0.05$ **, $p < 0.005$ ***, $p < 0.0005$, n.s. not statistically significant.

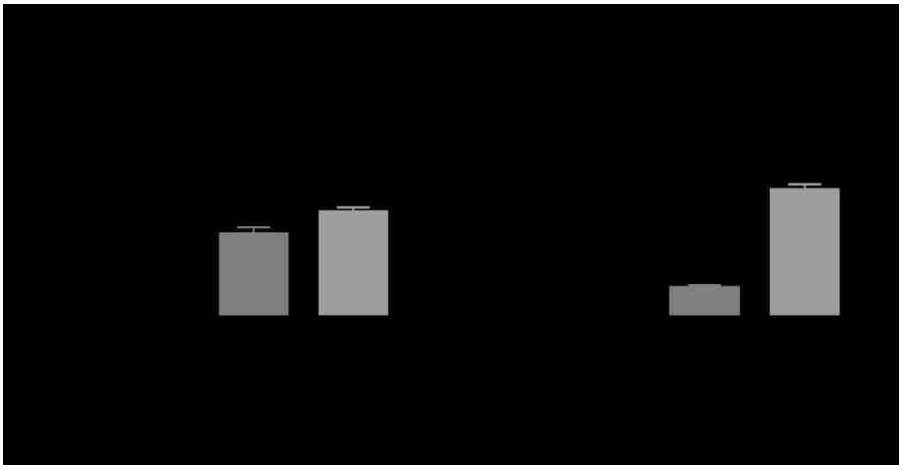

Figure S2. TPV drug loading (A) and encapsulation efficiency (B) when formulated in bare LCNP (TPV/LCNP), LCNP surface conjugated with α4β7 mAb (TPV/A4B7-LCNP) or liposome (TPV/Liposome). Data represents mean ± SD, n=3.

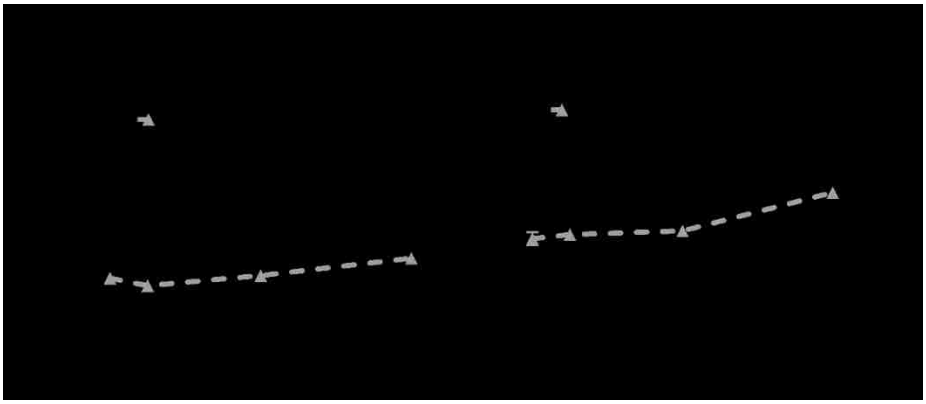

Figure S3. Delamination kinetics of fluorescently-labeled lipids DOPC-NBD (A) and DSPE-PEG-CF (B) from LCNPs in PBS at 37 °C or 4 °C. Data represents mean ± SD, n=3.

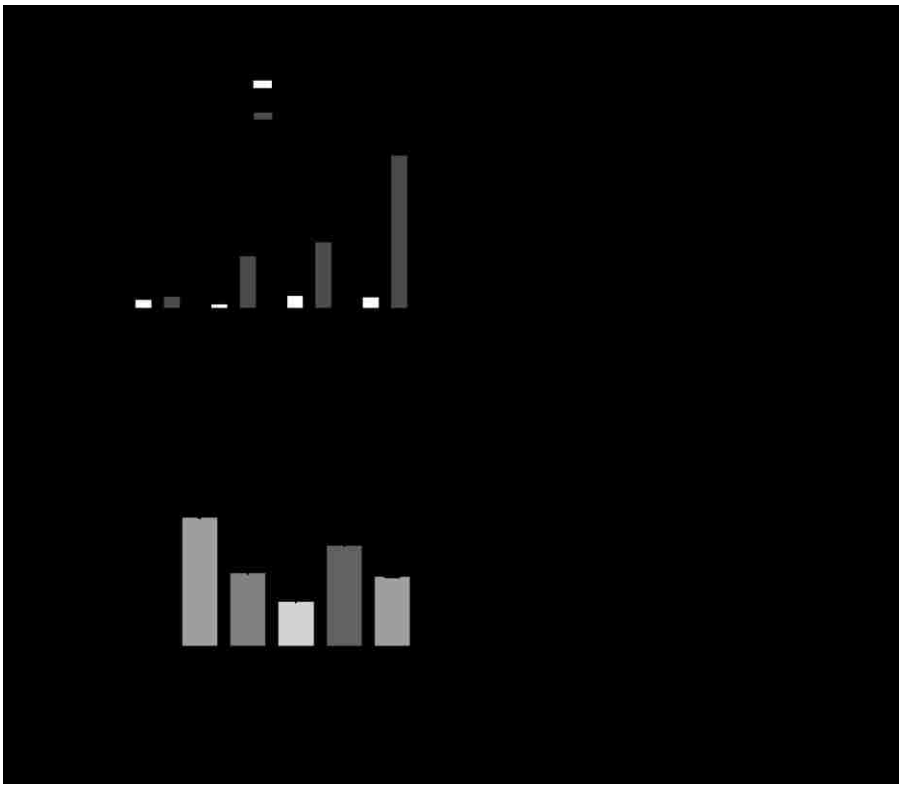

Figure S4. (A) Analysis of α4β7 expression on different T cell lines. Mean fluorescent intensity (MFI) of human T cell lines treated with anti-α4β7 APC at 4 °C for 30 min analyzed by flow cytometry. (B) Titration of APC conjugated α4β7 mAb (anti-α4β7 APC) used for cell-surface marking. MFI of HUT-78 cells treated with different concentration of anti-α4β7 APC at 4 °C for 30 min is analyzed by flow cytometry. (C) MFI of HUT-78 cells associated with rhodamine B labeled LCNPs, A4B7-LCNPs or Iso-LCNPs after 30 min incubation at 4°C. A receptor blocking study was done by blocking HUT 78 cells with soluble α4β7 mAb for 30 minutes, and then treating with different LCNP formulations. (D) MFI of HUT-78 cells decreased over time following 30 min incubation with anti-α4β7 APC and removal of free mAbs. *$p<0.05$, **$p<0.005$ ***$p<0.0005$, n.s., not statistically significant.

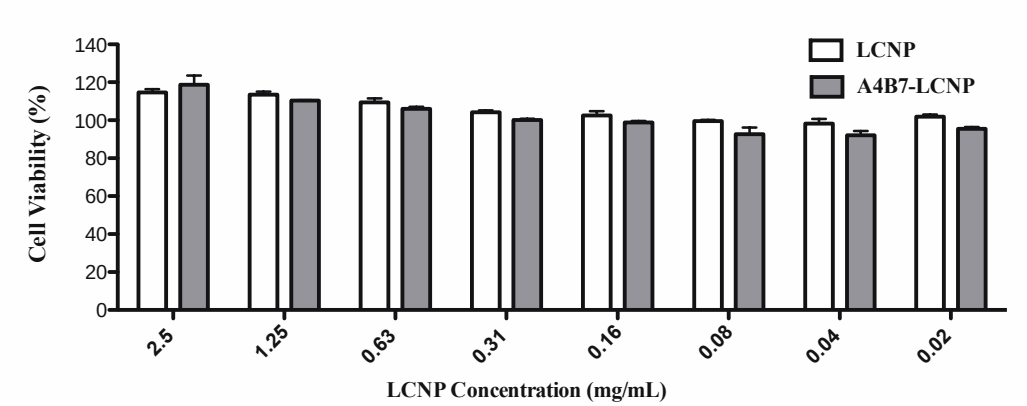

Figure S5. LCNPs and α4β7 mAb conjugated LCNPs (A4B7-LCNPs) showed no cytotoxicity to the HUT-78 cell line. Cell were incubated with LCNPs or A4B7-LCNPs at different concentrations for two days. Data represents mean ± SD, n=3.

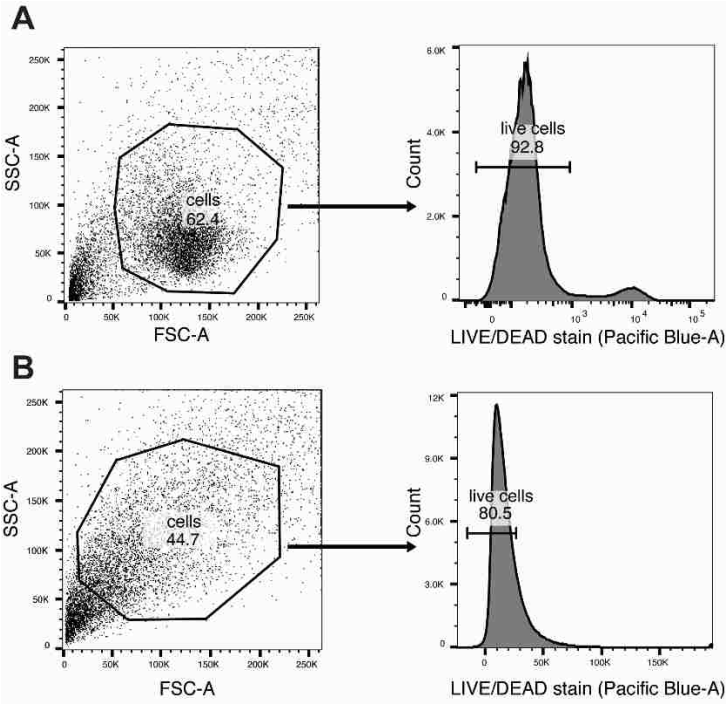

Figure S6. Representative flow cytometry gating strategies for analysis of (A) LPLs from rhesus macaque ileum for Figure 4, or (B) LPLs from mouse small intestines for Figure 6.

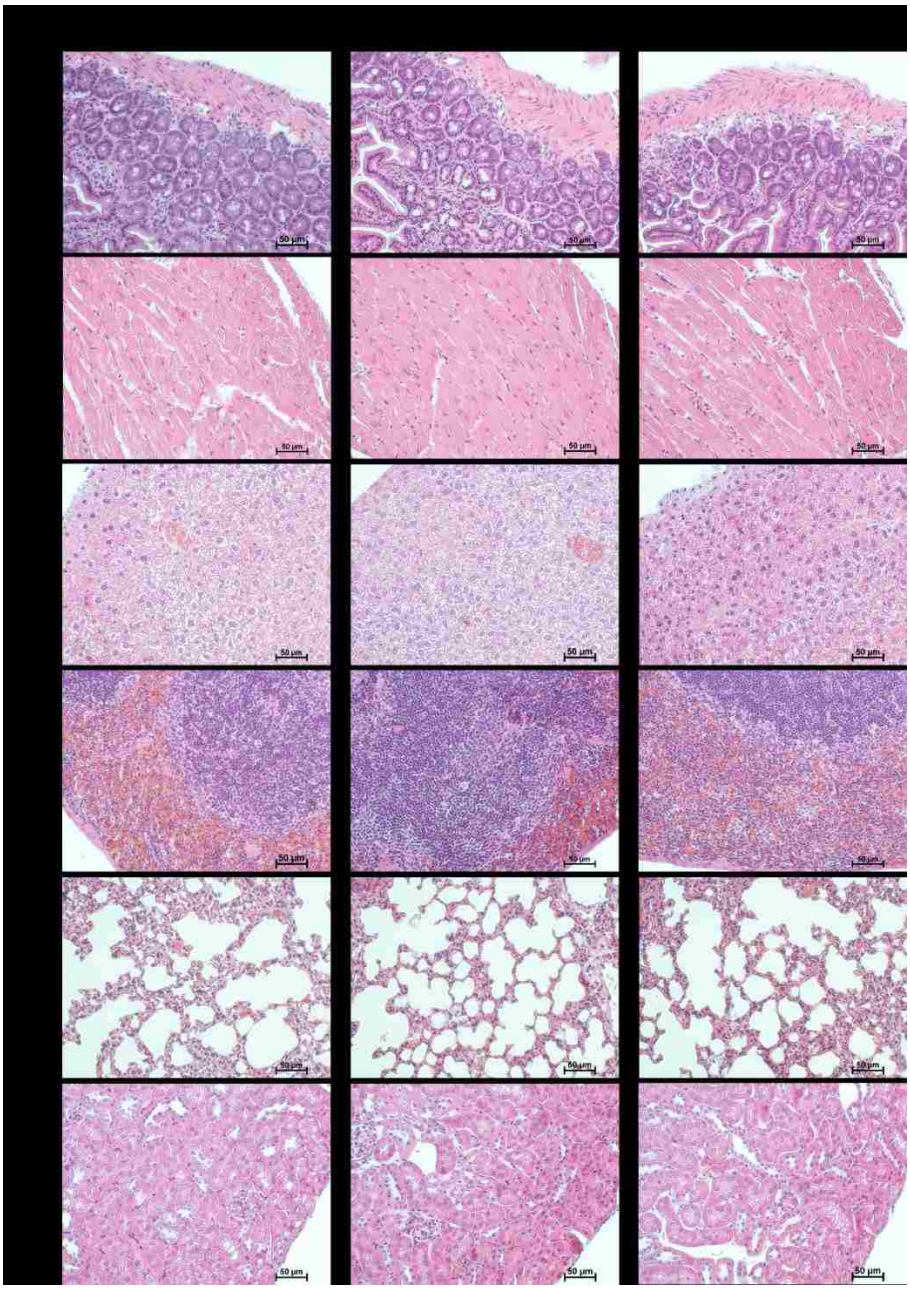

Figure S7. H&E staining of tissue slides from mice treated with 0.2 mL PBS, 50 mg/kg A4B7-LCNPs or 50 mg/kg Iso-LCNPs. The bar indicates 50 μm.

Figure S8. Dose of DiR loaded A4B7-LCNP or Iso-LCNPs in major organs or plasma of mice after intravenous administration. Data represents mean ± SD, n=4 mice per group.

Appendix III: Supplementary information for Chapter 5

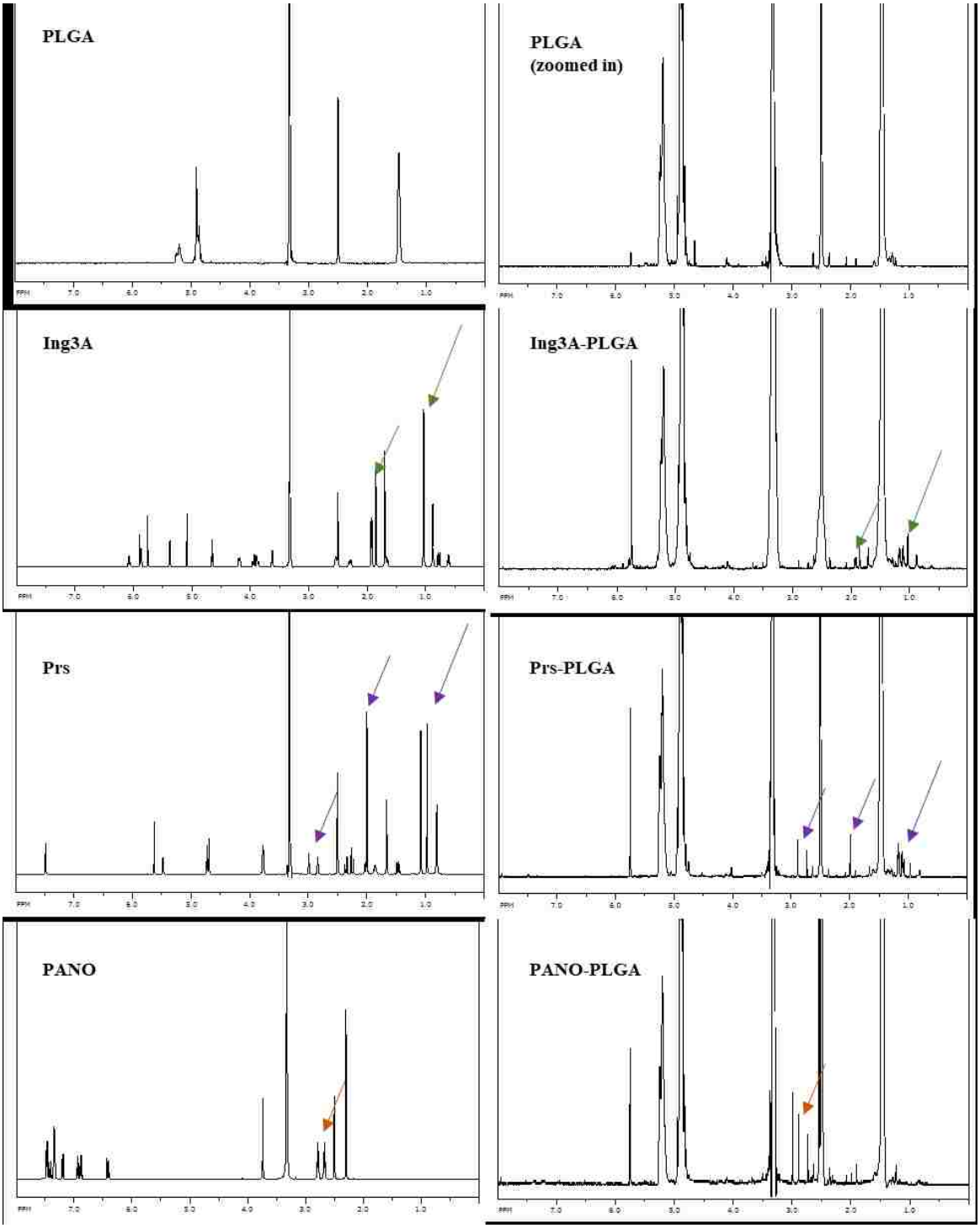

Figure S1. H-NMR analysis of PLGA, LRA and PLGA-LRA conjugates. Arrows indicate chemical shifts from LRAs. All shifts from LRAs in the conjugates were low due to conjugation of LRA (low m.w.) to PLGA (high m.w.) at 1:1 molar ratio.

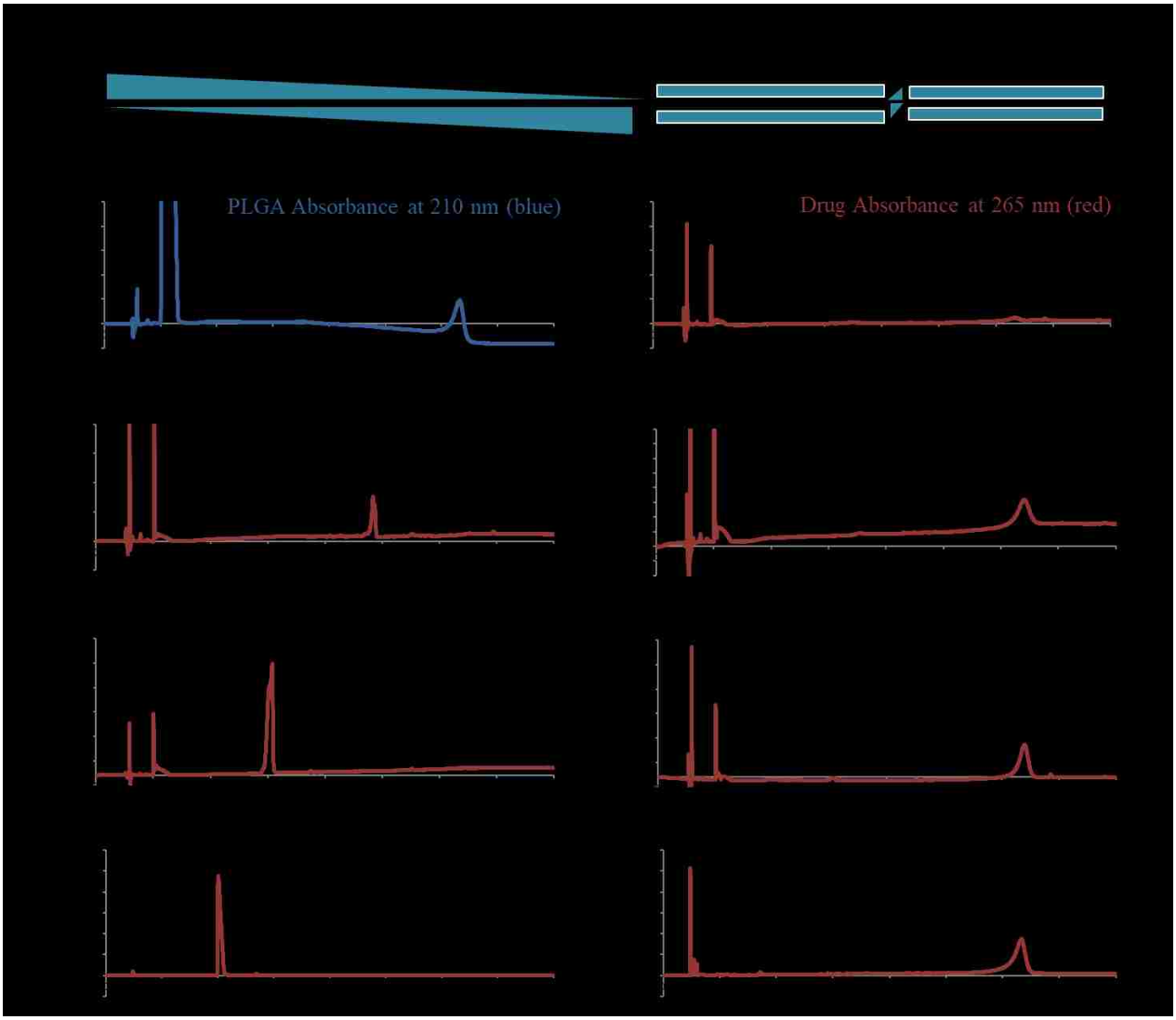

Figure S2. HPLC analysis of PLGA-LRA conjugates. (a) Water-acetonitrile (ACN) gradient eluting method for high performance liquid chromatography (HPLC) analysis of free LRA, PLGA and PLGA-LRA conjugates. **(b)** HPLC analysis of PLGA at 210 nm (blue) or 265 nm (red) wavelength, and free LRA and PLGA-LRA conjugates at 265 nm wavelength. PLGA and PLGA-LRA conjugates were eluted at 30-35 min.

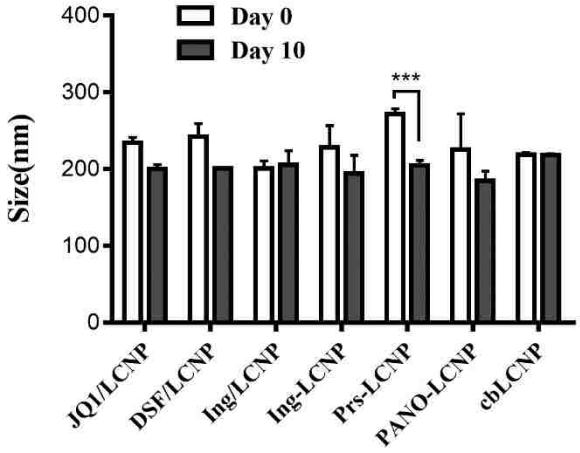

Figure S3. Colloidal stability of LRA loaded LCNPs. LCNPs were incubated in cell culture media at 37 °C for 10 days. Sizes were measured by DLS. Statistical significance was calculated using two-way ANOVA with Bonferroni's test. *** $p<0.0005$, otherwise not significant between day 1 and day 10. Data represent mean ± s.d.; $n = 3$.

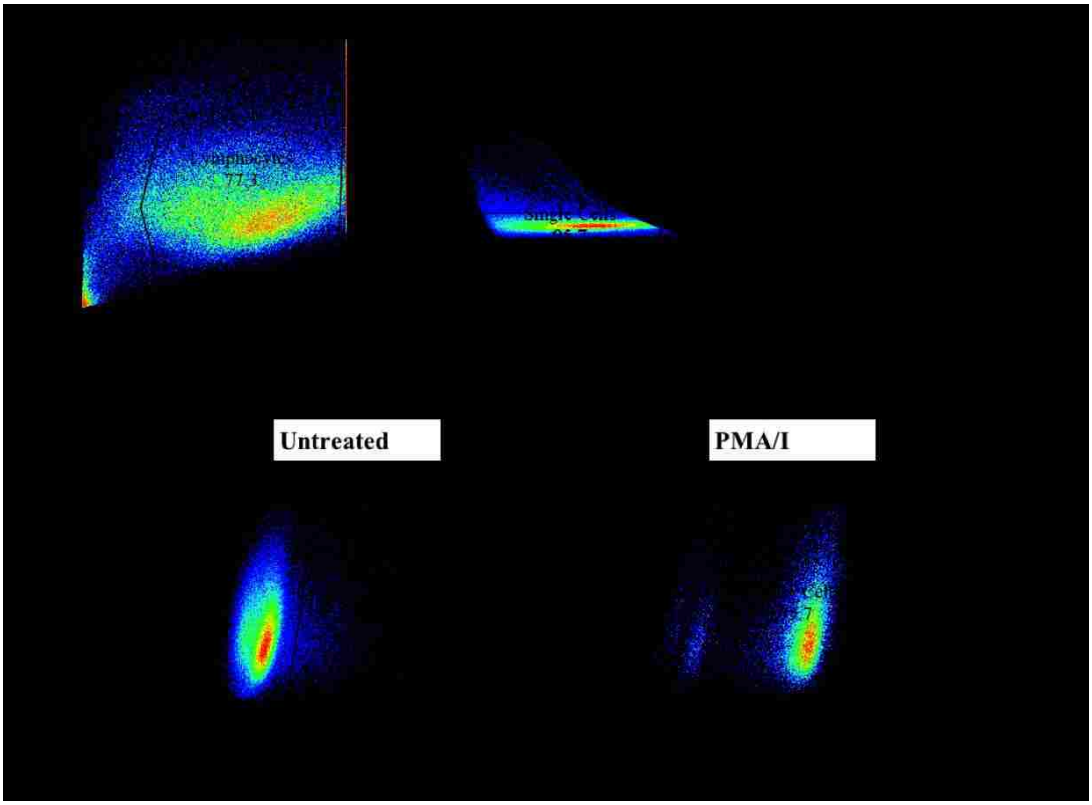

Figure S4. Flow cytometry dot plots showing the entire gating strategy utilized to identify GFP+ cell populations of J-Lat A1 cells. This gate strategy is applied to Figure 5.2B&C, Figure 5.3B, and Figure S5a&S6a.

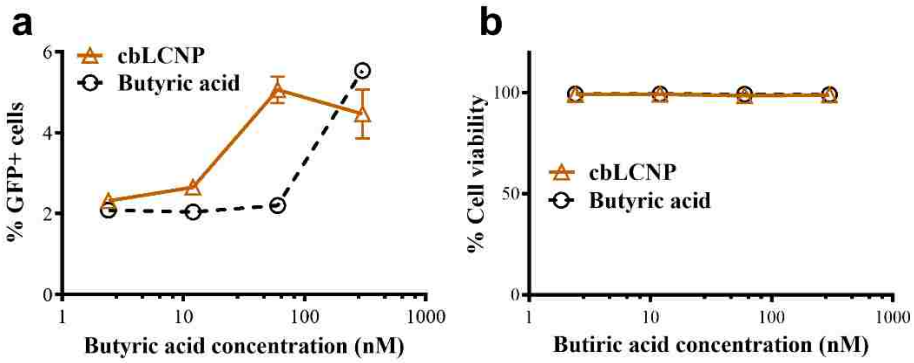

Figure S5. *In vitro* dose-response HIV-1 latency reversal and cytotoxicity by free butyric acid or its prodrug inserted into LCNPs. (a) Dose-response curve for latent HIV reactivation (indicated as a percentage of GFP+ cells) on J-Lat A1 cells incubated with butyric acid or cbLCNPs for 20 hours. cbLCNP: LCNPs with cholesteryl butyrate inserted into the lipid layer. (b) Cell viability after treating with butyric acid or cbLCNPs for 20 hours. Data represent mean ± s.d.; $n = 3$.

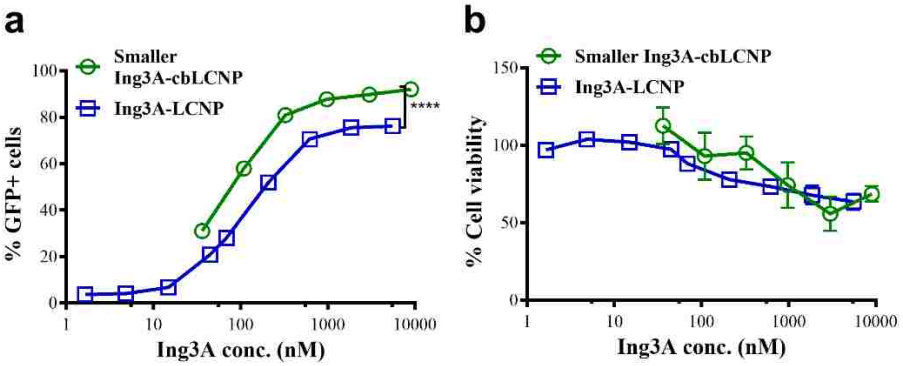

Figure S6. *In vitro* dose-response HIV-1 latency reversal and cytotoxicity by smaller Ing3A-cbLCNP compared to previous Ing3A-LCNP formulation. (a) Dose-response curve for latent HIV reactivation (indicated as a percentage of GFP+ cells) on J-Lat A1 cells incubated with smaller Ing3A-cbLCNPs (green circle) for 20 hours. The curve from previous Ing3A-LCNPs (blue square) was included here from main Figure 5.2B for comparison. (b) Cell viability after treating with smaller Ing3A-cbLCNPs for 20 hours. The cytotoxicity curve from previous Ing3A-LCNPs was included here from Figure 5.2D for comparison. Statistical analysis was performed using unpaired Student's *t* test after best-fit values from the nonlinear regression analysis. **** $p < 0.0001$. Data represent mean ± s.d.; $n = 3$.

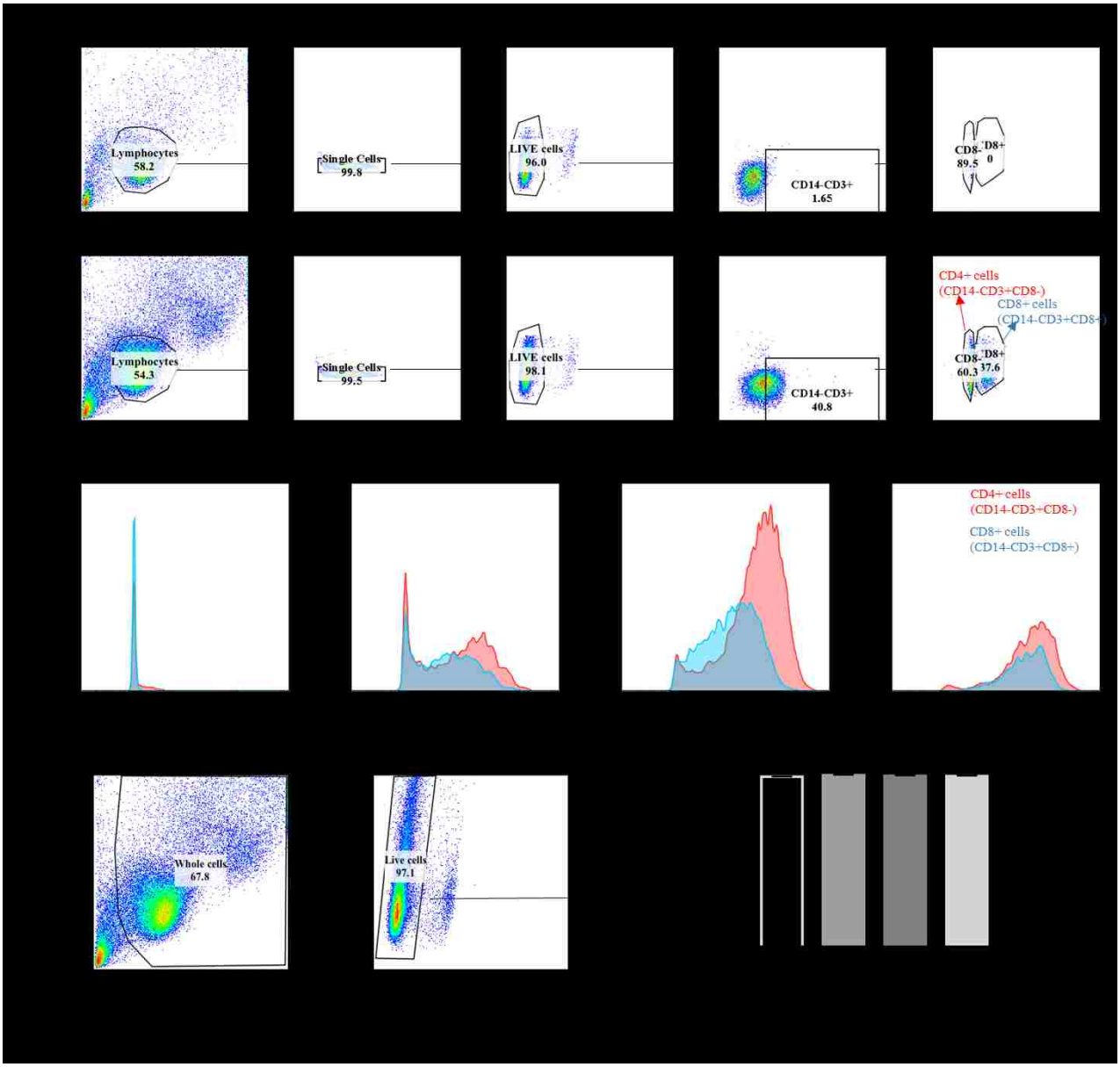

Figure S7. Comparison of CD69 expression between CD8+ and CD4+ T cells from non-human primates (NHP) PBMCs after treating with Ing3A formulations. (a,b) Flow cytometry dot plots showing the entire gate strategy utilized to distinguish CD4+ (CD14-CD3+CD8-) and CD8+ (CD14-CD3+CD8-) T cells in NHP PBMCs. Isotype control is shown in (a). Gate strategy for CD4+ T cells (CD14-CD3+CD8+) were chosen instead of direct anti-CD4 staining because that CD4-targeted LCNPs could block anti-CD4 staining. (c) Histograms of mean fluorescence intensity of CD69 expression by the indicated CD8+ (blue) or CD4+ (red) T cell subsets in NHP PMBCs. PBMCs were treated with free Ing3A, bare LCNPs, CD4-targeted LCNPs and isotype LCNPs for 20 hours. CD69 MFI data were plotted in Figure 5.5B. (d) Flow cytometry dot plots showing the gate strategy utilized to identify live cells from whole PBMC cells. Percentages of live cells after incubation with various Ing3A formulations are plotted in the right bar graph. Data represent mean ± s.d.; n = 3.

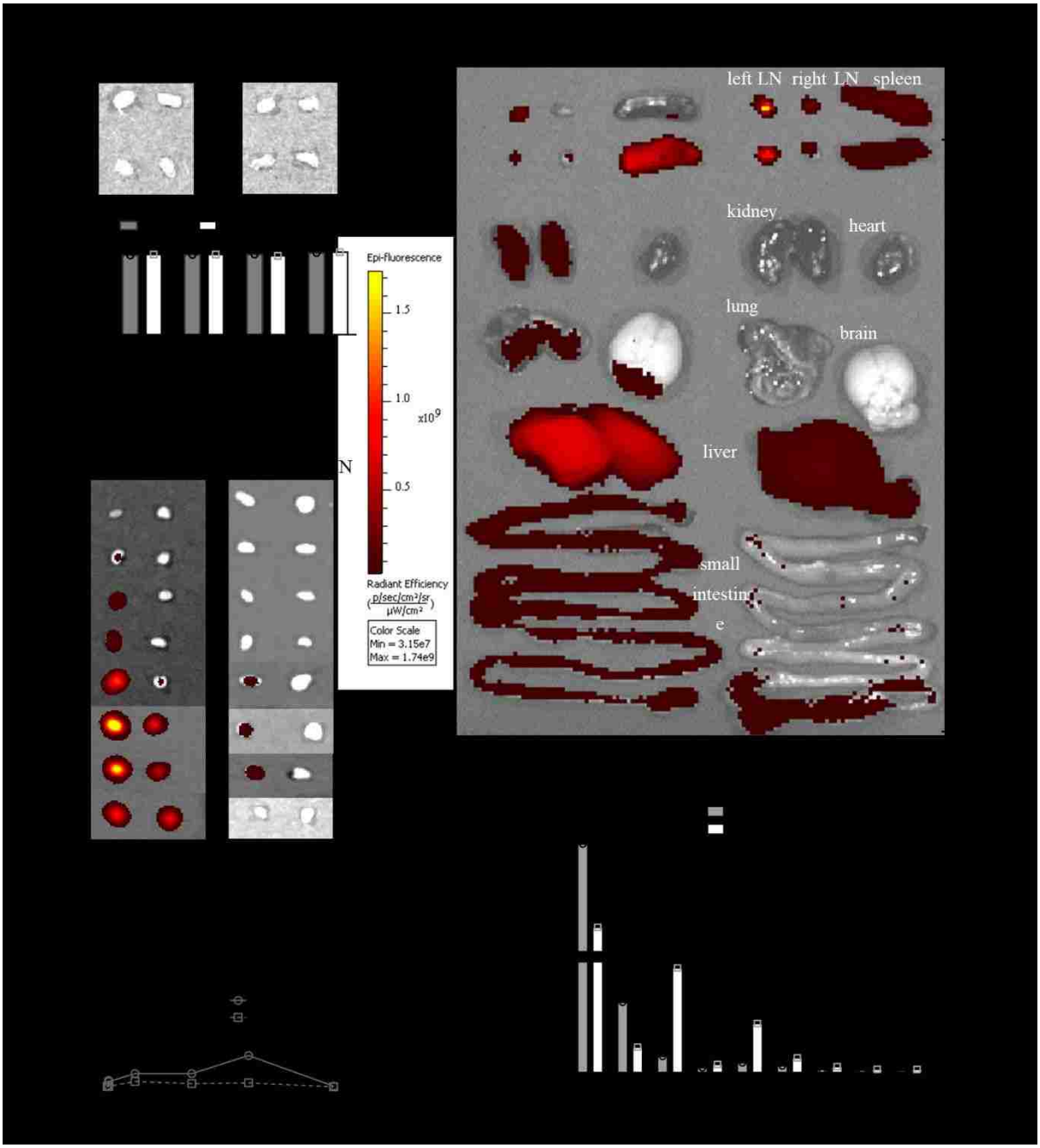

Fig. S8. Pilot mouse studies comparing biodistribution of different LCNP formulations. (a) Fluorescent images of inguinal lymph nodes (LNs) of mice after being subcutaneously injected with PBS or DiR labeled dtLCNPs (neutral LCNPs with DOTAP in the lipid bilayer) at 1 hour or 1 day. Fluorescent signals were not observed from both left and right LNs. Average radiant efficacies from those LNs were plotted below. **(b)** Fluorescent images of LNs of mice at different time points post-administration of DiR dye labeled cbLCNPs (negatively-charged LCNPs with cholesteryl butyrate inserted into the lipid bilayer) or equivalent free DiR dye (86 µg/mL DiR). Average radiant efficacies from those LNs were plotted below. **(c)** Fluorescent images of LNs and other major organs of mice after being subcutaneously injected with 200 nm or 100 nm DiR labeled cbLCNPs (25 µg/mL DiR) at 20 hours or 3 days. Total fluorescent signal normalized by tissue mass were plotted below. All fluorescent images share the same scale bar in the middle.

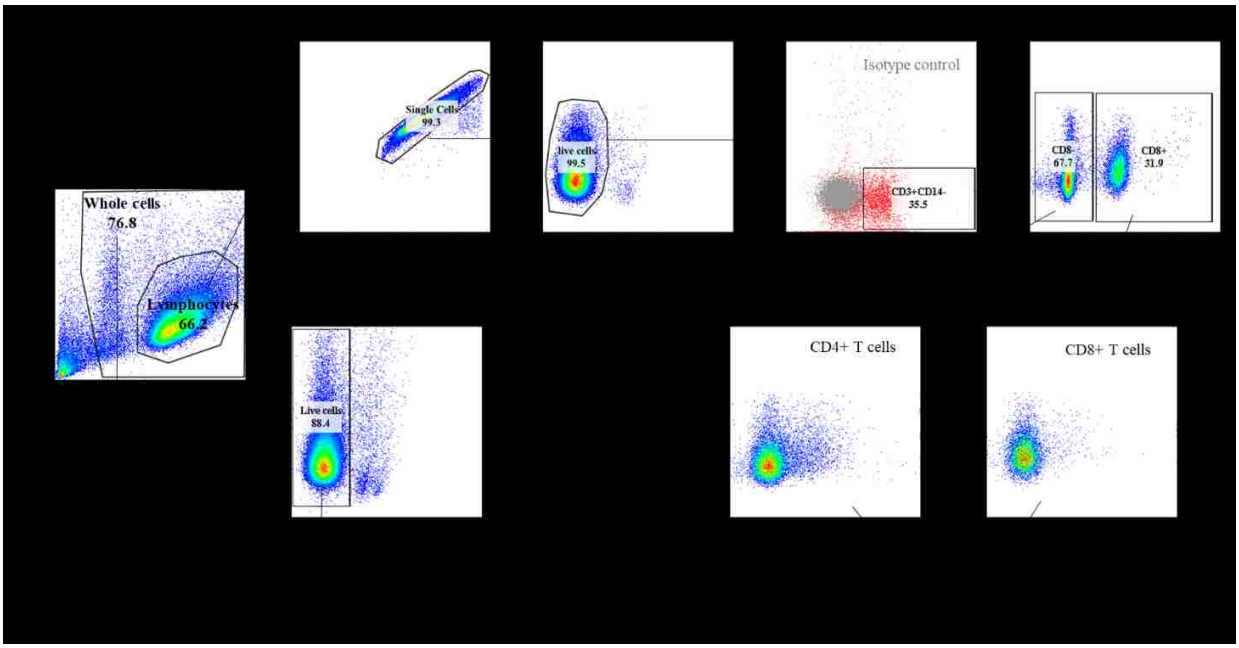

Figure S9. Flow cytometry dot plots showing the entire gating strategy applied in Figure 5.6A&B. Percentage of live cells in Figure 5.6B were gated from whole cells that include dead cells and other cell populations. Mean fluorescent intensity (MFI) of CD69 expression from distinguish CD4+ (CD14-CD3+CD8-) and CD8+ (CD14-CD3+CD8+) T cells were plotted in Figure 5.6A. The Figure 5.6C used a similar gating strategy, except for measuring MFI of DiD fluorescent signal instead of CD69-APC. Isotype control is shown in grey.

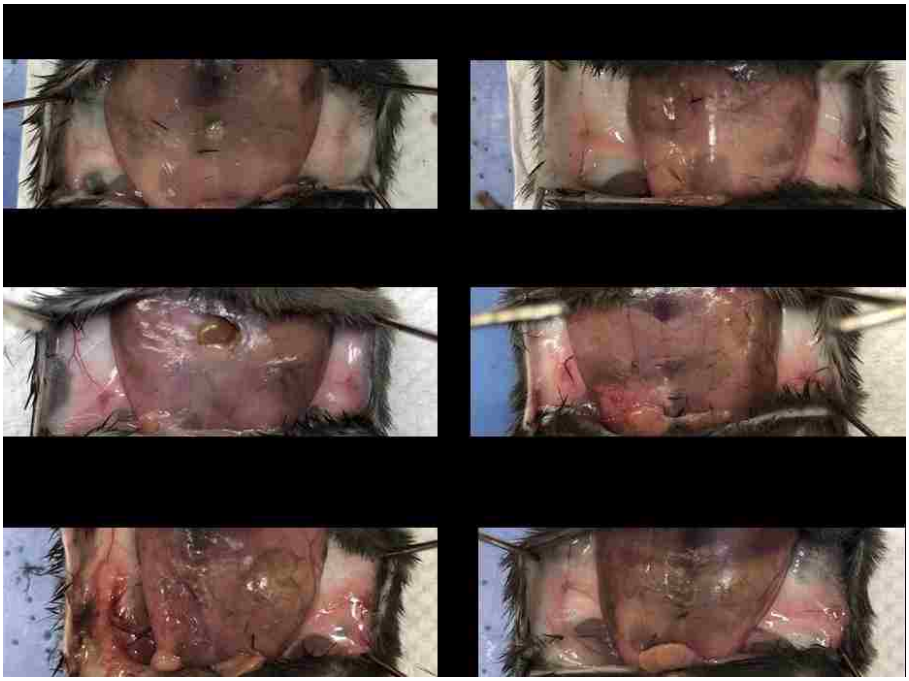

Figure S10. Representative images of mouse subcutaneous tissues at day 3 post-administration of different Ing3A formulations. Substances were injected subcutaneously into the left side flank of mice.

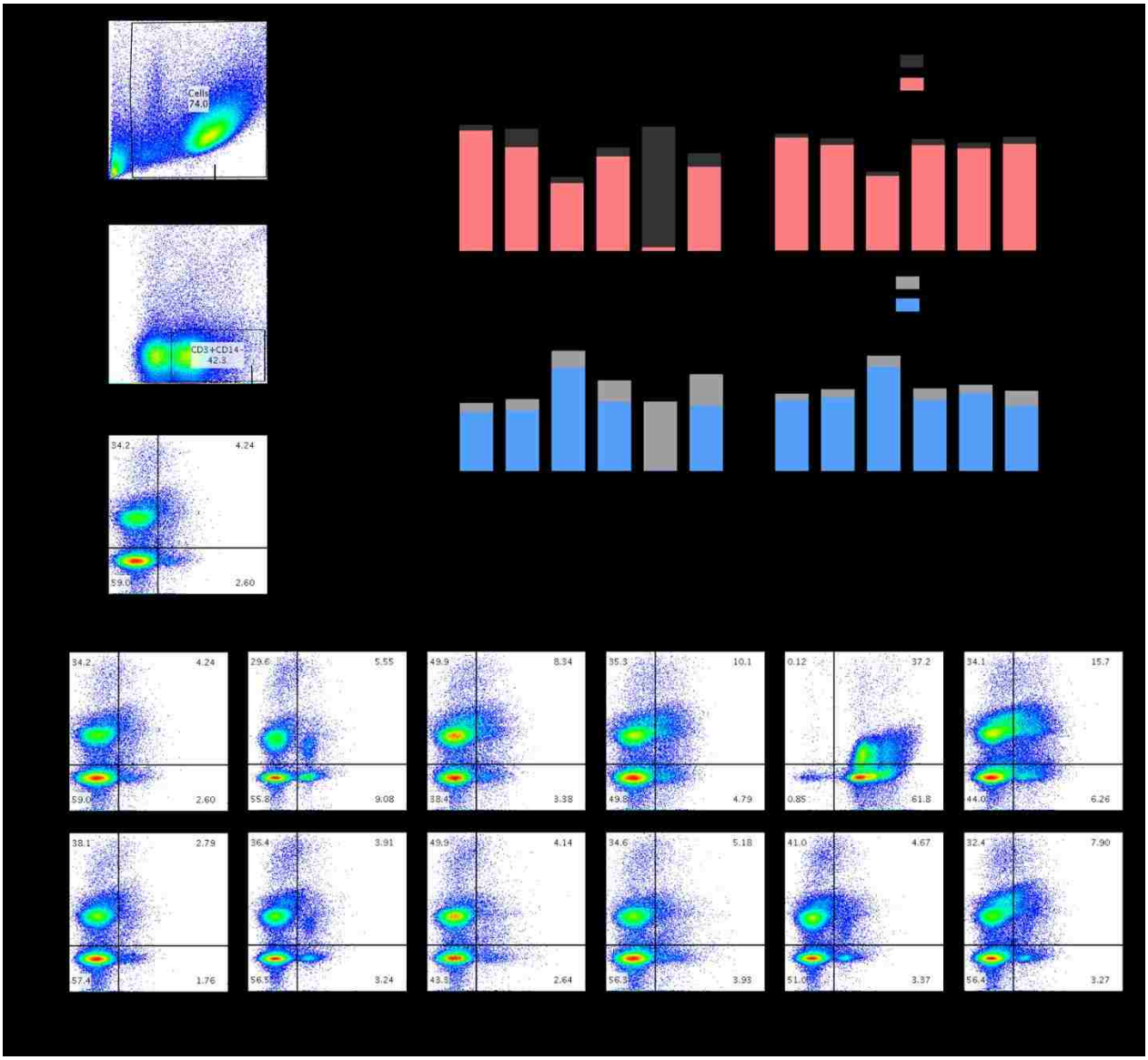

Fig. S11. Targeted LCNP-formulated Ing3A is nontoxic to CD4+ and CD8+ T cells in mice lymph nodes after subcutaneous dosing. (a) Flow cytometry dot plots of primary cells isolated from mice inguinal lymph nodes, showing the gating strategy applied in Fig. 11B, C. **(b)** Percentage of live or dead CD4+ (CD14-CD3+CD8-) and CD8+ (CD14-CD3+CD8+) T cells from CD3+CD14- cell populations in mice left or right inguinal lymph nodes at 20 hours after treatments. Data represent mean. **(c)** Representative flow cytometry dot plots for Fig. 11B. n = 3 mice per group.

Table S1. Physicochemical properties of LCNP formulated LRAs with unsatisfactory low drug loading.

LRAs	Prs[a]	Romidepsin	
Molecular Target	PKC	HDAC	
[b]Formulation Strategy	Single-emulsion (EtOAc)	Single-emulsion (EtOAc)	Single-emulsion (DCM)
[c]Size (d, nm)	209.0 ± 3.3	176.0 ± 2.9	234.0 ± 0.8
[c]Polydispersity Index	0.06 ± 0.01	0.06 ± 0.01	0.11 ± 0.05
Drug Input (wt%)	5	5	5
Drug Loading (wt%)	**<0.01**	**0.02 ± 0.002**	**0.18 ± 0.02**
[d]EE (%)	**<0.2**	**0.4 ± 0.2**	**3.8 ± 0.4**

[a]Data for Prs (prostratin) were from cbLCNP formulation with chol-but inserted into lipid layer;
[b]LRAs were dissolved in ethyl acetate (EtOAc) or dichloromethane (DCM) with PLGA following single-emulsion evaporation method;
[c]Size and polydispersity index were measured by DLS. Data present mean ± s.d., $n = 3$.
[d]EE: encapsulation efficiency is the ratio of the actual loading (wt%) to the drug input (wt%) expressed as a percentage.

Table S2. Physicochemical properties of LCNPs made of various PLGA.

[a]PLGA	Resomer®					Lactel®
	752H	**502H**	**503H**	**505**	**756S**	**B6013-2**
L:G ratio	72:25	50:50	50:50	50:50	72:25	75:25
Molecular Weight	4,000-15,000	7,000-17,000	24,000-38,000	54,000-69,000	76,000-115,000	~70,000-115,000[b]
End group	Acid	Acid	Acid	Ester	Ester	Ester
Transition Temperature (°C)	42-46	42-46	44-48	48-52	49-55	NA
Viscosity (dL/g, in chloroform)	0.14-0.22	0.16-0.24	0.32-0.44	0.61-0.74	0.71-1.0	0.55-0.75
[c]Size (d, nm)	194.2 ± 3.7	204.0 ± 34.6	165.9 ± 0.6	174.9 ± 2.8	181.6 ± 2.6	193.0 ± 1.9
[c]PDI	0.24 ± 0.01	0.23 ± 0.04	0.06 ± 0.05	0.08 ± 0.03	0.04 ± 0.01	0.07 ± 0.02
[c]ζ-potential (mV)	4.1 ± 0.6	8.1 ± 0.6	15.2 ± 1.7	17.3 ± 0.2	19.0 ± 0.4	9.4 ± 2.2
[d]Colloidal Stability	<1 d	<1 hr	>5 d	>5 d	>5 d	>5 d

[a]Properties of PLGA, including lactide:glycolide (L:G) ratio, molecular weight, end group, transition temperature, and viscosity were obtained from manufacturer's websites.
[b]Molecular weight of Lactel® PLGA is estimated based on its inherent viscosity using online sources.
[c]Size, PDI (polydispersity index), and ζ-potential were measured by DLS. Data present mean ± s.d.; $n = 3$.
[d]Colloidal stability is indicated as the time when the particle size changes and the PDI becomes larger than 0.3 in a physiological condition (cell culture media).

Table S3. Parameters from fitting to LRA release kinetics.

Treatment	Term	Estimate	Error	Statistic	P-Value	Release (%) at 20 hours
JQ1/LCNP	K	51.18587	3.637391	14.07214	4.32E-13	89.0646
	n	0.076936	0.017397	4.422411	0.00018	
	K0	38.59328	3.398875	11.35472	3.89E-11	
DSF/LCNP	K	43.15689	5.442451	7.92968	9.48E-08	53.9556
	n	0.270607	0.039021	6.934945	7.51E-07	
	K0	12.88075	4.74881	2.712416	0.013046	
Ing3A/LCNP	K	48.04601	7.163138	6.707397	1.23E-06	38.6922
	n	0.333127	0.049355	6.74961	1.12E-06	
	K0	-6.51646	6.101818	-1.06795	0.297665	
Ing3A-LCNP	K	7.978264	1.036291	7.698865	6.18E-08	3.9318
	n	0.584354	0.035957	16.25155	1.87E-14	
	K0	-3.23853	1.20181	-2.69471	0.012659	
Prs-LCNP	K	5.603765	0.541304	10.35235	2.49E-10	2.7266
	n	0.702044	0.02742	25.60345	6.17E-19	
	K0	-2.20247	0.738635	-2.98181	0.00648	
PANO-LCNP	K	47.76548	6.733931	7.093254	5.36E-07	43.5120
	n	0.244131	0.03581	6.8175	9.67E-07	
	K0	-2.16963	5.828599	-0.37224	0.713446	

$D(t) = Kt^n + K_0$

LRA/LCNP: LRA was physically encapsulated into LCNPs;
LRA-LCNP: LRA was chemically conjugated to the PLGA.

Table S4. Parameters from fitting to LRA dose-responsive curve.

Treatment	Slope	Lower Asymptote	Upper Asymptote	ED_{50} (nM)	rss
Free JQ1	-0.952364472	1.792652141	17.7039573	527.2488977	0.2392336006
JQ1/LCNP	-0.859372275	1.686678936	22.99286216	724.2970616	0.6315654068
Free DSF	-4.394655497	2.096852241	12.34579196	6018.806782	1.022873701
DSF/LCNP	-7.205209276	2.978245138	29.76341519	8494.777986	0.7526946443
Free Ing3A	-1.135179667	1.264189559	88.2731729	12.94915491	0.760276042
Ing3A/LCNP	-1.123422048	1.174486132	90.80389617	10.92800672	0.4822496735
Ing3A-LCNP	-1.246198532	2.439440274	77.57906768	116.4025408	0.9142957024
Free Prs	-1.849678762	1.888034372	84.616624	667.3110757	0.0955698905
Prs-LCNP	-1.34247879	2.983788141	100.1273641	27702.77825	0.4617669071
Free PANO	-1.683672937	2.453852081	79.20236538	22.74938412	0.8967216535
PANO-LCNP	-1.932296976	1.19373663	75.39156718	82.18765588	1.795007682

$f(x) = c + \frac{d-c}{1+e^{b(\log x - \log e)}}$

b = slope, e = ED50, c = lower asymptote, d = upper asymptote; rss, residual summary of squared error;
LRA/LCNP: LRA was physically encapsulated into LCNPs;
LRA-LCNP: LRA was chemically conjugated to the PLGA.

Table S5. Synthesis optimization for ultrasmall LCNPs.[a]

Formulations	PLGA (mg/mL)	Lipids (mg/mL)	Organic: Aqueous Ratio	Size, Z-ave (d, nm)	Size, Number Mean (d, nm)	Polydispersity Index
Original	10	1	1 : 2	219.27	196.83	0.057
Varying PLGA Concentration	1	1	1 : 2	172.72	113.07	0.144
	5	1	1 : 2	190.57	148.53	0.11
	20	1	1 : 2	260.53	210.43	0.132
Varying Organic: Aqueous Ratio	5	1	1 : 4	158.79	99.59	0.164
	5	1	1 : 6	235.7	91.34	0.305
	10	1	1 : 2.5	193.13	158.27	0.086
	10	1	1 : 4	166.4	126.07	0.113
	10	1	1 : 6	155.63	99.38	0.186
	10	1	1 : 10	246.07	98.59	0.213
Varying Lipid Concentration	5	2	1 : 4	183.74	93.79	0.287
	10	**2**	**1 : 4**	**146.2**	**100.04**	**0.141**
	10	3	1 : 4	168.03	94.05	0.244

[a]LCNP sizes were measured by dynamic light scattering (DLS) and presented as both Z-ave and number mean here. $n = 1$.

Appendix IV: Publications and presentations from this work

Publications

1. **Cao S**, Slack SD, Levy CN, Hughes SM, Jiang Y, Yogodzinski C, Roychoudhury P, Jerome KR, Schiffer JT, Hladik F, and Woodrow KA. Hybrid nanocarriers incorporating mechanistically distinct drugs for lymphatic CD4+ T cell reactivation and HIV latency reversal. *In revision.*
2. **Cao S**, Woodrow KA. Nanotechnology approaches to eradicating HIV reservoirs. *European Journal of Pharmaceutics and Biopharmaceutics.* 2018. In press. DOI: 10.1016/j.ejpb.2018.06.002
3. **Cao S**, Jiang Y, Zhang H, Kondza N, Woodrow KA. Core-shell nanoparticles for targeted and combination antiretroviral activity in gut-homing T cells. *Nanomedicine: Nanotechnology, Biology and Medicine.* 2018;14(7):2143-2153.
4. **Cao S**, Jiang Y, Levy CN, Hughes SM, Zhang H, Hladik F, and Woodrow KA. Optimization and comparison of CD4-targeting lipid-polymer hybrid nanoparticles using different binding ligands. *Journal of Biomedical Materials Research Part A.* 2018;106(5):1177-1188.
5. Krogstad EA, Ramanathan R, Nhan C, Kraft JC, Blakney AK, **Cao S**, Ho RJY, Woodrow KA. Nanoparticle-releasing Nanofiber Composites for Enhanced In Vivo Vaginal Retention. *Biomaterials.* 2017;11(144):1-16.
6. Jiang Y, **Cao S**, Bright DK, Bever AM, Blakney AK, Suydam IT, Woodrow KA. Nanoparticle-Based ARV Drug Combinations for Synergistic Inhibition of Cell-Free and Cell–Cell HIV Transmission. *Molecular pharmaceutics.* 2015;12(12):4363-74.

Presentations at National Conferences (presenter)

1. **Cao S**, Jiang Y, S.M. Hughes SM, Levy CN, Hladik F, and Woodrow KA. "Optimization and comparison of CD4-targeting lipid-polymer hybrid nanoparticles using different binding ligands" Society for Biomaterials Annual Meeting & Exposition. April 11-14, 2018. Atlanta, GA. Oral presentation.
2. **Cao S**, Jiang Y, Slack SD, Yogodzinski C, Hughes SM, Levy CN, Schiffer JT, Hladik F, Jerome KR, and Woodrow KA. "Lipid-polymer hybrid nanoparticles incorporating mechanistically distinct drugs for HIV cure" 2nd Bioengineering and Translational Medicine Conference. October 28-29, 2017, Minneapolis, MN. Oral presentation.
3. Creighton R, Ebner ME, Afunugo WE, Bever A, **Cao S**, Jiang Y, Woodrow KA, Suydam IT, "A prodrug strategy to improve drug loading and determine intracellular release from nanoparticle systems" BMES 2017 Annual Meeting. October 11-14, 2017, Phoenix, AZ. Oral presentation.
4. Afunugo WE, Ebner ME, Bever A, **Cao S**, Jiang Y, Woodrow K, Suydam IT, "Enhanced delivery of HIV integrase inhibitors with prodrugs designed for polymeric nanocarriers." 253rd American Chemical Society National Meeting & Exposition. April 2-6, 2017, San Francisco, CA. Poster presentation.
5. **Cao S**, Jiang Y, Zhang H, Kondza N, Woodrow KA, "In vivo targeting of gut-homing T cells with a dual-functional conjugated to lipid-polymer hybrid nanocarriers for HIV treatment" 7th

International Conference on Bioengineering and Nanotechnology. March 19-22, 2017, Chicago, IL. Oral presentation.

6. **Cao S**, Jiang Y, Kondza N, Woodrow KA, "Targeted co-delivery of dual-function monoclonal antibody and tipranavir to gut-homing T cells using lipid-coated PLGA nanoparticles" 43rd Annual Meeting & Exposition of the Controlled Release Society. July 17-20, 2016, Seattle, Washington. Poster presentation.
7. **Cao S**, Jiang Y, Woodrow KA, "Lipid-coated PLGA nanoparticles conjugated with a dual-function antibody for targeted delivery of ARVs to α4β7 expressing T cells" 13th International Nanomedicine and Drug Delivery Symposium. September 16-18, 2015, Seattle, Washington. Poster presentation.
8. Afunugo WE, Ebner ME, Jiang Y, **Cao S**, Woodrow KA, "Raltegravir prodrugs for improved nanoparticle delivery" 13th International Nanomedicine and Drug Delivery Symposium. September 16-18, 2015, Seattle, Washington. Poster presentation. Poster presentation.
9. Suydam IT, Ebner ME, Afunugo WE, Bever AM , Jiang Y, **Cao S**, Woodrow KA "Raltegravir Prodrugs for Improved Nanoparticle Delivery" 42nd Annual Meeting &Exposition of the Controlled Release Society. July 26-29, 2015, Edinburgh, Scotland. Oral presentation.
10. Jiang Y, **Cao S**, Bright D, Suydam IT, Woodrow KA, "Testing of nanoparticle-based ARV drug combinations for inhibiting cell-free and cell-cell HIV transmission" 32nd Annual Symposium on Nonhuman Primate Models for AIDS. November 11-14, 2014, Portland, Oregon. Poster presentation.
11. Jiang Y, **Cao S**, Bright D, Suydam IT, Woodrow KA, "Evaluation of nanoparticle-mediated delivery of ARV drug combinations." 31st Annual Symposium on Nonhuman Primate Models for AIDS. November 3-6, 2013, Atlanta, Georgia. Poster presentation.

VITA

Shijie Cao received his bachelor's degree in Pharmacy from Fudan University, China in 2013. His undergraduate research focused on nanoparticle design and evaluation for delivering chemotherapeutics to brain tumors. In 2013, he started to pursue his PhD in Bioengineering at the University of Washington under the supervision of Prof. Kim Woodrow. At UW, he worked in several projects on developing targeted drug delivery system for HIV treatment, and was particularly interested in synergistic combination therapy, as well as T cell and lymphatic tissue targeting. Currently, his research interests include biomaterials design, drug delivery, and immunoengineering.